UNIVERSIDAD COMPLUTENSE DE MADRID
FACULTAD DE CIENCIAS FÍSICAS
Departamento de Física Teórica I

CONTROL OF UTRASTRONGLY COUPLED SYSTEMS IN CIRCUIT QUATUM ELECTRODYNAMICS

CONTROL DE SISTEMAS ULTRAFUERTEMENTE ACOPLADOS EN ELECTRODINÁMICA CUÁNTICA DE CIRCUITOS

MEMORIA PARA OPTAR AL GRADO DE DOCTOR
PRESENTADA POR

Borja Peropadre

Bajo la dirección del doctor

Juan José García-Ripoll

Madrid, 2014

Departamento de Física Teórica I
Universidad Complutense de Madrid

Doctoral Thesis

Control of ultrastrongly coupled systems in circuit quantum electrodynamics

Author:
Borja Peropadre

Supervisor:
Dr. Juan José García-Ripoll

Instituto de Física Fundamental
Consejo Superior de Investigaciones Científicas

Departamento de Física Teórica I
Universidad Complutense de Madrid

Tesis Doctoral

Control de sistemas ultrafuertemente acoplados en electrodinámica cuántica de circuitos

Autor:
Borja Peropadre

Supervisor:
Dr. Juan José García-Ripoll

Instituto de Física Fundamental
Consejo Superior de Investigaciones Científicas

Contents

List of publications

This thesis has given rise to the following peer-reviewed articles:

- **Switchable Ultrastrong coupling in circuit QED**
  B. Peropadre, P. Forn-Díaz, E. Solano, J. J. García-Ripoll
  Phys. Rev. Lett. **105**, 023601 (2010)

- **Approaching perfect microwave photodetection in circuit QED**
  B. Peropadre, G. Romero, G. Johansson, C. M. Wilson, E. Solano, J. J. García-Ripoll
  Phys. Rev. A **84**, 063834 (2011)

- **Demonstration of a Single-Photon Router in the Microwave Regime**
  I.-C. Hoi, C.M. Wilson, G. Johansson, T. Palomaki, B. Peropadre, P. Delsing
  Phys. Rev. Lett. **107**, 073601 (2011)

- **Extracting past-future vacuum correlations using circuit QED**
  C. Sabin, B. Peropadre, M. del Rey, E. Martín-Martínez
  Phys. Rev. Lett. **109** 033602 (2012)

- **Fast microwave beam splitters from superconducting resonators**
  M. Haeberlein, D. Zueco, P. Assum, T. Weiβl, E. Hoffmann, B. Peropadre, J.J. García-Ripoll, E. Solano, F. Deppe, A. Marx, R. Gross
  arXiv:1302.0729, Submitted to App. Phys. Lett. (2012)

- **Scattering of coherent states on a single artificial atom**
  B. Peropadre, J. Lindkvist, I.-C. Hoi, C.M. Wilson, J.J. García-Ripoll, P. Delsing, G. Johansson
  New J. Phys. **15** 035009 (2013)

- **Tunable coupling engineering between superconducting resonators: from sidebands to effective gauge fields**
  B. Peropadre, D. Zueco, F. Wulschner, F. Deppe, A. Marx, R. Gross, J.J. García-Ripoll
  Phys. Rev. B **87**, 134504 (2013)

- **Microwave Quantum Optics with an Artificial Atom in 1D Open Space**
  I.-C. Hoi, C.M. Wilson, G. Johansson, J. Lindkvist, B. Peropadre, T. Palomaki, P. Delsing
  New J. Phys. **15** 025011 (2013)

Other scientific publications not included in this thesis

- **From Josephson junction metamaterials to tunable pseudo-cavities**
  D. Zueco, C. Fernández-Juez, J. Yago, U. Naether, B. Peropadre, J.J. García-Ripoll and J. J. Mazo
  Supercond. Sci. Technol. **26**, 074006 (2013)

- **Nonequilibrium and nonperturbative dynamics of ultrastrong coupling in open lines**
  B. Peropadre, D. Zueco, D. Porras, and J. J. García-Ripoll
  arXiv:1307.3870. Submitted to Phys. Rev. Lett. (2013)

- **Tunable and Switchable Coupling Between Two Superconducting Resonators**
  E. Hoffmann, A. Baust, M.Haeberlein, E.P. Menzel, D. Zueco, F. Quijandria, B. Peropadre J.J. García Ripoll, E. Solano, A. Marx. F. Deppe, and R. Gross
  Submitted to Phys. Rev. Lett. (2013)

Conferences

The work developed in the thesis has been presented in the following series of conferences and research visits:

1. *Tunable coupling engineering between superconducting resonators*, Talk.
   XXXIV Reunión Bienal de la Sociedad Española de Física,
   Valencia (Spain)–July, 2013

2. *Quantum Simulations with superconducting resonators*, Poster.
   QIPC International Conference, Florence (Italy)–July, 2013

3. *Controlling quantum systems in circuit QED designs*, Seminar.
   Harvard University, Cambridge (USA)–March, 2013

4. *Controlling quantum systems in circuit QED designs*, Seminar.
   Massachusetts Institute of Technology, Boston (USA)–March, 2013

5. *Extraction of on-chip past-future quantum correlations*, Talk.
   APS March Meeting, Baltimore (USA)–March, 2013

6. *Switchable ultrastrong coupling in circuit QED and relativistic simulations*, Seminar.
   Institute for Quantum Computing, Waterloo (Canada) –November, 2012

7. *Tunable interaction between superconducting resonators*, Talk.
   Central European Workshop of Quantum Optics, Sinaia (Romania) – July, 2012

8. *On-chip all-optical Quantum Information Processing*, Talk.
   XXIII Reunión Bienal de la RSEF, Santander (Spain) –September, 2011

9. *Approaching perfect microwave photodetection in circuit QED*, Poster.
   QIPC International Conference, Zurich (Switzerland) –September, 2011

10. *Towards Quantum Information Processing on a chip*, Talk.
International CEWQO, Madrid (Spain) –May, 2011

11. *Quantum circuits as a toolkit for Quantum Simulation*, Poster.
Quantum Simulations, Benasque (Spain) –February, 2011

12. *Perfect photodetection in circuit quantum electrodynamics*, Talk.
Workshop in Quantum Solid-State Devices, Bilbao (Spain) –November, 2010

13. *Circuit QED with propagating microwaves*, Poster.
Quantum Engineering of States and Devices, Obergurgl (Austria) –June, 2010

14. *Novel aspects in circuit QED*, Seminar.
Chalmers university of Technology, Göteborg (Sweden) –May, 2010

15. *Switchable ultrastrong coupling in circuit QED*, Poster.
Solid-State Systems for Quantum Information Processing, Bilbao (Spain) –February, 2010

Preface

The great technological development experienced by our society is, to a large extent, caused by the excellent progress in the miniaturization techniques of electronic devices. This brought the transistor, building block of electronics and ubiquitous in all integrated circuits, to the nanoscale regime, thereby improving information processing. However this miniaturization process can not be performed indefinitely and the technological progress, as we know it, will see the end when microchips reach a scale where quantum mechanics emerges. In such microscopic scales, electrons propagating in a waveguide could tunnel out of it (quantum tunneling effect), hence destroying the transmission of information that was taking place. It thus becomes crucial to progress towards a new theory that allows to bring together technological development and quantum mechanics.

That progress arose during the last decade with the advent of quantum information science [NC00]. It is an emerging and multidisciplinary field whose ultimate goal is to take advantage of quantum phenomena, such as superposition and entanglement, in order to improve the information storage, communication and computation. With it, a new paradigmatic framework arises, in which the information is stored and transported via quantum bits (qubits), and processed in a new prototype of processor, the quantum computer [Deu85]. This revolutionary idea would not only solve the problem of miniaturization, but also would solve problems which are simply inaccessible with a classical computer, such as the factorization problem [Sho97] or the dynamics of many-body quantum systems [AL97]. For these quantum computers to exceed their classical counterparts capabilities, it becomes essential that many qubits interact with each other, without losing their quantum properties. So far only few-qubit systems have been shown to preserve their quantum properties, which is not enough to talk about the breakthroug we pursue. However it is not all bad news, and until a universal quantum computer is developed, there is an alternative that allows for the simulation of

a smaller set of problems, as the dynamics of many-body quantum systems. This is the field of quantum simulation[Fey82, Llo96]: A quantum simulator [BN09] is a highly controllable experimental device, where we can control the quantum state of the system and the interactions between particles, to make the system behave as a particular model of interest.

There are several proposals for implementing both quantum computers and quantum simulators, all of them based on different physical systems. Trapped ions [CZ95, FSG+08], ultracold atoms [JZ05], NMR systems [VC05], quantum dots [BKKY08] or superconducting circuits [HTK12] are some examples of quantum simulators. Each of these platforms has different advantages and drawbacks with respect to the others, such as the ability of trapping particles and isolate them, control of the interactions between particles, improvement of decoherence, or the economic cost itself. However, all them share a common feature: the excellent control over individual quantum particles such as atoms, electrons and photons. Pioneering work in the field of trapped ions and quantum optics during the past decade has made this possible, and as such it has been recognised by the scientific community with the 2012 Nobel Prize to Dave Wineland and Serge Haroche for their "for groundbreaking experimental methods that enable measuring and manipulation of individual quantum systems". It is thus not surprising that researchers have focused their atention on the control and scalability of qunatum systems, towards a new revolution that allows for solving problems that are nowadays simply impossible. This thesis also pursues this goal, and we study the control of quantum systems on a particular platform: superconducting quantum circuits.

Quantum circuits [CW08] are integrated circuits whose degrees of freedom exhibit a quantum behaviour. In contrast to classical electrical circuits, where the degrees of freedom can take continuous values, the degrees of freedom of a quantum circuit can only take discrete values. The fundamental requirement for a quantum circuit to bahave quantum-mechanically is the absence of dissipation on it. Hence, quantum circuits are built with superconducting materials, since they have no resistance to the current flow. If the superconducting circuit is cooled down to cryogenic temperatures –typically on the order of millikelvins– where thermal fluctuations are negligible, we will finally observe its quantum nature.

In particular, superconducting circuits made out of linear elements such as inductors and capacitors, exhibit their quantum nature as excitations of the electromagnetic field on it, i.e, microwave photons. If instead we add nonlinear elements to the circuit, such as Josephson junctions, we can build artifi-

cial atoms or superconducting qubits, systems with only a few energy levels. These artificial atoms interact with the photons in the same way that real atoms and photons do, this is, ruled by the laws of quantum electrodynamics, giving rise to the field known as circuit quantum electrodynamics (*circuit QED* from now on). Circuit QED [BHW+04] is widely considered the on-chip realization of its optical counterpart *cavity QED*, since it studies the interaction between light and matter at the most fundamental level with quantum electrical circuits in one dimension. As we will see throughout this Thesis, this one-dimensional nature makes of circuit QED an advantageous platform, as the interaction between light and matter takes place in a more efficient way. In particular, it is possible to reach an interaction regime where the coupling strength "g" is comparable to the bare energies of superconducting qubits ω_q, and microwave photons ω_k. Under this condition, light and matter interact in the so-called *ultrastrong coupling regime* [BGA+09, NDH+10, FLM+10], unachievable in an optical system. In this rather unexplored regime, one can tailor strong photon-photon interactions [HBP06, PZW+12], generate strong correlations between light and matter [CRL+10, NC10b], or study the Kondo physics in the spin-boson model [LH12]. Along the lines of quantum technologies, the ultrastrong coupling regime has found application in the development of ultrafast quantum gates [RBW+12] and quantum memories [SPdRMM12] for quantum computing in circuit QED [NC11]. For all these reasons, circuit QED has become a unique platform for studying new regimes of interaction, as well as a strong candidate to be the first system that implements a quantum computer.

In this Thesis we will focus on the study of light-matter interaction in a quantum circuit, and the control of their interaction in the ultrastrong regime. In addittion to this, we propose different designs that allows for a switchable coupling, both statically and dynamically, and we show their potential application for quantum information science. This Thesis is written in the "article format", where the original publications that the realization of this Thesis has produced are presented after a brief summary and discussion of their main results. It is organized as follows: The first two chapters are devoted to a brief description of the basic concepts and tools used in this Thesis. In chapter 1 we show the general procedure to quantize electrical circuits, and show how these circuits behave as microwave photons and artificial atoms. More precisely, we will focus on those quantum circuits that have been relevant in the development of this Thesis. In chapter 2, we introduce the field of circuit QED, with special emphasis in the setups that lead to the strong and ultrastrong regimes of interaction. We also introduce the novel field of circuit QED in open space, and present the general treatment of open quantum systems for studying this novel framework. Then, in chapter 3 we present the origi-

nal publications, together with a brief motivation and summary of the main results. Our results can be dividied into two different approaches, namely

- Control of the interaction between photons and qubits, either confined in a resonator or an open line, via an engineered switchable coupling g.
- Control of propagating microwave photons moving in an open transmission line, by means of the scattering properties with an artificial atom.

In the first part of this Thesis, we will show how one can dynamically control the coupling g between qubits and microwave photons by using superconducting quantum interference devices (SQUID's), connecting and disconnecting the interaction in times that are on the nanosecond scale. The designs proposed in this Thesis can be used as quantum switches that allow for the implementation of ultrafast quantum gates, the generation of single photons on demand, as well as the simulation of relativistic quantum information problems, such as the extraction of quantum entanglement from the vacuum. These designs not only allow for a complete deactivation of the light-matter interaction, but also for coherent rotations of it, going from transverse to longitudinal interactions. Besides these applications, mostly focused in the development of quantum gates for quantum computing, our designs allow for the simulation of Kerr-type nonlinear media, and the generation of entangled pair of photons. Moreover, we propose different setups of coupled superconducting resonators whose interaction can be dynamically controlled by means of SQUID's. Using this devices, we it becomes possible to study and quantum simulate diverse interesting models in condensed matter physics, such as families of Bose-Hubbard models.

In the second part of the Thesis, we adopt a different approach for tuning the coupling. Motivated by the recent experiments which shows that light and matter can interact strongly even in the absence of confining cavities, we study the control of propagating photons in an open tranmission line through their scattering upon artificial atoms. We observe that the scattering of propagating photons by a two-level system results in a perfect reflection of the photon. By contrast, the photon scattering by a three-level artificial atom can result in perfect transmission of the photon. Hence, by playing with the internal structure of the artificial atom, we can control whether the photons are reflected or transmitted at will. We propose a practical application to address photons to different channels of a quantum network. Finally, we study the photodetection problem of propagating microwaves in circuit QED. Given the low cross section of microwave photons, it has not been possible to design

efficient single-photon detectors without introducing noise the detection process. Based on the scattering theory, we propose a simple design with a single phase qubit placed in a semi-infinite transmission line that works as a perfect absorber of the microwave photon. Below we present the most outstanding results derived from this thesis.

1

Quantum electrical circuits

In this chapter we present the minimal theoretical background to the field of superconducting circuits, to help the reader to understand the content of this Thesis. We introduce the standard quantization approach of electrical circuits, and the wide variety of quantum systems that result from it. In particular, we show those that have been of central importance in the development of this Thesis: microwave photons, superconducting qubits, and tunable couplers.

1.1 Classical & quantum circuits

For most purposes in physics, electrical circuits can be regarded as networks where electromagnetic fields propagate from one point to another. These electromagnetic fields are fully described by their classical degrees of freedom, the intensity $I(t)$ and voltage $V(t)$ defined at each point of the network, and their dynamics is governed by the Maxwell equations. Under this viewpoint we usually refer to these devices as *classical circuits*.

Nonetheless, electrical circuits can behave *quantum mechanically* under certain conditions. If we cool them down to very low temperatures ($T \simeq 20$mK), the circuit operates in the superconducting regime [OD91], opposing no resistance to the current flow[1]. Besides this absence of dissipation, at those cryogenic temperatures the typical energy of thermal fluctuations $K_B T$ is negligible, so the discreteness in the energy levels of the circuit and the quantum nature of the circuit degrees of freedom emerge. We refer to these microfabricated devices as *superconducting* or *quantum circuits*: macroscopic circuits that

[1] Superconductivity is a crucial requirement for a circuit to behave quantum mechanically, since dissipative elements such as resistances, induce energy relaxation and decoherence.

obey the laws of quantum mechanics [Leg80].

Under these conditions, the quantum circuit will be described by a macroscopic wavefunction $\Psi(\mathbf{r},t) = \sqrt{n(\mathbf{r},t)}e^{i\theta(\mathbf{r},t)}$, where $n(\mathbf{r},t)$ accounts for the density of Cooper pairs in the circuit, and $\theta(\mathbf{r},t)$ represents the phase of the superconducting condensate. The dynamics of the quantum circuit is ruled by the Schrödinger equation:

$$i\hbar\frac{\partial\Psi(\mathbf{r},t)}{\partial t} = H\Psi(\mathbf{r},t), \tag{1.1}$$

where H is the Hamiltonian operator associated to the quantum degrees of freedoms of the circuit.

In the reminder of this chapter we will show that it is possible to build a wide variety of circuits whose corresponding Hamiltonian and quantum degrees of freedoms resemble those of individual quantum systems, such as atoms and photons. This will be our testbed for building up devices that successfully reproduce the interaction between atoms and photons, or the dynamics of many-body quantum systems in a controllable way. Along our way to build up these systems, we first present the general procedure for obtaining the Hamiltonian H of any superconducting circuit.

1.1.1 Quantum Network Theory

In this section we show the general formalism that allows us to compute the Hamiltonian H of a superconducting circuit: it is based on the so-called Quantum Network Theory [YD84, Dev95]. This is an *effective theory*, which is formally similar to the classical description of electrical circuits [Pau94], with the only difference that we will impose canonical quantization rules to the circuit degrees of freedom.

Following the classical network analysis, we can divide any electrical circuit, typically made out of capacitors and inductors[2], into lumped elements[3], and identify the node points of the resulting network with the degrees of freedom of the circuit (see Fig. 1.1.1). Without loss of generality, these degrees of freedom will be the flux $\Phi(t)$ and the charge $Q(t)$ on each node of

[2]Since we have neglected dissipative elements like resistors R, the only passive elements we consider in an electrical circuit are capacitors C and inductors L. They are non-dissipative elements which store energy in the electric and magnetic field respectively.

[3]The lumped element approximation is valid when the size of a circuit is much smaller that the typical wavelength of the electric fields contained on it. When it is not this way, as in the case of transmission lines, an equivalent circuit based on lumped dements can always be found.

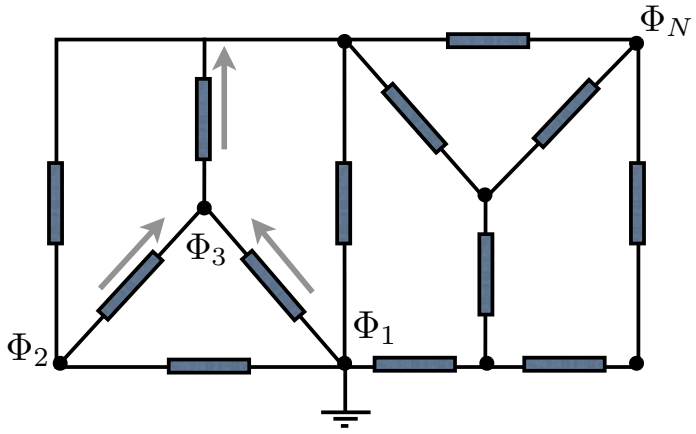

Figure 1.1: Lumped element description of an electrical circuit. The passive elements (typically capacitors and inductors) are represented by blue boxes. Kirchoff's laws at each node gives the equation of motion for the variables Φ_N.

the circuit. Notice that it is completely equivalent to describe the degrees of freedom either with flux-charge variables or voltage-intensity variables[4] , since the former variables are defined as the time integral of the latters

$$\Phi(t) = \int_{-\infty}^{t} V(t')dt', \quad Q(t) = \int_{-\infty}^{t} I(t')dt'. \tag{1.2}$$

This description is particularly suitable for superconducting circuits, because flux and charge variables are closely related to the superconducting phase $\theta(\mathbf{r}, t)$ of the circuit and the number of Cooper pairs $n(\mathbf{r}, t)$. Applying Kirchoff's laws at each node of the network[5], we find the equations of motion for the flux $\Phi(t)$, which correspond to the Euler-Lagrange equations

$$\frac{d}{dt}\left(\frac{\partial L}{\partial \dot{\Phi}_k}\right) - \frac{\partial L}{\partial \Phi_k} = 0, \quad k = 1, ..., n \tag{1.3}$$

associated to a certain Lagrangian L. Unsurprisingly, this Lagrangian L is nothing but the energy difference between the capacitive and inductive energies stored in the electromagnetic fields of the circuit[6]:

$$L(\dot{\Phi}_k, \Phi_k) = \frac{1}{2}\dot{\vec{\Phi}}^{\dagger} C\, \dot{\vec{\Phi}} - \frac{1}{2}\vec{\Phi}^{\dagger} L \vec{\Phi}, \tag{1.4}$$

[4]Like V and I, Φ and Q are canonically conjugated variables in the language of Hamiltonian mechanics, and therefore satisfy that their Poisson bracket is equal to one.

[5]In particular, we apply the Kirchoff's law for the current: the sum of all electrical currents arriving at a given node equals zero.

[6]In analogy with Hamiltonian mechanics, this Lagrangian describes the dynamics of a set of particles with mass matrix "C" moving in a potential "L".

where C and L accounts for the capacitance and inductance matrices of the circuit. Finally, the associated classical Hamiltonian H can be obtained by applying a Legendre transformation of the form

$$H(Q_k, \Phi_k) = \sum_k Q_k \dot{\Phi}_k - L, \tag{1.5}$$

being the charge $Q_k = \partial L / \partial \dot{\Phi}_k$ the canonically conjugated momentum of the flux Φ_k, fulfilling $\{\Phi_k, Q_{k'}\} = \delta_{kk'}$.

The above discussion corresponds to the classical description of an electrical circuit. If we now assume that the circuit is effectively cooled down to the absolute zero, its degrees of freedom Φ_k and Q_k become quantum, and we can apply canonical quantization rules[7] to them, rendering the following quantum Hamiltonian

$$H = \frac{1}{2}\vec{\hat{Q}}^{\dagger} C^{-1} \vec{\hat{Q}} + \frac{1}{2}\vec{\hat{\Phi}}^{\dagger} L \vec{\hat{\Phi}}, \tag{1.6}$$

where Φ and Q satisfy the canonical commutation ralation $[\Phi, Q] = i\hbar$. Notice that any superconducting circuit is fully characterized by its capacitance and inductance matrices C and L. So, knowing the particular form of those matrices we can determine the Hamiltonian H, and therefore the dynamics of any quantum circuit.

We will apply this formalism to different superconducting circuits of paramount importance, as they are the cornerstone of microwave photons and artificial two-level atoms. We start by analyzing the simplest superconducting circuit: the *quantum LC resonator*

1.2 Superconducting resonators: Microwave photons

1.2.1 Quantum LC resonator

A quantum LC resonator is a superconducting wire containing a capacitor C in parallel with an inductor L, as illustrated in Fig. 1.2a. The Kirchoff equation for the circulating current[8] implies that $I_L = I_C$, which yields a second-order differential equation for the flux variables

$$\frac{\Phi_2 - \Phi_1}{L} = C(\ddot{\Phi}_2 - \ddot{\Phi}_1) \tag{1.7}$$

[7] The classical variables Φ_k and Q_k will turn into quantum operators $\hat{\Phi}_k$ and $\hat{Q}_k$, satisfying the canonical commutation relations $\left[\hat{\Phi}_k, \hat{Q}_{k'}\right] = i\hbar\{\Phi_k, Q_{k'}\} = i\hbar\delta_{kk'}$

[8] The total current coming from inductive elements $I_L = \Phi/L$ equals the current going to capacitive elements $I_C = C\, dV_c/dt$.

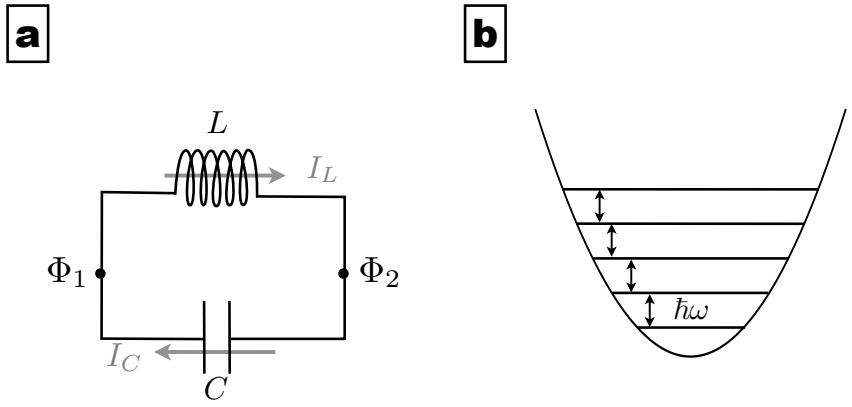

Figure 1.2: a) Lumped element model of an LC resonator. b) Discrete energy spectrum of the quantum LC resonator. It is identical to that of a quantum harmonic oscillator, with energy gap given by $\hbar\omega = 1/\sqrt{LC}$.

where we used eq. (1.2) to express the currents as a function of fluxes. Without loss of generality, we can always take the variable $\Phi_1 = 0$, by properly assigning the reference node[9]. In doing so, we can relabel the flux $\Phi_2 = \Phi$, and the equation (1.7) can be written as

$$\ddot{\Phi} - \frac{1}{LC}\Phi = 0. \tag{1.8}$$

In other words, the LC resonator behaves as a harmonic oscillator with frequency $\omega = 1/\sqrt{LC}$[10]. The above equation of motion yields the Lagrangian L and Hamiltonian H of the circuit, namely

$$L = \frac{C\dot{\Phi}^2}{2} - \frac{\Phi^2}{2L} \quad \longrightarrow \quad H = \frac{Q^2}{2C} + \frac{\Phi^2}{2L}, \tag{1.9}$$

where $Q = C\dot{\Phi}$ is the canonically conjugate momentum of Φ. Finally, and provided that the circuit is at zero temperature, we can promote the classical variables to their quantum counterparts, obeying $\left[\hat{\Phi}, \hat{Q}\right] = i\hbar$. If we now express these quantum operators in terms of the annihilation and creation

[9]The reference node is the node connected to the ground $V = 0$.

[10]Typical values of the inductance and capacitance are $L \sim 10$ nH and $C \sim 1$ pF, yielding a resonant frequency that is in the microwave regime ($\omega/2\pi \sim 1 - 5$ GHz).

operators a and $a^\dagger$

$$a = \frac{1}{\sqrt{2\hbar L\omega}}\hat{\Phi} + i\frac{1}{\sqrt{2\hbar C\omega}}\hat{Q}, \tag{1.10}$$

$$a^\dagger = \frac{1}{\sqrt{2\hbar L\omega}}\hat{\Phi} - i\frac{1}{\sqrt{2\hbar C\omega}}\hat{Q}, \tag{1.11}$$

the Hamiltonian of the LC resonator can be eventually written as

$$H = \hbar\omega(a^\dagger a + \frac{1}{2}), \tag{1.12}$$

where the operators a, $a^\dagger$ fulfill $[a, a^\dagger] = 1$. The eigenstates of (1.12) are Fock states $|n\rangle$ with equally spaced energy levels $\epsilon_n = \hbar\omega(n + 1/2)$, where n is the number of excitations (see Fig. 1.2b). We can interpret these quanta excitations as microwave photons with frequency ω, that have arisen from the quantization of the electromagnetic field in the resonator. Therefore, the LC resonator can be seen as a microwave cavity where photons get trapped.

However, the LC resonator is not the most suitable microwave cavity for practical purposes, as it can only support a single mode of the electromagnetic field –for this reason it is usually called zero-mode resonator. Nevertheless, understanding the physics of this simple quantum circuit is crucial for describing more complex devices. Coplanar waveguides such as microstrips, strip-lines and transmission line resonators are examples of distributed elements that admit a lumped element description in terms of LC oscillators. Particularly, in this Thesis we have mostly considered transmission line resonators for storing microwave photons.

1.2.2 Transmission line resonator

A transmission line is the two-dimensional analogue of a coaxial cable: it consists of two ground planes and one center conductor, where electromagnetic fields can propagate between two different points.

A *transmission line resonator* is a finite section of a transmission line, which can support standing modes of the electromagnetic field, as the one depicted in Fig. 1.3a. Such a resonator can be easily built by inserting a gap in the center conductor of the transmission line, where the "mirrors" are the resulting capacitors on the edges[11]. The capacitors create a node in the intensity field $\hat{I}(x,t)$, so that the current cannot flow out of the resonator.

[11] Alternatively, a transmission line resonator can be built by connecting the center conductor to the ground planes. This way, the shorted circuit creates a node in the voltage field $\hat{V}$. We will use this boundary condition in publication P8 for building up a semi-infinite cavity.

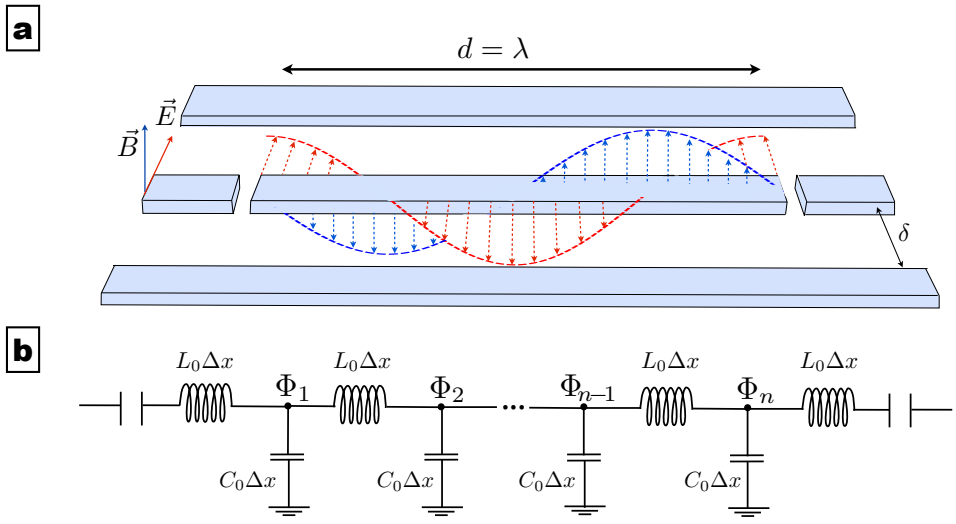

Figure 1.3: a) Full-wavelength transmission line resonator with standing electric and magnetic fields. b)Lumped equivalent circuit of the resonator depicted in a).

It is possible to describe these devices with a discretized equivalent circuit, by dividing the transmission line into infinitesimally small segments of length Δx, as shown in Fig. 1.3b. Each of these segments is a lumped LC oscillator, with characteristic inductance L_0 and capacitance C_0 per unit length. In this lumped approximation, current conservation renders the following Euler-Lagrange equations and associated Lagrangian:

$$C_0\Delta x\ \ddot{\Phi}_k + \frac{\Phi_{k+1} - 2\Phi_k + \Phi_{k-1}}{L_0\Delta x} = 0, \tag{1.13}$$

$$L = \frac{1}{2}\sum_k C_0\Delta x\ \dot{\Phi}_k^2 - \frac{1}{L_0\Delta x}(\Phi_{k+1} - \Phi_k)^2, \tag{1.14}$$

which in the continuum limit $\Delta x \to 0$ reads:

$$v_p^2\partial_x^2\Phi(x,t) - \partial_t^2\Phi(x,t) = 0, \tag{1.15}$$

$$L = \frac{1}{2}\int_0^d dx\left[\dot{\Phi}(x,t)^2 + \frac{1}{L_0}\left(\partial_x\Phi(x,t)\right)^2\right]. \tag{1.16}$$

Equation (1.15) is the well-known wave equation for the flux field $\Phi(x,t)$ with propagation velocity $v_p = 1/\sqrt{L_0C_0}$. It can be solved by decomposing

the field over normal modes in the form $\Phi(x,t) = \sum_n = \phi_n(t)u_n(x)$. Using open boundary conditions[12], we obtain that

$$\Phi(x,t) = \sqrt{\frac{2}{d}} \sum_{n_o=1} \phi_{n_o}(t) \cos\frac{n_o \pi x}{d} + \sqrt{\frac{2}{d}} \sum_{n_e=2} \phi_{n_e}(t) \sin\frac{n_e \pi x}{d}, \tag{1.17}$$

where $n_{e,o}$ respectively stands for the even and odd modes in the line. Substituting this normal mode expansion into (1.16), we obtain the diagonalized Lagrangian: a set of n independent harmonic oscillators:

$$L = \sum_{n=1}^{\infty} \frac{C_r}{2}\dot{\phi}_n^2 - \frac{C_r}{2}\omega_n^2\phi_n^2, \tag{1.18}$$

where $C_r = dC_0$ is the total capacitance of the transmission line resonator, and $\omega_n = n\pi/d\sqrt{L_0C_0}$ is the frequency of the n-th oscillator. The corresponding Hamiltonian follows from a Legendre transformation, yielding:

$$H = \sum_{n=1}^{\infty} \frac{1}{2C_r} q_n^2 + \frac{C_r}{2}\omega_n^2\phi_n^2, \tag{1.19}$$

where $q_n = C_r\dot{\phi}_n$ is the conjugate charge. We can now quantize this Hamiltonian in the usual form. In particular, if we express the quantum operators $\hat{\phi}_n$, $\hat{q}_n$ in terms of the annihilation and creation operators a_n, $a_n^\dagger$

$$\hat{\phi}_n = \sqrt{\frac{\hbar}{2C_r\omega_n}}(a_n^\dagger + a_n), \quad \hat{q}_n = i\sqrt{\frac{\hbar C_r\omega_n}{2}}(a_n^\dagger - a_n), \tag{1.20}$$

the transmission line Hamiltonian reduces to a discrete sum of infinite uncoupled harmonic oscillators:

$$H = \sum_{n=1}^{\infty} \hbar\omega_n(a_n^\dagger a_n + \frac{1}{2}). \tag{1.21}$$

The transmission line resonator can thus trap microwave photonic modes of frequency ω_n, exactly in the same way as an optical cavity does. For most of the purposes of this Thesis, it will be sufficient to restrict ourselves to the first (half-wavelength) or to the second mode (full-wavelength) of the resonator, so henceforth the resonator Hamiltonian will be written as

$$H = \hbar\omega_r(a^\dagger a + \frac{1}{2}), \tag{1.22}$$

being $\omega_r = 1/\sqrt{L_rC_r}$ the frequency of the resonator.

[12] Open boundary conditions, or zero current conditions yields $\partial_x\Phi(0,t) = \partial_x\Phi(d,t) = 0$.

Zero-point energy of the resonator

The ground state of the above Hamiltonian is the Fock state with zero photons in the resonator $|0\rangle$. However, even in the absence of photons the resonator contains some zero-point energy $\hbar\omega_r/2$, due to the quantum fluctuations of the voltage and intensity fields $\hat{V}$, $\hat{I}$:

$$V(x,t) = \frac{\partial\Phi(x,t)}{\partial t} = iV_{\text{rms}}(a-a^\dagger)\cos(kx), \tag{1.23}$$

$$I(x,t) = \frac{1}{L_0}\frac{\partial\Phi(x,t)}{\partial x} = I_{\text{rms}}(a+a^\dagger)\sin(kx), \tag{1.24}$$

where the zero-point voltage V_{rms} and intensity I_{rms} are given by[13]

$$V_{\text{rms}} = \sqrt{\frac{\hbar\omega_r}{C_r}}, \quad I_{\text{rms}} = \sqrt{\frac{\hbar\omega_r}{L_r}}. \tag{1.25}$$

The corresponding zero-point electric and magnetic field can be written as

$$E_{\text{rms}} = \frac{V_{\text{rms}}}{\delta} = \sqrt{\frac{\hbar\omega_r}{C_0 V}}, \quad B_{\text{rms}} = \frac{\mu_0 I_{\text{rms}}}{\pi\delta} = \frac{\mu_0}{\pi}\sqrt{\frac{\hbar\omega_r}{L_0 V}}, \tag{1.26}$$

where V is the effective volume in which the photons are confined[14]. Due to the one dimensional nature of the resonator, the confining volume V is very small, and thus the vacuum fluctuations of the electric and magnetic fields can be very large[15]. We will take advantage of these large vacuum fluctuations for increasing the light-matter interaction, which in the dipole approximation is given by

$$H_{\text{el}} = -\hat{\mathbf{d}}\cdot\hat{\mathbf{E}}, \quad H_{\text{mag}} = -\hat{\boldsymbol{\mu}}\cdot\hat{\mathbf{B}}, \tag{1.27}$$

where $\mathbf{d}$ and $\boldsymbol{\mu}$ are respectively the electric and magnetic dipole moments of the atom. Moreover, in the next section we will show that it is possible to build artificial two-level atoms with very large dipole moments, which can boost the light-matter interaction to the strong and ultrastrong regime.

To this end, it will be necessary to introduce a add a new ingredient: the anharmonicity. In contrast to photons, where all the energy transitions are degenerate, two-level atoms are highly anharmonic systems whose energy transitions are well-separated from all the others. We introduce a new element in

[13] The root mean square intensity I_{rms} is equal to the uncertainty in the intensity field $\Delta I = \sqrt{\langle 0|I^2|0\rangle - \langle 0|I|0\rangle^2}$, and analogously the root mean square voltage V_{rms}.

[14] The volume of the photonic mode $V = d\cdot\delta^2 \sim 10^{-6}\lambda^3$, being d the length of the cavity, and δ the distance between the ground plane and the central pin.

[15] For a 1D resonator, E_{rms} is 10^3 times larger the typical zero-point fields in an optical cavity.

the circuit architecture that provides us with the required non-linearity: the Josephson junction [Jos62].

1.3 Josephson-based qubits: Artificial atoms

1.3.1 Josephson junction & Josephson effect

A Josephson junction is the weak link between two superconductors, separated by a thin insulating layer (see Fig.1.4a). As we mentioned in the introduction of the chapter, the two superconductors are characterized by a macroscopic wavefunction of the form $\Psi_i = \sqrt{n_i}e^{i\theta_i}$. In 1962 Brian Josephson [Jos62] demonstrated that these two wavefunctions can overlap with each other, resulting in a tunneling of Cooper pairs between the two superconductors. The solution to the Schrödinger equation for this system shows that the flowing current through the junction can be related to the phase difference of the wavefunctions through

$$I = I_c \sin(\theta_2 - \theta_1) = I_c \sin \varphi_J, \tag{1.28}$$

where I_c is the critical current of the junction[16], and φ_J is the so-called gauge-invariant phase (see Fig.1.4b). The relation (1.28) is usually known as the dc-Josephson relation, as it shows a continuously flowing dc-current in the absence of any externally applied voltage bias V. For a non-zero applied voltage V between the two superconducting electrodes, Josephson demonstrated that it is related to the gauge invariant phase φ_J according to:

$$V = \frac{\Phi_0}{2\pi}\frac{d\varphi_J}{dt}, \tag{1.29}$$

where $\Phi_0 = 2e/h$ is the magnetic flux quantum[17]. This equation is known as the ac-Josephson relation, and together with (1.28), yields the *non-linear* oscillating current in the junction $I = I_c \sin(2\pi V t/\Phi_0)$. According to the relation[18] $L = V/\dot{I}$, we can derive the associated inductance to the Josephson junction,

$$L_J = \frac{\Phi_0}{2I_c \cos \varphi_J}, \tag{1.30}$$

so the junction is regarded as a non-linear inductor.

[16] The critical current of the junction depends on microscopic details, such as the area and the thickness of the junction.

[17] The quantity Φ_0 is known as the magnetic flux quantum, since the magnetic flux passing through a superconducting loop is quantize on units of Φ_0. This is shown in Appendix **??**.

[18] $L_J = \left(\frac{dI}{d\phi}\right)^{-1} = \left(\frac{dI}{dt}\frac{dt}{d\phi}\right)^{-1} = V/\dot{I}$

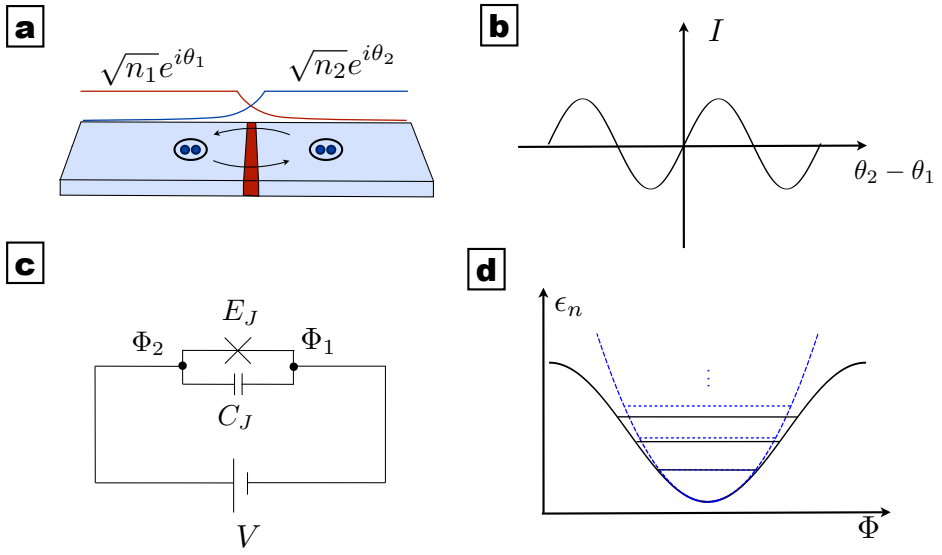

Figure 1.4: a) Pictorial view of a Josephson Junction; two superconducting electrodes (blue) are separated by a thin oxide layer (red). The overlap of the wavefunctions Ψ_1 and Ψ_2 yields the tunneling of Cooper pairs. b) Current-phase relation of the junction. c) Lumped equivalent circuit of the Josephson junction subject to an external bias V. d) Energy level comparison between the Josephson junction (solid black) and a harmonic oscillator (dashed blue).

In the equivalent circuit representation, the Josephson junction can be described by a capacitively shunted[19] non-linear inductance, and is usually represented with a cross in parallel with a capacitance, as shown in Fig.1.4c.

It is worth noting that the time derivative of the flux drop across the junction equals the external bias V:

$$V = \frac{d(\Phi_2 - \Phi_1)}{dt} = \frac{d\Phi}{dt}, \tag{1.31}$$

which combined with the ac-Josephson equation (1.29), reflects the intimate relation between the flux and the gauge invariant phase: $\varphi_J = 2\pi\Phi/\Phi_0$. So each time the flux changes in one flux quantum, the superconducting phase winds by 2π.

In our way to derive the Josephson junction Hamiltonian, we apply the

[19] Apart from assisting the tunneling of Cooper pairs, the insulating barrier acts as a capacitor, since it behaves as two parallel plates facing each other.

Kirchoff equation for the current in the circuit of Fig.1.4c, getting the equation $C_J\ddot{\Phi} = I_c \sin(2\pi\Phi/\Phi_0)$, with $\Phi = \Phi_2 - \Phi_1$, that corresponds to the Lagrangian

$$L = \frac{C_J}{2}\dot{\Phi}^2 - \frac{I_c\Phi_0}{2\pi}\left[1 - \cos\left(\frac{2\pi\Phi}{\Phi_0}\right)\right]. \tag{1.32}$$

Finally, the Josephson junction Hamiltonian readily follows from a Legendre transformation, yielding

$$H_J = \frac{\hat{Q}^2}{2C_J} - \frac{I_c\Phi_0}{2\pi}\cos\left(\frac{2\pi\hat{\Phi}}{\Phi_0}\right), \tag{1.33}$$

or equivalently in terms of the number and phase operators,

$$H_J = 4E_C\hat{n}^2 - E_J\cos\hat{\varphi}_J, \tag{1.34}$$

where we expressed the charge as a function of the the number of Cooper pairs in the junction $\hat{Q} = 2e\hat{n}$, and where $E_C = e^2/2C_J$ and $E_J = I_c\Phi_0/2\pi$ are respectively the charging energy and the Josephson energy of the junction. The cosine dependence of H in Eq. (1.33) endows the system with a highly non-linear potential, which in turn yields an anharmonic spectrum for the energy levels of the junction, as illustrated in Fig. 1.4d. In the next section we will use this feature for building up quantum circuits whose energy spectra are those of a few level systems, like two-level atoms, or *qubits*[20] in the language of quantum information.

1.3.2 Superconducting qubits

Quantum bits, or qubits [NC00], are quantum mechanical two-level systems in which we can codify quantum information in the internal states of the system, $|0\rangle$ and $|1\rangle$. In contrast to classical bits, which can only take either the logical value 0 or 1, quantum bits can hold arbitrary superpositions $|\psi\rangle = \alpha|0\rangle + \beta|1\rangle$, with complex probability amplitudes satisfying $|\alpha|^2 + |\beta|^2$. Together with quantum entanglement, this striking property has made of qubits a cornerstone in quantum information technologies, as they could perform computations much faster than a classical computer does[21]. One of the most promising platforms for developing these fascinating tasks are quantum circuits with *superconducting qubits*.

[20] A quantum bit is the minimal unit of quantum information.

[21] Besides this long-term goal, and among other applications, quantum bits have been used for unconditionally secure quantum communications, so it is not surprising that qubits are subject of large research and development.

Superconducting qubits are Josephson-junction based circuits that behave as quantum two-level systems. For this reason they are also called *artificial atoms*. During the past decade a number of Josephson-based qubits have been proposed [DWM, CW08]. They can be classified according to the different working regimes of the Josephson junction. These regimes are defined by the ratio of the charging and Josephson energy E_J/E_C, and basically tells us which term dominates the Hamiltonian (1.34):

- If the ratio $E_J/E_C \ll 1$, then the junction is said to be in the *charge regime*, and the number of Cooper pairs n on the junction is a good quantum number[22]. To this family of qubits belongs the *charge qubit* [BVJ+98].
- If on the other hand, the ratio $E_J/E_C \gg 1$, the junction is said to be in the *flux* (or *phase*) *regime*, and the flux (or phase) across the junction is well defined, while the number of Cooper pairs is not. This is the case of the *flux qubit* [OMT+99] and the *phase qubit* [MDC85].

In a nutshell, the charge qubit is a superconducting island connected to a superconducting reservoir through a junction. Since the number of Cooper-pairs on the island is a good quantum number, the logical states $|0\rangle$ and $|1\rangle$ will be the discrete number of charges in the island. The flux qubit is a superconducting ring interrupted by three Josephson junctions. Since it operates in the flux regime, the flux in the loop is well-defined, and the logical states will be superconducting persistent currents flowing clockwise and counterclockwise in the loop. The phase qubit is a current biased Josephson junction operating in the phase regime and therefore, two different values of φ_J define our quantum logic states. These three quantum circuits are considered the building blocks of superconductor based quantum information, since charge, flux and phase qubits, were the first to be developed and all the subsequent superconducting qubits are pretty much based on them. In particular, other Josephson-based superconducting qubits are the *quantronium* [VAC+02], *fluxonium* [MKGD09] or the *transmon qubit* [KYG+07]. They are essentially "improved" versions of the charge and flux qubits, which aim to extend the qubit lifetimes by reducing the flux and charge noise by their coupling to the environment.

Of paramount importance in this Thesis have been the flux, the transmon, and the phase qubits. In particular, in publications P1 and P2 we focus on the control of light-matter interaction with flux qubits. In publications P5,

[22] This in an immediate consequence of the Heisenberg uncertainty relation for the number and phase operators, $\Delta n \Delta \varphi_J \geq 1$, by which if one variable doesn't fluctuate, the other one is smeared out.

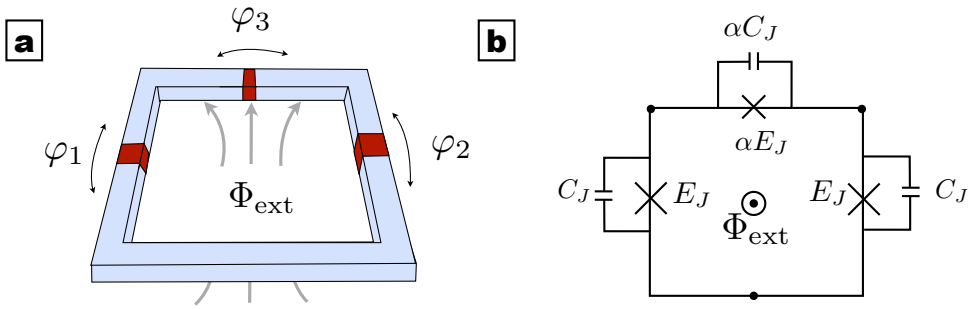

Figure 1.5: a) Superconducting ring interrupted by three-Josephson junctions. This quantum circuit is the so-called flux qubit. b) Equivalent circuit of the qubit.

P6 and P7 we put our attention in the scattering of photons with a transmon qubit. Lastly, publication P8 we have devoted to the study of phase qubits as candidates to quantum photon detectors. The next section is devoted to a thorough description of these qubits.

1.3.3 Flux qubit

The flux qubit or persistent current qubit [OMT+99, MOL+99], consists of a superconducting ring interrupted by three Josephson junctions, being one of the junctions smaller than the others by a factor α (this is schematically shown in Fig.1.5a&b). The flux qubit is threaded by an externally applied magnetic flux[23] Φ_{ext}, which eventually will control the state of our qubit. Neglecting the self-inductance of the loop[24], the Lagrangian of the circuit can be written as

$$L = \frac{1}{2}\sum_{i=1}^{3}\left(\frac{\Phi_0}{2\pi}\right)^2 C_i\dot{\varphi}_i^2 + E_{J_i}\cos\varphi_i, \tag{1.35}$$

where φ_i is the phase drop across the i-th junction. In principle it could seem that there are three independent variables, φ_1, φ_2 and φ_3, but we can eliminate one of them because the macroscopic wave function of the quantum circuit must be *single valued* around the closed loop. This imposes the phase

[23]The external magnetic flux can be generated by placing close to the qubit a small coil carrying that generates a magnetic field.

[24]For sufficiently large loops, the contribution of the self-inductance $\Phi^2/2L_{\text{loop}}$ might be important. This can be the case of the rf-SQUID's, but given the small size of the flux qubit we can safely neglect this term.

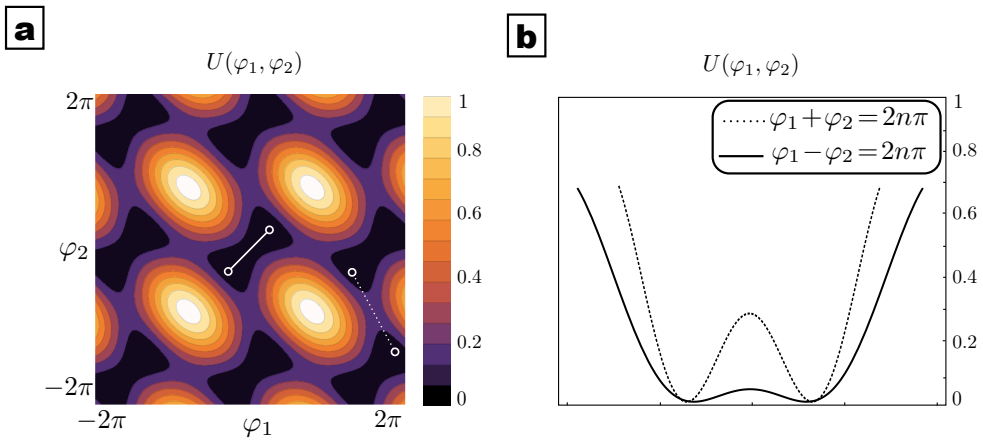

Figure 1.6: a) Potential landscape $U(\varphi_1, \varphi_2)$ of the flux qubit for $\Phi_{\text{ext}} = \Phi_0/2$. The black contours reveal a double-well structure. b) Cut along the curves $\varphi_1 = \pm\varphi_2$, showing the intra-cell and inter-cell double-well potentials.

quantization condition:

$$\varphi_1 - \varphi_2 + \varphi_3 + \frac{2\pi\Phi_{\text{ext}}}{\Phi_0} = 2\pi n, \quad n \in \mathbb{Z}. \tag{1.36}$$

Eq. (1.36) is also know as *fluxoid quantization*, and we will thoroughly discuss its derivation in Appendix 4. Under this condition, the Lagrangian (1.35) is reduced to:

$$L = \frac{C_J}{2}\left(\frac{\Phi_0}{2\pi}\right)^2\left[(\dot{\varphi}_1^2 + \dot{\varphi}_2^2) + \frac{\alpha}{2}(\dot{\varphi}_1 + \dot{\varphi}_2)^2\right] - U(\varphi_1, \varphi_2), \tag{1.37}$$

where $U(\varphi_1, \varphi_2)$ is the energy potential of the system, and is given by:

$$U(\varphi_1, \varphi_2) = -E_J\left[\cos\varphi_1 + \cos\varphi_2 + \alpha\cos\left(\frac{2\pi\Phi_{\text{ext}}}{\Phi_0} - (\varphi_2 - \varphi_1)\right)\right]. \tag{1.38}$$

For an externally applied magnetic flux $\Phi_{\text{ext}} = \Phi_0/2$, and $\alpha > 1/2$, the potential U shows a periodic double-well structure with two degenerate minima [25], as depicted in Fig.1.6a. The classical two degenerate minima correspond to clockwise and counterclockwise dc-persistent currents circulating in the superconducting ring. A particle subject to this potential could in principle tunnel either between intra-cell (white solid line) or inter-cell double wells (white dashed line), but it turns out that the inter-cell tunneling is strongly

[25] This point is usually called the symmetry point of the system, or "sweet spot".

suppressed due to its high tunnel barrier –this is clearly reflected in the companion from Fig.1.6b. This implies that the dynamics takes place along the orbit $\varphi_1 = \varphi_2$, and therefore U can be reduced to a one-dimensional potential, expressed in the basis $\varphi_\pm = (\varphi_2 \pm \varphi_1)/2$

$$U(\varphi_+, \varphi_-) = -E_J \left[2\cos\varphi_- + \alpha\cos\left(2\pi\Phi_{\text{ext}}/\Phi_0 - 2\varphi_-\right)\right], \tag{1.39}$$

which corresponds to the black solid line depicted in Fig.1.6b.

Finally, the quantum Hamiltonian describing the dynamics of the flux qubit can be written as:

$$H = \frac{\hat{Q}_-^2}{2C_J(1+\alpha)} - E_J[2\cos(\hat{\varphi}_-) + \alpha\cos(2\pi\Phi_{\text{ext}}/\Phi_0 - 2\hat{\varphi}_-)], \tag{1.40}$$

where $\hat{Q}_- = -i\hbar(2\pi/\Phi_0)\partial/\partial\hat{\varphi}_-$. We diagonalize (1.40) numerically, and get the first energy levels of the system, shown in Fig. 1.7a. In particular, we notice that for values of Φ_{ext}/Φ_0 close to symmetry point $1/2$, the two lowest energy levels approach each other, and the Hamiltonian (1.40) can be reduced to a two-level system:

$$H = \frac{1}{2}(\epsilon(\Phi_{\text{ext}})\sigma_z + \Delta\sigma_x) \tag{1.41}$$

Δ accounts for the tunneling between the two persistent current states $|\circlearrowright\rangle$ and $|\circlearrowleft\rangle$, $\epsilon(\Phi_{\text{ext}}) = 2I_p(\Phi_{\text{ext}} - \Phi_0/2)$ is the magnetic energy of the qubit due to the circulating current I_p, and σ_z, σ_x are the Pauli matrices expressed in the current state basis. Acting on (1.41) with the unitary rotation $U = e^{-i\theta\sigma_y}$, $\theta = \arctan(\Delta/\epsilon)$, we arrive at the diagonal form of the Hamiltonian:

$$H = \frac{\hbar\omega_q}{2}\sigma_z, \tag{1.42}$$

where $\omega_q = \sqrt{\Delta^2 + \epsilon(\Phi_{\text{ext}})^2}$, and where σ_z is the Pauli matrix now expressed in the eigenbasis $\{|g\rangle, |e\rangle\}$, given by

$$|g\rangle = \cos(\theta/2)|\circlearrowright\rangle + \sin(\theta/2)|\circlearrowleft\rangle, \quad |e\rangle = \sin(\theta/2)|\circlearrowright\rangle - \cos(\theta/2)|\circlearrowleft\rangle. \tag{1.43}$$

Far away the symmetry point, $\theta \to 0$ or π, and the ground and excited states of the qubit $|g\rangle$, $|e\rangle$, are essentially equal to the classical circulating currents $|\circlearrowright\rangle$ and $|\circlearrowleft\rangle$ –see the dashed lines of Fig. 1.7b. On the other hand, if we move towards the degeneracy point, where $\theta = \pi/2$, then the ground and excited states are in a quantum superposition of macroscopic circulating currents[26]. Given the large values that can be achieved for the circulating current I_p, the flux qubit can be regarded as a huge magnetic dipole with magnetic moment $m = I_p\, A$. This will in turn make possible the achievement of the strong and ultrastrong regimes of interaction between qubits and microwave photons.

[26]This happens because the degeneracy is lifted by the tunneling matrix element Δ between the two states.

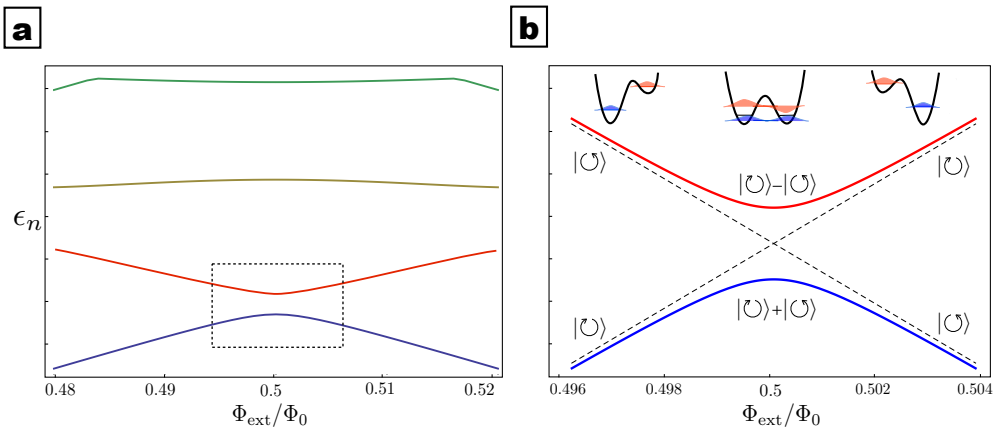

Figure 1.7: a) Energy levels of the 3-JJ flux qubit as a function of the external magnetic flux Φ_{ext}. From the picture it is clear how the system behaves as a two-level system in the region inside the dashed box. b) Closeup of the marked region, showing the classical solutions (dashed lines), the two-level anticrossing (blue and red solid lines), and the quantum states at different points of the hyperbolas.

1.3.4 Charge qubit & Transmon qubit

The transmon qubit is essentially a charge qubit operating in the regime where $E_J/E_C \gg 1$. In this regime, the transmon qubit is insensitive to the charge noise, and therefore its lifetime is orders of magnitudes larger than the charge qubit one. The underlying physics of both transmon and charge qubit is the same, so we will describe the original charge qubit, and then we will go through the novel features that the transmon qubit introduces.

Charge qubit

The charge qubit or Cooper-pair Box [BVJ+98], consists of a superconducting island connected to a superconducting reservoir of Cooper pairs by a tunnel junction, and capacitively coupled to a "gate voltage", which eventually will control the state of our charge qubit. A pictorial representation of the charge qubit is shown in Fig. 1.8a. Typically charge qubits operate in the charge regime, where $E_C \gg E_J$, so the quantum states describing the charge qubit are states with a well-defined number of Cooper pairs on the island.

We can readily compute the Lagrangian of the charge qubit as the energy

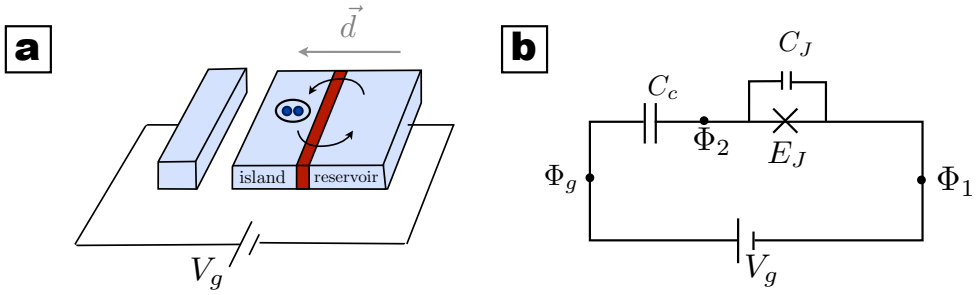

Figure 1.8: a) Schematic view of a voltage-biased Cooper pair box. Cooper pairs can tunnel from the reservoir to the island, to compensate the voltage V_g b) Equivalent circuit of the Cooper pair box represented in a).

difference of capacitive and inductive terms in the equivalent circuit model of Fig. 1.8b,

$$L = \frac{C_J}{2}(\dot{\Phi})^2 + \frac{C_c}{2}(\dot{\Phi} - V_g)^2 + E_J \cos\left(\frac{2\pi\Phi}{\Phi_0}\right), \tag{1.44}$$

where V_g is the voltage bias, and C_c is the coupling or gate capacitor. Notice that there is only one degree of freedom $\Phi = \Phi_2$, since one of the nodes is connected to the ground $\Phi_1 = 0$, and the other one is connected to the constant gate voltage, and therefore $\dot{\Phi}_g = V_g$. A Legendre transformation $H = Q\dot{\Phi} - L$, and canonical quantization rules brings us the charge qubit Hamiltonian:

$$H = \frac{2e^2}{2C_\Sigma}(\hat{n} - n_g)^2 - E_J \cos\left(\frac{2\pi\Phi}{\Phi_0}\right), \tag{1.45}$$

where $C_\Sigma = C_c + C_J$ is the total capacitance of the island, and the constant $n_g = C_c V_g/2e$ is the dimensionless gate charge, and works as a charge offset that changes the "zero charge" point. It is convenient to rewrite the above Hamiltonian in the Cooper-pair number basis $|n\rangle$, defined by $\hat{n}|n\rangle = n|n\rangle$:

$$H = 4E_C \sum_n (n - n_g)^2 |n\rangle\langle n| - \frac{E_J}{2}\sum_n |n+1\rangle\langle n| + |n\rangle\langle n+1|. \tag{1.46}$$

We introduced the charging energy $E_C = e^2/2C_\Sigma$, and the number state representation for the $\hat{\varphi}$ operator[27].

[27] The representation of $\hat{\varphi}$ in the $|n\rangle$ basis can be computed using the following relations:

$$e^{i\hat{\varphi}}|n\rangle = \frac{1}{2\pi}\int_0^{2\pi} d\varphi' e^{i\varphi'}|\varphi'\rangle\langle\varphi'|n\rangle = \frac{1}{2\pi}\int_0^{2\pi} d\varphi' e^{\varphi'} e^{in\varphi'} = \frac{1}{2\pi}\int_0^{2\pi} d\varphi' e^{i(n+1)\varphi'} = |n+1\rangle,$$

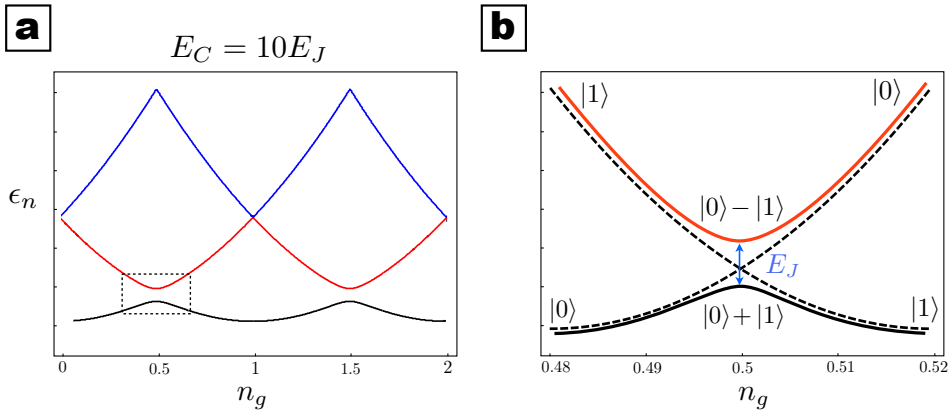

Figure 1.9: a) Energy spectrum of the Cooper pair box as a function of an offset charge. b)Closeup of the dashed box in a), showing the qubit structure of the Cooper pair box around $n_g = 1/2$. Dashed lines represent the classical solutions.

The energy spectrum associated to the Cooper pair box can be obtained numerically. The first three energy levels are represented in Fig. 1.9a. We observe that the energy spectrum is periodic as a function of the offset charge n_g[28]. Moreover, around the degeneracy point $n_g = 1/2$ the two lowest energy levels $|0\rangle$ and $|1\rangle$ are well-separated from higher energy levels[29], so (1.46) can be reduced to a two-level Hamiltonian

$$H = 2E_C(1 - 2n_g)\sigma_z - \frac{E_J}{2}\sigma_x, \tag{1.47}$$

with $\sigma_z = |1\rangle\langle 1| - |0\rangle\langle 0|$ and $\sigma_x = |0\rangle\langle 1| + |1\rangle\langle 0|$. As in the case of the flux qubit, we arrive at the diagonal form of (1.47) by rotating H an angle $\theta = -\arctan(E_J/E_{el})$. In doing so, we obtain

$$H = \frac{\hbar\omega_q}{2}\sigma_z \tag{1.48}$$

which is valid for all states $|n\rangle$, and therefore $e^{i\hat{\varphi}} = \sum_n |n+1\rangle\langle n|$. This finally leads to:

$$\cos\left(\frac{2\pi\Phi}{\Phi_0}\right) = \cos\hat{\varphi} = \frac{1}{2}(e^{i\hat{\varphi}} + e^{-i\hat{\varphi}}) = \frac{1}{2}\sum_n |n+1\rangle\langle n| + |n\rangle\langle n+1|$$

[28]This is because the integer part of the offset charge n_g can be cancelled out by transferring Cooper pairs from the reservoir to the superconducting island.

[29]At the degeneracy point $n_g = 1/2$, the adjacent charge states $|0\rangle$, $|1\rangle$ have the same charging energy E_C, and its energy difference is only due to the Josephson energy E_J. Higher states $|k\rangle$, $k \geq 2$, are separated from the previous states by an energy $k \times E_C$, so in the charge regime $E_C \gg E_J$ we can safely truncate the Hamiltonian to the charge states $|0\rangle$ and $|1\rangle$.

where $\omega_q = \sqrt{[E_C(1-2n_g)]^2 + E_J^2}$ is the energy of the charge qubit, and the Pauli matrix σ_z is expressed in the eigenbasis $\{|g\rangle, |e\rangle\}$:

$$|g\rangle = \cos(\theta/2)|0\rangle + \sin(\theta/2)|1\rangle, \quad |e\rangle = \sin(\theta/2)|0\rangle - \cos(\theta/2)|1\rangle, \quad (1.49)$$

being θ the mixing angle given by $\theta = \arctan[E_J/4E_C(1-2n_g)]$. For small values of E_J, and far away the degeneracy point, $\theta \to (0, \pi)$, and the solutions are similar to the classical ones (dashed lines in Fig. 1.9b), and the eigenstates are given by the classical charge states $|0\rangle$ and $|1\rangle$. By contrast, at the degeneracy point $E_{el} = 0$, $\theta = \pi/2$ and the eigenstates of (1.47) are quantum superpositions of the charge states $|0\rangle$ and $|1\rangle$, as shown in Fig. 1.9b.

In summary, the excess number of charges on the island defines the state of the charge qubit. This generates a charge imbalance with the reservoir, and thus a dipole moment $d = 2e \cdot |\hat{r}|$ between island and reservoir, where $|\hat{r}|$ is approximately the size of the Cooper pair box[30], typically around micrometers. If we compare this distance with the dipole moment in real atoms (nanometers), we realize that the charge qubit acts as a huge electrical dipole.

Charge qubit insensitive to charge noise: the transmon qubit

One of the major problems of the charge qubit is that it severely suffers from *charge noise*. In a charge qubit, the typical size of the superconducting island is very small on purpose, so that adding or subtracting a single Cooper pair significantly changes the energy of the system. This is a problem indeed, if we consider that the charge qubit is exposed to noisy sources, such as the presence of quasiparticles (electrons) in the environment. This effect of charge noise can be partially attenuated by preparing the charge qubit at the sweet spot, where the charge-noise contributions are of second order. While this has led to better qubit lifetimes, it does not represent a significant improvement in the qubit coherence, since still small perturbation can take the qubit out of the sweet spot. In 2007, J. Koch and co-workers came up with an elegant solution to the charge noise problem, presenting a charge-insensitive qubit which possesses a *sweet spot everywhere*: it is the so-called transmon qubit [KYG+07]. A transmon qubit is a charge qubit operating in the regime $E_J \gg E_C$. To reach this regime, rather than increasing the Josephson energy of the junction E_J , it is much more convenient to decrease E_C by increasing the junction capacitance C_J (using for instance the interdigitated finger-like structure depicted in Fig. 1.10). Under this condition, the Cooper pairs can tunnel

[30] Since the extra Cooper pair es completely delocalized in the condensate, we can safely say that the norm of the position operator $\hat{r}$ is approximately the size of the charge qubit.

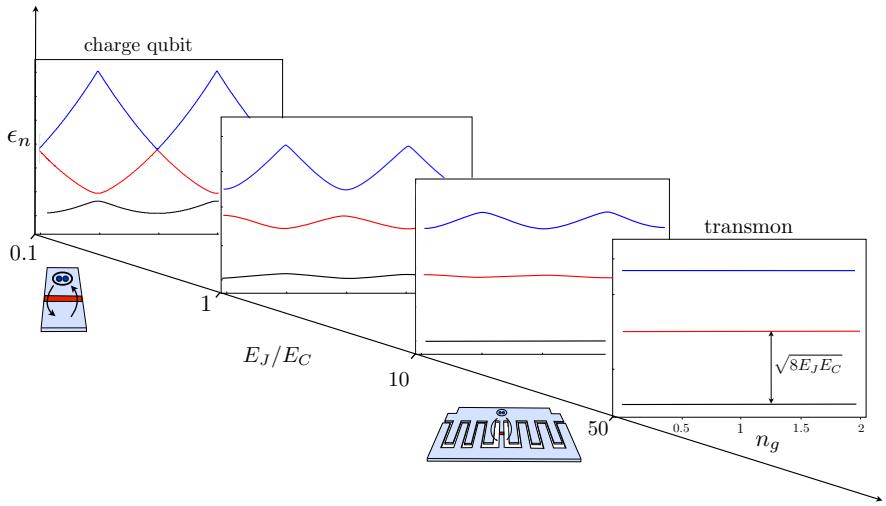

Figure 1.10: Energy spectrum of the first three energy levels for different values of E_J/E_C. In the charge regime $E_J/E_C \ll 1$, small changes in the charge offset n_g produces large variations in the energy levels ϵ, leading to decoherence. For the Cooper pair box operating in the transmon regime $E_J/E_C \gg 1$, the energy levels are practically flat, so they are insensitive to variations in n_g.

easily across the junction, increasing the coupling between charge states, and thus the level repulsion between energy levels. This effect has two important implications: firstly, the sweet spot spreads out on the energy band, thus reducing the noise sensitivity and increasing the coherence time of the qubit[31]. Secondly, the system starts losing anharmonicity, and resembles a harmonic oscillator, which in principle could be a drawback for quantum information purposes.

However, it turns out that while the noise decreases exponentially with the ratio E_J/E_C, the anharmonicity of the energy levels only decreases in a polynomial manner. It is thus possible to enhance the qubit coherence time (up to 100 microseconds) while preserving some degree of anharmonicity. As an example, for the transmon shown in Fig.1.10, the first three energy

[31] An alternative explanation for the reduced charge noise is the following: In the regime $E_J \gg E_C$, the number of charges on the island is no longer good a quantum number, and the ground and excited states of the transmon will be combination of multiple charge states. This makes the transmon less sensitive to changes in the charge, and therefore also to fluctuations in the charge induced by the environment.

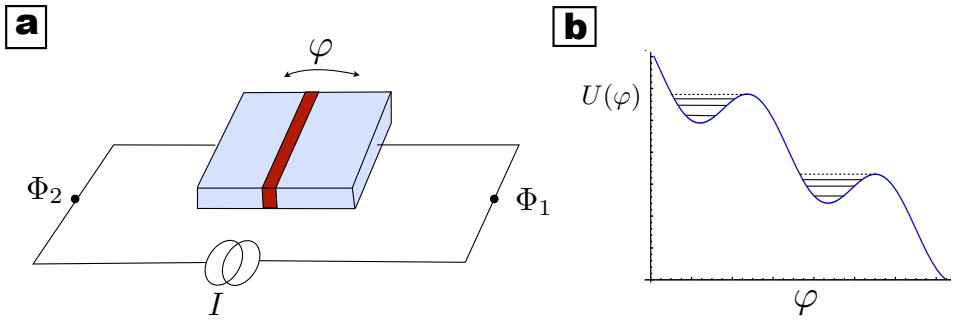

Figure 1.11: a) Schematic view of the current biased Josephson junction qubit b) Tilted washboard potential associated to the phase qubit. Due to the strong bias, the minima can only trap a few energy levels.

levels are fully flat with anharmonicity[32] $\alpha = 10\%$, which is sufficient for addressing individual qubit transitions. The transmon indeed works pretty well as a three-level ladder-system, feature that we will exploit in publications P5, P6 and P7 for controlling the state of propagating microwave photons by means of electromagnetically induced transparency.

1.3.5 Phase qubit

The phase qubit [MDC85] is a current biased Josephson junction operating in the very large regime $E_J \gg E_C$. A schematic view of the qubit is show in Fig. 1.11a. Due to the presence of the externally applied bias I, the usual periodic Josephson potential $U(\varphi)$ gets tilted, and the local minima in Fig. 1.11b can only trap a support a few metastable states. Particularly, for current bias I close to the critical current of the junction I_c, the potential is sufficiently anharmonic to observe a well-defined two level system with states $|0\rangle$ and $|1\rangle$ contained on it. Let us derive the phase qubit dynamics close to this working point:

The Kirchoff equation for the current applied to the the phase qubit gives us the Euler-Lagrange equation

$$C\ddot{\Phi} + I_c \sin(2\pi\Phi/\Phi_0) = I, \tag{1.50}$$

[32] We define the anharmonicity "α" as $\alpha = (E_{12} - E_{01})/E_{01}$, being $E_{ij} = E_j - E_i$.

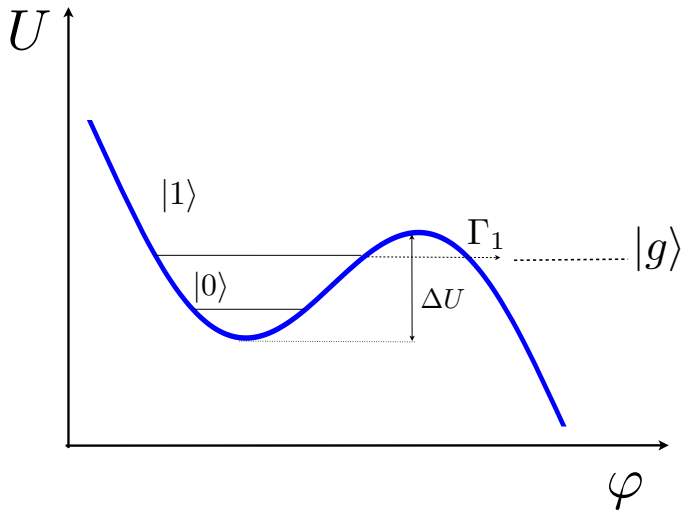

Figure 1.12: Current bias JJ potential around the local minimum $\varphi_{\min}$. For bias $I \simeq 0.95 I_c$, the minimum only traps a few energy levels, and the two lowest metastable levels $|0\rangle$ and $|1\rangle$ define the phase qubit. The state $|1\rangle$ can decay into a mesoscopically distinguishable state $|g\rangle$, that will serve as a photodetection method.

being $\Phi = \Phi_2 - \Phi_1$. The associated Lagrangian $L = T - U$ follows immediately from (1.50):

$$L = \frac{C_J}{2}\dot{\Phi}^2 - \frac{I_c \Phi_0}{2\pi}\left[1 - \cos\left(\frac{2\pi\Phi}{\Phi_0}\right)\right] + I\Phi. \tag{1.51}$$

Remembering that the Josephson energy $E_J = I_c\Phi_0/2\pi$, and the phase flux relation $\varphi = 2\pi\Phi/\Phi_0$, the potential $U(\Phi)$ can be rewritten as:

$$U(\varphi) = E_J\left[1 - \cos\varphi + \frac{I}{I_c}\varphi\right]. \tag{1.52}$$

Let us focus on the solutions around the minimum $\varphi_{\min} = \arcsin(I/I_c)$ of one of the wells of $U(\varphi)$. We expand the potential up to first anharmonic order, yielding:

$$U(\varphi) \simeq U_0 + E_J\sqrt{1 - \left(\frac{I}{I_c}\right)^2}\frac{(\delta\varphi)^2}{2} - E_J\frac{(\delta\varphi)^3}{6}. \tag{1.53}$$

Neglecting the phase-independent terms of the potential, we can finally find

the quantum Hamiltonian of the phase qubit:

$$H = -E_C \frac{\partial^2}{\partial(\delta\varphi)^2} + E_J \left[\sqrt{1 - \left(\frac{I}{I_c}\right)^2} \frac{(\delta\varphi)^2}{2} - \frac{(\delta\varphi)^3}{6} \right]. \tag{1.54}$$

From the above expression we can readily find the plasma frequency of the small phase oscillations around minimum

$$\omega_p = \frac{2\pi}{\Phi_0} \sqrt{\frac{E_J}{C_J}} \left[1 - (I/I_c)^2\right]^{1/4}, \tag{1.55}$$

and the height of the potential barrier:

$$\Delta U = \frac{2^{5/2}}{3} E_J \left[1 - (I/I_c)^2\right]^{3/2}. \tag{1.56}$$

It is possible to show that the number of metastable states N_s trapped in the potential is $N_s = \Delta U/\hbar\omega_p$, which in the typical conditions of an experiment is usually $N_s \approx 4$, with a significant anharmonicity $\alpha = 10\%$. Moreover, the tunneling rates out of the local well potential are given by the expression

$$\Gamma_N = \omega_p \frac{(432 N_s)^{n+1/2}}{\sqrt{2\pi} n!} E^{-35N_s/5}. \tag{1.57}$$

For typical values of actual experiments, the decay rate between consecutive levels fulfills $\Gamma_{n+1} = 1000\Gamma_n$, and together with the large anharmonicity, it is sufficient to keep the two lowest states $|0\rangle$ and $|1\rangle$. Truncating (1.54) to the effective two-dimensional Hilbert subspace spanned by the qubit states, we obtain the phase qubit Hamiltonian

$$H = -\frac{\hbar\omega_{01}(I)}{2}\sigma_z, \tag{1.58}$$

with $\omega_{01}(I) \approx \omega_p$. In contrast to the previous flux and transmon qubits, there is no direct external parameter that allows for a qubit state control. Instead, we can introduce a time-dependent modulation $\Delta I(t)$ in the current bias I. In doing so, the Hamiltonian (1.58) becomes

$$H = \begin{pmatrix} -\hbar\omega_{01} & 0 \\ 0 & \hbar\omega_{01} \end{pmatrix} + E_J \frac{\Delta I(t)}{I_c} \begin{pmatrix} \langle 0|\varphi|0\rangle & \langle 0|\varphi|1\rangle \\ \langle 1|\varphi|0\rangle & \langle 1|\varphi|1\rangle \end{pmatrix}. \tag{1.59}$$

For a modulation of the form $\Delta I(t) = I_x(t)\cos(\omega_{01}) + I_y(t)\sin(\omega_{01}) + I_z(t)$, where the amplitudes $I_{x,y,z}(t)$ are slow-varying functions of time, the Hamiltonian can be expressed in the interaction picture with respect to the free Hamiltonian as:

$$H = \sqrt{\frac{\hbar}{2C\omega_{01}}} \left(\frac{I_x(t)}{2}\sigma_x + \frac{I_y(t)}{2}\sigma_y \right) + \hbar \frac{\partial\omega_{01}}{\partial I} \frac{I_z(t)}{2}\sigma_z. \tag{1.60}$$

Thus, by controlling the amplitudes, it becomes possible to perform qubit rotations.

Apart from working as two-level system, the phase qubit can be used for photodetection tasks, a problem thoroughly studied in publication P8. The underlying physics behind this idea is the following: If we manage to tailor a decay rate Γ_1 of the first excited state $|1\rangle$ large enough, while keeping Γ_0 negligible[33], then a photon absorbed by the qubit will excite it to the $|1\rangle$ state, and it might decay to the state $|g\rangle$, generating a current that we can detect.

[33] In general, this is always true, because of the relation $\Gamma_1 = 1000\Gamma_0$.

1.4 Superconducting Quantum Interference Devices

In this section we show two Josephson-based devices of central importance in the development of this Thesis: the *Superconducting Quantum Interference Devices* or SQUID's [Cla89] . They are superconducting loops containing one or two Josephson junctions, and are famous for being very sensitive magnetometers, although they present much more applications: depending on their design, SQUID's can be used as quantum two-level systems, tunable Josephson-junctions, and very good *coupling elements*. In this Thesis we exploit the last property, and use SQUID's as *couplers* between other quantum circuits, such as superconducting resonators and qubits. Let us describe the two types of SQUID devices that we have considered: the rf-SQUID, and the dc-SQUID[34]:

1.4.1 rf-SQUID

The radio-frequency SQUID is a superconducting loop of inductance L interrupted by a Josephson junction, and threaded by a total magnetic flux Φ_{tot} as shown in Fig.1.13a[35]. It was firstly proposed to work as a superconducting qubit in Ref. [Leg80], using as qubit states the clockwise and counterclockwise supercurrents –for this reason, it is sometimes called one-junction flux qubit. The Lagrangian of the rf-SQUID follows from the equivalent circuit of Fig. 1.13b

$$L = \frac{C_J}{2}\dot{\Phi}^2 + E_J \cos\left(\frac{2\pi\Phi}{\Phi_0}\right) - \frac{1}{2L}(\Phi_{\text{ext}} - \Phi)^2. \tag{1.61}$$

As we did for the qubits, we study the SQUID dynamics around the minimum, given by $\partial_\Phi U = 0$:

$$\varphi = \frac{2\pi\Phi_{\text{ext}}}{\Phi_0} - \beta \sin\varphi. \tag{1.62}$$

$\beta = 2\pi L I_c/\Phi_0$ is the screening parameter, that accounts for the generated magnetic flux due to the circulating current in the loop. For $\Phi_{\text{ext}} \approx \Phi_0/2$, the potential $U(\Phi)$ shows a symmetric double-well around the minimum (Fig. 1.13c), that may trap only a few energy levels. For the energy levels of these states to form a qubit, it is necessary that the screening parameter $\beta > 1$, which implies that the size of the loop must be large as well. This is

[34]The prefix "rf" and "dc" for the SQUID's attend to their functioning nature: the rf-SQUID is based on ac-Josephson effect, while the dc-SQUID is based on the dc-Josephson effect.

[35]The total flux Φ_{tot} results from adding to the external flux Φ_{ext} the one generated by the circulating current LI_c.

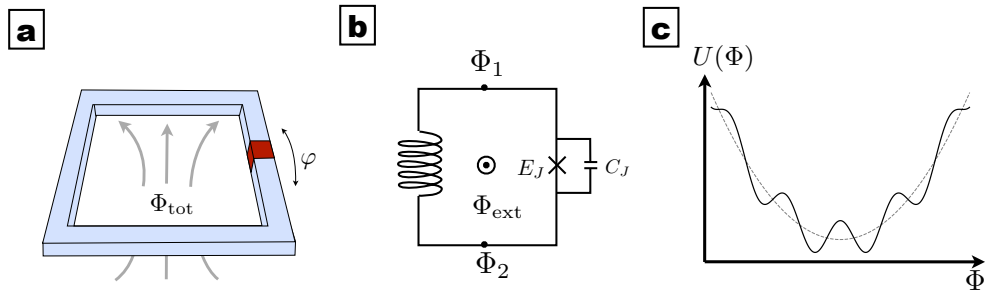

Figure 1.13: a) rf-SQUID: superconducting loop interrupted by one Josephson-Junction. b) Equivalent circuit of the setup shown in a). c) Potential energy of the SQUID (solid line), resulting from the periodic modulation of the harmonic potential (dashed gray).

a big inconvenient though, since large loops implies large sensitivity to flux noise, and therefore very low coherence times. For this reason, the rf-SQUID is hardly used as a quantum two-level system, and are usually fabricated in the limit of $\beta < 1$, where the contribution due to the self-inductance can be neglected.

As we mentioned at the beginning of this section, rf-SQUID's are very sensitive magnetometers and hence are widely used for the read-out of superconducting flux qubits [ref]. According to the fluxoid quantization condition in the SQUID loop

$$\varphi + 2\pi\frac{\Phi_{\rm ext}}{\Phi_0} = 2\pi n, \tag{1.63}$$

small variations of the external magnetic flux $\Phi_{\rm ext}$ will shift the value of the phase φ, dramatically changing the Josephson inductance L_J, given by eq.(1.30). Coupling the SQUID to a resonant circuit, this change in the Josephson inductance L_J can be detected.

Aside from these interesting applications, in publications P1, P2 and P3 we show that rf-SQUID's can act as powerful couplers between other quantum circuits. The idea relies on the fluxoid quantization, and *galvanic coupling*[36] between elements: we connect the SQUID in between the two circuits, and due to the fluxoid quantization we can get rid of the SQUID degree of freedom φ, ending up in a strongly coupled state between the two quantum circuits of interest.

[36]Galvanic coupling implies a direct contact between the superconducting leads of the circuits. Then, the dominant coupling mechanism is due to *kinetic inductance*, which boosts the circuit to the ultrastrong-coupling regime.

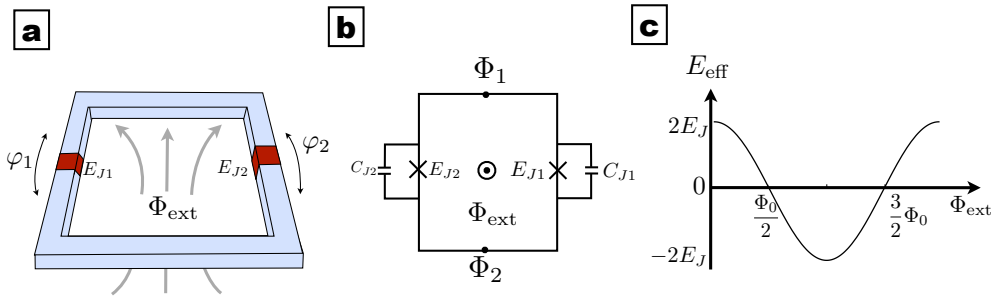

Figure 1.14: a) a) Pictorial view of the two-junction SQUID. b) Equivalent circuit in the limit $\beta \ll 1$. c) Tunable Josephson energy of the SQUID as a function of the external magnetic flux Φ_{ext}.

1.4.2 dc-SQUID

The dc-SQUID is a superconducting loop containing two Josephson junctions, like the one illustrated in Fig. 1.14a. We will work in the regime $\beta \ll 1$, so the self-inductance of the loop can be safely neglected. As we demonstrate below, the dc-SQUID is widely considered as a tunable Josephson junction, since the effective model that describes the SQUID yields a flux dependent Josephson energy E_J.

From the equivalent circuit of Fig. 1.14b, we derive the Lagrangian of the SQUID in the usual way,

$$L = \frac{C_{J1}}{2}(\dot{\Phi}_1)^2 + \frac{C_{J2}}{2}(\dot{\Phi}_2)^2 + E_{J1}\cos\left(\frac{2\pi\Phi_1}{\Phi_0}\right) + E_{J2}\cos\left(\frac{2\pi\Phi_2}{\Phi_0}\right). \tag{1.64}$$

For the sake of simplicity, we consider a symmetric[37] dc-SQUID, this is $E_{J1} = E_{J2} = E_J$ and $C_{J1} = C_{J2} = C_J$. It will be useful to write the above Lagrangian in the basis $\Phi_\pm = (\Phi_1 \pm \Phi_2)/2$:

$$L = \frac{2C_J}{2}(\dot{\Phi}_+^2 + \dot{\Phi}_-^2) + 2E_J\cos\left(\frac{2\pi\Phi_+}{\Phi_0}\right)\cos\left(\frac{2\pi\Phi_-}{\Phi_0}\right). \tag{1.65}$$

We can eliminate one of the SQUID variables by applying the fluxoid quantization condition:

$$\Phi_1 + \Phi_2 + \Phi_{\text{ext}} = n\Phi_0, \tag{1.66}$$

which in the new basis turns into $2\Phi_+ + \Phi_{\text{ext}} = n\Phi_0$. Inserting this expression into (1.65), we finally arrive at the reduced form of the dc-SQUID Lagrangian:

[37] In most practical cases it is not possible to build a perfectly symmetric SQUID, but this doesn't affect the functioning of the SQUID as a tunable device.

$$L = \frac{1}{2} C_{\text{eff}} \dot{\Phi}_-^2 + E_{\text{eff}} \cos\left(\frac{2\pi\Phi_-}{\Phi_0}\right), \tag{1.67}$$

where $C_{\text{eff}} = 2C_J$ and $E_{\text{eff}} = 2E_J \cos(\pi\Phi_{\text{ext}}/\Phi_0)$ are the effective Josephson capacitance and Josephson energy respectively. Equation (1.67) reveals that the SQUID works as a single junction with a tunable Josephson energy $E_{\text{eff}}(\Phi_{\text{ext}})$. In Fig.1.14c we represent its behavior; for values of the external flux equal to half flux quanta, the Josephson energy equals zero, whereas for integer values of Φ_0 the Josephson energy acquires a maximum value of $2E_J$. We can the use these quantum interference devices to dynamically tune the energy of a single junction. For instance, by replacing the Josephson junction in a transmon [KYG+07], or flux qubit [PFHM09] by a SQUID, it becomes possible to change the qubit energy gap just by varying the external magnetic flux through the SQUID. From the experimental viewpoint this is of great importance, since with a unique sample it is possible to prepare qubits with arbitrary energy gaps. Moreover, the use of SQUID's as tunable Josephson junctions allows for the correction of qubit parameters that might undergo imperfections during the fabrication process.

As we thoroughly discuss in chapter 3 (publications P1-P3), dc-SQUID's can also be used for coupling purposes. Along these lines, the dc-SQUID can act as a tunable coupler in two different ways, either detuning qubits from some the resonant frequency (by changing the qubit energy gap), or acting as a coupler between quantum circuits (since the interaction strength depends on E_{eff}).

2

Circuit Quantum Electrodynamics

So far we have seen how quantum electrical circuits can behave, under certain conditions, as microwave photons and "artificial" atoms. In this section we introduce the field of circuit QED[BHW+04, SG08, Zag11], which studies the light-matter interactions from a quantum mechanical perspective, using microware photons and Superconducting qubits to mimic visible light and atoms. But let us firstly recall the main features of light and matter interaction:

2.1 Light-matter interaction: cavity QED

The field of Quantum Optics [SZ97, WM08] studies the light-matter interaction at the most fundamental level, using the well established theory of *quantum electrodynamics (QED)* [Dir27]. Interactions in free space between light and individual photons are particularly weak. However, when atoms and molecules are placed in resonant cavities, light-matter interactions are dramatically enhanced in what is called the Purcell effect [PTP46]. This enhancement opened the door to a new field of research, called cavity-QED [HK89, WVEB06] , which results of particular interest for practical applications in quantum information [HR06, RBH01].

Consider a single mode of the electromagnetic field interacting with a two-level atom passing through it, as shown in Fig. 2.1a. The Hamiltonian of

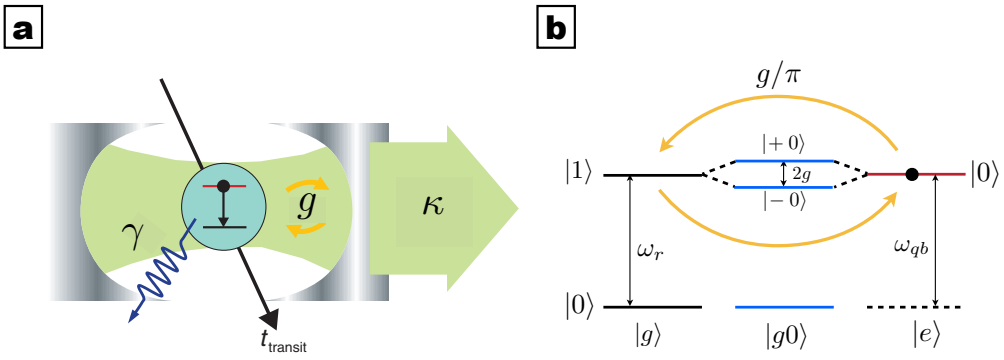

Figure 2.1: a) Schematic representation of a cavity QED system. A field mode interacts with an atom in a high-Q cavity. Due to the Purcell effect, they can strongly interact at a rate g. b) First energy levels of the free and coupled system, when the photon and the atom are on resonance.

this model can be written as:

$$H = \hbar\omega_0 \left(a^\dagger a + \frac{1}{2}\right) + \frac{\hbar\omega_q}{2}\sigma_z + \hbar g(a^\dagger + a)\sigma_x, \tag{2.1}$$

where is the first two terms account for the Hamiltonian of the bare systems, and the third term is the interaction Hamiltonian in the dipole approximation[1]. The coupling constant

$$g = \hbar^{-1} d \cdot E_{\text{rms}} \sin(kx) \tag{2.2}$$

represents the atom-field coupling at the position x of the atom, and in most cases we can be taken $g \ll \omega_0, \omega_q$, so we can apply the Rotating Wave Approximation (RWA)[2]. In doing so, we end up in the celebrated Jaynes-Cummings model [JC63], whose Hamiltonian reads

$$H = \hbar\omega_0 \left(a^\dagger a + \frac{1}{2}\right) + \frac{\hbar\omega_q}{2}\sigma_z + \hbar g(a^\dagger\sigma^- + a\sigma^+). \tag{2.3}$$

The Hamiltonian (2.3) is analytically solvable; its diagonalization yields the

[1]The dipole approximation assumes the size of the atom to be much smaller than the wavelength of the cavity mode, so the interaction Hamiltonian can be written as: $H_{\text{int}} = -\hat{d}\cdot\hat{E}$, where $\hat{d} = d_{\text{eg}}\sigma_x$ is the dipole moment of the atom, and

$$\hat{E}(x,t) = E_{\text{rms}}(a + a^\dagger)\sin kx,$$

the quantized electric field in the cavity, being $E_{\text{rms}} = \sqrt{\frac{\hbar\omega_0}{\epsilon_0 V}}$ the zero-point electric field.

[2]The RWA consists in neglecting the fast oscillating terms of (2.1), like $a^\dagger\sigma^+$.

following eigenenergies

$$E_{g,0} = \frac{\hbar\Delta}{2}, \tag{2.4}$$

$$E_{\pm,n} = (n+1)\hbar\omega_0 \pm \frac{\hbar}{2}\sqrt{4g^2(n+1)+\Delta^2}, \tag{2.5}$$

associated to the eigenstates $|g,0\rangle$, and

$$|+,n\rangle = \cos(\theta_n)|g,n+1\rangle + \sin(\theta_n)|e,n\rangle, \tag{2.6}$$

$$|-,n\rangle = -\sin(\theta_n)|g,n+1\rangle + \cos(\theta_n)|e,n\rangle. \tag{2.7}$$

In the previous equations, $\Delta = \omega_q - \omega_r$ is the atom-cavity detuning, and θ_n the mixing angle given by the expression

$$\theta_n = \frac{1}{2}\arctan\left(\frac{2g\sqrt{n}}{\Delta}\right). \tag{2.8}$$

If we consider the case where a single photon and the atom are on resonance ($\Delta = 0$), then the eigenstates of (2.3) are [3]

$$|\pm,0\rangle = \frac{1}{\sqrt{2}}(|g,1\rangle \pm |e,0\rangle), \tag{2.9}$$

with energy splitting $\Delta E_{\pm,0} = 2g$, also known as *vacuum Rabi splitting*. In Fig.2.1b we sketch the energy spectrum for the bare and dressed states, which can be interpreted as follows: if we prepare the initial state in $|e,0\rangle$ (atom excited and cavity with zero photons), the atom will coherently emit the photon into the cavity ($|g,1\rangle$) and absorb it back to the initial state ($|e,0\rangle$), with a frequency g/π. These oscillations are called *vacuum Rabi oscillations*, and last until the system dissipates the energy (in a time scale given by the atom and cavity losses, $\gamma + \kappa$).

In the so-called *strong coupling regime* where $g \gg \kappa, \gamma$, the vacuum Rabi splitting and many Rabi oscillations can be observed[4]. However, in order to achieve this regime, we need of large dipole moments d for the atoms and small cavity volumes for the confined photons, which is challenging in the usual cavity QED setups [RBH01]. By contrast, we have seen that this can be done with Josephson-based artificial atoms, and superconducting resonators, so we can consider the realization of cavity QED with superconducting circuits.

[3] This maximally entangled states $|\pm,n\rangle$ are excitations known as *polaritons*.

[4] Observing the strong coupling regime is a major breakthrough for various reasons: on the fundamental side, it unveils the quantum nature of light-matter interaction, and from a practical viewpoint, it would allow for the realization of quantum information processing.

2.2 Circuit QED: solid-state cavity QED

While the implementation of cavity QED systems was initially conceived with optical cavities and real atoms, its realization is not restricted to this setup. Whenever we can trap photons in a resonant cavity and make them interact with localized two-level systems, we will be implementing a cavity QED setup. This is the case of cavity QED with superconducting circuits, or *circuit QED*.

Circuit QED [BHW+04, Zag11] is the on-chip realization of cavity QED, where superconducting qubits interact with microwave photons trapped in superconducting resonators. It was the first solid-state system in achieving the strong coupling regime, and nowadays is a well established platform for studying microwave quantum optics, as it presents a number of advantages with respect to its optical counterpart, namely:

- In optical cavity QED, the system parameters such as the the frequency ω_q of the atoms or the coupling strength g, are characterized by "God-given" constants. On the other hand, in circuit QED these parameters can be design at will: in Josephson-based atoms the qubit frequencies can be tailored by changing the Josephson energy (using for instance dc-SQUID's), and the coupling constant depends on external capacitors, inductors, and the geometry design.

- In cavity QED, the interaction is limited by the time that the atom passes in the cavity (transit time), since the atoms are flying through the resonator[5]. Conversely, in circuit QED the transit time can be considered infinite, since the "atoms" are built in a fixed position in the superconducting resonator. This makes the coupling constant throughout the interaction time. Moreover, since we can choose the position of the qubit in the resonator, we can maximize or minimize the coupling to a particular field mode. Additionally, it is possible to put many qubits in the same resonator, and study their effective interaction through the photonic mode, and entanglement between qubits.

- The one dimensional nature of circuit QED inherently implies stronger interactions, since the coupling g varies with the inverse of volume of the photonic mode. Thus, when bounded to a 1D cavity rather than a 3D one, it is possible to reach smaller effective volumes, and therefore larger couplings. If we combine this idea with a proper resonator

[5] Additionally, since the atom moves across the cavity, the coupling with the field might not be constant throughout the transit time t_{transit}.

geometry, it becomes possible to boost the light-matter interaction the *ultrastrong regime*, which is unachievable in any other quantum optical system.

2.2.1 Strong coupling in circuit QED

In this section we describe some outstanding circuit QED implementations that have led to the strong and ultrastrong coupling regime of interaction. Due to the different regimes of superconducting qubits (like the charge and flux regime), we can couple them to the microwave photons in two different ways. For charge-based qubits, like the charge and the transmon qubits, we will couple them to the photon mode via *capacitive coupling*. This means, by an electric dipole interaction of the qubit with the electric field. On the other hand, for a flux qubit, we will couple it to the field via *inductive coupling*. That is, by a magnetic dipole interaction of the qubit with the magnetic field.

2.2.2 Charge qubit in a transmission line resonator: capacitive coupling

Let us consider the system depicted in Fig.2.2, where a charge qubit is fabricated inside a full-wave length transmission line resonator. In particular, it is placed between the center conductor and a ground plane, in a position where the electric field of the resonator is maximum. Since the charge qubit behaves as a large electric dipole d, we expect a strong dipole interaction with the electric field.

The typical size of the qubit is much smaller than the relevant wavelengths of the transmission line[6], so we can describe the circuit QED system with the equivalent model depicted at the bottom of Fig.2.2: a split Cooper-pair box capacitively coupled[7] to a transmission line resonator, via the coupling capacitor C_g[BHW+04, WSB+04]. We derive the full Hamiltonian from the equivalent circuit in the usual way, yielding

$$H = \hbar\omega_r \left(a^\dagger a + \frac{1}{2}\right) + 4E_C(1 - 2\hat{n}_g)\sigma_z - \frac{E_{\text{eff}}}{2}\sigma_x, \tag{2.10}$$

where ω_r is the frequency of the transmission line resonator, and $E_{\text{eff}} =$

[6]The size of the charge qubit is $\Delta x = 10^{-6}$m, or 10^4 times smaller than the relevant microwaves.

[7]The center conductor and the charge qubit define an effective capacitance $C_g = \epsilon_0 A/z$, where A is the area of the transmon, and z the distance between the conductor and the qubit.

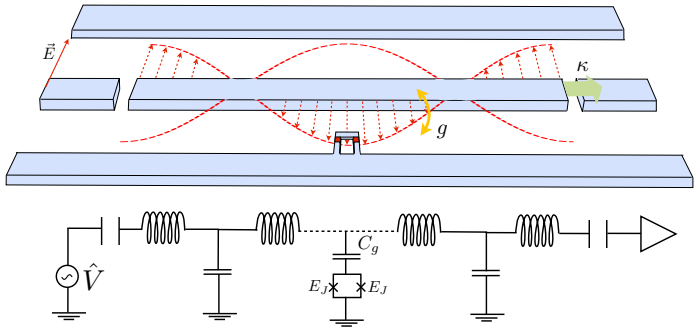

Figure 2.2: Circuit QED implementation with a transmon qubit, capacitively coupled to a transmission line resonator. We place the transmon close to the center conductor, in an antinode of the electric field. The equivalent circuit of this layout is displayed below.

$2E_J\cos(\pi\Phi_{\text{ext}})$ the effective Josephson energy. The above expression resembles pretty much to the bare Hamiltonians of the transmission line resonator (1.22) and the charge qubit (1.47). There is however a subtle difference: the dimensionless gate charge, defined as $\hat{n}_g = C_g\hat{V}_g/2e$, now possesses two contributions due to the voltage in the transmission line

$$\hat{V}_g = V_g^{\text{dc}} + V_{\text{rms}}(a + a^\dagger), \tag{2.11}$$

i.e, a classical dc-bias V_g^{dc} that adds up to the qubit Hamiltonian, and a zero-point voltage V_{rms} due to the quantum field in the resonator. Inserting this expression in (2.10), we finally end up with the Hamiltonian of the interacting system

$$H = \hbar\omega_r\left(a^\dagger a + \frac{1}{2}\right) + E_C(1 - 2n_g^{\text{dc}})\sigma_z - \frac{E_J}{2}\sigma_x + \hbar g(a + a^\dagger)\sigma_z, \tag{2.12}$$

or in the qubit eigenbasis:

$$H = \hbar\omega_r\left(a^\dagger a + \frac{1}{2}\right) + \frac{\hbar\omega_q}{2}\sigma_z + \hbar g(a + a^\dagger)(\sin\theta\sigma_x - \cos\theta\sigma_z), \tag{2.13}$$

where ω_q and θ are the qubit frequency and the mixing angle, and whose expressions were derived in the charge qubit section. Finally, the coupling constant g is given by the expression

$$\hbar g = e\frac{C_g}{C_\Sigma}V_{\text{rms}}. \tag{2.14}$$

Applying the RWA, we can neglect the fast oscillating terms[8] in (2.13), obtaining the Hamiltonian that describes the qubit-resonator interaction

$$H = \hbar\omega_r \left(a^\dagger a + \frac{1}{2}\right) + \frac{\hbar\omega_q}{2}\sigma_z + \hbar g \sin\theta (a^\dagger \sigma^- + a\sigma^+). \tag{2.15}$$

When the qubit is at the degeneracy point, $\sin\theta = 1$ and the coupling g with the field is maximum[9]. In particular, using realistic experimental values, $V_{\rm rms} \simeq 1\mu V$, and the ratio $C_g/C_\Sigma \sim 0.1$, so the coupling (2.14) $g \sim 100$MHz, value that is much greater than the typical cavity and qubit decay rates $\kappa, \gamma \sim$ 5MHz. It is sometimes useful to give the coupling constant relative to the qubit or photon frequencies, $g/\omega_r \sim 2 - 5 \cdot 10^{-3}$. However, the coupling cannot be much larger than that, since it is upper-bounded by the ratio $C_g/C_\Sigma \leq 1$ [DGS07]. In order to reach greater couplings that can go beyond the strong coupling regime, we should look for other proposals.

2.2.3 Flux qubit in a transmission line resonator: inductive coupling

Another circuit QED implementation that achieves the strong coupling regime is the one shown in Fig. 2.3. A superconducting flux qubit inductively coupled to a transmission line resonator [LWH+07], via magnetic dipole interaction $H_{\rm int} = -\hat{\mu}\cdot\hat{B}$. The large magnetic moment μ of the qubit and the large zero-point magnetic field of the resonator provides the strong coupling $B_{\rm rms}$ provides the necessary ingredients for the strong coupling regime.

From the equivalent circuit of Fig.(2.3) we readily derive the Hamiltonian of the circuit QED system

$$H = \hbar\omega_r (a^\dagger a + 1/2) + \frac{1}{2}(\hat{\epsilon}\sigma_z + \Delta\sigma_x), \tag{2.16}$$

where $\hat{\epsilon} = 2I_p(\hat{\Phi}_{\rm ext} - \Phi/2)$. The above expression resembles again the bare Hamiltonians of the resonator and the flux qubit. The difference lies now in the total magnetic flux threading the loop, which is given by $\hat{\Phi}_{\rm ext} = \Phi^{\rm dc}_{\rm ext} + \delta\hat{\Phi}$, i.e a dc-external control bias $\Phi^{\rm dc}_{\rm ext}$, and a small modulation $\delta\hat{\Phi}$ due to quantum fluctuations of the resonator field

$$\delta\hat{\Phi} = M\cdot\hat{I}_r = M\sqrt{\frac{\hbar\omega_r}{2L_r}}(a + a^\dagger), \tag{2.17}$$

[8] As in the cavity QED case, we neglect the counterrotating terms of the Hamiltonian, $a^\dagger\sigma^+ e^{i(\omega_r+\omega_q)} + H.c$. Additionally, we can neglect the fast oscillating terms $a^\dagger\sigma_z e^{i\omega_r} + H.c$

[9] On the other hand, notice that when the qubit is off resonance $\sin\theta \to 0$, and then the coupling term disappears. That means that we can protect the qubit from decoherence by far detuning the qubit from the cavity [PTP46].

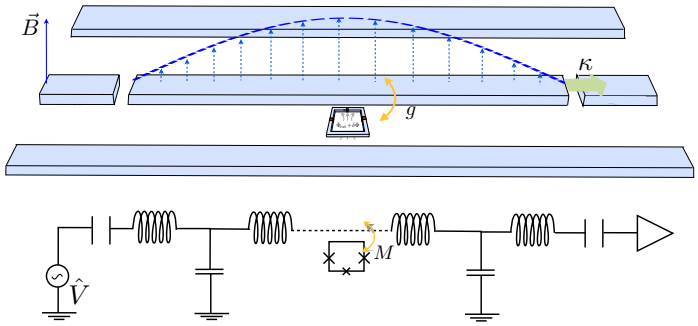

Figure 2.3: Circuit QED realization with a flux qubit inductively coupled to a transmission line resonator, and its equivalent circuit.

where M is the mutual inductance coefficient between the flux qubit and the resonator. Using this expression we can rewrite the Hamiltonian (2.16) as

$$H = \hbar\omega_r \left(a^\dagger a + \frac{1}{2}\right) + \frac{1}{2}(\epsilon\sigma_z + \Delta\sigma_x) + \hbar g(a + a^\dagger)\sigma_z, \tag{2.18}$$

with coupling constant

$$\hbar g = M I_p I_{\text{rms}}. \tag{2.19}$$

Provided that $g \ll \omega_q, \omega_r$, we can invoke the RWA, and the above Hamiltonian can be written in the qubit eigenbasis as

$$H = \hbar\omega_r \left(a^\dagger a + \frac{1}{2}\right) + \frac{\hbar\omega_q}{2}\sigma_z + \hbar g \sin\theta(a^\dagger\sigma^- + a\sigma^+), \tag{2.20}$$

with the mixing angle given by $\theta = \arctan(\Delta/\epsilon)$. Working at the degeneracy point, qubit and resonator are on resonance and the coupling between is maximum. A rough estimation of the coupling using realistic experimental values[10], yields a coupling constant $g \simeq 10 - 100$MHz, of equivalently $g/\omega_r \sim 1 - 5 \cdot 10^{-3}$, in any case much greater than the qubit and resonator decay rates $\kappa, \gamma \sim 1MHz$. The coupled system is then able to undergo many vacuum Rabi oscillations before the system decays.

The coupling g can be enhanced by increasing the qubit area A, since the mutual inductance M depends on it. However, as we discussed for the rf-SQUID, this fact limits the coherence time of the qubit and thus the time operation for developing quantum gates.

[10]The zero-point current in a transmission line resonator is $I_{\text{rms}} \sim 40$nA, the critical current of a flux qubit $I_p = 400\text{n}A$, and the mutual inductance can be estimated by for a square loop as $M = A\mu_0/\pi\delta$, where A is the qubit area, and δ the distance between ground plate and center conductor.

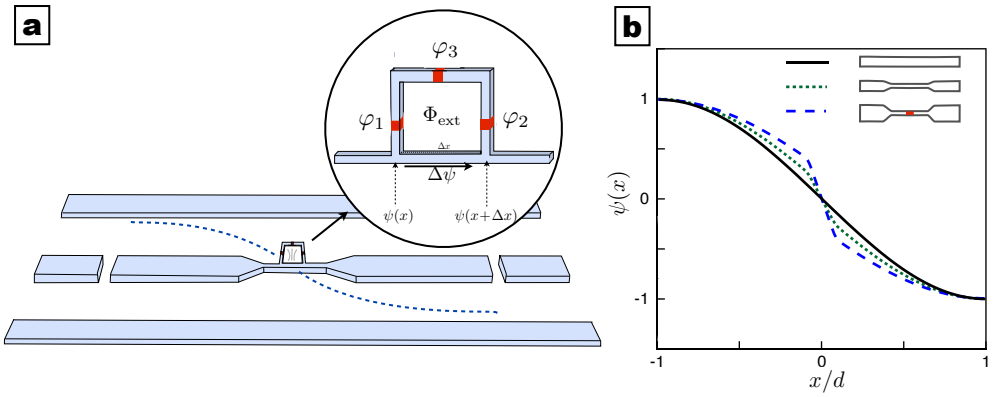

Figure 2.4: a) Schematic view of the ultrastrong coupling setup. A flux qubit is galvanically connected to the center conductor of an inhomogeneous transmission line resonator, and coupled to the field via kinetic inductance. b) Spatial dependence of the photon mode eigenfunction for different degrees of constrictions.

2.3 Ultrastrong coupling regime

In the previous section we have demonstrated that capacitive and inductively coupled circuit QED setups can reach the strong-coupling regim, by taking advantage of the large dipole moments of the charge and flux qubits, and the high vacuum fluctuations in the transmission line resonator. By contrast, both systems are bounded to that regime due to the nature of the coupling C_g and M. In this section we introduce a new setup that can bring the light-matter interaction to the ultrastrong regime [CBC05, GAH+09, BGA+09], where $g \simeq \omega_q, \omega_r$, and the ubiquitous RWA, and the celebrated Jaynes-Cummings model no longer apply.

The setup we consider is depicted in Fig. 2.4a. A superconducting flux qubit is *directly connected* to the central line of a transmission line resonator [BGA+09, AAAN+08]. By changing the width of the center conductor in the coupling region, it becomes possible to locally increase the inductance of the resonator[11], and hence the coupling with the qubit. We compute the Hamiltonian of this circuit QED setup using the standard approach[12], obtaining

[11]The total inductance of the central line $L = L_g + L_k$ has an additional contribution, the so-called kinetic inductance term, that can be dominant in the constriction.

[12]For the sake of simplicity, we only write the dominant contributions to the Hamiltonian, given by the Josephson energies. This is well justified, since in the flux regime $E_J \gg E_C$.

$$H = \hbar\omega_r \left(a^\dagger a + \frac{1}{2}\right) - \sum_{n=1}^{3} E_{J_n} \cos\varphi_n, \tag{2.21}$$

where E_{J_n} and φ_n are the energy and the phase drop across the n-th junction. From now on, we will assume the standard flux qubit configuration for the Josephson junctions[13]. The fluxoid quantization on the closed loop imposes the following condition,

$$\varphi_1 + \varphi_2 - \varphi_3 + \Delta\hat{\psi} = 2\pi\frac{\Phi_{\text{ext}}}{\Phi_0}, \tag{2.22}$$

where we have taken into account the phase slip $\Delta\hat{\psi}$ in the shared branch due to the photon eigenmode in the resonator[14]. Using this expression one can get rid of one of the Junctions variables, so the total Hamiltonian reads

$$\begin{aligned} H &= \hbar\omega_r \left(a^\dagger a + \frac{1}{2}\right) \\ &- E_J \left[\cos\varphi_1 + \cos\varphi_1 + \alpha\cos\left(\varphi_1 + \varphi_2 + \Delta\hat{\psi} - \frac{2\pi\Phi_{\text{ext}}}{\Phi_0}\right)\right]. \end{aligned} \tag{2.23}$$

For most practical cases $|\Delta\hat{\psi}| \ll 1$, so we can expand the above Hamiltonian up to first order in $\Delta\hat{\psi}$, yielding

$$H = H_r + H_{qb} + H_{\text{int}}, \tag{2.24}$$

being H_r and H_{qb} the usual resonator and flux qubit Hamiltonians, and the interaction term H_{int} is given by

$$H_{\text{int}} = \alpha E_J \Delta\hat{\psi} \sin\left(\varphi_1 + \varphi_2 - 2\pi\frac{\Phi_{\text{ext}}}{\Phi_0}\right), \tag{2.25}$$

where the field operator $\Delta\hat{\psi} = |\Delta\psi|(a + a^\dagger)$, and the qubit operator can be projected onto the qubit eigenbasis $\{|g\rangle, |e\rangle\}$:

$$\sum_{k,k'=e,g} |k\rangle\langle k| \sin\left(\varphi_1 + \varphi_2 - 2\pi\frac{\Phi_{\text{ext}}}{\Phi_0}\right) |k'\rangle\langle k'|. \tag{2.26}$$

At the sweet spot $\Phi_{\text{ext}} = \Phi_0/2$, this operator is antisymmetric, and only couples states with different parity. This finally yields the following interaction Hamiltonian

$$H_{\text{int}} = \hbar g (a + a^\dagger)\sigma_x, \tag{2.27}$$

with a coupling constant g given by

$$\hbar g = \alpha E_J |\Delta\psi| \langle g| \sin(\varphi_1 + \varphi_2) |e\rangle. \tag{2.28}$$

[13] For a typical flux qubit $E_{J_1} = E_{J_2} = E_J$, and $E_{J_3} = \alpha E_J$, where $E_J \sim 250$GHz, and the relative size of the junctions $\alpha \sim 0.8$.

[14] Specifically, the photon generates a flux $\Delta\Phi$ across the common branch, that is proportional to the phase slip $\Delta\psi$ according to the Josephson relation $\Delta\dot{\Phi} = (\hbar/2e)\Delta\dot{\psi}$.

Estimation of the coupling strength

From the above expression we notice that the coupling g mainly depends on the value of the Josephson energy E_J, and the phase slip $|\Delta\psi|$ of the resonator. In particular, for a flux qubit sharing a branch of length Δx with the resonator, the phase slip can be written as:

$$|\Delta\psi| = |\psi(x_0 + \Delta x) - \psi(x_0)| = |\partial_x \psi(x)|_{x_0} \Delta x, \tag{2.29}$$

where $\partial_x\psi$ is the slope of the photon mode eigenfunction at the qubit position $x_0 = 0$ in the resonator[15]. In Fig. 2.4b we show the profiles of $\psi(x)$ for different constrictions in the central line. We have considered three cases: a homogeneous resonator (solid line), an inhomogeneous resonator (dotted line), and finally an inhomogeneous resonator interrupted by a Josephson junction[16] (dashed line). We observe that as long as we make the central line narrower, the slope of the photon mode increases and hence the phase slip. In particular, for the three proposed geometries we have numerically obtained the following phase slips: $|\Delta\psi| = 2 \cdot (10^{-4}, 10^{-3}, 10^{-2})\mu\text{m}^{-1}$. Using typical junction parameters for the flux qubit[17], and substituting everything in (2.28), we obtain the corresponding coupling constants: $g = (50\text{ MHz}, 500\text{ MHz}, 5\text{ GHz})$. While the galvanic coupling to a homogeneous resonator doesn't improve the previous circuit QED setups, the direct coupling to resonators with constrictions in the line can boost the coupling to the ultrastrong regime. Moreover, ratios $g/\omega_r \sim 12\%$ has been already measured [NDH+10, FLM+10], opening the door to novel and interesting phenomena, such as the observation of the superradiant phase in cavity QED [NC10a], the degeneracy of the vacuum state [NC10b] and qubit protection [NC11], or the generation of photons from the vacuum [RLSH12, SRDS+13, RSH13].

This Thesis is extensively focused on this fascinating regime. In particular, in publications P1, P2 , P3 and P4 we will be interested in the development of an ultrastrong switchable interaction, either between light-and matter, or between photons themselves. This would allow for a countless number of applications, ranging from applications in quantum optics [RVDS+10], quantum computing [RBW+12], or relativistic quantum information [SDRGRL11, SGRSL10, SPdRMM12].

[15] A major advantage of this setup is that the coupling constant g scales with the length of the shared branch Δx, and not with the qubit area A as in the case of mutual inductance coupling. This allows for larger couplings without increasing the qubit sensitivity to flux noise.

[16] Adding a large Josephson junction to the central line can enhance even more the inductance of the wire:.In the considered case, the total inductance is given by $L = L_J + L_k + L_g$, where the Josephson inductance in the line $L_J \gg L_k, L_g$ is the dominant contribution.

[17] $\alpha E_J = 200$GHz, $\Delta x = 5\mu$m, and matrix element $\langle g|\sin 2\varphi_+|e\rangle \sim 0.78$.

2.4 Circuit QED in 1D open space

2.4.1 Propagating microwave photons

Aside from the remarkable achievements in intracavity light-matter coupling, circuit QED has started to focus on the strong interaction between propagating microwave photons and superconducting qubits, giving rise to a new area of research: *propagating quantum microwave technologies* [AAZ+10, HWJ+11, HPL+12, SF05b, SF05a]. This promising field aims to generate, control, and detect propagating microwave photons for the development of scalable quantum information processing and communications with quantum microwaves, in the same spirit of all-optical QIP. Along these lines we put our attention in the second part of this Thesis. In particular, we demonstrate a high degree of control of propagating photons in publications P5, P6 and P7. Additionally, in publication P8 we exploit this large control over the photons to propose a single-shot single-photon detector in the microwave regime.

In this section we present the mathematical tools needed for the study of light-matter interaction in 1D open space [Pur01], which we will eventually use for the control and manipulation of individual photons: this is the so-called *scattering theory*. We will introduce the so-called "input-output" theory [GZ91]. This formalism allows us to express the outgoing scattered fields as a function of the incoming fields and some interaction with a localized quantum system, which can be a harmonic oscillator, atoms in cavities, etc. In this Thesis, the localized systems will be the transmon and the phase qubits. We will see that their dynamics cannot be fully determined by analytical means, so we we will derive a master equation, which is an approximate equation for the qubit dynamics. With this toolkit, we will be able to describe the interaction of propagating quantum microwaves with the artificial atoms.

2.4.2 Scattering theory: Input-Output formalism

Let us consider a two-level system interacting with an electromagnetic field environment in an open transmission line. The total Hamiltonian $H = H_{\text{sys}} + H_{\text{res}} + H_{\text{int}}$ can be written as

$$H = \hbar\frac{\omega_q}{2}\sigma_z + \int_{-\infty}^{\infty}\hbar\omega a_\omega^\dagger a_\omega \mathrm{d}\omega + \int_{-\infty}^{\infty}\hbar g(\omega)\sigma_x(a_\omega + a_\omega^\dagger)\mathrm{d}\omega, \tag{2.30}$$

where the field operators a_ω obey the bosonic canonical commutation relations $[a_\omega, a_{\omega'}^\dagger] = \delta(\omega - \omega')$ and $[a_\omega, a_{\omega'}] = 0$. We are interested in obtaining

the equations of motion of the system. To this end, it is convenient to work in the the Heisenberg picture, where the time evolution of any operator $\hat{O}$ is given by

$$\frac{\mathrm{d}\hat{O}}{\mathrm{d}t} = \frac{i}{\hbar}[H, \hat{O}]. \tag{2.31}$$

We will be working in the weak and strong coupling regimes of interaction in an open line[18], so we can simplify the Hamiltonian (2.30) by performing a rotating wave approximation:

$$H = \hbar\frac{\omega_q}{2}\sigma_z + \int_{-\infty}^{\infty}\hbar\omega a_\omega^\dagger a_\omega \mathrm{d}\omega + \int_{-\infty}^{\infty}\hbar g(\omega)(\sigma^+ a_\omega + \sigma^- a_\omega^\dagger)\mathrm{d}\omega. \tag{2.32}$$

Let us focus on the Heisenberg equations for the field operators. Using the bosonic commutation relations for the field, we can compute the equations of motion for a_ω

$$\frac{\mathrm{d}a_\omega}{dt} = -i\omega a_\omega - ig(\omega)\sigma^-, \tag{2.33}$$

and the corresponding Hermitian conjugate equations for $a_\omega^\dagger$.

1. Input field

The field equation (2.33) can be formally integrated as follows

$$a_\omega(t) = e^{-i\omega(t-t_0)}a_\omega(t_0) - ig(\omega)\int_{t_0}^{t} e^{-i\omega(t-\tau)}\sigma^-(\tau)d\tau, \tag{2.34}$$

where $t_0 < t$ is an initial time, and is taken to be the remote past. For reasons that will be clear later, it is convenient to integrate the above expression over the frequency range. In doing so, we obtain that

$$\frac{1}{\sqrt{2\pi}}\int_{-\infty}^{\infty} a_\omega(t)\mathrm{d}\omega = b_{\mathrm{in}}(t) - \frac{i}{\sqrt{2\pi}}\int_{-\infty}^{\infty}\int_{t_0}^{t} g(\omega)e^{-i\omega(t-\tau)}\sigma^-(\tau)\mathrm{d}\tau\mathrm{d}\omega, \tag{2.35}$$

where we have defined the "input" field $b_{\mathrm{in}}(t)$ as

$$b_{\mathrm{in}}(t) = \frac{1}{\sqrt{2\pi}}\int_{-\infty}^{\infty} e^{-i\omega(t-t_0)}a_\omega(t_0)\mathrm{d}\omega. \tag{2.36}$$

Since we are in the weak or strong coupling regimes, we can perform the first Markov approximation, which assumes that the coupling with environment

[18] This is well justified, since the spin-boson Hamiltonian (2.30) in the ultrastrong regime is practically intractable, and hardly unachievable in an open quantum system.

is approximately constant, $g(\omega) = \sqrt{\gamma/2\pi}$. In doing this and after some algebra[19], one can rewrite eq. (2.35) as

$$\frac{1}{\sqrt{2\pi}}\int_{-\infty}^{\infty} a_\omega(t)\mathrm{d}\omega = b_{\mathrm{in}}(t) - \frac{\sqrt{\gamma}}{2}\sigma^-(t). \tag{2.37}$$

2. Output field

The solution to the field equation (2.33) can be also specified in terms of a final condition $t_1 > t$, which can be assumed to be in the remote future:

$$a_\omega(t) = e^{-i\omega(t-t_1)}a_\omega(t_1) + ig(\omega)\int_t^{t_1} e^{-i\omega(t-\tau)}\sigma^-(\tau)d\tau, \tag{2.38}$$

where the plus sign in the second term arises from the presence of the time t in the lower limit of integration. Proceeding in the same way as before, we integrate over frequencies, obtaining

$$\frac{1}{\sqrt{2\pi}}\int_{-\infty}^{\infty} a_\omega(t)\mathrm{d}\omega = b_{\mathrm{out}}(t) + \frac{\sqrt{\gamma}}{2}\sigma^-(t), \tag{2.39}$$

where the solution is now given in terms of the "output" field

$$b_{\mathrm{out}}(t) = \frac{1}{2\pi}\int_{-\infty}^{\infty} e^{-i\omega(t-t_1)}a_\omega(t_1)\mathrm{d}\omega. \tag{2.40}$$

We finally combine eqs. (2.37) and (2.39) to arrive at the *input-output* relation

$$b_{\mathrm{out}}(t) = b_{\mathrm{in}}(t) - \sqrt{\gamma}\,\sigma^-(t). \tag{2.41}$$

This important equation tells us that we can completely determine the state of any output field after the interaction with the atom, by knowing the input state and the dynamics of the atom operator $\sigma^-(t)$. To find this dynamics, we have to solve the equations of motion for the qubit operators $\sigma^{\pm}$, σ_z, given by its Heisenberg equations. Using the commutation relations for the

[19] For the ease of understanding, the second term in (2.35) can be written as

$$-\frac{\sqrt{\gamma}}{2\pi}\int_{-\infty}^{\infty}\sigma^-(\tau)\int_{t_0}^{t} e^{-i\omega(t-\tau)}\mathrm{d}\tau\mathrm{d}\omega = -\gamma\int_{t_0}^{t}\sigma^-(\tau)\delta(t-\tau)\mathrm{d}\tau = -\frac{\gamma}{2}\sigma^-(t),$$

where the factor $1/2$ is because the peak of the delta function is at the end of the interval of integration. This result corresponds with a delta-correlated noise or memory-less interaction.

Pauli operators $[\sigma_z, \sigma^{\pm}] = \pm 2\sigma^{\pm}$, $[\sigma^+, \sigma^-] = \sigma_z$, and the derived expression for the input field $b_{\text{in}}(t)$, these equations read

$$\dot{\sigma}^- = -(i\omega_q + \frac{\gamma}{2})\sigma^- + \sqrt{\gamma}\,\sigma_z b_{\text{in}}(t), \tag{2.42}$$

$$\dot{\sigma}^+ = (i\omega_q - \frac{\gamma}{2})\sigma^+ + \sqrt{\gamma}\,\sigma_z b_{\text{in}}^\dagger(t), \tag{2.43}$$

$$\dot{\sigma}_z = -\gamma(1+\sigma_z) - 2\sqrt{\gamma}\,(\sigma^+ b_{\text{in}}(t) + b_{\text{in}}^\dagger(t)\sigma^-). \tag{2.44}$$

These set of equations are formally equivalent to quantum Langevin equations[20], where the input field $b_{\text{in}}(t)$ is the quantum noise term. These equations are not exactly solvable though, so in principle it could seem that one cannot fully determine the state of the outgoing fields $b_{\text{out}}(t)$. However, for our purposes it is not necessary to know the detailed correlation between the noise $b_{\text{in}}(t)$ and the system. We rather can average the system over all possible states b_{in}, using the statistics given by $b_{\text{in}}(t)$. To this end, we derive a master equation $\rho_{\text{sys}}(t)$ for the system, and obtain the expectation value $\langle\sigma^-(t)\rangle$, which we will finally introduce in (2.41) to get the outgoing fields.

2.4.3 Master equation

A master equation [BP07, Car91] is an approximate equation for the time evolution of the density operator of a quantum system coupled to a noisy reservoir. It is an extremely powerful tool in describing the dynamics of open quantum systems, since it accounts for the irreversible processes of dissipation and decoherence in the system (usually called relaxation and dephasing). In this section we present a detailed derivation of the master equation, with special emphasis on the case of a two-level artificial atom coupled to an open transmission line, which has been of central importance in publications P5-P8.

Consider a quantum system described by H_{sys} coupled to a large reservoir described by H_{res}. The total Hamiltonian can be decomposed into free and interaction terms

$$H = H_{\text{sys}} + H_{\text{res}} + H_{\text{int}} = H_0 + H_{\text{int}}. \tag{2.45}$$

[20] A quantum Langevin equation for a system operator Y,

$$\dot{Y} = \frac{i}{\hbar}[H_{\text{sys}}, Y] + \frac{i}{2\hbar}[\gamma\dot{X} - 2\sqrt{\gamma c}\,\dot{b}_{\text{in}}, [X, Y_+]]$$

is a stochastic differential equation that accounts for the exact dynamics of a quantum system interacting with a quantum noisy environment $b_{\text{in}}(t)$.

Let χ_{tot} be the total density operator of the system plus reservoir. The equation of motion in the Schrödinger picture is given by the von Neumann equation [21]

$$\dot{\chi}_{\text{tot}} = -\frac{i}{\hbar}[H, \chi_{\text{tot}}]. \tag{2.46}$$

It is convenient to write this equation in the interaction picture, defined by the transformation

$$\rho_{\text{tot}} = U\chi_{\text{tot}}U^{\dagger}, \quad U = e^{iH_0 t/\hbar}. \tag{2.47}$$

In taking the time derivative of ρ_{tot}, we obtain

$$\dot{\rho}_{\text{tot}} = -\frac{i}{\hbar}[H_{\text{int}}(t), \rho_{\text{tot}}], \tag{2.48}$$

where $H_{\text{int}}(t) = UH_{\text{int}}U^{\dagger}$. The equation above can be formally integrated, yielding the following integro-differential equation

$$\rho_{\text{tot}}(t) = \rho_{\text{tot}}(0) - \frac{i}{\hbar}\int_0^t \mathrm{d}\tau[H_{\text{int}}(\tau), \rho_{\text{tot}}(\tau)]. \tag{2.49}$$

We now insert this expression into the right-hand side of (2.48) and get[22]

$$\dot{\rho}_{\text{tot}}(t) = -\frac{i}{\hbar}[H_{\text{int}}(t), \rho_{\text{tot}}(0)] - \frac{1}{\hbar^2}\int_0^t \mathrm{d}\tau[H_{\text{int}}(t), [H_{\text{int}}(\tau), \rho_{\text{tot}}(\tau)]. \tag{2.50}$$

We will be interested in the system dynamics, so we can trace over the reservoir degrees of freedom. In doing so, we obtain the reduced density matrix of the system $\rho_{\text{sys}}(t) = \text{Tr}_{\text{res}}\{\rho_{\text{tot}}(t)\}$ which follows the equation

$$\begin{aligned}\dot{\rho}_{\text{sys}}(t) = &- \frac{i}{\hbar}\text{Tr}_{\text{res}}[H_{\text{int}}(t), \rho_{\text{tot}}(0)] \\ &- \frac{1}{\hbar^2}\int_0^t \mathrm{d}\tau \text{Tr}_{\text{res}}[H_{\text{int}}(t), [H_{\text{int}}(\tau), \rho_{\text{tot}}(\tau)]].\end{aligned} \tag{2.51}$$

The above expression is an exact equation for the reduced density matrix of the system. Our aim is to transform this integro-differential equation into a first-order differential equation, for which we assume the following approximations:

- First, we consider that the system and reservoir at time $t = 0$ are uncorrelated, so that $\rho_{\text{tot}}(0) = \rho_{\text{sys}}(0) \otimes \rho_{\text{res}}(0)$.

[21] The von Neumann equation can be straightforwardly obtained, by taking the derivative of $\rho = |\Psi\rangle\langle\Psi|$ and applying the Schrödinger equation $i\hbar\partial_t|\Psi\rangle = H|\Psi\rangle$.

[22] Since the system-reservoir coupling is typically small, we can drop terms higher than second order in the iterative solution of ρ_{tot}.

- Second, we can assume without loss of generality that

$$\mathrm{Tr}_{\mathrm{res}}[H_{\mathrm{int}}(t), \rho_{\mathrm{tot}}(0)] = 0. \tag{2.52}$$

  If this condition is not satisfied, we can always redefine H_{sys} and H_{res}, while keeping H constant, in such a way that (2.52) is fulfilled.

- Born approximation: We assume that the coupling is so weak and the reservoir so large, that the reservoir density operator is not affected due to the interaction with the system. Then, $\rho_{\mathrm{tot}}(\tau) \simeq \rho_{\mathrm{sys}}(\tau) \otimes \rho_{\mathrm{res}}(0)$ and (2.51) can be written as

$$\dot{\rho}_{\mathrm{sys}}(t) = -\frac{1}{\hbar^2}\int_0^t \mathrm{d}\tau \mathrm{Tr}_{\mathrm{res}}[H_{\mathrm{int}}(t), [H_{\mathrm{int}}(\tau), \rho_{\mathrm{sys}}(\tau) \otimes \rho_{\mathrm{res}}(0)]]. \tag{2.53}$$

- Markov approximation: The memory of the reservoir is short-lived, and therefore the system does not depend on its past history. We can then drop the τ-dependence on the system density operator by replacing $\rho_{\mathrm{sys}}(\tau)$ by $\rho_{\mathrm{sys}}(t)$ in (2.54). In doing this, we can finally write down the celebrated master equation in the Born-Markov approximation:

$$\dot{\rho}_{\mathrm{sys}}(t) = -\frac{1}{\hbar^2}\int_0^t \mathrm{d}\tau \mathrm{Tr}_{\mathrm{res}}[H_{\mathrm{int}}(t), [H_{\mathrm{int}}(\tau), \rho_{\mathrm{sys}}(t) \otimes \rho_{\mathrm{res}}(0)]]. \tag{2.54}$$

To understand this better, let us consider a particular interaction Hamiltonian of the form (in the interaction picture):

$$H_{\mathrm{int}}(t) = \hbar \sum_i \sigma_i(t) b_i(t), \tag{2.55}$$

where $\sigma_i(t)$, $b_i(t)$ are the system and reservoir operators respectively. The master equation in the Born approximation is now

$$\dot{\rho}_{\mathrm{sys}}(t) = -\sum_{i,j}\int_0^t \mathrm{d}\tau \mathrm{Tr}_{\mathrm{res}}[\sigma_i(t) b_i(t), [\sigma_j(\tau) b_j(\tau), \rho_{\mathrm{sys}}(\tau) \otimes \rho_{\mathrm{res}}(0)]]. \tag{2.56}$$

Expanding the commutators, and using the cyclic property of the trace $\mathrm{Tr}[AB] = Tr[BA]$, we end up with:

$$\begin{aligned}\dot{\rho}_{\mathrm{sys}}(t) = & -\sum_{i,j}\int_0^t \mathrm{d}\tau \left\{ [\sigma_i(t)\sigma_j(\tau)\rho_{\mathrm{sys}}(\tau) - \sigma_j(\tau)\rho_{\mathrm{sys}}(\tau)\sigma_i(t)] \left\langle b_i(t) b_j(\tau) \right\rangle \right. \\ & + \left. [\rho_{\mathrm{sys}}(\tau)\sigma_j(\tau)\sigma_i(t) - \sigma_i(t)\rho_{\mathrm{sys}}(\tau)\sigma_j(\tau)] \left\langle b_j(\tau) b_i(t) \right\rangle \right\},\end{aligned} \tag{2.57}$$

where the two-time correlation functions are given by

$$\begin{aligned}\left\langle b_i(t) b_j(\tau) \right\rangle &= \mathrm{Tr}_{\mathrm{res}}[b_i(t) b_j(\tau) \rho_{\mathrm{res}}(0)], \\ \left\langle b_j(\tau) b_i(t) \right\rangle &= \mathrm{Tr}_{\mathrm{res}}[b_j(\tau) b_i(t) \rho_{\mathrm{res}}(0)].\end{aligned} \tag{2.58}$$

The large size of the reservoir and the weak interaction with the system, makes that any change in the reservoir caused by the system will die down very fast, so that reservoir correlations can be considered delta-correlated

$$\langle b_i(t) b_j(\tau) \rangle \propto \delta(t-\tau), \tag{2.59}$$

and thus $\rho_{\text{sys}}(\tau) = \rho_{\text{sys}}(t)$, leading to the master equation (2.56).

1. Decay of a two-level atom

Let us solve the master equation for the specific case we have considered in this Thesis: an artificial two-level system coupled to a electromagnetic reservoir. The Hamiltonian of this system is given by (2.32). In particular, the interaction Hamiltonian in the interaction picture

$$H_{\text{int}}(t) = \hbar \int_{-\infty}^{\infty} g(\omega) \left(\sigma^+ a_\omega e^{i(\omega_q - \omega)t} + \sigma^- a_\omega^\dagger e^{-i(\omega_q - \omega)t} \right) \mathrm{d}\omega \tag{2.60}$$

can be written in the form of (2.55)

$$H_{\text{int}}(t) = \hbar \left(\sigma^+(t) b(t) + \sigma^-(t) b^\dagger(t) \right), \tag{2.61}$$

where

$$\sigma^+(t) = \sigma^+ e^{i\omega_q t}, \qquad b(t) = \int_{-\infty}^{\infty} g(\omega) a_\omega e^{-i\omega t} \mathrm{d}\omega. \tag{2.62}$$

Assuming that the reservoir is initially in a thermal state[23] at temperature T, we find the following correlation functions:

$$\langle b(t) b(\tau) \rangle = \langle b^\dagger(t) b^\dagger(\tau) \rangle = 0, \tag{2.63}$$

$$\langle b^\dagger(t) b(\tau) \rangle = \int \mathrm{d}\omega |g(\omega)|^2 n_\omega e^{i\omega(t-\tau)}, \tag{2.64}$$

$$\langle b(t) b^\dagger(\tau) \rangle = \int \mathrm{d}\omega |g(\omega)|^2 (n_\omega + 1) e^{i\omega(t-\tau)}. \tag{2.65}$$

Substituting these expressions in (2.57) and performing the time integrals of the reservoir correlation functions[24], we finally obtain the quantum optical

[23] The statistics of a thermal state ρ_{th} yields the following expectation values:

$$\langle a_\omega a'_\omega \rangle = \langle a_\omega^\dagger a^\dagger \omega' \rangle = 0, \langle a_\omega^\dagger a_{\omega'} \rangle = n_\omega \cdot \delta(\omega - \omega'), \text{ where } n_\omega = (e^{\hbar\omega/KT} - 1)^{-1}.$$

[24] We use the relation $\int_\infty^\infty \mathrm{d}\omega f(\omega) \int_0^\infty \mathrm{d}\tau e^{-i\omega\tau} = \int \left[\pi\delta(\omega) - i\text{PV}\left(\frac{1}{\omega}\right) \right] f(\omega) \mathrm{d}\omega$, where PV stands for the Cauchy principal value. This term accounts for the radiative corrections that are known as the Lamb shift of the atom.

master equation:

$$\dot{\rho}_{\rm sys}(t) = \frac{\Gamma_\downarrow}{2}(2\sigma^-\rho_{\rm sys}\sigma^+ - \sigma^+\sigma^-\rho_{\rm sys} - \rho_{\rm sys}\sigma^+\sigma^-) \quad (2.66)$$

$$- \frac{\Gamma_\uparrow}{2}(2\sigma^+\rho_{\rm sys}\sigma^- - \sigma^-\sigma^+\rho_{\rm sys} - \rho_{\rm sys}\sigma^-\sigma^+). \quad (2.67)$$

where $\Gamma_{\uparrow\downarrow}$ are the relaxation and excitation rates

$$\Gamma_\downarrow = 2\pi g(\omega_q)^2|n_{\omega_q}+1|^2, \quad \Gamma_\uparrow = 2\pi g(\omega_q)^2|n_{\omega_q}|^2. \quad (2.68)$$

The coupling $g(\omega)$ straightforwardly follows from the tools presented in the previous chapter:

$$g(\omega) = \frac{2e}{\hbar}\frac{C_c}{C_\Sigma}\sqrt{\frac{\hbar Z_0\omega}{4\pi}}\langle 1|\hat{n}|0\rangle. \quad (2.69)$$

Projecting the master equation on the qubit eigenbasis, we arrive at the following equation for the time evolution of the qubit populations:

$$\dot{\rho}_{00} = -\Gamma\rho_{00}, \quad \dot{\rho}_{11} = -\dot{\rho}_{00}, \quad (2.70)$$

where $\Gamma = \Gamma_\uparrow + \Gamma_\downarrow$ is the total decay rate, and $T_1 = 1/\Gamma$ is the relaxation time of the qubit. In quantum optics, it is common that the two-level atom couples to a reservoir at $T = 0$, $\Gamma_\uparrow = 0$, so the decay rate that accounts for the relaxation of the atom becomes $\Gamma = \Gamma_\downarrow = 2\pi g(\omega_q)^2\omega_q$.

2. Pure dephasing

Relaxation of the qubit is not the only decoherence mechanism. Another important channel of decoherence in the system is due to *pure dephasing*. This happens when weak fluctuations in the system parameters such as the gate voltage, induce small oscillations in the qubit energies – this is for instance the so-called charge noise in charge-based qubits.

Formally, a qubit Hamiltonian subject to a perturbation δn_g in the gate voltage can be written as

$$H_{\rm sys} = \frac{\hbar}{2}\left(\omega_q(n_g)\sigma_z + \frac{\partial\omega_q(n_g)}{\partial n_g}\delta n_g\sigma_z\right). \quad (2.71)$$

It can be shown that the last contribution in (2.71) adds up to the interaction Hamiltonian due to the coupling with a heat bath, as

$$H_{\rm int}(t) = \hbar\sigma_z(t)\left(b(t) + b^\dagger(t)\right). \quad (2.72)$$

Proceeding as before, we can derive a master equation that accounts for the pure dephasing

$$\dot{\rho}_{\text{sys}} = \Gamma_\phi(\sigma_z \rho_{\text{sys}} \sigma_z - \rho_{\text{sys}}), \tag{2.73}$$

where the pure dephasing decay rate is

$$\Gamma_\phi = \frac{e^2}{8E_C^2}\frac{C_c}{C_\Sigma}\frac{KT}{\hbar}\left|\frac{\partial_{\omega_q}(n_g)}{\partial n_g}\right|^2. \tag{2.74}$$

Including the dephasing due to relaxation processes, the off-diagonal elements of the density matrix evolve as

$$\dot{\rho}_{01} = -\gamma_{01}\,\rho_{01} = (\Gamma_\phi + \frac{\Gamma_\downarrow}{2})\rho_{01}, \tag{2.75}$$

where the total dephasing time is defined as

$$\frac{1}{T_2} = \frac{1}{2T_1} + \frac{1}{T_\phi}. \tag{2.76}$$

With this results, we have fully determined the master equation, and one can compute any qubit operator expectation value. In particular, we were interested in computing $\langle\sigma^-\rangle$, which straightforwardly follows from the solution of

$$\frac{\mathrm{d}}{\mathrm{d}t}\langle\sigma^-\rangle = \mathrm{Tr}(\dot{\rho}_{\text{sys}}\sigma^-) = \mathrm{Tr}(\sigma^-\mathcal{L}\rho_{\text{sys}}), \tag{2.77}$$

provided that we know the expression of the Lindblad operator.

3
Results

3.1 Switchable ultrastrong coupling in circuit QED

As we have shown in chapter 2, the large dipole moments of artificial atoms combined with the strong vacuum fields attainable in superconducting resonators have made possible the achievement of the strong and ultrastrong coupling regimes in circuit QED. In this latter regime, the coupling "g" is comparable to the qubit and photon frequencies ($g \simeq \omega_0, \Omega$), and the renowned Jaynes-Cummings model does not properly describe the dynamics of the system, opening the door to a wide variety of studies around the rather unexplored physics beyond the rotating wave approximation. However, this regime lacks an important ingredient, namely, the ability to tune or switch the coupling strength. Only in the case of a qubit confined in a resonator, the coupling might be adjusted by detuning the qubit from the cavity, but at the price of moving the qubit away from its symmetry point, with the subsequent reduction of qubit lifetime. For a qubit placed in an open transmission line this argument is not even valid, since the qubit is coupled to a continuum of field modes, regardless it is detuned or not.

3.1.1 Summary and discussion of results

In the first work of this Thesis we show how different circuit QED designs can fully control the interaction between light and matter in the ultrastrong coupling regime, either in an open or a closed transmission line. By adding superconducting ring couplers to the standard circuit QED architecture (like the one shown in Fig.3.1a), we manage to effectively rotate the interaction basis, or completely suppress all the couplings. A thorough description of these

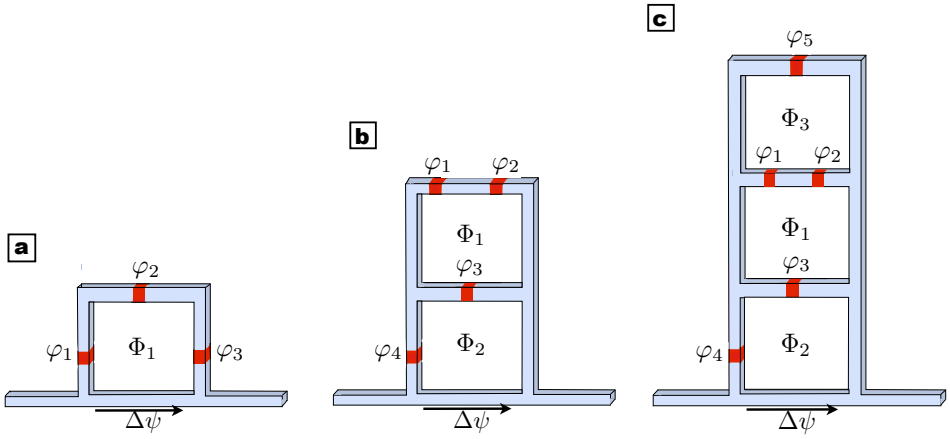

Figure 3.1: a) Schematic layout for the ultrastrong coupling in circuit QED b) By adding a second superconducting loop (a rf-SQUID), the coupling can be modulated. c) A three-loop design allows for a selective tunability of the coupling, such as the enhancement of non-linear photon-photon interactions.

proposals, together with diverse applications in Quantum Information Processing and Relativistic Quantum Information, are the topics of publication P1, whose main results can be summarized as follows:

- We have proposed a tunable coupling design, consisting of two superconducting loops galvanically coupled to a transmission line (see Figure 3.1b). The top loop stands for the 3JJ-flux qubit, while the loop in between (an rf-SQUID) acts as a coupling element. It introduces a control parameter, the external magnetic flux Φ_2 passing through the SQUID, whose effect is to induce a quantum interference between the flux qubit and the photons passing through the transmission line[1]. By controlling this additional magnetic flux, we can rotate the light-matter interaction basis,[2] going from transversal interactions of the form $H_{\text{int}} = g_x\sigma_x(a + a^\dagger)$ to longitudinal Hamiltonians $H_{\text{int}} = g_z\sigma_z(a + a^\dagger)$. This rotation can be performed in times that are within the subnanosecond scale –much faster than the qubit and photon dynamics, while preserving the ultrastrong nature of the interaction.

- By means of an additional loop (Figure 3.1c), we propose a more ver-

[1]Such a quantum interference arises from the fluxoid quantization on the loops, which merges qubit and field operators with classical control parameters.

[2]It is worth pointing out that this can be done while keeping the qubit at its symmetry point, where the noise contributions appear at second order.

satile design that allows us to switch on and off *different orders* of the interaction Hamiltonian. Thus, it becomes possible to enhance the relevance of non-linear contributions of the form $H_{\text{int}} = g_x^{(2)}\sigma_x(a + a^\dagger)^2$, by switching off only the light-matter interaction at first order. This second-order process becomes an appreciable process, for it can reach significant couplings $g_x^{(2)} \sim 25 - 250$ GHz , provided that we remain in the ultrastrong regime of interaction.

- Finally, we present a device that could disconnect *all the couplings* present in the system at a time, both linear, non-linear and possible spurious couplings that might arise from capacitive channels. This can be done by replacing the fourth Josephson junction in Fig3.1b by a dc-SQUID. Controlling the magnetic flux over this quantum interference device, we can dynamically tune the Josephson energy of the Junction and ultimately the coupling.

We envision numerous applications for all these proposals. The immediate one would concern the field of Quantum Information Processing, with the creation of ultrafast quantum gates [RBW+12] between two arbitrary pair of qubits in a row coupled to a transmission line. This is possible by decoupling all qubits from the line, except those who have to implement two-qubit gate. The second application would be the qubit protection from decoherence. By switching off all the couplings we can isolate the qubit from the environment [GHB11]. Moreover, this can be used for measuring the qubit once its ultrafast dynamics is frozen. Another application is the generation of propagating single-photons (two-photons) on demand. This is accomplished by the following protocol: we prepare the qubit in its ground state. We drive the qubit the qubit to the excited state, and immediately connect an ultrastrong linear (nonlinear) interaction to the line, as described above. Finally, the qubit will decay by emitting a propagating single-photon (two-photons). Last but not least, a tunable coupling with propagating photons can be of paramount importance in the field of relativistic quantum information. With these designs, it becomes possible to measure the light-cone of photons, as well as the propagation of quantum correlations between qubits in a common transmission line.

In summary, we have proposed several devices that allows for a precise control of the ultrastrong light-matter interaction, both in resonators and open lines. We have proposed a plethora of applications that would be of interest in the fields of microwave quantum optics and quantum information science. A more fundamental and striking application in relativistic quantum information is presented in publication P2.

3.1.2 Publication 1: Switchable ultrastrong coupling in circuit QED. B. Peropadre, P. Forn-Díaz, E. Solano, J. J. García-Ripoll. Phys. Rev. Lett. 105, 023601 (2010)

Switchable Ultrastrong Coupling in Circuit QED

B. Peropadre,[1] P. Forn-Díaz,[2] E. Solano,[3,4] and J. J. García-Ripoll[1]

[1]*Instituto de Física Fundamental, CSIC, Serrano 113-bis, 28006 Madrid, Spain*

[2]*Quantum Transport Group, Kavli Institute of Nanoscience, Delft University of Technology, Lorentzweg 1, 2628 CJ Delft, The Netherlands*

[3]*Departamento de Química Física, Universidad del País Vasco—Euskal Herriko Unibertsitatea, Apartado 644, 48080 Bilbao, Spain*

[4]*IKERBASQUE, Basque Foundation for Science, Alameda Urquijo 36, 48011 Bilbao, Spain*

(Received 19 January 2010; published 6 July 2010)

We propose different designs of switchable coupling between a superconducting flux qubit and a microwave transmission line. They are based on two or more loops of Josephson junctions which are directly connected to a closed (cavity) or open transmission line. In both cases the circuit induces a coupling that can be modulated in strength, reaching the so-called ultrastrong coupling regime in which the coupling is comparable to the qubit and photon frequencies. Furthermore, we suggest a wide set of applications for the introduced architectures.

DOI: 10.1103/PhysRevLett.105.023601 PACS numbers: 42.50.−p, 03.67.Lx, 85.25.−j

Superconducting quantum circuits [1] possess ingredients for quantum information processing and for developing on-chip microwave quantum optics [2]. After the first manipulations of few-level superconducting systems (qubits) [3–5], the real boost came with the achievement of the strong coupling regime between qubits and confined microwave photons [6–8]. The initial qubit-cavity couplings of 10–100 MHz exceeded by orders of magnitude the rate at which photons leak out of the resonator, but the use of the transmon qubit [9] improved those numbers by a factor of 2–3 reaching a strength that is comparable only to the state of the art in microwave quantum optics [10,11]. More recently, proof-of-principle theoretical and experimental studies have paved the way to the ultrastrong coupling regime [12–14], where the coupling approaches the qubit transition frequency and the Jaynes-Cummings model of cavity QED [10,14] breaks down [15,16], and a door opens to the rather unexplored physics beyond the rotating-wave approximation [17,18].

The strong coupling regime in circuit QED has made possible an incredible variety of experiments, such as dispersive readouts of qubits [19], resolving the photon numbers in cavity [20], multiphoton excitations of the Jaynes-Cummings model [21], preparing nonclassical states of a resonator [22], full quantum tomography of the microwave radiation field [23], or the Tavis-Cummings model [24], etc. However, all those experiments have something in common: The microwave field is confined inside a resonator. In other words, the transmission line spectrum is discrete and the coupling between qubits and photons could be switched on and off by tuning the qubit [25] or cavity frequency [26]. While the switchability of the coupling has been proposed for open lines [27,28], this has not been achieved in the ultrastrong coupling regimes.

In this work, we will introduce a novel circuit QED design where the qubit is ultrastrongly coupled to a transmission line, open or not, with a coupling that can be tuned in strength and kind by applying an external flux bias. Our proposal uses the type of designs shown in Fig. 1, where the qubit is built in direct contact with the transmission line. It has been shown theoretically [14], and demonstrated experimentally [13], that the system admits an effective description based on a two-level system—the current in the loop—ultrastrongly coupled to the photons in the line. We will boost these ideas and show that, by means of induced quantum interference, one is capable of cancelling the ultrastrong coupling, effectively rotating the qubit basis, or activating higher-order nonlinearities. This fully controllable coupling tunability opens the path for new experimental results and nontrivial applications. A very important one is switching on and off the interaction in order to control the qubit evolution with subnanosecond resolution, allowing one to resolve the emission and propagation of single photons, measuring their light cone, and studying the propagation of entanglement between qubits coupled to the same transmission line [29]. Straightforward

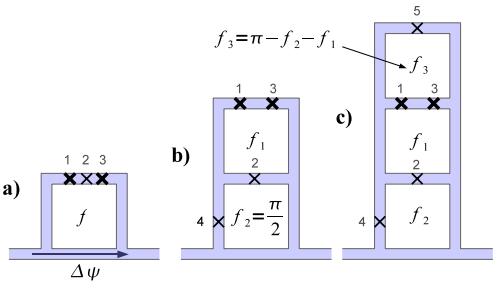

FIG. 1 (color online). Schemes for ultrastrong coupling between a qubit and a transmission line. (a) Basic setup of a qubit coupled directly to the line. $\Delta\psi$ is the phase difference between the nodes in which the qubit and line intersect. (b) With a second loop, the coupling can be modulated. (c) A slightly improved setup in which the qubit is better decoupled from the flux f_2.

extensions of this work will also allow the implementation of ultrafast quantum switches between cavities and remote qubits or the design of qutrits with tunable couplings.

The basic design of the switchable coupling can be understood by using a few rules that focus on the inductive terms of the Hamiltonian. More precisely, we will concentrate on the dominant contributions to the energy, which are given by the Josephson junctions as $V(\phi_n) = -E_{Jn}\cos(\phi_n)$. Here, E_{Jn} denotes the Josephson energy of the nth junction, and ϕ_n is the phase difference between both sides of the junction. These phases are by the Josephson relation proportional to the flux across the device, $\phi = \varphi/\varphi_0$ with the reduced flux quantum $\varphi_0 = \hbar/2e$. The next rule is that around close loops the total flux is quantized in a multiple of $h/2e$. This quantization imposes relations between the flux jumps on different junctions, reducing the complexity of the problem, $\sum_n \phi_n = f + 2\pi n$, but it also introduces a control parameter which is the externally applied magnetic flux inside the loop, $f\varphi_0$. Finally, we will include an additional flux difference $\Delta\psi$ along the segment that is shared with the transmission line [see Fig. 1(a)] and which is the source of the coupling.

With these rules, one can analyze the setup from Fig. 1(a) and impose the usual flux qubit configuration, with two equal junctions $E_{J1} = E_{J3} = E_J$, and a smaller one $E_{J2} = \alpha E_J (\alpha < 1)$, and the quantization $\phi_1 + \phi_2 + \phi_3 - \Delta\psi = f + 2\pi n$. The result is an effective Hamiltonian that, for $f = \pi$, reads

$$\begin{aligned} H_J &= -E_J\cos(\phi_1) - \alpha E_J\cos(\phi_2) - E_J\cos(\phi_3) \\ &= E_J[\alpha\cos(\phi_+) - 2\cos(\phi_-/2)\cos(\phi_+/2)] \\ &\quad + \alpha E_J \Delta\psi\sin(\phi_+) + O(\Delta\psi^2). \end{aligned} \tag{1}$$

Note how this model combines a flux qubit term [4], where the most important variable is the linear combination $\phi_+ = \phi_3 + \phi_1$, with a coupling between the qubit degrees of freedom and the transmission line. When we introduce the capacitive terms, the qubit can be diagonalized and the model becomes

$$H \sim \tfrac{1}{2}\Omega\sigma_z + \alpha E_J \Delta\psi\sigma_x. \tag{2}$$

It is noteworthy to mention that the qubit-line coupling can remain in the ultrastrong regime [14], because it is proportional to the Josephson energy αE_J. However, the coupling always has the form $\sigma_x\Delta\psi$, and there are no parameters to tune the interaction.

A more versatile design, shown in Fig. 1(b), separates the three qubit junctions and the transmission line by a loop. The new Josephson junction adds a contribution to the energy, which is of the form $E_{J4}\cos(\phi_4) = \alpha_4 E_J\cos(f_2 - \phi_2 - \Delta\psi)$, while keeping the flux qubit quantization independent of the transmission line flux, $\Delta\psi$. The result is now

$$\begin{aligned} H = E_J[&-\alpha\cos(f_1 - \phi_+) - 2\cos(\phi_-/2)\cos(\phi_+/2)] \\ &+ \alpha_4 E_J\cos(f_1 + f_2 - \Delta\psi + \phi_+), \end{aligned} \tag{3}$$

with two independently adjustable parameters f_1 and $f_1 + f_2$. A numerical evaluation of the Hamiltonian in the qubit basis reveals that for $f_2 = \pi$ the effective coupling

$$H \sim \frac{1}{2}\Omega\sigma_z + \alpha_4 E_J \Delta\psi \sum_{r=x,y,z} c_r^1(\alpha, \alpha_4, f_1)\sigma_r \tag{4}$$

is linear in the field and has a tunable orientation $c_r^1(\alpha, \alpha_4, f_1)$.

Moreover, since the coupling term is strictly independent of the qubit Hamiltonian, it now becomes possible to switch on and off the interaction. The simplest way is to replace the fourth junction E_{J4} with a SQUID, so that a control flux over this loop will allow us to dynamically tune the coupling strength α_4. By using this technique, the mutual influence between the qubit and the transmission line can be completely suppressed in times of about 0.1 ns, which is much faster than the qubit-resonator dynamics [30]. Remark that in the ultrastrong coupling regime the rotating-wave approximation cannot be made, and the physics of Rabi oscillations does not apply.

A different setup which we consider in this work is shown in Fig. 1(c). We now included two equal junctions $E_{J5} = E_{J4} = \alpha_4 E_J$, and we add a new loop above the qubit with a control flux f_3. Working at $f_3 = \pi - f_2 - f_1$ we cancel a contribution $\cos(f_1 + f_2 + \phi_+)$ that appears in Eq. (3) when we move away from $f_2 = \pi$. The effective Hamiltonian now reads

$$H = \frac{1}{2}\Omega\sigma_z + \alpha_4 E_J \sum_{n=1,2\ldots} \Delta\psi^n \sum_{r=x,y,z} c_r^n(\alpha, \alpha_4, f_1, f_2)\sigma_r. \tag{5}$$

With the two free parameters $\{f_1, f_2\}$ we can (i) switch on and off the interaction, (ii) change the orientation, and (iii) increase the relevance of higher-order couplings.

We have analyzed these setups numerically, confirming that the coupling is ultrastrong and can be arbitrarily tuned. In order to do so, we first completed the theoretical model to include the capacitive terms which appear in the junctions and the line itself. We then diagonalized the Hamiltonian of what we identify as the qubit degrees of freedom and verified that they can still be treated under a two-level approximation. Finally, we expanded the interaction between the qubit and the transmission line in powers of the flux $\Delta\psi$ and computed the matrix elements of the interaction in the qubit basis.

The main results are shown in Figs. 2 and 3, corresponding to setups in Fig. 1(b) and 1(c). In the first figure we have explored the simplest switchable setup for various configurations of the qubit α and of the externally applied flux f_1. It is important to remark that we have a very good qubit for values of α well above the 0.8 which is normally considered. Furthermore, when $f_1 = \pi$ for both $\alpha < 1$ and

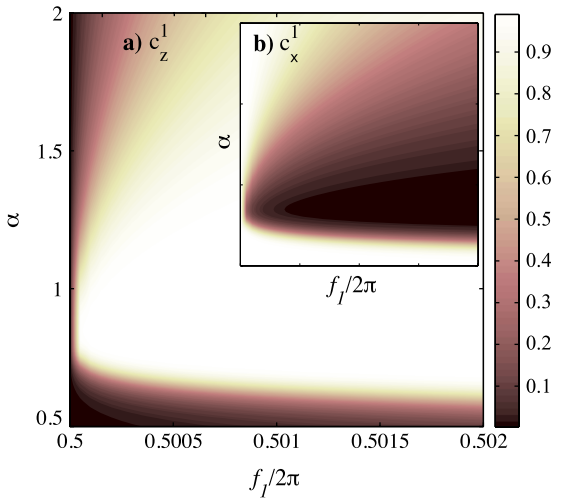

FIG. 2 (color online). For the Fig. 1(b) setup, coupling strengths as a function of the external flux f_1 and the qubit junction size $\alpha = E_{J2}/E_{J1}$, for $f_2 = \pi$. We plot (a) the normalized first-order coupling along the Z direction, $c_z^1 \sigma_z \Delta\psi$, and (b) across the XY plane.

$\alpha > 1$, the ground states are superpositions of left- and right-moving currents, and the interaction is proportional to σ_x, transversely to the qubit basis. When we apply a small flux difference increasing or decreasing f_1, we unbalance the populations of the two current states, the ground state acquires an effective magnetic dipole, and the interaction rotates from σ_z to $\sigma_{x,y}$.

The second set of plots is shown in Fig. 3 and corresponds to the three-loops setup [Fig. 1(c)]. We have chosen $\alpha = 2$ because it allows for a finer control in the rotation of the interaction σ_x to σ_z, but it is not essential. The tunability of the qubit manifests as follows: When f_1 is increased, the strength of $c_x^{1,2}$ decreases, causing an increase of $c_z^{1,2}$, much like in Fig. 2. But in addition to this, we now have complete freedom to change the value of f_2. Changes in this second flux result in a simultaneous deactivation of all couplings $c_{x,y,z}$, which become zero as seen in the dark horizontal stripes for $f_2 = (2n + 1)\pi/2$ in Fig. 3(a) and in the zeros of c_x in Fig. 3(b). The switching capability, measured as $\min c_x/c_z$, is rather strong, 6×10^{-4} in this example, and improves by increasing α.

We may now address the absolute strength of the qubit-line coupling. For clarity, we will restrict to the case in which the line forms a single-mode resonator, which admits a trivial generalization to the continuum by summing over modes. The phase slip then becomes approximately [14]

$$\Delta\psi = \frac{\partial_x u(x)\Delta x}{\varphi_0}\sqrt{\frac{\hbar}{\omega C}}(a + a^\dagger) = \frac{2\pi\partial_x \Psi(x)\Delta x}{\Phi_0}(a + a^\dagger).$$

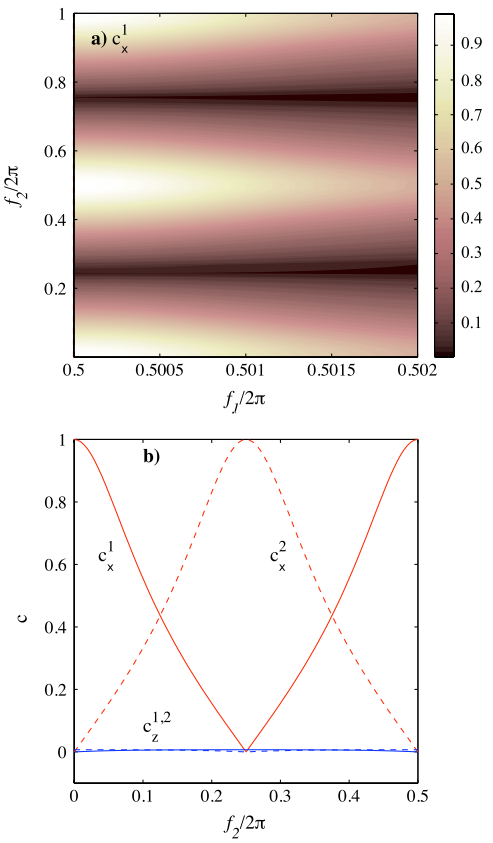

FIG. 3 (color online). (a) Following Eq. (5), normalized transverse coupling c_x^1 as a function of external fluxes f_1 and f_2 for the setup in Fig. 1(c), using $\alpha = 2.0$ and $\alpha_4 = 0.1$. (b) Cut at $f_1 = 0.5$ shows first-order (solid line) and second-order couplings (dashed line) of longitudinal (c_z, blue line) and transverse (c_x, red line).

Here $u(x)$ is the photon mode eigenfunction in the cavity, Δx is the separation between the two qubit-line intersections, ω is the cavity mode frequency, and C the resonator total capacitance. The dependence is thus similar to previous works meaning that we can achieve comparable ultrastrong couplings. Assuming a flux gradient $|\partial_x \Psi| = 65 \times 10^{-6}\Phi_0/\mu\text{m}$ and a qubit size $\Delta x = 5\ \mu\text{m}$, we reach a coupling $g = 2 \times 10^{-3} E_J$, which for a typical junction with $E_J = 250$ GHz implies a very strong 500 MHz coupling. The previous numbers are, however, pessimistic. An aluminum thin film penetration depth $\lambda_L = 150$ nm allows a larger flux gradient, of $1.7 \times 10^{-3}\Phi_0/\mu\text{m}$ or 25 times the previous coupling strength, that is up to 10 GHz. Either with these values, or by enhancing the phase slip with the use of an auxiliary junction [14], the fact is one can take the coupling strength deep in the ultrastrong regime with an interesting consequence, namely, the possibility of inducing nonlinearities in the transmission line [Fig. 3]. In the crudest approximation, the second-order coupling strength is proportional to $\alpha_4 E_J (2\pi\Delta x \partial_x \psi/\Phi_0)^2$. For a phase slip

of 0.01–0.03, that means a coupling $E_J \times (10^{-4}$–$10^{-3})$, or 25 to 250 MHz, according to the values mentioned before.

Throughout this work we neglected the coupling between the qubit and photons induced by the capacitive energy of the junctions, that is, terms of the form

$$H_{\mathrm{cap}} = \frac{\alpha_4}{1 + 2\alpha + 4\alpha_4} 2\pi\hbar\omega \frac{\partial_x \psi}{\Phi_0} \Delta x i(a - a^\dagger) q_+, \quad (6)$$

where $q_+ = (-i\partial/\partial\phi_+)$ is the conjugate operator to the flux qubit variable ϕ_+. This term, and a similar one for E_{J5} [Fig. 1(c)], gives a negligible coupling strength $\sim 10^{-3}\hbar\omega$.

We envision several applications of the switchable coupling introduced before. The first one would be to perform quantum gates between arbitrary qubit pairs of a row coupled to a transmission line. By decoupling all qubits except those chosen to perform a two-qubit gate, it should be possible to perform operations as the swap of quantum information between the qubit and the line modes or between both qubits. This scheme has an important advantage, namely, that the qubit switching happens for precise flux values, depending only on geometric properties and not on the precise eigenenergies or fabricated junction properties. A second application would be decoupling a qubit from the transmission line and coupling it to slower measurement devices, especially after having performed an ultrastrong coupling evolution [31]. Furthermore, since the coupling may be switched on and off in about 0.1 ns, this enhanced resolution can also be used for the measurement of quantum microwaves. More precisely, given that one qubit may act as a perfect mirror for individual photons, a combination of one or more may be used as streak camera for stroboscopic measurements of wave packets. A fourth application is the deterministic generation of propagating single- and two-photon pulses. This would work by decoupling the qubit, exciting it, and then activating an ultrastrong coupling dynamics. The qubit would decay in a few nanoseconds, emitting either a single photon (linear coupling) or two of them (nonlinear one) in a wave packet whose shape can be tailored with a second qubit.

In conclusion, we believe that the future access to the physics of switchable ultrastrong coupling will pave the way to novel and otherwise inaccessible physics, including key applications to quantum microwave technologies.

P. F.-D. acknowledges support from NanoNed. E. S. acknowledges funding from UPV-EHU Grant No. GIU07/40, Spanish MEC Project No. FIS2009-12773-C02-01, EuroSQIP, and SOLID European projects. J. J. G.-R. and B. P. thank funding from Spanish Projects No. MEC FIS2006-04885 and No. CSIC 200850I044 and the CSIC JAE-PREDOC2009 grant.

[1] J. Clarke and F. K. Wilhelm, Nature (London) **453**, 1031 (2008).
[2] R. J. Schoelkopf and S. M. Girvin, Nature (London) **451**, 664 (2008).
[3] V. Bouchiat, D. Vion, P. Joyez, D. Esteve, and M. H. Devoret, Phys. Scr. **T76**, 165 (1998).
[4] J. E. Mooij *et al.*, Science **285**, 1036 (1999).
[5] J. M. Martinis, M. H. Devoret, and J. Clarke, Phys. Rev. Lett. **55**, 1543 (1985).
[6] A. Blais, R.-S. Huang, A. Wallraff, S. M. Girvin, and R. J. Schoelkopf, Phys. Rev. A **69**, 062320 (2004).
[7] A. Wallraff *et al.*, Nature (London) **431**, 162 (2004).
[8] I. Chiorescu *et al.*, Nature (London) **431**, 159 (2004).
[9] J. Koch *et al.*, Phys. Rev. A **76**, 042319 (2007).
[10] S. Haroche and J.-M. Raymond, *Exploring the Quantum* (Oxford University Press, New York, 2006).
[11] M. Brune *et al.*, Phys. Rev. Lett. **101**, 240402 (2008).
[12] M. Devoret, S. Girvin, and R. Schoelkopf, Ann. Phys. (N.Y.) **16**, 767 (2007).
[13] A. A. Abdumalikov, O. Astafiev, Y. Nakamura, Y. A. Pashkin, and J. Tsai, Phys. Rev. B **78**, 180502 (2008).
[14] J. Bourassa *et al.*, Phys. Rev. A **80**, 032109 (2009).
[15] C. Ciuti, G. Bastard, and I. Carusotto, Phys. Rev. B **72**, 115303 (2005).
[16] G. Günter *et al.*, Nature (London) **458**, 178 (2009).
[17] F. De Zela, E. Solano, and A. Gago, Opt. Commun. **142**, 106 (1997).
[18] A. P. Hines, C. M. Dawson, R. H. McKenzie, and G. J. Milburn, Phys. Rev. A **70**, 022303 (2004).
[19] S. Filipp *et al.*, Phys. Rev. Lett. **102**, 200402 (2009).
[20] D. I. Schuster *et al.*, Nature (London) **445**, 515 (2007).
[21] F. Deppe *et al.*, Nature Phys. **4**, 686 (2008).
[22] M. Hofheinz *et al.*, Nature (London) **454**, 310 (2008).
[23] M. Hofheinz *et al.*, Nature (London) **459**, 546 (2009).
[24] J. M. Fink *et al.*, Phys. Rev. Lett. **103**, 083601 (2009).
[25] M. Mariantoni *et al.*, Phys. Rev. B **78**, 104508 (2008).
[26] J. R. Johansson, G. Johansson, C. M. Wilson, and F. Nori, Phys. Rev. Lett. **103**, 147003 (2009).
[27] Y.-D. Wang, A. Kemp, and K. Semba, Phys. Rev. B **79**, 024502 (2009).
[28] A. J. Kerman and W. D. Oliver, Phys. Rev. Lett. **101**, 070501 (2008).
[29] C. Sabín, J. J. García-Ripoll, E. Solano, and J. León, Phys. Rev. B **81**, 184501 (2010).
[30] C. M. Wilson (private communication).
[31] I. Lizuain, J. Casanova, J. J. García-Ripoll, J. G. Muga, and E. Solano, Phys. Rev. B (to be published).

3.1.3 Application to Relativistic Quantum Information

One of the most striking properties of quantum field theory is that the vacuum of a quantum field is an entangled state. This fascinating result, while demonstrated time ago, didn't capture a great deal of attention since it hardly found practical applications. Astonishingly, in 2005 B. Reznik and coworkers [RRS05] showed that it is possible to exploit this property of the vacuum, and transfer the entanglement contained on it to a pair of qubits. This made that vacuum entanglement acquired a prominent interest, for it can be used as a resource of entanglement for quantum information [RCR05, SGRSL10].

In their original proposal, a pair of *space-like separated qubits* in a separable state, interact strongly with the vacuum of a quantum field for a finite time T. After the interaction, the qubits can get entangled with each other, even if they are causally disconnected. This result has been recently extended by J. Olson and T. Ralph [OR11] to scenarios where the qubits are *time-like separated*, i.e, the qubits extract quantum correlations from the vacuum, by interacting with it *at different times*[3]. Unfortunately, the realization of these proposals relies on quite unrealistic physical parameters[4] [OR12], and therefore seems to be unfeasible from the experimental viewpoint. In this regard, circuit QED pops up as an actual alternative, since it is endowed with the unique properties of large vacuum fluctuations, ultrastrong light-matter interaction and high degree of control in the coupling constant.

3.1.4 Summary and discussion of results

In publication P2, we exploit all these features with a circuit QED proposal that would allow for the extraction of past-future quantum correlations from the vacuum to a pair of flux qubits. The extraction protocol that we propose is the following (which is shown in Fig.3.2a for the sake of clarity): two superconducting flux qubits P (for the past) and F (for the future), initially prepared in the separable state $|eg\rangle_{PF}$ and separated a fixed distance d, are directly attached to an open transmission line, that supports the vacuum of a quantum field $|0\rangle_f$. By means of a tunable coupling device, like the one schematically shown in Fig.3.2b, we connect an ultrastrong interaction between the qubit P and the field for a time T_{on}, while keeping the qubit F disconnected from the line. After this time we switch off the coupling for

[3] We will refer to this kind of correlations as *past-future* quantum correlations.

[4] In order to amplify the weak vacuum correlations, the existing proposals rely on super-oscillatory coupling constants and time-dependent qubit energy gaps which suffer from infrared and ultraviolet divergences.

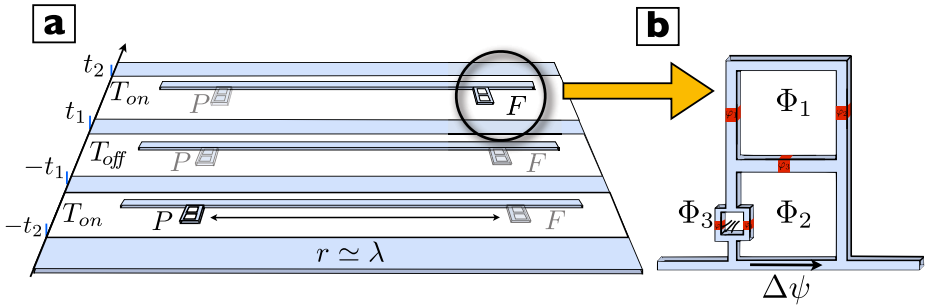

Figure 3.2: a) Protocol for the extraction of past-future quantum correlations from the vacuum. b) Flux qubit ultrastrongly coupled to a quantum field $\Delta\psi$ with a switchable interaction mediated by the flux Φ_3 through the SQUID.

a time T_{off}, time in which the system freely evolves. Lastly, we switch on the interaction of the qubit F with the field for a time T_{on}, while keeping P disconnected. After this protocol, the system ends up in a highly entangled state. Since we are interested only in the entanglement between the qubits, we trace over the field degrees of freedom and compute the concurrence[5] for the reduced density matrix of the qubits P and F. We have thoroughly studied this entanglement measure as a function of the distance d, and the interaction times T_{on} and T_{off}. These parameters basically tell us whether the qubits are inside or outside their mutual light-cone. In what follows, we summarize the main results we have obtained:

- When the separation between the qubits d is much smaller than the typical wavelength of the qubit energy gap λ, we observe that the qubits get entangled outside their mutual light cone. This means, even when the exchange of real photons is not allowed, qubits P and F exhibit strong quantum correlations. This is possible as the qubits have extracted the entanglement from the genuine vacuum correlations contained in the field.

- As the distance between the qubits increases, past-future quantum correlations die down. In particular, for distances $d > \lambda$, there is no entanglement in causally disconnected regions, but rather inside the light-cone of the qubits, and assisted by real photon exchange. However, we observe a high degree of entanglement concentrated in the vicinity of

[5] We use the concurrence as entanglement measure, since it is more suitable in measuring the degree of entanglement between non-pure two-qubit states. Nevertheless, other entanglement measures as the negativity can be used, yielding the same results.

the light-cone, even in the absence of projective measurements. This non-trivial correlations can only be explained by the one dimensional nature of circuit QED, which allows for a much more efficient interaction.

- We discuss the possibility of using our setup for developing *quantum teleportation in time*. Based on the extraction of past-future quantum correlations, we can generate entangled states $P - F$ in time, and therefore a third qubit P' could be teleported to the future following the next protocol: we let the joint system PP' interact with the quantum field for the time T_{on}. During the time of no interaction T_{off}, we Bell-measure the state PP' and write down the result. We finally connect a qubit F to the field, and given that it is entangled with P we can retrieve the state P', by properly using the classical information stored before, and locally acting on F[6].

- The previous teleportation protocol can be seen as a rudimentary quantum memory, where the state of a qubit P' is codified in the vacuum for a time T_{off}, and recovered in the future. Interestingly enough, this can be done regardless of whatever happened P after the Bell measurement.

Summing up, based on switchable ultrastrong interactions, in this publication we propose an experimentally feasible circuit QED setup to test the extraction of quantum correlations between different times contained in the vacuum of a quantum field. We have shown in particular that sizable past-future vacuum correlations can be transferred to a pair of qubits P and F, which only interact with the field in the past or the future respectively, and *do not coexist at the same time*. Moreover, we discuss the potential technological applications of that entanglement extraction and the particular use of our scheme to work as a novel kind of quantum memory.

[6]The fidelity of the teleportation protocol will depend on the amount of entanglement shared by P and F. For the numbers show in this work, the corresponding fidelity is well above the classical limit, and therefore can be used to distille some pure past-future entanglement.

3.1.5 Publication 2: Extracting past-future vacuum correlations using circuit QED. C. Sabin, B. Peropadre, M. del Rey, E. Martín-Martínez. Phys. Rev. Lett. 109 033602 (2012)

Extracting Past-Future Vacuum Correlations Using Circuit QED

Carlos Sabín,[1] Borja Peropadre,[1] Marco del Rey,[1] and Eduardo Martín-Martínez[1,2]
[1]*Instituto de Física Fundamental, CSIC, Serrano 113-B, 28006 Madrid, Spain**
[2]*Department of Physics and Astronomy and Department of Applied Mathematics, Institute for Quantum Computing, University of Waterloo, 200 University Avenue West, Waterloo, Ontario, N2L 3G1, Canada*
(Received 15 February 2012; revised manuscript received 25 May 2012; published 17 July 2012)

We propose a realistic circuit QED experiment to test the extraction of past-future vacuum entanglement to a pair of superconducting qubits. The qubit P interacts with the quantum field along an open transmission line for an interval T_{on} and then, after a time-lapse T_{off}, the qubit F starts interacting for a time T_{on} in a symmetric fashion. After that, past-future quantum correlations will have transferred to the qubits, even if the qubits do not coexist at the same time. We show that this experiment can be realized with current technology and discuss its utility as a possible implementation of a quantum memory.

DOI: 10.1103/PhysRevLett.109.033602 PACS numbers: 42.50.−p, 03.65.Ud, 03.67.Lx, 85.25.−j

Introduction.—The fact that the vacuumof a quantum field presents quantum entanglement was discovered long ago [1–3], but it was considered a mere formal result until it was addressed from an applied perspective in [4]. Since then, this intriguing property has attracted a great deal of attention as a possible new resource for quantum-information tasks [5–8].

As shown in [4], the entanglement contained in the vacuum of a scalar field can be transferred to a pair of two-level spacelike separated detectors interacting with the field at the same time. Unfortunately, this theoretical result seems to be very difficult to translate into an experiment, even in the context of a trapped-ion simulation [5]. Recently, it has also been proven [9] that the vacuum of a massless scalar field contains quantum correlations [10] between the future and the past light cones. A theoretical method of extraction by transfer to detectors interacting with the field at different times has also been proposed [11], but the particular time dependence of the energy gaps seems extremely challenging from the experimental viewpoint. Another ideal proposal was provided in [12] with a setting that seems even more difficult to tackle experimentally.

On the other hand, circuit QED [13] provides a framework in which the interaction of two-level systems with a quantum field can be naturally considered. The combination of superconducting qubits with transmission lines implement an artificial 1D matter-radiation interaction, with the advantage of a large experimental accessibility and tunability of the physical parameters. Using these features, fundamental problems in quantum field theory hitherto considered as ideal are now accessible to experiment [14]. In particular, the possibility of achieving an ultrastrong coupling regime [15–17] has already been exploited to propose a feasible experimental test of the extraction of vacuum entanglement to a pair of spacelike separated qubits [7].

In this work, we will take advantage of the aforementioned features of circuit QED in the ultrastrong coupling regime in order to propose a realistic experiment for the extraction of past-future correlations [18] contained in the vacuum of a quantum field. We will consider a setup consisting of a pair of superconducting qubits P and F with constant energy gaps in a common open transmission line [Fig. 1(a)]. First, the interaction of P with the vacuum of the field is on for a time interval T_{on} (we call this interval "the past"). Then, P is disconnected from the field during a time T_{off}. Finally, the interaction of F is switched on during T_{on} ("future") while keeping P disconnected. After this procedure, we will show that the qubits can end up in a strongly correlated quantum state, in spite of not having interacted with the field at the same time. We will consider three different spacetime configurations: that the qubits are spacelike or timelike separated and, in the latter case, with or without photon exchange allowed. Perhaps the most surprising result is that, even if photon exchange is forbidden, the qubits can get entangled by a transference of vacuum correlations, as we will show. However, this is not the only interesting aspect of our scheme. If there is

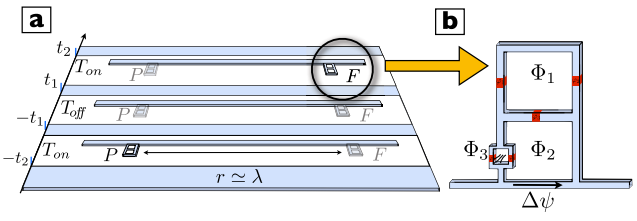

FIG. 1 (color online). Experimental proposal for past-future entanglement extraction. (a) Time evolution of our protocol: the qubit P interacts with the vacuum field ($\Delta\psi$) for a time T_{on}. After a certain time T_{off} with no interaction, a second qubit F interacts with the field getting entangled with the qubit P. (b) Switchable coupling design: a flux qubit (top ring) is coupled to the field $\Delta\psi$ by ways of two loops. Varying the magnetic fluxes Φ_2 and Φ_3, we deactivate the qubit-field coupling.

a certain probability of photon exchange, some classical correlations between the qubits are obviously expected. But it is also remarkable that, due to the peculiarities of our circuit QED setup, these correlations are quantum and attain a high degree without the need of a projective measurement of the field. We stress that our proposal is free of idealized requirements such as gaps with unfeasible time dependences. Our switching scheme is fully within reach of current circuit QED technologies, as shown below.

Our protocol also has an important applied counterpart. As suggested in [11], the extraction of past-future quantum correlations enables its use as a quantum channel for quantum teleportation "in time." We will show how this opens the door to a novel kind of quantum memory in which the information of the quantum state of some ancillary qubit P' is codified in the field during $T_{\rm off}$ and then recovered in F using classical information stored in the past—regardless or whatever happens to P after its interaction with the field.

Theoretical model.—We focus on a setup of circuit-QED with two superconducting qubits P and F interacting via a quantum field. The states $|e\rangle$ and $|g\rangle$ are separated by a constant energy $\hbar\Omega$. The 1-D field, $\Delta\psi(x)$, propagates along an open microwave guide or transmission line that connects them

$$\Delta\psi(x) = i\int_{-\infty}^{\infty} dk\sqrt{N\omega_k}e^{ikx}a_k + \text{H.c.} \tag{1}$$

This field has a continuum of Fock operators $[a_k, a_{k'}^\dagger] = \delta(k-k')$ and a linear spectrum $\omega_k = v|k|$, where v is the propagation velocity of the field. The normalization N and the speed of photons, $v = (cl)^{-1/2}$. depend on the microscopic details such as the capacitance and inductance per unit length, c and l. We will assume qubits that are much smaller than the relevant wavelengths, $\lambda = 2\pi v/\Omega_J$, $(J = P, F)$ and the fixed distance r. Thus, the Hamiltonian, $H = H_0 + H_{\rm I}$ splits into a free part $H_0 = \frac{1}{2}\hbar(\Omega_P\sigma_P^z + \Omega_F\sigma_F^z) + \int_{-\infty}^{\infty} dk\hbar\omega_k a_k^\dagger a_k$ and a pointlike qubit-field interaction:

$$H_{\rm I} = -\sum_{J=P,F} d_J\Delta\psi(x_J)\sigma_J^x = H_{\rm IP} + H_{\rm IF}. \tag{2}$$

Here x_J are the fixed positions of the atoms, and $d_J\sigma_J^x$ comes from a dimensional reduction of the matter—radiation interaction Hamiltonian with two-level atoms and the electromagnetic field analogous—but not fully equivalent—to the Unruh–de Witt model [19].

We choose the following initial state $|\Psi(-t_2)\rangle = |eg0\rangle$, where only P has been excited, in order to analyze the interplay between photon exchange and vacuum correlation effects in the generation of entanglement. According to our past-future scheme [Fig. 1(a)], the system evolves in the interaction picture into the state

$$|\Psi(t_2)\rangle = \mathcal{T}e^{-i\int_{-t_2}^{t_2} dt'/\hbar[\Theta(-t'-t_1)H_{\rm IP}^{(t')} + \Theta(t'-t_1)H_{\rm IF}^{(t')}]}|eg0\rangle, \tag{3}$$

$\mathcal{T}$ being the time ordering operator.

We use the formalism of perturbation theory up to the second order and beyond rotating-wave approximation [7] and trace over the field degrees of freedom to obtain the corresponding two-qubit reduced density matrix ρ_{PF} evaluated at t_2. The degree of entanglement of this X-state can be characterized with the concurrence, which is given by $\mathcal{C}(\rho_{PF}) = 2[|X| - (\sum_k|A_{1,k}|^2\sum_k|B_{1,k}|^2)^{1/2}]$, X standing for the amplitude of photon—real and virtual—exchange and $\sum_k|A_{1,k}|^2$, $\sum_k|B_{1,k}|^2$ for the probability of single-photon emission by P and F, respectively. These terms can be computed—following similar techniques as in [7]—as a function of four dimensionless parameters, $\xi_{\rm on}$, $\xi_{\rm off}$, K_P, and K_F. The first two, $\xi_{\rm on} = vT_{\rm on}/r$, $\xi_{\rm off} = vT_{\rm off}/r$ allow us to discriminate the different spacetime regions. The remaining ones are dimensionless coupling strengths for qubits P and F: $K_J = 4d_J^2N/(\hbar^2 v) = 2(g_J/\Omega_J)^2$. We will restrict to $2K_J\Omega_J t_2 \ll 1$ where our perturbative approach remains valid.

Three different regions emerge from the parameters above [see Fig. 2(a)]. If $T_{\rm off} < r/v$, we discriminate between two possibilities. First, if $2T_{\rm on} + T_{\rm off} < r/v$ (region I), there cannot be real photon exchange, but vacuum correlations—or virtual photon exchange—are allowed at any time. If $2T_{\rm on} + T_{\rm off} > r/v$ (region II), F may start to absorb radiation emitted by P in the past sometime in the future after an interval with no possible absorption (if $T_{\rm on} + T_{\rm off} < r/v$, region IIa) or start to absorb radiation at $t = t_1$ and stop to receive radiation sometime in the future while the interaction is still on $(T_{\rm on} + T_{\rm off} > r/v$, region IIb). Finally, if $T_{\rm off} > r/v$ (region III) F cannot absorb radiation at all, as in region I. The difference between these two regions is that the qubits are spacelike separated in region I and timelike separated in region III. Only in regions I and III are we dealing with a pure effect of transference of the past-future quantum correlations contained in the vacuum. In region II, these correlations may be assisted by a certain probability of photon exchange during a given time interval.

In Figs. 2(b) and 2(c), we show numerical results for the behavior of the concurrence as a function of $T_{\rm on}$ and $T_{\rm off}$, for coupling strengths $g_J/\Omega_J \simeq 0.1$, such as in cutting-edge experiments of ultrastrong coupling in circuit QED [16,17] and accessible values of the qubit's gaps and distance. We note that qubit-qubit entanglement is sizable in region II. However, the existence or not of entanglement in regions I and III depends much on the distance r, as expected. Figures 2(b) and 2(c) show a certain amount of entanglement in regions I and III, entailing a pure transference of vacuum correlations. Remarkably, Fig. 2(c) displays an interesting symmetry between regions I and III: for a given interaction time the entanglement that can

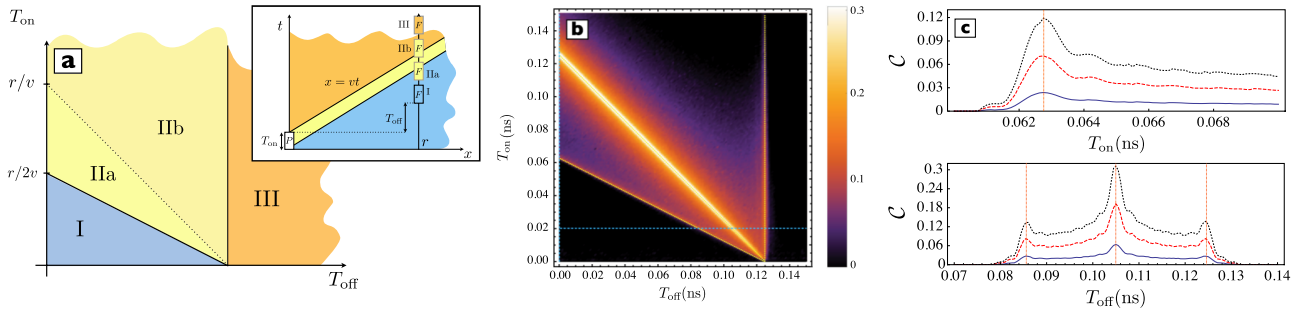

FIG. 2 (color online). (a) Diagram of the different spacetime regions. (b) Concurrence vs. T_{on} and T_{off} for $g = g_P = g_F$, $\Omega = \Omega_P = \Omega_F = 2\pi \times 1$ GHz, $g/\Omega = 0.19$, $r/\lambda = 0.125$. Significant entanglement is generated at both sides of the lines that discriminate between regions. (c) Concurrence vs. T_{on} with T_{off} fixed and vice versa along the blue lines shown in b. The peaks match the position of the region edges. Entanglement is generated in region I and III for three different values of the coupling strength $g/\Omega = 0.09$ (blue, solid), 0.15 (red, dashed), and 0.19 (black, dotted) and $T_{off} = 0$. T_{off} with $T_{on} = 0.02$ ns. Ω and r are the same as in b. The generated entanglement displays a remarkable symmetry for regions I and III.

be generated only by transference of vacuum correlations is the same regardless of whether the qubits are spacelike or timelike separated. This kind of entanglement vanishes as the distance grows (see Fig. 3). In general, entanglement is concentrated around $\Omega_J T_{on} \simeq \Omega_J T_{off} \simeq 1$ and $\xi_{on} \simeq \xi_{off} \simeq 1$. Thus, for qubit distances of the order of λ as in Fig. 3, entanglement shows up in the ns regime but drifts towards shorter times as the distance diminishes, as can be seen in Fig. 2(b).

From the experimental viewpoint, our protocol is equally interesting—and probably more amenable—if the qubits are in region II, although the origin of entanglement generation may seem, at first glance, less theoretically tantalizing. Notice however that even if photon exchange is allowed, our scheme does not include a projective measurement of the field state but a trace over all the field degrees of freedom instead. Then the generation of entanglement immediately after the light-cone crossing is not trivial. For instance, in the standard 3-D matter-radiation Hamiltonian, the atoms would only get classical correlations until much longer times [20]. Indeed, the relationship of the light cone with entanglement without measurements is a peculiarity of circuit QED in the ultrastrong coupling regime, together with the very high degree of entanglement that can be achieved. Thus, even in region II, what we are introducing here is a novel way of entanglement generation, remarkably different from the standard ones, including quantum buses in superconducting cavities [21].

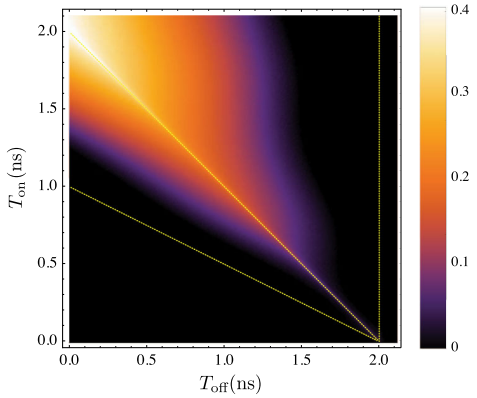

FIG. 3 (color online). Same as in Fig. 2(b) except for $r/\lambda = 2$ and $g/\Omega = 0.09$. Entanglement is restricted to region II for long distances.

We note that in our scheme, concurrence is 0 for $r = 0$. This could seem at variance with the results in [11], where extraction of vacuum correlations to a pair of timelike separated qubits in the same space point is reported. But notice that in [11], a tailor-made time-dependence for the qubit gap ($\propto 1/t$) is introduced, while in our scheme the gap is constant and we just switch on and off the interaction. As a matter of fact, the proposal in [11] exploits a formal analogy [9]—only fulfilled for massless fields—between the past and the future light cones and the left-right Rindler wedges. However, one must be very careful about the extent to which this analogy is valid: while it is possible to think of the vacuum state as entangled in the modes observed by causally disconnected observers in the spacetime left-right wedges [22], it is not clear whether this way of thinking can be transported to the past-future light cones [23]. This was the reason for the singular—and arguably difficult to implement experimentally—energy gap in [11]. However, we have shown that if the qubits are separated by a given distance r and the interaction can be switched on and off fast enough to have finite interaction times, past-future entanglement can be generated between qubits with constant energy gaps.

Circuit QED realization.—We will, thus, focus on the following setting, aiming to test the results shown in Fig. 2. As mentioned in the introduction, it consists of a circuit QED design, where two superconducting qubits interact with the vacuum field in such a way that the interaction is on during a finite time [24] and not at the same time for each qubit [see Fig. 1(a)]. After that, entanglement can be

quantified with quantum state tomography [25]. This qualitative scheme is based on switchable ultrastrong interactions that can be engineered using the design depicted in Fig. 1(b). A superconducting flux qubit—upper three-junction loop—is galvanically coupled to a quantum field $\Delta\psi$ transmission line by means of two additional loops. These extra loops are essential since they will allow us to decouple the qubit from the field in an extremely fast way. We assume the Josephson energy E_{J_i} of each junction to be much greater than its charging energy E_{C_i}. Thus the three-loop Hamiltonian can be reduced to a sum of the inductive energies, $H_J = -\sum_{j=1}^{5} E_{J_j}\cos\varphi_j$, where φ_i is the superconducting phase of the i-th junction.

We can simplify the expression of H_J due to the flux quantization around each closed loop, that imposes: $\sum_j \varphi_j = 2\pi f_i$, $(i = 1, 2, 3)$, where the magnetic frustration parameters $f_i = \Phi_i/\Phi_0$ depend on the external magnetic fluxes Φ_i. Assuming the standard flux qubit configuration, $E_{J1} = E_{J2} = \alpha E_{J3}$, together with $E_{J4} = E_{J5} = \alpha_4 E_{J1}$, the Hamiltonian is

$$H_J = -E_J[\cos(\varphi_1) + \cos(\varphi_2) + \alpha\cos(2\pi f_1 + \varphi_1 + \varphi_2)] - \alpha_{\text{eff}} E_J \cos(2\pi f_{\text{eff}} - \Delta\psi + \varphi_1 + \varphi_2), \quad (4)$$

where $\alpha_{\text{eff}} = 2\alpha_4\cos(\pi f_3)$ and $f_{\text{eff}} = f_1 - f_2 + f_3/2$ is an effective magnetic frustration. After a proper diagonalization, the first line of (4) can be identified with the flux qubit Hamiltonian, whereas the second line represents the qubit-field interaction. The shape of this interaction depends on f_1 and f_2, and the interaction strength given by α_{eff} can be adjusted through f_3. A numerical evaluation of H_J for $(f_1, f_2, f_3) = (0.5, 0.75, 1)$ yields the following effective Hamiltonian in the qubit basis: $H = \int dk\omega_k a^\dagger a + \hbar\frac{\Omega}{2}\sigma_z + \alpha_4 E_J \sigma_x \Delta\psi$, where $\Delta\psi$ is given by (1), and we have included the free Hamiltonian of the field. On the other hand, if we vary the SQUID magnetic flux up to $f_3 = 0.5$, the interaction is switched off, and the Hamiltonian is $H = \int dk\omega_k a^\dagger a + \hbar\frac{\Omega}{2}\sigma_z$. Therefore, with a fast change of f_3 the model given by Eqs. (2) and (3) can be realized in the laboratory. Current technology with Al qubits [14] allows us to vary f_3 in times of less than 0.1 ns and this value can be further improved while remaining below the plasma frequency of the junctions.

Discussion.—The extraction of past-future entanglement from the field to a pair of qubits could be used to implement a device which teleports a quantum state in time—as first suggested in [11]. In other words, we could use the field in the transmission line for building up a novel kind of quantum memory. To achieve this goal, an observer—say, Paula—in possession of P and another qubit P' that she wants to teleport, carries out measurements on her qubits once the interaction is off at $-t_1$. After t_2, an observer—say, Frank—would use the results of Paula's measurements stored as classical information and manipulate F in order to transfer the state of P' to F. The fidelity will be a function of the amount of quantum correlations between P and F. Note that during $T_{\text{of,f}}$ the information of the state of P' is codified in the field, regardless of what happened to P after its interaction and measurement. The information is recovered and embodied in F after its T_{on} and the use of the stored classical bits.

The experimental realization of quantum teleportation has already been achieved in cQED [26] and teleportation with mixed states is considered in [27,28]. As shown in Fig. 3, entanglement is strong enough to consider high-fidelity teleportation for T_{off} of nanoseconds. This interval might, in principle, be even similar to the coherence times of the qubit and the scheme might be used as a quantum memory, provided that the coherence of the field is long enough. In our setting, that time-lapse grows with the qubit spatial separation and the inverse of the qubit gap.

Conclusions.—We have proposed a circuit QED setup in which past-future correlations can be transferred from a quantum field to a pair of qubits P and F, which only interact with the field in the past or the future, respectively. We discuss the possible technological uses of that entanglement extraction and the potential of our scheme to work as a quantum memory.

The authors would like to acknowledge J. J. García-Ripoll, T. C. Ralph, A. Dragan, I. Fuentes, G. Adesso, J. Louko, N. Friis, C. M. Wilson, P. Delsing, P. Forn-Díaz, and J. León for useful comments. This work was supported by Spanish MICINN Projects No. FIS2011-29287 and No. FIS2009-10061 and CAM research consortium QUITEMAD Grant No. S2009-ESP-1594. B. Peropadre and M. del Rey were supported by a CSIC JAE-PREDOC grant. M. del Rey was also supported by Ayuntamiento de Madrid.

*csl@iff.csic.es

[1] W. G. Unruh, Phys. Rev. D **14**, 870 (1976).
[2] S. J. Summers and R. F. Werner, Phys. Lett. **110A**, 257 (1985).
[3] S. J. Summers and R. F. Werner, J. Math. Phys. (N.Y.) **28**, 2448 (1987).
[4] B. Reznik, A. Retzker, and J. Silman, Phys. Rev. A **71**, 042104 (2005).
[5] A. Retzker, J. I. Cirac, and B. Reznik, Phys. Rev. Lett. **94**, 050504 (2005).
[6] S. Marcovitch, A. Retzker, M. B. Plenio, and B. Reznik, Phys. Rev. A **80**, 012325 (2009).
[7] C. Sabín, J. J. García-Ripoll, E. Solano, and J. León, Phys. Rev. B **81**, 184501 (2010).
[8] M. Cliche and A. Kempf, Phys. Rev. A **81**, 012330 (2010).
[9] S. J. Olson and T. C. Ralph, Phys. Rev. Lett. **106**, 110404 (2011).
[10] Although in [9] these correlations are referred to as entanglement, such a wording might not be appropriate since quantum states in past and future belong to Hilbert spaces defined in different simultaneity planes. Nevertheless, quantum correlations of this sort can, in

principle, be extracted to physical systems and exploited as a resource for quantum-information tasks as in the case of typical entanglement.

[11] S. J. Olson and T. C. Ralph, Phys. Rev. A **85**, 012306 (2012).

[12] A. Dragan and I. Fuentes, arXiv:1105.1192.

[13] J. Q. You and F. Nori, Nature (London) **474**, 589 (2011).

[14] C. M. Wilson, G. Johansson, A. Pourkabirian, J. R. Johansson, T. Duty, F. Nori, and P. Delsing, Nature (London) **479**, 376 (2011).

[15] J. Bourassa, J. M. Gambetta, A. A. Abdumalikov, O. Astafiev, Y. Nakamura, and A. Blais, Phys. Rev. A **80**, 032109 (2009).

[16] P. Forn-Díaz, J. Lisenfeld, D. Marcos, J. J. García-Ripoll, E. Solano, C. J. P. M. Harmans, and J. E. Mooij, Phys. Rev. Lett. **105**, 237001 (2010).

[17] T. Niemczyk, F. Deppe, H. Huebl, E. P. Menzel, F. Hocke, M. J. Schwarz, J. J. Garcia-Ripoll, D. Zueco, T. Hümmer, E. Solano *et al.*, Nature Phys. **6**, 772 (2010).

[18] Note that we will use the term "past-future" correlations to refer to a different and more general notion than "time-like entanglement" or "entanglement between the past and the future light cones".

[19] DeWitt, *General Relativity: An Einstein Centenary Survey* (Cambridge University Press, Cambridge, England, 1980).

[20] J. León and C. Sabín, Phys. Rev. A **79**, 012304 (2009).

[21] J. Majer, J. M. Chow, J. M. Gambetta, J. Koch, B. R. Johnson, J. A. Schreier, L. Frunzio, D. I. Schuster, A. A. Houck, A. Wallraff *et al.*, Nature (London) **449**, 443 (2007).

[22] D. E. Bruschi, J. Louko, E. Martín-Martínez, A. Dragan, and I. Fuentes, Phys. Rev. A **82**, 042332 (2010).

[23] To have a mirror interpretation for a plane-wave-like basis like that provided in [9], we would need observers undergoing forbidden trajectories in the spacetime horizontal hyperbolas in past and future light cones.

[24] B. Peropadre, P. Forn-Díaz, E. Solano, and J. J. García-Ripoll, Phys. Rev. Lett. **105**, 023601 (2010).

[25] M. Steffen, M. Ansmann, R. C. Bialczak, N. Katz, E. Lucero, R. McDermott, M. Neeley, E. M. Weig, A. N. Cleland, and J. M. Martinis, Science **313**, 1423 (2006).

[26] M. Baur, A. Fedorov, L. Steffen, S. Filipp, M. P. da Silva, and A. Wallraff, Phys. Rev. Lett. **108**, 040502 (2012).

[27] G. Bowen and S. Bose, Phys. Rev. Lett. **87**, 267901 (2001).

[28] S. Albeverio, S. M. Fei, and W. Yang, Commun. Theor. Phys. **38**, 301 (2002).

3.2 Tunable coupling in arrays of superconducting resonators

In the early works of this Thesis, we have introduced the field of circuit QED as a suitable framework for studying light-matter interaction in the ultrastrong coupling regime. Moreover, we have demonstrated the tunability of the coupling parameter and proposed diverse potential applications to the fields of Quantum Optics and QIP. In this work, we now focus on circuit QED as a testbed for studying the many-body dynamics of low-dimensional quantum systems, as it could be the quantum simulation of Bose-Hubbard model [LH10], extending the ideas of tunable coupling to diverse scenarios.

3.2.1 Summary and discussion of results

In publication P3 we revisit the architecture of coupled superconducting cavities, designing a tunable coupling beween nearest-neighbor resonators. We will see that this can represent a breakthrough for this type of systems, because the dynamical tunability of the resonator coupling makes it possible to engineer a huge variety of photon-photon interactions, or simply cancel the unavoidable cross-talk between neighboring resonators. The main results derived from publication P3 can be summarized as follows:

- We consider the case that usually takes place in a real experiment: two superconducting resonators approach each other in a small region of the space, and get coupled due to an inductive and capacitive crosstalk. Using the tools presented in Chapter 1, we derive a microscopic model for the two coupled resonators and their coupling $g_{\mathrm{i,c}}$. The coupling is *static* and weak, and yields a permanent beam-splitter type interaction $H_{\mathrm{int}} = (g_{\mathrm{c}} + g_{\mathrm{i}})(a^{\dagger}b + ab^{\dagger})$ between the resonators –which eventually can be used for QIP purposes, as we show in publication P4.

- Based on simple quantum circuits such as rf- and dc- SQUID's, we propose two designs that allows for a tunable coupling between resonators (see Fig. 3.3a&b). In the first proposal, the coupling is controlled through the effective Josephson energy of the SQUID, that can be modulated with an external magnetic field. In the second one, the tunability relies on the flux quantization over the SQUID loop, that merges the photon operators $\Delta\psi_1$, $\Delta\psi_2$ in a linear or non-linear way, depending on the value of the external flux $\Phi_{\circlearrowleft}$. With both setups, we manage to completely suppress the geometric crosstalk of the previous configuration.

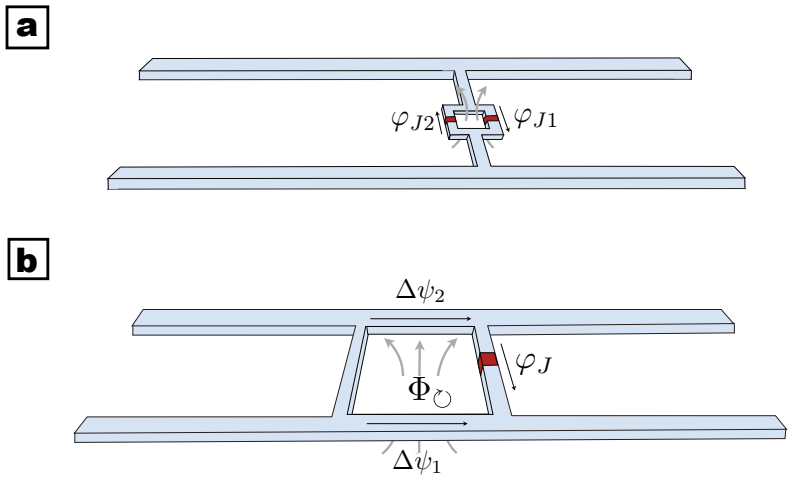

Figure 3.3: a) dc-SQUID and. b) rf-SQUID as tunable couplers between superconducting resonators. Varying the magnetic flux through the SQUID we can boost the coupling the u-strong regime, or fully isolate the resonators.

- On the other hand, the galvanic coupling between resonators provided by the SQUID's, can boost the resonator-resonator interaction to the ultrastrong regime[7]. In doing so, counterrotating terms of the form $H_{\text{int}} = \hbar g(a^\dagger b^\dagger + \text{H.c.})$ can become important and contribute to the dynamics.

- We estimate possible sources of error, as it could be a large size of the superconducting loop, that can jeopardize the switchable capability of our device if the screening parameter $\beta > 1$. We show that for loop sizes $\sim$ 5% of the cavity length, we can still reach the ultrastrong regime, while preserving full control over the coupling g.

For constant magnetic fluxes $\Phi_{\circlearrowleft}$ passing through the SQUID's, we can only couple or decouple the resonators. By contrast, the application of time-dependent fluxes can yield *arbitrary linear couplings* between resonators. This can be done in the following manner[8]:

We consider resonators with different frequencies ω_a, ω_b, subject to an external time-dependent magnetic flux of the form $\Phi_{\circlearrowleft} = \Phi_0 + \delta\Phi\cos\omega t$. By

[7] More precisely, this can be done by means of the techniques presented in the introduction for enhancing the coupling g.

[8] For further details, we refer the reader to the main body of publication P3.

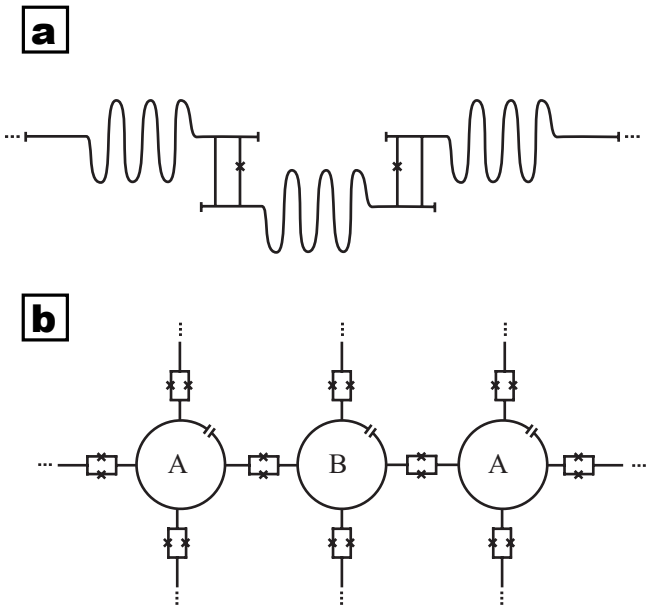

Figure 3.4: Schematic setup of a) one-dimensional array and b) two-dimensional lattice of resonators with tunable nearest neighbors interactions.

properly choosing the frequency ω, we can engineer a two-color driving for the coupling, of the form

$$g(t) = g_1 \cos(\omega_- t + \phi_1) + g_2 \cos(\omega_+ t + \phi_2), \tag{3.1}$$

where $\omega_\pm = \omega_a \pm \omega_b$, and where the driving weights g_1, g_2 and the phases ϕ_1, ϕ_2 can be controlled with high precision. The effective dynamics of the resonators under this coupling parameter is given by

$$H_{\text{eff}} = g_1 a^\dagger b e^{i\phi_1} + g_2 a^\dagger b^\dagger e^{i\phi_1} + \text{H.c.}, \tag{3.2}$$

that is, a linear combination of red and blue sidebands. By properly choosing the drive parameters, we can explore very rich and different physics, ranging from quantum optics, to condensed matter, or quantum simulations. To this end, our proposals can be easily cascaded into 1D and 2D networks of resonators [LDM+12], as it is shown in Fig.3.4a&b.

Below we summarize the most important applications:

- Microwave Quantum Optics:

  - Tunable microwave beam splitters: by setting $g_2 = 0$ and modulating g_1 in (3.2), we control the transference of excitations in the network in a controlled way. This is highly desirable for future realizations of quantum computing with microwave flying photons.
  - Frequency conversion of photons and generation of squeezed states through the blue sideband, as well as parametric generation of photons, by setting $g_1 = 0$, $g_2 \neq 0$ in (3.2).

- Condensed Matter:
  - The study of dynamical quantum phase transitions in harmonic and anharmonic models[9], by adiabatically sweeping the flux across a quantum critical point.
  - Thermalization and propagation of excitations after a quench. A sudden change in the external flux takes the system out of equilibrium, and we can study how an excitation in the chain relaxes.

- Quantum Simulations:
  - Simulation of spin-like Hamiltonians and Bose-Hubbard models, with or without photon pairing,

$$H = \sum_{\langle ij \rangle} t_{ij} a_i^\dagger a_j + U \hat{n}_i(\hat{n}_i - 1), \quad H = \sum_{\langle ij \rangle} t_{ij} a_i^\dagger a_j^\dagger + \text{H.c.} + U \hat{n}_i(\hat{n}_i - 1).$$

  - Simulation of abelian gauge fields by creating non-trivial hopping terms $t_{ij} = |t_{ij}| e^{i\theta_{ij}}$, which simulate the dynamics of magnetic fluxes on the lattice plaquettes [KHHG10, NKG11].

To sum up, in publication P3 we demonstrate the tunability of coupled superconducting resonators via galvanic coupling with SQUID's. We show that it is possible to go from ultrastrong coupling, to perfect decoupling. Moreover, we propose arbitrary linear and nonlinear couplings in arrays of resonators, as well as countless applications to the fields of microwave quantum optics and condensed matter physics. We envision that all these proposals can be realized in the near future. In particular, in the next work we present a first experiment on coupled resonators, which is a proof-of-principle towards multiresonator experiments.

[9] Adding elements such as qubits and Josephson junctions to the resonators, can produce a non-linear Kerr-type interactions.

3.2.2 Ultrafast beam splitters from superconducting resonators:

As we discussed in P3, beam splitters are ubiquitous components in the realization of all-optical quantum information processing, as they can implement one-qubit and two-qubit KLM gates[10] [KLM01]. For a quantum computation to be successful, a considerable number of these gates must be carried out before the information is lost by decoherence. It is then desirable to build up beam splitters that carry out computations in very fast times. We have shown that this can be done in the framework of circuit QED by coupling superconducting resonators.

In particular, in publication P4 we show that geometrically coupled resonators can implement ultrafast microwave beam-splitters, with gate times[11] that are much faster than the resonators decay rate. –and therefore many gate operations could be performed. The main results of this work can be summarized as follows:

- We propose a *distributed coupling* model[12] that brings the geometric coupling to the ultrastrong regime. As a consequence, we obtain undesired nonlinear effects due to the counterrotating terms in the Hamiltonian

$$H/\hbar = \omega_0(a^\dagger a + b^\dagger b) + g_{\mathrm{BS}}(a^\dagger b + a b^\dagger) + g_{\mathrm{TMS}}(a^\dagger b^\dagger + a b), \qquad (3.3)$$

  where $g_{\mathrm{BS}} = g_{\mathrm{i}} + g_{\mathrm{c}}$, and $g_{\mathrm{TMS}} = g_{\mathrm{i}} - g_{\mathrm{c}}$ arise from the superposition of both capacitive and inductive couplings.

- We look for asymmetric designs that can suppress the effect of the counterrotating terms, by studying the dependence of g_{i} and g_{c} with the physical coupling positions of the layout. In particular, we find that it is possible to achieve a configuration such that $g_{\mathrm{c}} = g_{\mathrm{i}}$, and thus $g_{\mathrm{TMS}} = 0$, yielding a pure beam-splitter interaction.

- We have experimentally validated our model, by analyzing several samples with different geometries. The most important results are:

  – Spectroscopic measurements in transmission for the coupled resonators shows asymmetrical splitting of the normal modes $w_\pm$

[10] Knill-Laflamme-Milburn or KLM gates [KLM01], are heralded C-NOT gates for scalable quantum computation with photons using solely linear devices such as beam splitters, ancillary photons and measurements.

[11] The gate time is defined as the time needed to perform a quantum operation, and is given by the inverse of the coupling $t = 2\pi/g$. In publication P4 this time is about $1 - 10$ ns.

[12] In distributed coupling models, resonators approach each other in a large region of the space, comparable with their lengths themselves.

with respect to the bare resonator frequencies w_0. This is a clear signature of the presence of counterrotating terms in the Hamiltonian (3.3).

- We obtain a beam splitter coefficient $g_{\mathrm{BS}} \simeq 20\%$ regardless the geometry of the layouts, while g_{TMS} depends linearly on it, according to the proposed model. In particular, for the analyzed samples we demonstrated a tunability of the coupling ratio $g_{\mathrm{TMS}}/g_{\mathrm{BS}}$ between 16% and 43%.
- By extrapolation of our results, we show that it would be possible to reach a pure ultrastrong beam-splitter interaction (this is, $g_{\mathrm{BS}}/\omega_0 \simeq 20\%$ and $g_{\mathrm{TMS}} = 0$), as well as standard ultrastrong interaction between resonators in absence of galvanic coupling (with $g_{\mathrm{BS}}/\omega_0 \simeq 20\%$, $g_{\mathrm{TMS}}/\omega_0 \simeq 13\%$).

In summary, we have proposed a fast beam splitter with geometrically coupled resonators. Based on a distributed coupling model, we have shown that the interaction can be boosted to the ultrastrong regime. Moreover, we have studied the role that the coupling position plays in the resonator dynamics. In this sense, we have shown for different layouts a significant on-off ratio in the two-mode squeezer term. These results are a proof-of-principle of the viability of ultrafast beam splitters for quantum computing and quantum simulations with photons.

3.2.3 Publication 3: Tunable coupling engineering between superconducting resonators: from sidebands to effective gauge fields B. Peropadre, D. Zueco, F. Wulschner, F. Deppe, A. Marx, R. Gross, J.J. García-Ripoll. Phys. Rev. B 87, 134504 (2013)

PHYSICAL REVIEW B **87**, 134504 (2013)

Tunable coupling engineering between superconducting resonators: From sidebands to effective gauge fields

Borja Peropadre,[1] David Zueco,[2,3] Friedrich Wulschner,[4] Frank Deppe,[4,5] Achim Marx,[4]
Rudolf Gross,[4,5] and Juan José García-Ripoll[1]

[1]*Instituto de Física Fundamental, IFF-CSIC, Calle Serrano 113b, E-28006 Madrid, Spain*

[2]*Instituto de Ciencia de Materiales de Aragón y Departamento de Física de la Materia Condensada, CSIC–Universidad de Zaragoza, Calle de Pedro Cerbuna 12, E-50009 Zaragoza, Spain*

[3]*Fundación ARAID, Paseo María Agustín 36, E-50004 Zaragoza, Spain*

[4]*Walther-Meißner-Institut, Bayerische Akademie der Wissenschaften, D-85748 Garching, Germany*

[5]*Physik Department, Technische Universität München, James-Franck-Straße, D-85748 Garching, Germany*

(Received 6 November 2012; revised manuscript received 19 February 2013; published 5 April 2013)

In this work we show that a tunable coupling between microwave resonators can be engineered by means of simple Josephson junctions circuits, such as dc and rf superconducting quantum interference devices. We show that by controlling the time dependence of the coupling it is possible to switch on and off and modulate the cross-talk and boost the interaction towards the ultrastrong regime, as well as to engineer red and blue sideband couplings, nonlinear photon hopping, and classical gauge fields. We discuss how these dynamically tunable superconducting circuits enable key applications in the fields of all-optical quantum computing, continuous-variable quantum information, and quantum simulation—all within the reach of the state of the art in circuit-QED experiments.

DOI: 10.1103/PhysRevB.87.134504 PACS number(s): 42.50.Pq, 03.67.Lx, 85.25.−j

I. INTRODUCTION

The field of circuit quantum electrodynamics (circuit QED) studies the interaction between artificial atoms and artificial photons,[1,2] both of them implemented with the same technology: superconducting circuits cooled to millikelvin temperatures. A key feature of these systems is that, based on the same microscopic model, both the photonic degrees of freedom and the artificial atoms have similar energy scales and may interact very strongly. Hence, they show effects which are beyond those explored in the optical domain. A paradigmatic example is the failure of the rotating-wave approximation when the qubit-photon coupling approaches the qubit and photon energies.[3,4] Aside from the development of qubits and the control of their interactions,[5–7] circuit QED has recently started to focus on the photons themselves, mostly in the context of two different experimental configurations. In the first type of setup, cavities are replaced with open transmission lines and propagating microwave photons that move and interact with localized qubits. This allows us to study one-dimensional artificial QED, atom-light interaction,[8] electromagnetically induced transparency,[9] causality,[10] and quantum metamaterials[11–15] and to implement photodetectors[16–18] and routers.[19] The other type of setup is based on polariton physics:[20,21] by coupling multiple cavity-qubit systems it is possible to build lattices on which dressed photons hop and interact, either attractively or repulsively, implementing Hubbard-type models or spin Hamiltonians.[22,23] This gives rise to well-known models, such as the Tonks-Girardeau gas;[24] however, the architecture based on superconducting cavities and Josephson junctions also allows for the exploration of new phenomena, such as gauge fields and frustration.[25]

In this work we reconsider the architecture of coupled superconducting cavities, designing a tunable coupling between nearest-neighbor resonators. The setup that we have in mind consists of an array of linear resonators, *directly connected* through different types of Josephson junction (JJ) circuits (see Fig. 4). The fixed circuit structure is associated with static, geometry-dependent capacitive and inductive couplings between the resonators, while the interactions created by the JJ circuits can be tuned in amplitude, phase, and form by external magnetic fields.

The coupling elements in this coupled-resonator framework can be operated in two ways: (i) with a stationary configuration of magnetic fields that determines the associated coupling matrix between oscillator modes or (ii) with a periodic multicolor driving that allows for engineering a variety of *photon-photon interactions*, from red and blue sidebands to gauge fields, passing through correlated photon hopping and Kerr nonlinearities, or simply canceling the usual cross-talk between resonators. In particular, we show how to engineer couplings of the form $\eta_1 a^\dagger b + \eta_2 ab + \text{H.c.}$ between any two resonators a and b, with adjustable strengths $\eta_{1,2}$ and possibly complex phases in front of each term.

We must remark that our coupling circuits are based on superconducting quantum interference devices (SQUIDs), those ubiquitous devices which are used for anything from measuring magnetic fields and qubits to parametrically controlling microwave transmission lines.[26,27] Despite the widespread use of SQUIDS, the framework that we introduce here combines in a single design original solutions to many different problems that were addressed only individually in previous works. First of all, the design we present here is *nondispersive*. This is in contrast to other proposals based on dispersive couplings via qubits[28–30] and disconnected SQUID loops.[31] While in those works the coupling is limited by the dispersive condition, the setup in this work allows us to reach the *strong- and ultrastrong-coupling regimes*—larger than the corresponding decay rates or comparable to the cavity frequencies, respectively. This demands on our side a careful microscopic derivation that merges ideas from the work of

Bourassa *et al.*[32] with the field of coupled cavities. Second, our SQUID coupling works between separate resonators, allowing for *scalable architectures* with one- and two-dimensional configurations as shown in Fig. 4. This is in contrast with other works that showed coupling between different modes of the same resonator,[33–36] or which couple a few nonlinear resonators.[37] Third, unlike other scalable proposals based on circulator-type devices,[25,38] our setup is minimalistic and relies on a very robust circuit which is not sensitive to charge noise and does not require a precise balance of junctions. Finally, our design achieves full tunability, regardless of other elements that may coexist with the cavities, such as qubits or magnetic impurities.

As short-term applications of this work we would like to address two fields. The first one has been sketched above: by tuning the coupling between different cavities it is possible to tune the lattice topology, the coupling strength, and even the phase of the hopping terms in polariton arrays. This nicely complements existing proposals which show how to tune the photon nonlinearity by manipulating the qubit inside the cavity[22] and gives access to effective gauge fields without relying on fragile coupling elements.[25] The second type of application points along the line of quantum information and the manipulation of continuous-variable states. By means of the coupling circuits in this toolbox one may implement any nearest-neighbor quadratic Hamiltonian with any time dependence and geometry, as far as it is embeddable in a two-dimensional (2D) manifold. Notice that our implementations are limited to a frequency scale which is well below the plasma frequency of the SQUID, where it behaves as a passive device. However, this is always true for the purposes of this work.[39] This Hamiltonian can be used to implement interesting states, such as two-dimensional continuous-variable Gaussian states,[40] whose tomography could be supplemented by embedded qubits[41] or moving probes.[42]

The paper is organized as follows. In the first part (Sec. II) we study two superconducting resonators that are close together and subject to a mutual inductive and capacitive interaction. Using the Lagrangian quantization, we will show that, in both the weak- and strong-coupling regimes, the geometric cross-talk gives rise to a constant beam-splitter type of interaction. In the second part of this work (Sec. III) we propose two quantum circuits that dynamically tune the inductive coupling between the resonators. The first one is a SQUID which is galvanically coupled to two resonators. The second one uses instead two coupling wires, creating an interference device between resonators. We will discuss both models analytically, demonstrating that they can tune and switch off the overall resonator-resonator coupling. In Sec. III C we study the validity of our designs under realistic experimental conditions, estimating the coupling strengths that can be attained in current experiments. In Sec. IV A we consider the situation of a time-dependent resonator coupling. We show that a periodic modulation of the coupling makes it possible to engineer sidebands not only in a nonperturbative fashion,[43] but also in a controlled way, tuning the strength and phase of both the rotating and counterrotating terms. Finally, in Sec. IV C we summarize our results and suggest a large set of potential applications, ranging from quantum information to quantum simulation.

II. STATIC COUPLING

In this section we derive the Hamiltonian that rules the dynamics of two coupled superconducting stripline resonators, and give a general expression for the different coupling constants that arise from the model. First we consider the simplest case of coupling, caused by the mutual inductance and mutual capacitance due to the spatial proximity of the resonators. Since the coupling is time independent and determined by the detailed spatial arrangement of the resonators, we refer to it as static geometric coupling. The discussion of this interaction is done for a particular configuration of parallel resonators, but the objective is just to exemplify how this coupling manifests itself as a beam-splitter interaction.

Consider two superconducting stripline resonators of length $2l$, as depicted in Fig. 1(a). In this particular layout, the coupling occurs mainly within a middle section of length $2l_c$, where the resonators approach each other. Assuming that the cross-talk is given by the mutual inductance l_m and mutual capacitance c_m induced in this middle region,[44,45] we can write down the following Lagrangian density:

$$\mathcal{L} = \sum_{i,j} \int_{-l}^{l} \left[\frac{\hat{c}_{ij}}{2} \dot{\phi}_i \dot{\phi}_j - \left(\frac{1}{2\hat{l}} \right)_{ij} \partial_x \phi_i \partial_x \phi_j \right] dx, \tag{1}$$

where both the flux fields $\phi_i(x)$ and the capacitance $\hat{c}$ and inductance matrices $\hat{l}$, depend on the position along the transmission line:

$$\hat{c} = c_0(x) + c_m(x)(\mathbb{I} - \sigma_x), \tag{2}$$

$$\hat{l} = l_0(x) + l_m(x)\sigma_x, \tag{3}$$

where σ_x is the Pauli matrix. A full derivation of Eq. (1) can be obtained from the lumped circuit equivalent of the striplines [Fig. 1(b)] and it is thoroughly discussed in Appendix A.

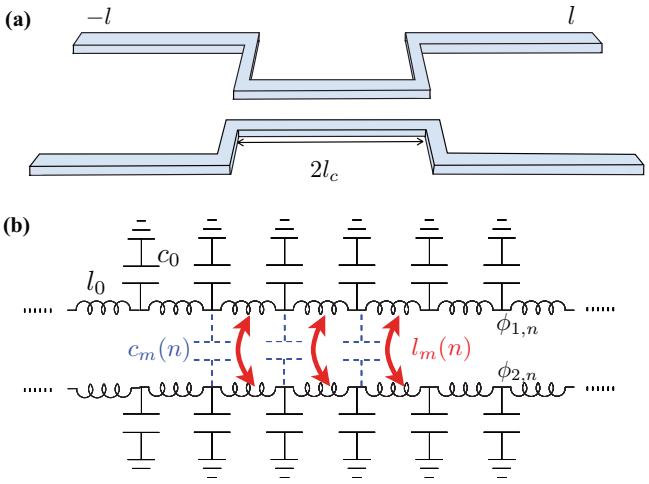

FIG. 1. (Color online) (a) Sketch of the geometrical arrangement of the two coupled superconducting stripline resonators of length $2l$. A finite interaction is present only in the coupling region of length $2l_c$ and is negligible elsewhere. (b) Schematics for the lumped circuit equivalent. We explicitly draw the mutual capacitances (dashed blue lines) and the mutual inductive coupling (red arrows). The node flux ϕ_n is also indicated.

For the sake of simplicity, we will consider the capacitance and inductance per unit length of each line, $c_0(x)$ and $l_0(x)$, to be constant, and use piecewise-constant functions for the mutual inductance and capacitance:

$$c_m(x) = \begin{cases} c_m, & |x| < l_c, \\ 0 \quad \text{otherwise}, \end{cases} \qquad l_m(x) = \begin{cases} l_m, & |x| < l_c, \\ 0 \quad \text{otherwise}. \end{cases} \tag{4}$$

We derive a normal-mode expansion for the flux $\phi_j(x,t) = \sum_n q_{j,n}(t)u_n(x)$ in each resonator $j = 1,2$. In what follows we restrict ourselves to the fundamental mode of each resonator with frequency ω_0 and total capacitance $C_r = \int_{-l}^{l} c_0(x)dx$. This is always true if we remain in the strong-coupling limit, where $g \ll \omega_1 - \omega_0$, or we work with zero-mode resonators, like the ones used in Ref. 4. Within this subspace and mode expansion, the interaction term gives rise to off-diagonal terms, as expected from an interaction between two cavities, but also diagonal terms that induce a renormalization (dressing) of the oscillator frequencies. This dressed resonance frequency is

$$\omega = \omega_0 \sqrt{\frac{1+C}{1+2C}\left(1 + \frac{1}{\nu}\frac{L^2}{1-L^2}\right)}, \tag{5}$$

expressed in terms of two *overlap* integrals

$$\Delta_1 = \int_{-l_c}^{l_c} [u_0(x)]^2\, dx, \quad \Delta_2 = \int_{-l_c}^{l_c} [\partial_x u_0(x)]^2 dx, \tag{6}$$

where $C = c_m\Delta_1/C_r$, $L = l_m/l_0$, and $\nu = \omega_0^2 C_r l_0/\Delta_2$ is a geometric factor.

We finally proceed with the quantization of this model, introducing the oscillator length $a_0 = \sqrt{\hbar(1+C)/C_r\omega(1+2C)}$. We express the phase-space operators in terms of the Fock operators $q_j = a_0(a_j + a_j^\dagger)/\sqrt{2}$ and $p_j = i\hbar(a_j^\dagger - a_j)/\sqrt{2}a_0$. This leads to

$$H = \hbar\omega \sum_{j=1,2} a_j^\dagger a_j - \hbar g_c(a_1^\dagger - a_1)(a_2^\dagger - a_2) - \hbar g_i(a_1^\dagger + a_1)(a_2^\dagger + a_2). \tag{7}$$

The coupling constants g_c and g_i account for the static capacitive and inductive contributions to the coupling, respectively,

$$g_c = \frac{\omega_0}{2}\sqrt{\frac{C^2}{(1+C)(1+2C)}\left(1 + \frac{1}{\nu}\frac{C^2}{1-C^2}\right)}, \tag{8}$$

$$g_i = \frac{\omega_0}{2}\frac{1}{\nu}\frac{L}{1-L^2}\sqrt{\frac{1+C}{1+2C}\frac{1}{1+\frac{1}{\nu}\frac{L^2}{1-L^2}}}. \tag{9}$$

The usual limits in quantum optics correspond to the weak-coupling and strong-coupling regimes. In both of them $g_{c,i}/\omega_0 \ll 1$, so that the frequency renormalization becomes negligible (provided that $C, L \ll 1$). We can then invoke the rotating-wave approximation (RWA) and transform (7) to the beam-splitter model,

$$H \simeq \hbar\omega_0 \sum_{j=1,2} a_j^\dagger a_j - \hbar(g_i - g_c)(a_1^\dagger a_2 + a_2^\dagger a_1). \tag{10}$$

Note how the resulting Hamiltonian can be interpreted as an exchange or *hopping* of excitations between modes, similar to optical lattice and tight-binding models.

This type of static geometric coupling is implicit in the experimental configurations of coupled-cavity models,[20,21] although previous designs have inclined to consider a capacitive coupling taking place at the electric field nodes (current antinodes) of the resonator,[22,25,38] sometimes enhanced by an additional JJ circuit.[25,38]

III. TUNABLE COUPLING

In this section we study alternative mechanisms for coupling two or more linear resonators. On the one hand we aim at a larger coupling strength, and on the other hand we wish to achieve real-time tunability of the couplings. For both goals it will be advantageous to rely on inductive rather than capacitive coupling. First of all, the inductive coupling realized by JJs and loops intersected by JJs (e.g., SQUIDs) can be tuned by an applied magnetic field varying the magnetic flux threading the JJs or loops. Second, and equally important, inductive interactions can be enhanced, profiting both from the kinetic inductance of thin superconducting films and from embedded junctions working in the linear regime.[32] Based on the two previous ideas, we envision the two coupling elements sketched in Fig. 2. We will study these designs analytically, deriving expressions for the effective interactions and coupling strengths.

A. The SQUID as a coupler

Given the large inductance provided by the Josephson junctions, one could naively think of connecting both cavities with a superconducting wire interrupted by a Josephson junction. In doing so one would achieve a static ultrastrong coupling. However, for tuning the Josephson inductance of a single junction we have to generate a magnetic flux of the order of a flux quantum threading the junction area. Due to the small junction area unpractically large magnetic fields would be required. Fortunately, we can design a much better tunability by using a SQUID configuration, as depicted in

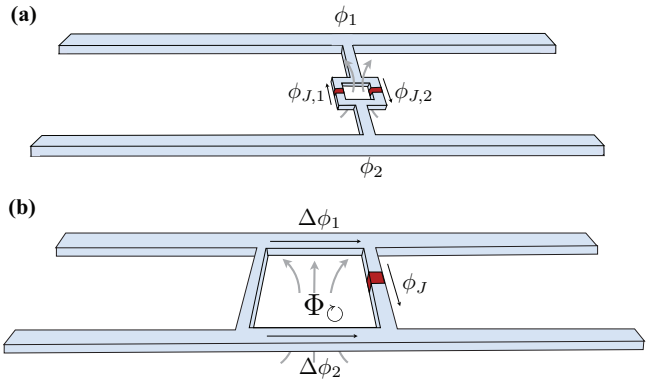

FIG. 2. (Color online) Architectures leading to a tunable microwave beam splitter. (a) A dc SQUID (superconducting loop intersected by two Josephson junctions) mediates the coupling between two stripline resonators (ground planes not shown). The established pointlike contact between the resonators takes the coupling to the ultrastrong domain. (b) A superconducting ring intersected by a Josephson junction now partially shares its branches with the cavities, improving the switching capability.

Fig. 2(a). Since the SQUID loop area is much larger than the junction area, much smaller control fields are required. Note that the use of the dc SQUID to achieve fast tunability is quite common in circuit QED. For instance, they have been used to very rapidly change the effective length of resonators[46] to observe the dynamical Casimir effect,[26,27] and through similar principles they underlie the basis of recent Josephson parametric amplifiers.[47–49] More related to our work, SQUIDs have also been suggested as a coupling element for flux qubits,[50] using an external flux to control their mutual inductance. However, the peculiarities of our setup, which deals with continuous variables and has subtle differences, merits a separate discussion below.

A short line with the SQUID as depicted in Fig. 2(a) represents a small contribution to the original Lagrangian density (1). Following Ref. 51 we compute $\mathcal{L}_t = \mathcal{L} + \mathcal{L}_{\rm SQUID}$ with

$$\mathcal{L}_{\rm SQUID} = \sum_{k=1}^{2} \frac{C_{J,k}}{2}\dot{\phi}_{J,k}^2 + E_{J,k}\cos\left(\frac{2\pi\phi_{J,k}}{\Phi_0}\right), \qquad (11)$$

where $\phi_{J,k}$ represent the flux differences along the junctions $k = 1,2$. We use fluxoid quantization along the SQUID loop, $\phi_{J,1} + \phi_{J,2} + \Phi_{\circlearrowleft} = n\Phi_0$, to express the Lagrangian in terms of the variables $\phi_\pm = \frac{1}{2}(\phi_{J,1} \pm \phi_{J,2})$ and the total flux enclosed by the loop, $\Phi_{\circlearrowleft}$. For simplicity, we assume $\Phi_{\circlearrowleft} \simeq \Phi_{\rm ext}$, that is, we are neglecting the additional flux generated by the circulating loop current. This is equivalent to restricting our discussion to screening parameters $\beta_L = 2\pi L I_c/\Phi_0 < 1$ as discussed in more detail below. Here, L is the loop inductance and I_c the critical current of the Josephson junctions. If the SQUID is symmetric, $C_{J,1} = C_{J,2}$ and $E_{J,1} = E_{J,2}$, the coupling becomes $E_{\rm eff}\cos(\pi\phi_-/\Phi_0)$, with an effective Josephson coupling energy that depends on the flux threading the SQUID loop,

$$E_{\rm eff} = 2E_J\cos(\pi\Phi_{\circlearrowleft}/\Phi_0 a). \qquad (12)$$

The voltage-phase relation $\dot{\phi}_- = \dot{\phi}_1(x) - \dot{\phi}_2(x)$ allows us to express ϕ_- in terms of the voltages at the edges of the connecting wire. In the linear limit of small fluxes, i.e., small photon number (see Appendix B), we can write a quadratic coupling between fields,

$$\mathcal{L}_{\rm SQUID} \simeq C_J(\dot{\phi}_1 - \dot{\phi}_2)^2 - \frac{2\pi^2 E_{\rm eff}}{\Phi_0^2}(\phi_1 - \phi_2)^2, \qquad (13)$$

which by means of the normal-mode decomposition adopts the form of Eq. (7). The cross-term of Eq. (13) adds up to the static inductive coupling (9), making it tunable. This tunability relies on the fact that the Josephson energy $E_{\rm eff}$ is flux dependent,[52] and thus

$$g_i = g_i^{\rm static} + \frac{4\pi^2\hbar}{\Phi_0^2 C_r\omega}E_J\cos(\pi\Phi_{\circlearrowleft}/\Phi_0) \qquad (14)$$

in Eq. (10) can be changed in magnitude and sign. For an appropriate value of the external flux (close to $\Phi_{\circlearrowleft} = \Phi_0/2$ if $|g_c| \ll |g_i|$) we can fully deactivate the coupling. Note that in this treatment the SQUID variables are not independent and introduce no new modes: the fluxoid quantization allows us to express them in terms of the cavity modes. This topic and the linearization are discussed in more detail in Appendix B 3 using exact diagonalizations.

We finally note that our setup is robust against small differences in the two junction energies, $E_{J1,2} = E_J(1 \pm \varepsilon)$. In this case one can still expand $\phi_{1,2} = \frac{1}{2}\Phi_{\circlearrowleft} \pm \phi_-$, linearizing around $\phi_- \simeq 0$ to obtain

$$\mathcal{L}_{\rm SQUID} \pm 2\varepsilon E_J\sin(\pi\Phi_{\circlearrowleft}/\Phi_0)\frac{2\pi\phi_-}{\Phi_0}. \qquad (15)$$

The linear term in this equation amounts just to a displacement of the oscillators and does not add up to the total coupling, preserving the tunability of the setup. We will use this idea in the following setup.

B. Superconducting ring coupler

The second design is shown in Fig. 2(b). It consists of a superconducting ring interrupted by a single Josephson junction. Since both resonators share a branch of the loop that couples them, the Lagrangian acquires new contributions with the kinetic inductance of the superconductor.[32] This kinetic coupling can be very strong, while still retaining the switching capability due to the fluxoid quantization inside the loop, similar to previous designs for superconducting qubits.[53]

Note that in comparison to previous studies of SQUID-mediated entanglement between cavities,[54–56] this setup is much simpler because there are no degrees of freedom for the SQUID: the flux through the SQUID is the same as the flux to the cavities. Additionally, this design profits from the stronger interaction due to the galvanic coupling of the circuit elements.

Our derivation is based on two nonessential constraints. The first one is that the loop is small enough for its self-inductance to be neglected ($\beta_L \ll 1$). The second one is that the wire without junction touches the resonators at points where the flux of the coupled modes is zero,[57] $u_0(x_1) = 0$. Under these circumstances the coupling term reads

$$\mathcal{L}_{JJ} = \frac{C_J}{2}\dot{\phi}_J^2 + E_J\cos\left(\frac{2\pi\phi_J}{\Phi_0}\right). \qquad (16)$$

The fluxoid quantization inside the loop, $\Delta\phi_2 - \Delta\phi_1 + \phi_J = -\Phi_{\circlearrowleft}$, allows us to get rid of the flux variable ϕ_J and rewrite the coupling in terms of the branch fluxes $\Delta\phi_{1,2}$,

$$\mathcal{L}_{JJ} = \frac{C_J}{2}(\Delta\dot{\phi}_1 - \Delta\dot{\phi}_2)^2 + E_J\cos\left[\frac{2\pi(\Delta\phi_1 - \Delta\phi_2 + \Phi_{\circlearrowleft})}{\Phi_0}\right]. \qquad (17)$$

At this point we will repeat the linearization of the cosine, much as in Eq. (13). However, now the Taylor expansion will depend on the external flux $\Phi_{\circlearrowleft}$, producing linear and quadratic contributions of different magnitude. We start with the normal-mode decomposition of the branch fluxes and restrict ourselves to the lowest-energy modes

$$\Delta\phi_j = \phi_j(x_2) - \phi_j(x_1) \simeq q_{j,0}\partial_x u_0(x)|_{x_1}\Delta x. \qquad (18)$$

Substituting these terms in Eq. (17) produces the quadratic Lagrangian for the fundamental modes,

$$L_{JJ} = \frac{1}{2}\sum_{j=1,2}\left(\alpha_J \dot{q}_j^2 - \beta_J q_j^2\right) + \gamma_J(q_1 - q_2) - \alpha_J \dot{q}_1\dot{q}_2 + \beta_J q_1 q_2. \quad (19)$$

The expressions for all coefficients can be computed from first principles,

$$\alpha_J = C_J\,[\partial_x u_0(x=0)]^2\,\Delta x^2, \quad (20)$$

$$\beta_J = E_J\frac{4\pi^2}{\Phi_0^2}\,[\partial_x u_0(x=0)]^2\,\Delta x^2\cos\left(\frac{2\pi\,\Phi_{\circlearrowleft}}{\Phi_0}\right), \quad (21)$$

$$\gamma_J = E_J\frac{2\pi}{\Phi_0}\,[\partial_x u_0(x=0)]\,\Delta x\sin\left(\frac{2\pi\,\Phi_{\circlearrowleft}}{\Phi_0}\right), \quad (22)$$

where we have assumed that the superconducting loop is placed around $x = 0$. Of these terms, γ_J is a linear displacement of the cavity eigenmodes and does not transfer energy. The capacitive and inductive terms α_J and β_J are the only ones that contribute to the intercavity coupling g_c and g_i, and to the frequency renormalization. More precisely, we obtain the model (7) with mode frequency

$$\omega = \omega_0\sqrt{1 + \frac{\beta_J}{C_r\omega_0^2}} \quad (23)$$

and coupling strengths

$$g_i = g_i^{\text{static}} + \frac{\beta_J}{2C_r\omega}, \quad g_c = g_c^{\text{static}} + \frac{\alpha_J C_r\omega}{2}. \quad (24)$$

In general we will find that for a junction that works in the flux regime the term β_J dominates all other contributions. But even without this assumption, it is true that while g_c is fixed, the value of g_i depends entirely on β_J and can be changed in magnitude and sign, either enhancing the strength of the beam-splitter coupling (10), or switching it off entirely for a value of $\Phi_{\circlearrowleft} \simeq \Phi_0/4$.

While the coupling strength grows with the loop size Δx, we cannot make it arbitrarily large because then we are no longer allowed to neglect the additional flux ϕ_L caused by the circulating loop current due to the increasing value L of the self-inductance of the loop.[58] In this case the total flux threading the loop is given by the sum of the external flux Φ_{ext} and the flux Φ_L. However, as explained in Ref. 58, Chap. 8.4, provided that

$$\beta_L = \frac{2\pi L I_c}{\Phi_0} < 1 \quad (25)$$

we can ensure that the $\Phi_{\circlearrowleft}$ versus Φ_{ext} dependence is single valued, allowing us full tunability of the coupling. This condition means that the maximum loop current I_c cannot generate more than a single flux quantum. It restricts us to loop sizes of around 5% of the resonator length. We now study various methods to increase the coupling strength while preserving the condition above.

C. Estimation of the coupling strength

We are interested in an upper bound for the coupling strength g. More precisely we would like to access both the strong- and ultrastrong-coupling regimes. Strong coupling means that it is possible to observe Rabi oscillations between the two cavities because the coupling g is larger than the resonator decay rate κ. On the other hand, ultrastrong coupling occurs when the RWA fails, which in this case implies that the number of photons in the ground state, which is proportional to g/ω, approaches 1.

Looking at the first proposal [see Fig. 2(a) and Sec. III A] we note that the maximum coupling is reached for an external flux $\Phi_{\circlearrowleft} = n\Phi_0$ threading the SQUID loop, and thus yielding

$$g_i \simeq \frac{4e^2}{2C_r}\frac{E_J}{\hbar^2\omega}|u_0(x)|^2 = \frac{\pi I_c}{\Phi_0}Z|u_0(x)|^2, \quad (26)$$

where I_c is the critical current of the junction, Z is the resonator impedance, and the eigenmode $u_0(x)$ satisfies $0 < |u_0(x)| < \sqrt{2}$. To preserve the power field expansion, we suppose the SQUID to be built at a position such that $|u_0(x)| \leqslant 0.1$ (see Sec. IV B). Under this condition, and using a critical current $I_c \simeq 5\times10^{-6}$ A, together with $Z = 50\ \Omega$, it would be possible to reach a coupling strength up to $g_i \simeq 1.2$ GHz.

On the other hand, for the second proposal [see Fig. 2(b) and Sec. III B] the coupling (24) in the loop becomes

$$g_i \simeq E_J\left(\frac{2\pi}{\Phi_0}\frac{\partial\psi(x)}{\partial x}\Delta x\right)^2, \quad (27)$$

with $\partial_x\psi = \partial_x u\sqrt{\frac{\hbar}{2C_r\omega}}$. For a homogeneous resonator [see (A 1)], we can straightforwardly assess the slope of $u_0(x)$, finding an exact expression for g:

$$g = \pi^2\frac{\omega_J\omega_c}{\omega_0}\left(\frac{\Delta x}{2l}\right)^2, \quad (28)$$

where $\omega_J = E_J/\hbar$, $\omega_c = E_C/\hbar = (2e)^2/2\hbar C_r$ is the characteristic charging frequency of the resonator, and ω_0 is the first-mode frequency. Using available values for Nb striplines and junction parameters, we find that the homogeneous resonator remains in the weak-coupling regime, as we envisioned before. For a loop size Δx of 1% of the resonator length, we obtain $g \simeq 2$ MHz which represents 0.03% of the resonator frequency ω (see Fig. 3).

Adding a constriction to the central part of the resonator increases the field slope and thus the coupling. To this end, for a suitable Nb inhomogeneous transmission line resonator,[32] this enhances the coupling up to $g \simeq 100$ MHz, or equivalently to 1.8% of the resonator frequency (Fig. 3, red dashed line).

Finally, the coupling can be further enhanced by interrupting the transmission line with a Josephson junction. Due to the presence of the junction, the flux eigenmode presents a constant phase slip $\Delta\phi_0$ at $x = 0$, which depends on the Josepshon coupling energy of the junction.[32,59] This additional phase jump enhances the coupling as follows:

$$g_i \simeq E_J\left(\frac{2\pi}{\Phi_0}\frac{\partial\psi(x)}{\partial x}\Delta x + \Delta\phi_0\right)^2. \quad (29)$$

Optimal parameters for the junction attached to the resonator ($E_{J\text{res}} \simeq 7E_{J\text{loop}}$) could lead to extremely large couplings of around $g \sim 600$ MHz (9% of ω).

The previous numbers have to be compared with similar figures from other setups, such as a circulator-based coupling

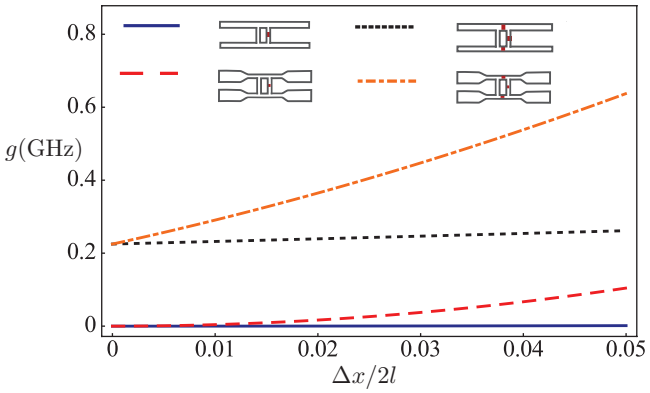

FIG. 3. (Color online) Coupling strength for differerent niobium transmission lines, as a function of the loop size. While homogeneous resonators (blue) hardly reach the strong-coupling regime, inhomogeneous ones (red dashed) do. The coupling strength can be further increased with a Josephson junction interrupting the center conductor, as shown for the homogeneous case (dotted) and the inhomogeneous one (dot dashed). We have considered for each resonator a frequency $\omega_0/2\pi = 6.65$ GHz.

between resonators,[25,38] or the dispersive coupling based on SQUID loops[31] or qubits.[28] In these three cases the coupling element works with a high detuning Δ from the resonator frequency. This means that the effective coupling takes the form g^2/Δ, where g is the coupling of one resonator to the circulator, SQUID loop, or qubit, Δ is the detuning from the resonator frequency and the dispersive condition $g \ll \Delta < \omega$ limits the maximum achievable strength to a few percentage points of ω.

IV. APPLICATIONS

A. Sidebands

So far we have discussed the possibility of tuning the coupling strength between two resonators, constructing a classical switch that allows us to control the exchange of photons. In this section we discuss a second type of tunability, which consists of engineering an arbitrary linear type of coupling between two resonators:

$$H_{\rm int} = g_1 e^{i\phi_1} a^\dagger b + g_2 e^{i\phi_2} ab + \text{H.c.}, \tag{30}$$

represented by the Fock operators a and b. This would enlarge the applicability of our setup, extending it to the realization of almost any quadratic model with nearest-neighbor interactions.

In order to demonstrate that this is possible we start our discussion by noting that both the dc SQUID and the ring coupler provide us with a flux-dependent coupling

$$H = \hbar\omega_a a^\dagger a + \hbar\omega_b b^\dagger b + g(\Phi_{\circlearrowleft})(a^\dagger + a)(b^\dagger + b). \tag{31}$$

If we now engineer the two resonators to have very different frequencies ω_a and ω_b, the static coupling $|g| \ll \omega_{a,b}$ will be effectively suppressed, giving rise to a small dispersive term

$$H \sim \hbar\omega_a a^\dagger a + \hbar\omega_b b^\dagger b + \frac{g^2}{|\omega_b - \omega_a|} a^\dagger a b^\dagger b. \tag{32}$$

However, if we allow for a two-tone driving of the coupling,

$$g(t) = g[\Phi_{\circlearrowleft}(t)] = g_1 \cos[(\omega_b - \omega_a)t + \phi_1] + g_2 \cos[(\omega_a + \omega_b)t + \phi_2], \tag{33}$$

then this driving effectively activates the rotating and counterrotating terms, with the phases given above. To show this we switch to an interaction picture with respect to the two harmonic oscillators,

$$H_I = g(t)(a^\dagger b e^{i(\omega_a - \omega_b)t} + ab e^{-i(\omega_a + \omega_b)t} + \text{H.c.}). \tag{34}$$

The oscillating terms in Eq. (33) will precisely cancel the ones in the previous time-dependent Hamiltonian, leaving behind some other nonresonant terms which act only in higher-order perturbation theory, $O(g^2/\omega)$. The result should be the desired combination of sidebands

$$H_{\rm eff} = g_1 a^\dagger b e^{i\phi_1} + g_2 ab e^{i\phi_2} + \text{H.c.} \tag{35}$$

It is worth mentioning that the previous sideband engineering is not perturbative: while we still need to impose the requirement that $|g_{1,2}| \ll |\omega_b - \omega_a|$, the resulting coupling is larger than the dispersive term. This strong coupling and the individual tuning of photon terms would be a wonderful tool to explore the different phase transitions predicted for exotic Bose-Hubbard models, as discussed for instance in Ref. 60.

Another very important feature of the two-tone driving method is that it allows us to control the phases of the rotating and counterrotating terms, for this is related to the phase of the two-tone driving. As we discuss below, this is a very important property, as it allows us to implement effective gauge fields that control the hopping of photons between resonators. Moreover, we achieve this effect by a simple driving of a standard SQUID, without the need of time-reversal symmetry-breaking circuits which might be very sensitive to other noise sources.[25]

Finally, even though the realization of the time dependence (33) might seem complicated, in practice we do not need to tune the flux in a very complicated manner. A simple driving of $\Phi_{\circlearrowleft}(t) \simeq \Phi + \delta\Phi\cos(\omega t)$, when introduced in the sinusoidal coupling (14) $g \simeq \cos(2\pi\Phi_{\circlearrowleft}/\Phi_0)$ produces, via the Jacobi-Anger expansion,

$$g(t) \simeq \cos(2\pi\Phi/\Phi_0) J_0(\delta\Phi) + \sin(2\pi\Phi/\Phi_0) J_1(\delta\Phi)\cos(\omega t) + \cdots \tag{36}$$

in terms of the Bessel functions J_0 and J_1. This series contains the basic driving plus higher harmonics which will be spectrally suppressed in the coupling term. Alternatively, a suitable dependence for $\Phi_{\circlearrowleft}$ can be engineered with around 0.1 ns resolution using appropriate signal generators.[61] Again, out of this signal only the resonant terms, with frequencies around $\omega_a \pm \omega_b$ will contribute to the coupling. Discretization errors in the signal, and higher harmonics, will be averaged out.

B. Nonlinear photon hopping

So far we have worked with the Josephson junctions in the linear regime, neglecting higher-order terms, which are of the order $\frac{1}{24} E_J (2\pi\phi/\Phi_0)^4$. This approximation is valid only when the argument of the trigonometric functions, $2\pi\phi/\Phi_0$, is small, a condition which can be recast as a restriction on the

number of photons that can populate the resonator. Roughly, for the SQUID we have the condition

$$\phi \sim u(x)\sqrt{\frac{\hbar Z}{2}n} \ll \frac{\Phi_0}{2\pi} = \frac{\hbar}{2e}, \tag{37}$$

where Z is the impedance of the resonators, n is the average number of photons, and $u(x)$ is the mode wave function at the coupling points. Using, in the same way as above, the value $u(x) = 0.1$ restricts the number of photons to $n < 1000$ (see Appendix B 1), which does not represent a restriction for the few photon applications that we envision.

The question now is what happens when we do not neglect the nonlinear terms. In this case we have the potential to introduce new interactions between resonators, which are now of higher order and include on-site nonlinearities n_i^2, nearest-neighbor attractive or repulsive interactions $n_i n_j$, photon-pair hopping $a_i^{\dagger 2} a_j^2$, etc. (see Appendix B 2). Of these terms some are already strongly suppressed because of being off resonant; this is the case for interactions with odd powers, such as $a_i^{\dagger 3} a_j$. The Kerr nonlinearities will always be present and give rise to extended Bose-Hubbard physics. Finally, the correlated hopping terms $a_i^{\dagger 2} a_j^2$ can be resonantly enhanced using the same technique that we employ for the sidebands: introducing a frequency mismatch between neighboring cavities and driving with exactly the frequency which is needed to select this process, $2(\omega_i - \omega_j)$. With all these tools we envision the possibility of engineering very interesting models, such as a condensate of pairs of photons,[62] which are very hard to engineer in other systems.

C. Outlook and discussion

Summing up, in this work we have studied two different ways to engineer the coupling between superconducting resonators: one is geometric and static in nature, while the other relies on nonlinear coupling circuits and can be easily tuned in and out of the strong-coupling regime. Both elements together form a powerful toolbox for implementing almost arbitrary models consisting of a low-dimensional (from 1D to 2D) array of resonators with tunable nearest-neighbor interactions, as in the model sketched in Fig. 4. Let us now discuss some of the potential applications of such circuits.

1. Traditional quantum optics

The implementation of tunable sidebands in coupled resonators opens the door to many well-known processes from quantum optics. Some of them are the squeezing of different modes via those sidebands, frequency conversion of photons as they are transferred between cavities, parametric generation of photons via $a^\dagger b^\dagger + ab$ terms, entanglement production at high temperatures,[63] etc. The beam-splitter Hamiltonian is also the cornerstone of all-optical quantum information processing, as suggested in Ref. 37 for a different circuit-QED architecture.

2. Harmonic models

The most immediate application of our design would be to implement arbitrary quasilocal and quadratic Hamiltonians, with the aim of studying the dynamical or static properties of many-body Gaussian states. This includes a variety of

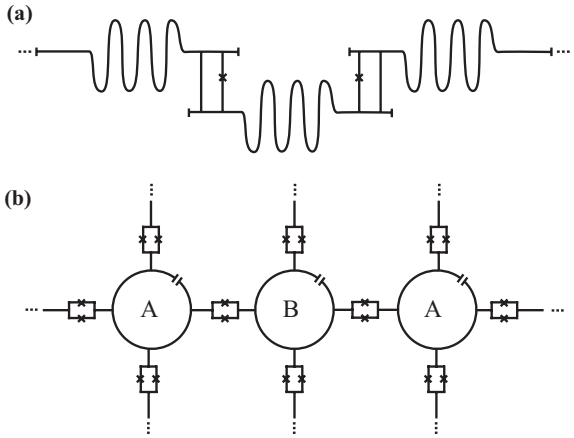

FIG. 4. (a) One-dimensional array of cavities coupled by means of a superconducting ring coupler. (b) Two-dimensional lattice of circular resonators, coupled by dc SQUIDs. Both lattices are bipartite. Using different resonator frequencies for each sublattice, $\omega_A \neq \omega_B$, we can use the techniques from Sec. IV A to engineer any sideband interaction between the arrays.

studies, such as the static correlations in the model[64] and their relation to the underlying entanglement, dynamical quantum phase transitions from trivial to critical phases, the study of propagation of correlations in nonequilibrium models and their relation to Lieb-Robinson bounds,[65–67] etc. In this context, the tunability of the coupling plays two different roles. On the one hand it allows us to change the parameters of the Hamiltonian in an abrupt or smooth way, for instance to study a dynamical quantum phase transition or a quench. On the other hand and equally important, by switching off all couplings we can freeze the quantum state of the oscillators, giving us time to measure the properties of the system, either with different measurement qubits or through a movable probe.[42]

3. Anharmonicity and thermalization

The interest of the harmonic problems lies in their simplicity and the possibility of obtaining analytical and numerical results for different geometries and sizes. However, as soon as we introduce a small nonlinearity in our system, we can say very little about their dynamical and static properties and many of the simulations which we mentioned in the previous paragraph become open problems. In particular, one very simple problem which deserves being studied is that of thermalization. The basic idea is to replace the linear resonators in Fig. 4 with resonators that host a tunable and weak nonlinearity in the form of a SQUID (similar to Ref. 27 but outside the linear regime). One would then prepare the ground state of the cavities with a value of the coupling, and then abruptly quench this coupling to a different (larger or smaller) value in which the prepared state is not a ground state. Throughout this process it will be possible to track the relaxation of the oscillator chain or lattice, studying how its behavior is modified by the presence of the nonlinearity. Note that it is well known that the simulation of such time-dependent many-body problems becomes numerically intractable for a few resonators. For instance, assuming a truncation basis with ten photons per cavity, a state of ten

coupled cavities requires already 10 gigabytes of memory. But the problem of time evolution is worse, for truncation and rounding errors introduce a very fast growth of errors such that after a short runaway time, even the most sophisticated density matrix renormalization group (DMRG) many-body simulation methods[68] provide only qualitative results.[69] In this sense, having good quantum simulators would be an invaluable tool to advance the understanding of these nonequilibrium processes beyond those regimes which can be simulated with more straightforward methods.[72]

4. Coupled cavities and gauge fields

Along the lines of anharmonic systems, another interesting problem is the study of coupled cavities or Jaynes-Cummings lattices.[20,21] The setup would be that of Fig. 4, but with one qubit attached to each resonator. The coupled qubit-resonator system behaves as a highly nonlinear element, implementing a quasiparticle known as a "polariton," which may hop from resonator to resonator through our tunable coupling elements. This can be roughly formulated as a Bose-Hubbard Hamiltonian

$$H = \sum_{ij} t_{ij} a_i^\dagger a_j + U(a_i^\dagger a_i), \tag{38}$$

with a very nonlinear on-site interaction U and a hopping t_{ij} which, unlike in previous proposals,[22] is now dynamically tunable. This allows us to explore the quantum phase transitions from weak interactions $U \ll |t|$ to hard-core particles $U \gg |t|$ simply by reducing the hopping instead of arbitrarily boosting the qubit-resonator interaction—something which might be more challenging from the theoretical and experimental point of view.

In addition to the usual Mott-superfluid phase transition, we now have control over the phase of the hopping, $t_{ij} = |t| \exp i\theta_{ij}$. The procedure, as described in the previous section, consists of engineering two coupled sublattices [A and B in Fig. 4(b)] of resonators with different frequencies, $\omega_A \neq \omega_B$. Applying a multitone driving on the bonds that connect the two sublattices, we can create an array of phases θ_{ij} which have a nontrivial flux around each plaquette. This will allow us to probe integer quantum Hall physics with polaritons,[25] without the use of circulators.

In summary, we have shown that in circuit QED, tunable coupling between resonators can be implemented via simple Josephson circuits. We have developed this initial idea into a profound theoretical basis for exciting multiresonator experiments ranging from arbitrary sideband interactions to setups scalable towards the many-body regime. On the theoretical side, our results lend themselves to being expanded to advanced scenarios, such as the relation between our circuit models and Josephson junction arrays, the influence of decoherence, or even the design of models with tunably dissipative elements.

ACKNOWLEDGMENTS

We thank Juan José Mazo for useful discussions. This work was supported by the EU Projects PROMISCE and CCQED, Spanish MICINN Projects No. FIS2009-10061 and No. FIS2011-25167, and CAM Research Consortium QUITEMAD No. S2009-ESP-1594. B.P. acknowledges financial support from CSIC Contract JAE-PREDOC2009. F. W., F. D., A. M., and R. G. acknowlegde support by the German Research Foundation via SFB 631 and the German Excellence Initiative via the Nanosystems Initiative Munich (NIM).

APPENDIX A: LUMPED ELEMENT MODEL OF TWO COUPLED RESONATORS

Here we derive the density Lagrangian (1) of Sec. II from the quantum network theory perspective. The appendix is divided into three parts: in the first one we review the quantization of a single microstrip resonator. In the second one, we consider the equivalent circuit of the coupled striplines shown in Fig. 1(a) in its lumped element model [see Fig. 1(b)]. The Kirchhoff equations derived here will give rise to the Lagrangian (1) in the continuum limit.

1. Single-oscillator description

Here, we detail the description for the single-resonator case. The transmission line field equations are obtained from their lumped circuit equivalent. Neglecting losses, it can be described as a series of LC circuits.[58] In the continuum limit, the resulting field equations can be obtained from the Lagrangian

$$\mathcal{L}_0 = \frac{1}{2}\int_{-l}^{l} dx[c_0(x)\dot{\phi}(x,t)^2 - l_0(x)^{-1}\partial_x\phi(x,t)^2], \tag{A1}$$

where $c_0(x)$ and $l_0(x)$ are the capacitance and inductance per unit of length, respectively; otherwise, $\phi(x) = (\Phi_0/2\pi)\varphi(x)$ is the magnetic flux variable with $\Phi_0 = h/2e$ the magnetic flux quantum and $\varphi(x)$ the phase of the macroscopic wave function describing the superconductor. The stationary modes are found by solving the eigenvalues and eigenvectors for the equation of motion (the Euler-Lagrange equations)

$$\partial_x[l_0(x)^{-1}\partial_x\phi(x,t)] = c_0(x)\partial_t^2\phi(x,t), \tag{A2}$$

which is nothing but the wave equation in one dimension. The solution to this equation is expanded in normal modes and time-dependent amplitudes,

$$\phi(x,t) = \sum_n q_n(t)u_n(x), \tag{A3}$$

such that $\ddot{q}_n = -\omega_n q_n$, with ω_n the resonator frequencies. Therefore the *eigenstates* u_n satisfy the differential equation $\partial_x[l_0(x)^{-1}\partial_x u_n(x)] = -\omega_n c_0(x)u_n(x)$. The u_n satisfy the orthogonal relation

$$\int_{-l}^{l} c_{0,j}(x)u_{m,j}(x)u_{n,j}(x)dx = C_r\delta_{nm}, \tag{A4}$$

with $C_r = \int_{-l}^{l} c_0(x)dx$ the total capacitance of the resonator.

For homogeneous resonators, l_0 and c_0 are constant, and we obtain the well-known case of equispaced eigenfrequencies $\nu_n = (2n-1)/2l\sqrt{l_0c_0}$ with $2l$ the length of the superconducting resonator and $u_n = \sqrt{2}\sin[(2n-1)\pi x/2l]$.

2. Two coupled oscillators

Consider the lumped element model depicted in Fig. 1(b). The discrete modes of the electromagnetic field inside the strips are described as arrays of LC oscillators, together with the mutual inductances and capacitances, representing the cross-talk. By applying the current conservation law at each node of the circuit, we obtain a set of dynamical equations for the node fluxes $\phi_{j,n}$:

$$\begin{aligned}&\Delta x c_0(n)\ddot{\phi}_{1,n} + \Delta x c_m(n)(\ddot{\phi}_{1,n} - \ddot{\phi}_{2,n})\\ &= \frac{l_0(n)}{\Delta x}\frac{(\phi_{1,n-1}-\phi_{1,n})}{l_0(n)^2 - l_m(n)^2} - \frac{l_0(n)}{\Delta x}\frac{(\phi_{1,n}-\phi_{1,n+1})}{l_0(n)^2 - l_m(n+1)^2}\\ &\quad - \frac{l_m(n)}{\Delta x}\frac{(\phi_{2,n-1}-\phi_{2,n})}{l_0(n)^2 - l_m(n)^2} - \frac{l_m(n+1)}{\Delta x}\frac{(\phi_{2,n+1}-\phi_{2,n})}{l_0(n)^2 - l_m(n+1)^2},\end{aligned} \tag{A5}$$

and the equivalent equation for the second resonator. Above, $c_0(n)$ and $l_0(n)$ are the capacitance and inductance per unit length, respectively, while $c_m(n)$ and $l_m(n)$ represent the mutual capacitance and mutual inductance coefficients. Notice that, in general, all these parameters are position dependent.

The former equations of motion are nothing but the Euler-Lagrange equations associated with the following Lagrangian:

$$L = T - V, \tag{A6}$$

with

$$T = \frac{\Delta x}{2}\sum_{n,j} c_0\dot{\phi}_{j,n}^2 + c_m(n)(\dot{\phi}_{j,n} - \dot{\phi}_{j+1,n})^2, \tag{A7}$$

$$\begin{aligned}V = &\frac{1}{2\Delta x}\sum_{n,j}\frac{l_0}{l_0^2 - l_m(n)^2}(\phi_{j,n} - \phi_{j,n-1})^2 - \frac{l_m(n)}{l_0^2 - l_m(n)^2}\\ &\times(\phi_{j,n} - \phi_{j,n-1})(\phi_{j+1,n} - \phi_{j+1,n-1}).\end{aligned} \tag{A8}$$

We can now take the continuum limit $\Delta x \to 0$, which implies

(a) $\phi_{j,n} \to \phi_j(x)$,

(b) $\frac{(\phi_{j,n}-\phi_{j,n-1})}{\Delta x} \to \partial_x\phi_j(x)$,

(c) $\Delta x\sum_n \to \int_{-l}^{l} dx$.

Hence, the Lagrangian (A6) ends up as Eq. (1) in the main text that we rewrite here for completeness,

$$\mathcal{L} = \frac{1}{2}\sum_{j=1,2}\int_{-l}^{l} dx\left[\hat{c}_{ij}\dot{\phi}_i(x)\dot{\phi}_j(x) - \hat{l}_{ij}^{-1}\partial_x\phi_i(x)\partial_x\phi_j(x)\right]. \tag{A9}$$

The fluxes $\phi_i(x)$ are thus coupled by the capacitance $\hat{c}(x)$ and inductance $\hat{l}(x)$ matrices given in the main text (2). The diagonal terms of these matrices represent the single-resonator Lagrangian $\mathcal{L}_0$ derived in the previous section, which depends on $l_0(x)$ and $c_0(x)$. On the other hand, the off-diagonal contributions represent the coupling Lagrangian $\mathcal{L}_1$, described by the parameters $l_{jj} = l_0, l_{ij} = l_m, c_{jj} = c_0 + c_m$, and $c_{ij} = -c_m$.

3. Generalization to more oscillators

We now show that the quantum description of two coupled resonators presented above can be generalized to the case of N coupled resonators. We therefore extend the sum in Eq. (A9) to N:

$$\mathcal{L} = \frac{1}{2}\sum_{i,j=1}^{N}\int_{-l}^{l} dx\left[\hat{c}_{ij}\dot{\phi}_i(x)\dot{\phi}_j(x) - \hat{l}_{ij}^{-1}\partial_x\phi_i(x)\partial_x\phi_j(x)\right], \tag{A10}$$

where the $\hat{c}(x)$ and $\hat{l}(x)$ are now given by $N \times N$ matrices with self-capacities (self-inductances) on the diagonal and the mutual capacities (self inductances) on the off diagonal. Following the same procedure as above we restrict ourselves to the fundamental modes, split off the single-resonator Lagrangians, and write the interaction part as

$$\begin{aligned}L_1 = &\frac{1}{2}\sum_{N}\left(c_m\Delta_1\dot{q}_j^2 - \frac{l_m^2}{l_0(l_0^2 - l_m^2)}\Delta_2 q_j^2\right)\\ &+ \sum_{i=1}^{N-1}\left(-c_m\Delta_1\dot{q}_i\dot{q}_{i+1} + \frac{l_m}{l_0^2 - l_m^2}\Delta_2 q_i q_{i+1}\right),\end{aligned} \tag{A11}$$

taking into account only nearest-neighbor interaction. The Hamiltonian can finally be written as

$$\begin{aligned}H/\hbar = &\sum_{j=1}^{N}\omega a_j^\dagger a_j - \sum_{j=1}^{N-1} g_c(a_j^\dagger - a_j)(a_{j+1}^\dagger - a_{j+1})\\ &- \sum_{i=1}^{N-1} g_i(a_j^\dagger + a_j)(a_{j+1}^\dagger + a_{j+1}),\end{aligned} \tag{A12}$$

with ω, g_c, and g_i the same as in the two-resonator case. In particular, from the resulting total Hamiltonian H the normal frequencies can be found, giving

$$\begin{aligned}\omega_- &= \omega_0\sqrt{\frac{1}{1+2C}\left(1 + \frac{L}{\nu(1-L)}\right)},\\ \omega_+ &= \omega_0\sqrt{1 - \frac{L}{\nu(1+L)}}.\end{aligned} \tag{A13}$$

We finally notice that by making $l_c \to l(\nu \to 1)$, i.e., two straight parallel resonators, the formulas for the normal modes match the case of two coupled LC circuits.

APPENDIX B: LINEAR AND NONLINEAR COUPLINGS

The motivation in this Appendix is twofold. On the one hand we estimate the validity of the linear approximation; on the other hand, we explicitly compute the first nonlinear corrections to the coupling.

We first expand the cosine in $\mathcal{L}_{\text{SQUID}}$ (11),

$$\begin{aligned}&-\cos\left(\frac{2\pi}{\Phi_0}\phi_-\right)\\ &= -1 + \frac{1}{2}\left(\frac{2\pi}{\Phi_0}\right)^2\phi_-^2 - \frac{1}{24}\left(\frac{2\pi}{\Phi_0}\right)^4\phi_-^4 + \cdots.\end{aligned} \tag{B1}$$

We recall that

$$\phi_- = u_0\sqrt{\hbar Z}(a_-^\dagger + a_-) \quad \text{and} \quad a_- = \frac{1}{\sqrt{2}}(a_1 - a_2). \tag{B2}$$

Assuming $Z = 50\ \Omega$ and defining

$$\xi \equiv u_0^2 \left(\frac{2\pi}{\Phi_0}\right)^2 2\hbar Z = u_0^2 \frac{\pi^2}{10^2} \cong 10^{-1} u_0^2, \tag{B3}$$

we can write for the expansion

$$-\cos\left(\frac{2\pi}{\Phi_0}\phi_-\right) = -1 + \frac{\xi}{4}(a_-^\dagger + a_-)^2 - \frac{\xi^2}{96}(a_-^\dagger + a_-)^4. \tag{B4}$$

1. Linear regime

The linear approximation is justified when the second-order terms in Eq. (B1), or equivalently the average value and fluctuations of the flux in Eq. (B4), are small. How does this relate to actual experiments? In order to determine a condition based on the number of photons we study the fluctuations $\langle \phi_-^2 \rangle$, which are related to the expectation value

$$\langle (a_-^\dagger + a_-)^2 \rangle \cong 2(\langle a_1^\dagger a_1 \rangle + \langle a_2^\dagger a_2 \rangle) \equiv 4n \tag{B5}$$

with n the number of photons. Using the previous series we conclude that linearization is strictly justified whenever $n \ll 10/u_0^2$, where u_0 is the value of the mode wave function. For the ring coupler layout, the same reasoning follows by replacing $u_0 \to \partial_x u_0 \Delta x$ in Eqs. (B2) and (B3).

2. Nonlinear hopping terms

With the help of Pathak's results,[73] we compute,

$$(a_- + a_-^\dagger)^4 = a_-^4 + 4(a_-^\dagger)^3 a_- + 6(a_-^\dagger)^2 a_-^2 + 6a^\dagger a + 3 + \text{H.c.} \tag{B6}$$

Notice that $a_- = \frac{1}{\sqrt{2}}(a_1 - a_2)$ [Eq. (B2)], so the above ends up in a long expression hard to deal with. To make it simpler, we assume that sidebands will select a_-^2 or $a^\dagger a$ and we resort to a RWA argument to write

$$(a_- + a_-^\dagger)^4 \cong 6(a_-^\dagger)^2 a_-^2 + 12a^\dagger a + 6(a_-^\dagger)^2 + 6a_-^2 + 3. \tag{B7}$$

Looking at each term we rewrite them in terms of the *local* bosonic operators a_1 and a_2:

$$4(a_-^\dagger)^2 a_-^2 = (a_1^\dagger)^2 a_1^2 + (a_2^\dagger)^2 a_2^2 + 2a_1^\dagger a_2^\dagger a_1 a_2 - 2a_1^\dagger a_2^\dagger \left(a_1^2 + a_2^2\right) + \text{H.c.}, \tag{B8}$$

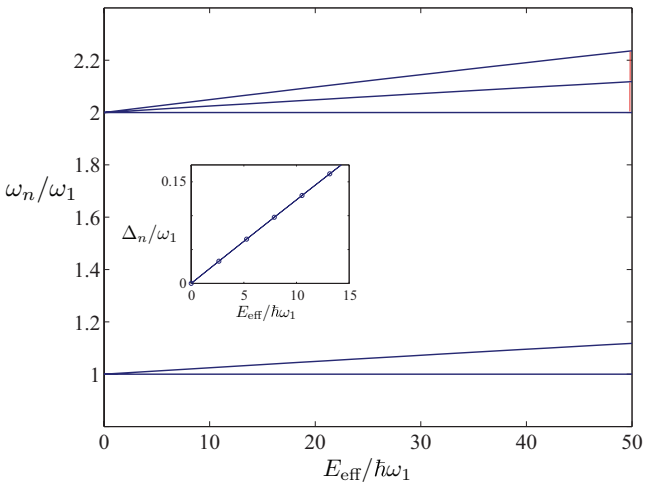

FIG. 5. (Color online) Energies of the full Hamiltonian of two *LC* resonators with frequency ω_1 coupled by a SQUID (11), as a function of the effective Josephson energy $E_{\rm eff}$. We plot the transition frequencies relative to the ground state, $\omega_n = (E_n - E_0)/\hbar$. Note the splitting between energy levels which is linear with $E_{\rm eff}$. The inset shows the energy splitting Δ_n, for $n = 1$ (solid) and 2 (circles) photons, in perfect agreement with our linearized theory.

$$2(a_-^\dagger)^2 = (a_1^\dagger)^2 + (a_2^\dagger)^2 - 2a_1^\dagger a_2^\dagger, \tag{B9}$$

$$2a_-^\dagger a_- = a_1^\dagger a_1 + a_2^\dagger a_2 - a_1^\dagger a_2 - a_2^\dagger a_1. \tag{B10}$$

3. Full diagonalization

We conclude this Appendix by computing the full diagonalization of the Hamiltonian associated with Eq. (11). More precisely, we consider two zero-mode resonators connected by a single SQUID element and diagonalize everything in the Fock basis of the oscillators. The SQUID acts as a nonlinearity whose bounded strength can be faithfully reproduced using Fock operators in a truncated basis. In Fig. 5 we show the resulting spectrum, with the energy splitting induced by the effective coupling, which is approximately linear in the SQUID strength. Note that for a small number of photons the energy splitting is the same, demonstrating the linear behavior of the element.

[1] A. Blais, R.-S. Huang, A. Wallraff, S. M. Girvin, and R. J. Schoelkopf, Phys. Rev. A **69**, 062320 (2004).

[2] A. Wallraff, D. Schuster, A. Blais, L. Frunzio, R.-S. Huang, J. Majer, S. Kumar, S. M. Girvin, and R. J. Schoelkopf, Nature (London) **431**, 162 (2004).

[3] T. Niemczyk, F. Deppe, H. Huebl, E. P. Menzel, F. Hocke, M. J. Schwarz, J. J. Garcia-Ripoll, D. Zueco, T. Hümmer, E. Solano *et al.*, Nat. Phys. **6**, 772 (2010).

[4] P. Forn-Díaz, J. Lisenfeld, D. Marcos, J. J. García-Ripoll, E. Solano, C. J. P. M. Harmans, and J. E. Mooij, Phys. Rev. Lett. **105**, 237001 (2010).

[5] T. Hime, P. A. Reichardt, B. L. T. Plourde, T. L. Robertson, C.-E. Wu, A. V. Ustinov, and J. Clarke, Science **314**, 1427 (2006).

[6] A. O. Niskanen, K. Harrabi, F. Yoshihara, Y. Nakamura, S. Lloyd, and J. S. Tsai, Science **316**, 723 (2007).

[7] S. H. W. van der Ploeg, A. Izmalkov, A. M. van den Brink, U. Hübner, M. Grajcar, E. Il'ichev, H.-G. Meyer, and A. Zagoskin, Phys. Rev. Lett. **98**, 057004 (2007).

[8] O. Astafiev, A. M. Zagoskin, A. A. Abdumalikov, Y. A. Pashkin, T. Yamamoto, K. Inomata, Y. Nakamura, and J. S. Tsai, Science **327**, 840 (2010).

[9] A. A. Abdumalikov, O. Astafiev, A. M. Zagoskin, Y. A. Pashkin, Y. Nakamura, and J. S. Tsai, Phys. Rev. Lett. **104**, 193601 (2010).

[10] C. Sabín, M. del Rey, J. J. García-Ripoll, and J. León, Phys. Rev. Lett. **107**, 150402 (2011).

[11] A. L. Rakhmanov, A. M. Zagoskin, S. Savel'ev, and F. Nori, Phys. Rev. B **77**, 144507 (2008).
[12] C. Hutter, E. A. Tholén, K. Stannigel, J. Lidmar, and D. B. Haviland, Phys. Rev. B **83**, 014511 (2011).
[13] D. Zueco, J. J. Mazo, E. Solano, and J. J. García-Ripoll, Phys. Rev. B **86**, 024503 (2012).
[14] A. M. Zagoskin, A. L. Rakhmanov, S. Savel'ev, and F. Nori, Phys. Status Solidi B **246**, 955 (2009).
[15] P. D. Nation, M. P. Blencowe, A. J. Rimberg, and E. Buks, Phys. Rev. Lett. **103**, 087004 (2009).
[16] G. Romero, J. J. García-Ripoll, and E. Solano, Phys. Rev. Lett. **102**, 173602 (2009).
[17] Y.-F. Chen, D. Hover, S. Sendelbach, L. Maurer, S. T. Merkel, E. J. Pritchett, F. K. Wilhelm, and R. McDermott, Phys. Rev. Lett. **107**, 217401 (2011).
[18] B. Peropadre, G. Romero, G. Johansson, C. M. Wilson, E. Solano, and J. J. García-Ripoll, Phys. Rev. A **84**, 063834 (2011).
[19] I.-C. Hoi, C. M. Wilson, G. Johansson, T. Palomaki, B. Peropadre, and P. Delsing, Phys. Rev. Lett. **107**, 073601 (2011).
[20] M. J. Hartmann, F. G. S. L. Brandão, and M. B. Plenio, Nat. Phys. **2**, 849 (2006).
[21] D. G. Angelakis, M. F. Santos, and S. Bose, Phys. Rev. A **76**, 031805 (2007).
[22] M. Leib and M. J. Hartmann, New J. Phys. **12**, 093031 (2010).
[23] M. Leib, F. Deppe, A. Marx, R. Gross, and M. Hartmann, New J. Phys. **14**, 075024 (2012).
[24] I. Carusotto, D. Gerace, H. E. Tureci, S. De Liberato, C. Ciuti, and A. Imamoğlu, Phys. Rev. Lett. **103**, 033601 (2009).
[25] A. Nunnenkamp, J. Koch, and S. M. Girvin, New J. Phys. **13**, 095008 (2011).
[26] J. R. Johansson, G. Johansson, C. M. Wilson, and F. Nori, Phys. Rev. Lett. **103**, 147003 (2009).
[27] C. M. Wilson, G. Johansson, A. Pourkabirian, J. R. Johansson, T. Duty, F. Nori, and P. Delsing, Nature (London) **479**, 376 (2011).
[28] M. Mariantoni, F. Deppe, A. Marx, R. Gross, F. Wilhelm, and E. Solano, Phys. Rev. B **78**, 104508 (2008).
[29] G. M. Reuther, D. Zueco, F. Deppe, E. Hoffmann, E. P. Menzel, T. Weißl, M. Mariantoni, S. Kohler, A. Marx, E. Solano, R. Gross, and P. Hänggi, Phys. Rev. B **81**, 144510 (2010).
[30] D. I. Tsomokos, S. Ashhab, and F. Nori, Phys. Rev. A **82**, 052311 (2010).
[31] L. Tian, M. S. Allman, and R. W. Simmonds, New J. Phys. **10**, 115001 (2008).
[32] J. Bourassa, J. M. Gambetta, A. A. Abdumalikov, O. Astafiev, Y. Nakamura, and A. Blais, Phys. Rev. A **80**, 032109 (2009).
[33] J.-Q. Liao, Z. R. Gong, L. Zhou, Y.-x. Liu, C. P. Sun, and F. Nori, Phys. Rev. A **81**, 042304 (2010).
[34] E. Zakka-Bajjani, F. Nguyen, M. Lee, L. R. Vale, R. W. Simmonds, and J. Aumentado, Nat. Phys. **7**, 599 (2011).
[35] E. Flurin, N. Roch, F. Mallet, M. H. Devoret, and B. Huard, Phys. Rev. Lett. **109**, 183901 (2012).
[36] F. Nguyen, E. Zakka-Bajjani, R. W. Simmonds, and J. Aumentado, Phys. Rev. Lett. **108**, 163602 (2012).
[37] L. Chirolli, G. Burkard, S. Kumar, and D. P. DiVincenzo, Phys. Rev. Lett. **104**, 230502 (2010).
[38] J. Koch, A. A. Houck, K. L. Hur, and S. M. Girvin, Phys. Rev. A **82**, 043811 (2010).
[39] H. Brenning, S. Kubatkin, and P. Delsing, J. Appl. Phys. **96**, 6822 (2004).
[40] N. C. Menicucci, P. van Loock, M. Gu, C. Weedbrook, T. C. Ralph, and M. A. Nielsen, Phys. Rev. Lett. **97**, 110501 (2006).
[41] M. Hofheinz, H. Wang, M. Ansmann, R. C. Bialczak, E. Lucero, M. Neeley, A. D. O'Connell, D. Sank, J. Wenner, J. M. Martinis *et al.*, Nature (London) **459**, 546 (2009).
[42] W. E Shanks, D. L. Underwood, and A. A. Houck, arXiv:1303.0874.
[43] J. R. Johansson, G. Johansson, C. M. Wilson, and F. Nori, Phys. Rev. A **82**, 052509 (2010).
[44] C. R. Paul, *Analysis of Multiconductor Transmission Lines* (Wiley-Interscience, New York, 1994).
[45] C. R. Paul, IEEE Trans. Electron. Compat. **44**, 413 (2002).
[46] M. Sandberg, C. M. Wilson, F. Persson, T. Bauch, G. Johansson, V. Shumeiko, T. Duty, and P. Delsing, Appl. Phys. Lett. **92**, 203501 (2008).
[47] M. A. Castellanos-Beltran and K. W. Lehnert, Appl. Phys. Lett. **91**, 083509 (2007).
[48] M. A. Castellanos-Beltran, K. D. Irwin, G. C. Hilton, L. R. Vale, and K. W. Lehnert, Nat.. Phys. **4**, 929 (2008).
[49] T. Yamamoto, K. Inomata, M. Watanabe, K. Matsuba, T. Miyazaki, W. D. Oliver, Y. Nakamura, and J. S. Tsai, Appl. Phys. Lett. **93**, 042510 (2008).
[50] M. Grajcar, Y.-x. Liu, F. Nori, and A. M. Zagoskin, Phys. Rev. B **74**, 172505 (2006).
[51] M. H. Devoret, in *Quantum Fluctuations: Les Houches Session LXIII*, edited by S. Reynaud, E. Giacobino, and J. Zinn-Justin (Elsevier, North-Holland, Amsterdam, 1997), pp. 351–386.
[52] J. Clarke, Proc. IEEE **77**, 1208 (1989).
[53] B. Peropadre, P. Forn-Díaz, E. Solano, and J. J. García-Ripoll, Phys. Rev. Lett. **105**, 023601 (2010).
[54] M. J. Everitt, T. D. Clark, P. Stiffell, H. Prance, R. J. Prance, A. Vourdas, and J. F. Ralph, Phys. Rev. B **64**, 184517 (2001).
[55] M. J. Everitt, P. Stiffell, T. D. Clark, A. Vourdas, J. F. Ralph, H. Prance, and R. J. Prance, Phys. Rev. B **63**, 144530 (2001).
[56] M. J. Everitt, T. D. Clark, P. B. Stiffell, A. Vourdas, J. F. Ralph, R. J. Prance, and H. Prance, Phys. Rev. A **69**, 043804 (2004).
[57] Typically this happens at the middle point for the fundamental mode. This is equivalent to choosing the phase $\varphi_1(x_1) = 2\pi\phi_1(x_1)/\Phi_0 = \varphi_2(x_2) = 2\pi\phi_2(x_2)/\Phi_0 = 0$ and neglecting the phase drop along the connecting wires compared to that across the Josephson junction. In this case the fluxoid quantization in the loop reads $\Delta\phi_1 - \Delta\phi_2 + \phi_J + \Phi_{\circlearrowleft} = n\Phi_0$. The former assumption can always be made since the current flowing in the resonator depends only on the spatial derivative of the phase and not on its absolute value. The latter is a good approximation as long as the Josephson inductance is large compared to the kinetic inductance of the wires. This is the case as long as the superconducting wire is not made extremely narrow.
[58] T. P. Orlando and K. A. Delin, *Foundations of Applied Superconductivity* (Addison-Wesley, New York, 1991).
[59] J. Bourassa, F. Beaudoin, J. M. Gambetta, and A. Blais, Phys. Rev. A **86**, 013814 (2012).
[60] M. Schiró, M. Bordyuh, B. Öztop, and H. E. Türeci, Phys. Rev. Lett. **109**, 053601 (2012).
[61] C. M. Wilson and P. Forn-Díaz (private communication).
[62] M. Eckholt and J. J. García-Ripoll, Phys. Rev. A **77**, 063603 (2008).
[63] F. Galve, L. A. Pachón, and D. Zueco, Phys. Rev. Lett. **105**, 180501 (2010).
[64] M. Cramer and J. Eisert, New J. Phys. **8**, 71 (2006).
[65] J. Eisert and D. Gross, Phys. Rev. Lett. **102**, 240501 (2009).

[66]M. Cramer, A. Serafini, and J. Eisert, in *Quantum Information and Many Body Quantum Systems*, edited by S. M. M. Ericsson, CRM Series No. 8 (Publications of the Scuola Normale Superiore, Pisa, 2008), pp. 51–72.

[67]M. B. Plenio, J. Hartley, and J. Eisert, New J. Phys. **6**, 36 (2004).

[68]J. J. García-Ripoll, New J. Phys. **8**, 305 (2006).

[69]Note that we mention DMRG because of its widespread use in the field of Bose-Hubbard simulations (Ref. 70) and its enormous potential for nonequilibrium and dissipative dynamics (Ref. 71). In some context, such as weak nonlinearities, other methods based on the Heisenberg picture or stochastic equations could be used.

[70]A. J. Daley, C. Kollath, U. Schollwck, and G. Vidals, J. Stat. Mech. (2004) P04005.

[71]J. Prior, A. W. Chin, S. F. Huelga, and M. B. Plenio, Phys. Rev. Lett. **105**, 050404 (2010).

[72]J. Johansson, P. Nation, and F. Nori, Comput. Phys. Commun. **184**, 1234 (2013).

[73]A. Pathak, J. Phys. A **33**, 5607 (2000).

3.2.4 Publication 4: Fast microwave beam splitters from superconducting resonators. M. Haeberlein, D. Zueco, P. Assum, T. Weiβl, E. Hoffmann, B. Peropadre, J.J. García-Ripoll, E. Solano, F. Deppe, A. Marx, R. Gross.

arXiv:1302.0729, Submitted to App. Phys. Lett. (2012)

Fast microwave beam splitters from superconducting resonators

M. Haeberlein,[1,2,*] D. Zueco,[3,4] P. Assum,[1] T. Weißl,[5] E. Hoffmann,[1,2] B. Peropadre,[6] J.J. García-Ripoll,[6] E. Solano,[7,8] F. Deppe,[1,2] A. Marx,[1] and R. Gross[1,2]

[1] *Walther-Meißner-Institut, Bayrische Akademie der Wissenschaften, D-85748 Garching, Germany*
[2] *Physik-Department, Technische Universität München, D-85748 Garching, Germany*
[3] *Instituto de Ciencia de Materiales de Aragón y Departamento de Física de la Materia Condensada, CSIC-Universidad de Zaragoza, Pedro Cerbuna 12, 50009 Zaragoza, Spain*
[4] *Fundación ARAID, Paseo María Agustín 36, 50004 Zaragoza, Spain*
[5] *Institut Néel, CNRS, F-38042 Grenoble cedex 9*
[6] *Instituto de Física Fundamental, IFF-CSIC, Serrano 113-B, E-28006 Madrid, Spain*
[7] *Departamento de Química Física, Universidad del País Vasco UPV/EHU, Apartado 644, 48080 Bilbao, Spain*
[8] *IKERBASQUE, Basque Foundation for Science, Alameda Urquijo 36, 48011 Bilbao, Spain*

(Dated: February 5, 2013)

Coupled superconducting transmission line resonators have applications in quantum information processing and fundamental quantum mechanics. A particular example is the realization of fast beam splitters, which however is hampered by two-mode squeezer terms. Here, we experimentally study superconducting microstrip resonators which are coupled over one third of their length. By varying the position of this coupling region we can tune the strength of the two-mode squeezer coupling from 2.4 % to 12.9 % of the resonance frequency of 5.44 GHz. Nevertheless, the beam splitter coupling rate for maximally suppressed two-mode squeezing is 810 MHz, enabling the construction of a fast and pure beam splitter.

Recent advances in quantum electrodynamics with superconducting circuits (circuit QED) allowed for the experimental implementation of basic quantum computation algorithms [1]. Based on important results such as single photon generation [2] and multi-qubit gates [3, 4], advanced schemes for quantum error correction [5] and quantum feedback control [6] were proposed. In such digital approaches, superconducting quantum circuits substitute classical bits and bus systems, allowing one to construct a general purpose quantum computation device. However, digital quantum simulations typically require a large number of qubits and sophisticated error correction schemes [7], which is still a significant technological challenge to date. Therefore, in the short term it is more promising to focus on what is called analog quantum computation or simulation. In this approach, a model quantum system is used to set up a quantum mechanical evolution similar to the physical system of interest. However, contrary to the physical system, the input and output channels of the model system are easily accessible. Superconducting quantum circuits interacting with quantum microwave fields represent a particularly attractive model system [8]. If the microwave fields are confined inside cavities, proposals and early experiments towards the simulation of manybody Hamiltonians exist [9, 10]. Beyond that, recent work on systems involving propagating quantum microwaves [11, 12] suggests that it is possible implement all-optical quantum simulation schemes [13] in the microwave regime. This route seems particularly attractive, because superconducting circuits offer extraordinarily large nonlinearities [14] and therefore promise deterministic gates. A qubit can, for example, be encoded in an entangled state of two spatially separated superconducting waveguides. In such a situation, linear microwave beam splitters play an important role for the realization of single qubit rotations and two qubit Knill-Laflamme-Milburn gates [15, 16]. At this point, it is important to consider decoherence effects. In order to minimize them, a beam splitter should be fast in the sense that its coupling rate is a significant fraction of the frequency of the propagating microwaves. In such an ultrastrong coupling scenario, it is well-known [14, 17] that nonlinear effects arise for dipolar coupling. Hence, these nonlinear effects must be taken care of in order to ensure a pure beam splitter functionality. In this work, we first develop a theoretical model for fast and pure microwave beam splitters based on two frequency-degenerate coupled superconducting transmission line resonators with low external quality factors. We confirm this model with proof-of-principle experiments using microstrip resonators with a resonance frequency of $\omega_0/2\pi = 5.44\,\mathrm{GHz}$ and medium quality factors ranging between 150 and 600. Notably, we reach a beam splitter coupling strength of above 800 MHz while suppressing the nonlinear coupling by a factor of six by exploiting the 90° phase shift between the inductive and the capacitive coupling channel. This allows for many operations within decoherence times of superconducting tramsission line circuits [18]. We first introduce our model, which is based on Ref. 19. As we aim at the realization of a pure beam splitter, the Hamiltonian describing our experimental system ideally should read as

$$\mathcal{H} = \hbar\omega_0 \left(a^\dagger a + b^\dagger b\right) + \hbar g_{\mathrm{BS}} \left(a^\dagger b + a b^\dagger\right). \qquad (1)$$

Here, $a^\dagger$, $b^\dagger$, a, and b are the bosonic creation and annihilation operators of the two resonators and g_{BS} is the

beam splitter coupling rate. The beam splitter interaction term $g_{\mathrm{BS}}(a^\dagger b + a b^\dagger)$ splits the single resonance symmetrically, resulting in two new normal modes at the angular frequencies $\omega_\pm = \omega_0 \pm g_{\mathrm{BS}}$. We can apply Eq. (1) to the case of two transmission line resonators coupled in a small region around a position where either the magnetic field (current) or the electric field (voltage) has an antinode. While this scenario allows one to neglect either the capacitive or the inductive coupling channel, it limits practical devices to coupling rates smaller than approximately $g/\omega_0 \approx 2\%$. In order to achieve higher coupling rates, we distribute the coupling over a region spanning a significant fraction of the resonator length. As a consequence of the large coupling strength, the rotating wave approximation breaks down, giving rise to a two-mode squeezer (TMS) term in the Hamiltonian. Introducing the TMS coupling rate g_{TMS}, we find

$$\mathcal{H} = \hbar\widetilde{\omega}\left(a^\dagger a + b^\dagger b\right) + \hbar g_{\mathrm{BS}}\left(a^\dagger b + a b^\dagger\right) + \hbar g_{\mathrm{TMS}}\left(a^\dagger b^\dagger + a b\right). \tag{2}$$

This Hamiltonian describes two coupled harmonic oscillators of renormalized frequency $\widetilde{\omega}$, which is split – in general asymmetrically with respect to ω_0 – into two normal modes of frequencies $\omega_\pm$. The detailed definition of $\widetilde{\omega}$ is not relevant for this work and can be found in Ref. 19. The total coupling rate results from a superposition of a capacitive (g_{c}) and an inductive (g_{i}) coupling channel. The corresponding two channels couple via 90°-shifted single mode fields. Therefore, we find $g_{\mathrm{BS}} \equiv (g_{\mathrm{i}} + g_{\mathrm{c}})$ and $g_{\mathrm{TMS}} \equiv (g_{\mathrm{i}} - g_{\mathrm{c}})$. The coupling rates g_{c} and g_{i} depend solely on the resonator geometry. For a suitable resonator design, we can achieve $g_{\mathrm{c}} = g_{\mathrm{i}}$ and thus $g_{\mathrm{TMS}} = 0$. In other words, our distributed coupling approach allows for the realization of a pure beam splitter described by the Hamiltonian of Eq. (1) with large coupling rates g_{BS}.

In the remainder of this work, we experimentally validate the distributed coupling model of Eq. (2) by varying g_{c} and g_{i} in a controlled way. To this end, we fabricate samples containing two coupled microstrip resonators. Our design is shown in Fig. 1. For the fabrication of the chip shown in Fig. 1(a), we first sputter 100 nm Niobium on both sides of a 250 µm thick SiO_2 (50 nm) coated silicon wafer. One side is then patterned by optical lithography and reactive ion etching, the other one serves as ground plane. Our microstrip waveguides have a width of 204 µm to match an impedance of 50 Ω. As shown in Fig. 1(a), the two resonators have the same shape. In order to avoid geometry effects, we shift the position of the coupling capacitors defining both ends of the resonators rather than redesigning the coupling region. In this way, we investigate seven different configurations where the resonators are coupled over a length of $\ell_{\mathrm{c}} = 3$ mm at different physical coupling positions ℓ_{left} [see Fig. 1(b)]. For each two-resonator sample, we fabricate a single resonator sample with the same parameters for comparison.

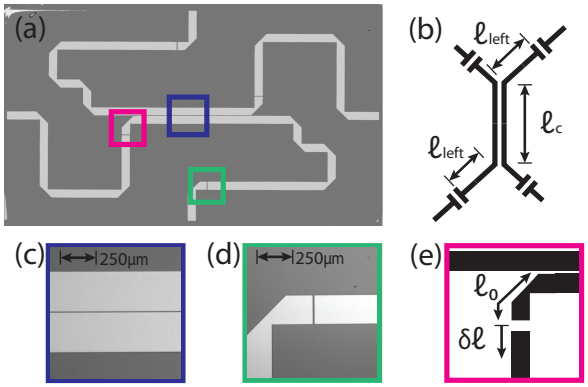

FIG. 1. Sample layout. (a) Reworked photograph of two coupled resonators on a 10 mm × 6 mm silicon wafer. (b) Schematic circuit diagram. The resonators couple over an electrical length ℓ_{c}. The coupling region starts at the electrical length ℓ_{left}. (c, d) Enlarged view of the region marked with the blue (green) box in (a). (e) Sketch of the region marked with the purple box in (a).

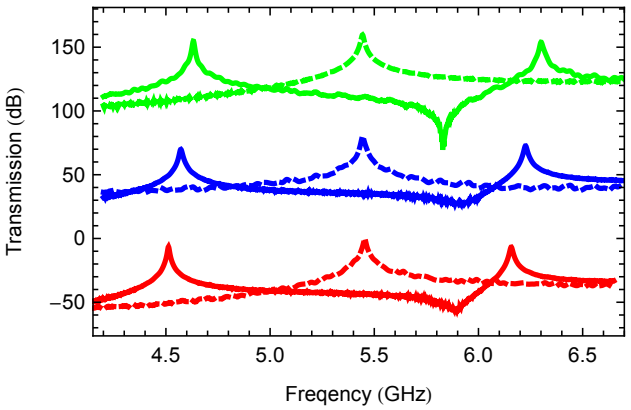

FIG. 2. Transmission spectra of three resonators coupled over a length of 3 mm, with $\delta\ell = 0$ µm (bottom), 300 µm (middle), and 600 µm (top). The top and middle curves are shifted by 160 dB and 80 dB, respectively. The dashed lines show the respective single resonator transmission spectra.

In our experiments, we measure transmission spectra of the fundamental mode of single and coupled microstrip resonators at 4.2 K and extract the resonance frequencies ω_0 and $\omega_\pm$, respectively. Typical examples are shown in Fig. 2. It can be seen that the two transmission peaks of the coupled resonators split asymmetrically with respect to the peak of the single resonator. This already indicates that the coupling is described by Eq. 2. Furthermore, we find that $\omega_0 = 5.44$ GHz is independent of the position of the coupling capacitors as expected. Hence, also the total electrical length $\ell_{\mathrm{tot}} = \pi c/(\omega_0\sqrt{\epsilon_{\mathrm{eff}}})$ is the same for all configurations. With $c = 2.99 \times 10^8$ m/s and the effective dielectric constant $\epsilon_{\mathrm{eff}} = 7.59$, we find $\ell_{\mathrm{tot}} = 9.963$ mm.

In order to extract the coupling parameters g_c and g_i, we make use of the microscopic model [19] leading to Eq. (2). The input parameters to this model are the ratio of the self-inductance (capacitance) per length to the mutual inductance (capacitance) per unit length $L_{\rm rat}$ ($C_{\rm rat}$) and the electrical position of the coupling region. The latter cannot be determined directly from the sample geometry because the physical length of the transmission line differs from the electrical one whenever there is a bend in the resonator. Furthermore, the ratios $L_{\rm rat}$ and $C_{\rm rat}$ depend implicitly on the electrical coupling position. Hence, the first step in our analysis is the determination of the electrical position of the coupling

$$\ell_{\rm left} = \ell_0 + \delta\ell. \tag{3}$$

Here, as shown in Fig. 1(e), ℓ_0 is the minimum distance between the coupling capacitor and the border of the coupling region and $\delta\ell$ accounts for the varying position of the coupling capacitor. We obtain $\delta\ell$ directly from the resonator geometry because in good approximation the electrical length of a straight segment of the resonator equals its physical length. With the definition of Eq. (3) and the model in Ref. 19, we can write

$$L_{\rm rat} = \frac{\nu_{\rm L}\omega_+^2}{\omega_0^2 - \nu_{\rm L}\omega_+^2}$$
$$C_{\rm rat} = \frac{\nu_{\rm C}(\omega_0^2-\omega_-^2) + \nu_{\rm C}\omega_0^2\omega_+^2/(\omega_0^2 - 2\nu_{\rm L}\omega_+^2)}{2\omega_-^2}.$$

Here, $\nu_{\rm L,C} = \ell_{\rm tot}/\Delta_{\rm L,C}$ are geometry factors. The expressions $\Delta_{\rm L,C}$ represent the overlap integrals of the magnetic (electric) field modes. For our scenario of homogeneous resonators and fundamental mode coupling, we can set $2\pi\Delta_{\rm L,C} = \ell_c \mp \ell_{\rm tot}\,[\sin(2\pi(\ell_{\rm left}+\ell_c)/\ell_{\rm tot}) - \sin(2\pi\ell_{\rm left}/\ell_{\rm tot})]$. In order to extract ℓ_0 from the measured peak positions ω_0 and $\omega_\pm$, we first assume that the field in the resonators is a TEM-mode and, consequently, $L_{\rm rat}$ and $C_{\rm rat}$ are independent of $\ell_{\rm left}$. Subsequent minimization of the normalized variance of $L_{\rm rat} + C_{\rm rat}$ for all seven capacitor configurations yields $\ell_0 = 1.271\,$mm. Figure 3(a) shows that indeed for this value of ℓ_0, the parameters $L_{\rm rat}$ and $C_{\rm rat}$ do not deviate more than 3 % from their average value. This gives evidence that our model is self-consistent.

In the next step, we use $L_{\rm rat}$, $C_{\rm rat}$, and $\ell_0 + \delta\ell$ to calculate $g_{\rm BS}$, $g_{\rm TMS}$, and $\tilde{\omega}$. In Fig. 3(b), we show $g_{\rm BS}/\omega_0$ and $g_{\rm BS}/g_{\rm TMS}$ as a function of $\ell_{\rm rel} \equiv \ell_{\rm left}/(\ell_{\rm tot} - \ell_c)$. We observe a maximum suppression of the TMS coupling rate to $g_{\rm TMS}/g_{\rm BS} = 16\%$ and a minimum suppression of $g_{\rm TMS}/g_{\rm BS} = 43\%$ while the beam splitter coupling rate stays nearly constant at $g_{\rm BS} = (816 \pm 7)\,$MHz. An extrapolation of the model prediction suggests that the TMS coupling should vanish at the relative coupling position $\ell_{\rm rel} = 14\,\%$. Nevertheless, the beam splitter coupling rate

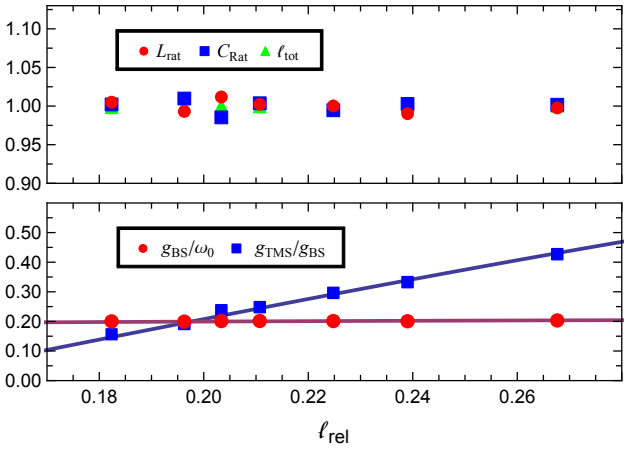

FIG. 3. Top: The parameters $L_{\rm rat}$, $C_{\rm rat}$, and $\ell_{\rm tot}$ divided by their respective average value displayed against the relative coupling position. Bottom: Coupling ratios as a function of the relative coupling position. The solid line is obtained using the average values of $L_{\rm rat}$, $C_{\rm rat}$, and $\ell_{\rm tot}$.

at this position still exceeds 780 MHz. This configuration is ideally suited for the realization of a fast beam splitter and can in principle be reached with our geometry. Finally, we analyze the potential of our devices for the investigation of ultrastrong coupling. In this context, we note that the coupling between the two resonators can be ultrastrong in the same way as the qubit-resonator coupling discussed in Ref. 14. For our samples, we achieve a maximum TMS coupling rate of 351 MHz for $\ell_{\rm rel} = 27\%$. When moving the coupling region to the center of the resonators, the maximum rate would become 702 MHz and $g_{\rm TMS}/\omega_0 = 12.9\%$. This implies that the relative coupling rate of our device is equally large as in Ref. 14. Since our devices do not require nonlinearities and are therefore much easier to fabricate, they provide a promising way of studying the dynamics of ultrastrong coupling.

In summary, we use linear superconducting circuits to implement a Hamiltonian with a beam splitter coupling strength of more than 800 MHz, where the TMS term is suppressed by a factor of six. We demonstrate a tunability of the coupling ratio $g_{\rm TMS}/g_{\rm BS}$ between 16 % and 43 %. An extrapolation of our result shows that an ultrastrong coupling scenario as well as a pure beam splitter Hamiltonian can be reached with our sample design. This paves the way for studying ultrastrong coupling dynamics and, by design of a suitable capacitor configuration [16], building fast beam splitter circuits for analog quantum computation and simulation with both standing-wave and propagating quantum microwaves.

We acknowledge support from the Deutsche Forschungsgemeinschaft via SFB 631, the German excellence initiative via the Nanosystems Initiative Munich (NIM), from the EU projects SOLID, CCQED and PROMISCE, EPSRC EP/H050434/1,

Basque Government IT472-10, and Spanish MINECO FIS2009-12773-C02-01, FIS2011-25167, and FIS2012-36673-C03-02.

* max.haeberlein@wmi.badw-muenchen.de

[1] E. Lucero, R. Barends, Y. Chen, J. Kelly, M. Mariantoni, A. Megrant, P. O'Malley, D. Sank, A. Vainsencher, J. Wenner, T. White, Y. Yin, A. N. Cleland, and J. M. Martinis, Nat. Phys. **8**, 719 (2012).

[2] M. Hofheinz, E. M. Weig, M. Ansmann, R. C. Bialczak, E. Lucero, M. Neeley, A. D. OConnell, H. Wang, J. M. Martinis, and A. N. Cleland, Nature **454**, 310 (2008).

[3] L. DiCarlo, J. M. Chow, J. M. Gambetta, L. S. Bishop, B. R. Johnson, D. I. Schuster, J. Majer, A. Blais, L. Frunzio, S. M. Girvin, and R. J. Schoelkopf, Nature **460**, 240 (2009).

[4] A. Fedorov, L. Steffen, M. Baur, M. P. d. Silva, and A. Wallraff, Nature **481**, 170 (2012).

[5] D. P. DiVincenzo and P. W. Shor, Phys. Rev. Lett. **77**, 3260 (1996).

[6] R. Vijay, C. Macklin, D. H. Slichter, S. J. Weber, K. W. Murch, R. Naik, A. N. Korotkov, and I. Siddiqi, Nature **490**, 77 (2012).

[7] I. Buluta and F. Nori, Science **326**, 108 (2009).

[8] R. J. Schoelkopf and S. M. Girvin, Nature **451**, 664 (2008).

[9] M. Leib and M. J. Hartmann, New J. Phys. **12**, 093031 (2010).

[10] A. A. Houck, H. E. Tureci, and J. Koch, Nat. Phys. **8**, 292 (2012).

[11] E. P. Menzel, R. Di Candia, F. Deppe, P. Eder, L. Zhong, M. Ihmig, M. Haeberlein, A. Baust, E. Hoffmann, D. Ballester, K. Inomata, T. Yamamoto, Y. Nakamura, E. Solano, A. Marx, and R. Gross, Phys. Rev. Lett. **109**, 250502 (2012).

[12] I.-C. Hoi, C. M. Wilson, G. Johansson, T. Palomaki, T. M. Stace, B. Fan, and P. Delsing, ArXiv e-prints (2012), arXiv:1207.1203 [quant-ph].

[13] J. L. O'Brien, Science **318**, 1567 (2007).

[14] T. Niemczyk, F. Deppe, H. Huebl, E. P. Menzel, F. Hocke, M. J. Schwarz, J. J. Garcia-Ripoll, D. Zueco, T. Hmmer, E. Solano, A. Marx, and R. Gross, Nat. Phys. **6**, 772 (2010).

[15] E. Knill, R. Laflamme, and G. J. Milburn, Nature **409**, 46 (2001).

[16] L. Chirolli, G. Burkard, S. Kumar, and D. P. DiVincenzo, Phys. Rev. Lett. **104**, 230502 (2010).

[17] J. Casanova, G. Romero, I. Lizuain, J. J. Garcia-Ripoll, and E. Solano, Phys. Rev. Lett. **105**, 263603 (2010).

[18] R. Barends, J. Wenner, M. Lenander, Y. Chen, R. C. Bialczak, J. Kelly, E. Lucero, P. O'Malley, M. Mariantoni, D. Sank, H. Wang, T. C. White, Y. Yin, J. Zhao, A. N. Cleland, J. M. Martinis, and J. J. A. Baselmans, Appl. Phys. Lett. **99**, 113507 (2011).

[19] B. Peropadre, D. Zueco, F. Wulschner, F. Deppe, A. Marx, R. Gross, and J. J. García-Ripoll, ArXiv e-prints (2012), arXiv:1207.3408 [cond-mat.supr-con].

3.3 Scattering by an artificial atom

In this second part of the Thesis, we leave aside the control of quantum systems using switchable couplers, to rather focus on the control of propagating photons through their scattering on an artificial atom [SF05b, SF05a]. Our interest stems from the first experiments showing the strong interaction between light and individual atoms in the absence of confining cavities. The coherent coupling between the photon and the atoms manifests as a quantum interference in the scattering process, that can result in a perfect extinction of the forward propagating wave. This fascinating effect has been observed in light scattered by individual atoms [WGH+07], but with just a 12% of extinction in the forward direction. This is because of the frequency mismatch between incident and scattered waves[13], and the extremely challenging task of addressing individual atoms with lasers.

By contrast, this frequency mismatch does not occur in circuit QED, where light-matter interaction takes place in one dimension, which is by far much more efficient than in 3D. In one dimension, the spontaneous emission by the artificial atom produces a photon propagating either backwards of forward in the open line, that is, the emitted photon is a plane wave as the incident photon. Recent experiments in circuit QED have confirmed the theoretical predictions with impressive results, showing extinctions of 94% in the transmitted wave [AZA+10]. This brings with it important consequences in the photon dynamics: as the photon can only propagate forward or backwards, the overall effect is that the photon has been reflected by the atom. In this Thesis we will exploit this coherent coupling to control the transport properties of propagating photons in an open transmission line. Moreover, we will show how these properties depend on the scatterer internal structure. Finally, we propose several applications for quantum information processing with flying photons.

3.3.1 Summary and discussion of results

In publication P5 we focus on an in-depth theoretical study of propagating microwaves in an open transmission line scattering off a single artificial atom (this is schematically shown in Fig.3.5). Our atom will be a transmon qubit, which possesses a three-level energy structure, as we shown in Chapter 1. We will show that, depending on whether the transmon behaves as a two-

[13] Notice that the spontaneously emitted wave by the atom is an spherical wave, while the incident one is a plane wave.

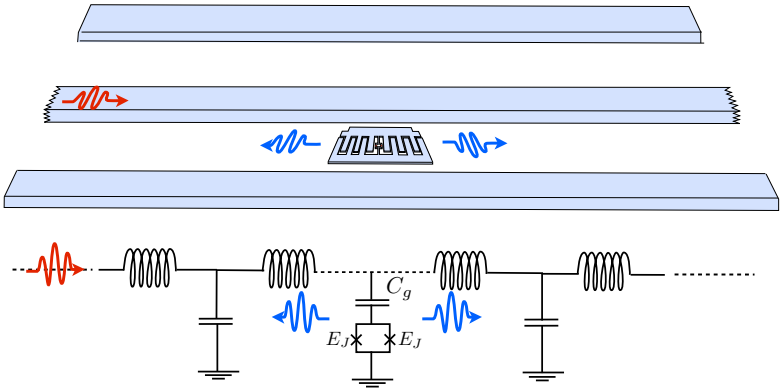

Figure 3.5: Schematics of a propagating photon facing an individual artificial atom in an infinite transmission line, and its equivalent circuit.

or a three-level system, very different physics takes place. In particular, for a transmon qubit working in the two-level approximation, the qubit acts as a saturable mirror for the incident photons. On the other hand, by driving a strong coherent field to the second transition of the transmon, the atom becomes transparent, yielding to perfect transmission of the incident photons. We finally study the photon antibunching of the reflected field, and its dependence with finite temperature and detection bandwidth. Below we present the main results of this work:

- We consider a transmon qubit capacitively coupled to a semi-infinite transmission line. Starting from a fully microscopic description, we derive the equations of motion for the coupled system. Within the rotating wave approximation[14] the equation of motion can be interpreted as a quantum Langevin equation for the transmon, and an input-output relation for quantum fields.

- As we shown in Chapter 2, Langevin equations are generally not solvable, so we derive a master equation for the transmon in its Lindblad form. We derive closed expressions for the relaxation and pure dephasing rates Γ_{ij}, Γ_ϕ as a function of the microscopic details of the system. We generalize these results to the case of N semi-infinite transmission lines meeting at the transmon position. We place especial emphasis in the case of $N = 2$, i.e. a transmon qubit placed in an infinite transmission line.

[14] In this particular setup,s the rotating wave approximation is always valid.

- Using the master equation and the input-output relation, we study the scattering of a coherent signal by a transmon qubit in the two-level approximation, as a function of the input power and frequency of the drive. These parameters together with the qubit decay rates, determine the reflection and transmission coefficients that fully characterize the dynamics of the output fields. In particular, for a low-amplitude drive on resonance with the qubit, we obtain the experimentally observed perfect reflection of the photon by the atom.

- We consider the scattering problem in the three-level approximation of the transmon: a coherent probe at the single photon level scatters off the transmon at the first transition, while a strong control pulse drives the second transition. We observe that the reflection and transmission coefficients of the probe depends on the frequency and drive amplitude of the control pulse. Thus, we can employ the strong control pulse to control the reflection and transmission at the probe frequency. This is usually called Electromagnetically Induced Transparency (EIT) [BIH91, AAZ+10], which in this case is assisted by the splitting of the second transition –usuall called Autler-Townes splitting [AT55].

- Finally, we study second order correlations functions $g_2(\tau)$ for the reflected and the transmitted field through the transmon . For low amplitude drives, we observe strong antibunching in the reflected field, and strong bunching in the transmitted one. The transmon acts as a photon-number filter, reflecting back to the line the one-photon Fock state $|1\rangle$ and transmitting higher multiphoton states [HPL+12]. We include finite temperature and finite detection bandwidth in the system. This can be done by adding a single-mode transmission line resonator in resonance with the transmon, acting as a frequency filter.

In conclusion, we have reported on a comprehensive study of the scattering of coherent states on a single transmon, from a microscopic viewpoint. From the equations of motion, we have derived an input-output relation for the quantum fields and a master equation for the transmon. Our results show that the transmon in the two-level approximation behaves as a saturable mirror for the incoming photons. On the other hand, a strong control pulse addressing the second transition of the transmon induces an Autler-Townes splitting on the excited energy levels, yielding to perfect transmission at the probe frequency. Our theoretical results are in excellent agreement with circuit QED experiments, in particular with those presented in publication P6 and P7.

3.3.2 Publication 5: Scattering of coherent states on a single artificial atom. B. Peropadre, J. Lindkvist, I.-C. Hoi, C.M. Wilson, J.J. García-Ripoll, P. Delsing, G. Johansson. New J. Phys. 15 035009 (2013)

New Journal of Physics
The open access journal for physics

Scattering of coherent states on a single artificial atom

B Peropadre[1,3], J Lindkvist[2,3], I-C Hoi[2], C M Wilson[2], J J Garcia-Ripoll[1], P Delsing[2] and G Johansson[2,4]

[1] Instituto de Física Fundamental, CSIC, Calle Serrano 113-bis, Madrid E-28006, Spain

[2] Department of Microtechnology and Nanoscience, Chalmers University of Technology, Göteborg, Sweden

E-mail: Goran.L.Johansson@chalmers.se

New Journal of Physics **15** (2013) 035009 (17pp)
Received 5 October 2012
Published 6 March 2013
Online at http://www.njp.org/
doi:10.1088/1367-2630/15/3/035009

Abstract. In this work, we theoretically analyze a circuit quantum electrodynamics design where propagating quantum microwaves interact with a single artificial atom, a single Cooper-pair box. In particular, we derive a master equation in the so-called transmon regime, including coherent drives. Inspired by recent experiments, we then apply the master equation to describe the dynamics in both a two-level and a three-level approximation of the atom. In the two-level case, we also discuss how to measure photon antibunching in the reflected field and how it is affected by finite temperature and finite detection bandwidth.

[3] These two authors contributed equally to the manuscript.

[4] Author to whom any correspondence should be addressed.

Contents

1. Introduction

In recent years, the field of circuit quantum electrodynamics (circuit QED) [1, 2] has become one of the most promising platforms in the study of light–matter interaction. One of the most important breakthroughs in this field was the achievement of a strong coupling between light and matter, or microwave photons and Josephson-based artificial atoms [3, 4]. Since then, many experiments have been carried out within the framework of superconducting circuits [5–9], revealing a wide variety of novel quantum phenomena. Most of these experiments share a common feature, namely the interaction between artificial atoms and isolated modes of the electromagnetic field in a cavity. Within circuit QED, there is now growing interest in studying propagating fields interacting with artificial atoms, owing to, e.g., its potential interest for condensed matter [10] and all-optical quantum information [11]. Theoretically, coherent coupling between an atom or superconducting qubit and a one-dimensional continuum of modes has been discussed for some time [12–17], and there exist now a growing number of experiments investigating this system in a circuit QED setup [18–25].

In this paper, we report on an in-depth microscopic description of the coherent coupling between a field propagating through an open transmission line (TL) and a superconducting artificial atom based on the single Cooper-pair box (SCB) [26–32]. In more detail, we analyze the so-called transmon regime [8, 33] and study the photon transport properties of this system according to different approximations. On the one hand, in the two-level approximation and under certain conditions, the qubit behaves like a saturable mirror [12, 13]. On the other hand, by including a second excited state of the transmon, we can effectively make the medium transparent for the incident photons using a coherent control field in resonance with this second transition. Finally, we also discuss how the photon antibunching observed in the reflected field is reduced by finite temperature and finite detection bandwidth. Our theoretical predictions are in full agreement with recent experiments [22, 23, 25].

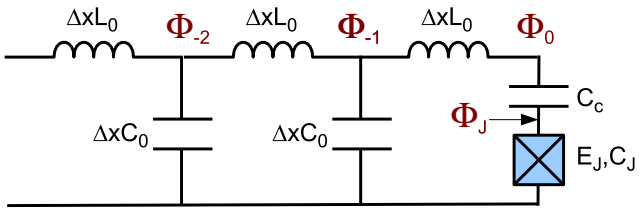

Figure 1. Discretized circuit describing the interaction of an SCB with microwaves photons propagating in a semi-infinite TL.

This paper is organized as follows. In section 2, we derive the master equation of an SCB coupled to an open TL. In section 2.1, we start from a discretized lumped-element description of the TL and in section 2.2 we proceed to the continuum description. In section 2.3, we discuss the regime where the system can be described as an SCB weakly coupled to the voltage of the TL, at the coupling point. We thus arrive at the Hamiltonian of a voltage-biased SCB, weakly coupled to a bath of harmonic oscillators, i.e. the electromagnetic modes of the TL. Making standard weak coupling approximations, we then derive a master equation in Lindblad form in section 2.4 and attach a coherent drive in section 2.5. For simplicity, we go through these derivations considering an SCB at the end of a semi-infinite TL, but in section 2.6 we discuss how the master equation can be straightforwardly extended to an arbitrary number of semi-inifinte TLs, all meeting at the SCB. In particular, this includes the important case of a single infinite TL.

In section 3, we then apply the master equation to a few experimentally relevant cases [22, 23]. Section 3.1 is devoted to the reflection and transmission of a single near resonant coherent drive, while section 3.2 includes two coherent drives, where one is used to control the transmission of the other. Finally in section 3.3, we investigate how the photon antibunching observed in the reflected field is influenced by finite temperature and finite detection bandwidth.

2. The model

In this section, we present a general formalism of the light–matter scattering in a one-dimensional continuum from a microscopic point of view. We start from a Hamiltonian description, arriving at the well-known input–output relations for the microwave field. We then follow the usual approach [34] to describe the joint state of the light–matter system by introducing dissipation, resulting in the standard quantum optical master equation.

2.1. The discrete circuit model, Hamiltonian and equations of motion

Consider a semi-infinite TL with characteristic inductance L_0 and capacitance C_0 per unit length. We discretize the TL [35] in units of the small length Δx, which we take to zero at the end of the calculation. The TL nodes are numbered with negative integers, while the SCB island node has index J and its Josephson junction has a capacitance C_J to ground and a Josephson energy E_J. The SCB is coupled to the TL at the zeroth node, through the capacitance C_c, as depicted in figure 1.

To describe the circuit dynamics, we use the node fluxes $\Phi_\alpha(t) = \int^t \mathrm{d}t' V_\alpha(t')$ as coordinates [36]. They are the time integrals of the node voltages and although less intuitive than

the voltages, this choice greatly simplifies the description of the Josephson junction. Starting from a circuit Lagrangian, we can derive the discrete circuit Hamiltonian [37]

$$H_{\mathrm{d}} = \frac{(p_0 + p_{\mathrm{J}})^2}{2C_{\mathrm{J}}} + \frac{p_0^2}{2C_{\mathrm{c}}} - E_{\mathrm{J}} \cos\left(\frac{2e}{\hbar}\Phi_{\mathrm{J}}\right) + \frac{1}{\Delta x}\sum_{n<0}\frac{p_n^2}{2C_0} + \frac{(\Phi_{n+1} - \Phi_n)^2}{2L_0}, \tag{1}$$

where the charges p_α are the conjugate momenta to the node fluxes Φ_α, fulfilling the canonical commutation relations

$$[\Phi_\alpha, p_\beta] = \mathrm{i}\hbar\delta_{\alpha,\beta}, \quad [\Phi_\alpha, \Phi_\beta] = [p_\alpha, p_\beta] = 0,$$

where $\delta_{\alpha,\beta}$ denotes Kronecker's delta. From the Hamiltonian, we obtain Heisenberg's equations of motion for the TL operators ($n < 0$)

$$\partial_t \Phi_n = \frac{p_n}{\Delta x C_0}, \quad \partial_t p_n = \frac{\Phi_{n-1} - 2\Phi_n + \Phi_{n+1}}{\Delta x L_0} \tag{2}$$

and for the SCB operators

$$\partial_t p_0 = \frac{\Phi_{-1} - \Phi_0}{\Delta x L_0}, \tag{3}$$

$$\partial_t \Phi_0 = \frac{p_0 + p_{\mathrm{J}}}{C_{\mathrm{J}}} + \frac{p_0}{C_{\mathrm{c}}} = \frac{C_\Sigma}{C_{\mathrm{c}} C_{\mathrm{J}}} p_0 + \frac{p_{\mathrm{J}}}{C_{\mathrm{J}}}, \tag{4}$$

$$\partial_t p_{\mathrm{J}} = -E_{\mathrm{J}} \frac{2e}{\hbar} \sin\left(\frac{2e}{\hbar}\Phi_{\mathrm{J}}\right), \tag{5}$$

$$\partial_t \Phi_{\mathrm{J}} = \frac{p_0 + p_{\mathrm{J}}}{C_{\mathrm{J}}}, \tag{6}$$

where $C_\Sigma = C_{\mathrm{c}} + C_{\mathrm{J}}$.

2.2. Continuum limit

In the continuum limit $\Delta x \to 0$, the charge of each TL node will go to zero together with the node capacitance. Thus, we define a charge density field $p(x_n, t) = p_n(t)/\Delta x$ and a flux field $\Phi(x_n, t) = \Phi_n(t)$, where we define the spatial coordinate $x_n = n\Delta x$ for $n < 0$, along the TL. The continuum equations of motion for the TL ($x < 0$) are

$$\partial_t p(x) = \frac{\partial_x^2 \Phi(x)}{L_0}, \quad \partial_t \Phi(x) = \frac{p(x)}{C_0}. \tag{7}$$

These are the equations of motion for the massless Klein–Gordon field, having freely propagating left- and right- moving solutions with velocity $v = 1/\sqrt{L_0 C_0}$. Therefore, we can write the general solution for $x < 0$ as a linear combination of right- and left- moving second-quantized fields

$$\begin{aligned} \Phi_{\rightleftarrows}(x, t) &= \sqrt{\frac{\hbar Z_0}{4\pi}} \int_0^\infty \frac{\mathrm{d}\omega}{\sqrt{\omega}} \left(a_\omega^{\rightleftarrows} \mathrm{e}^{-\mathrm{i}(\omega t \mp k_\omega x)} + \mathrm{h.c.}\right), \\ p_{\rightleftarrows}(x, t) &= -\mathrm{i}\sqrt{\frac{\hbar Z_0}{4\pi}} \int_0^\infty \mathrm{d}\omega \sqrt{\omega} \left(a_\omega^{\rightleftarrows} \mathrm{e}^{-\mathrm{i}(\omega t \mp k_\omega x)} - \mathrm{h.c.}\right), \end{aligned} \tag{8}$$

where $k_\omega = \omega/v$ and $Z_0 = \sqrt{L_0/C_0}$ is the characteristic impedance of the TL. The operators $a_\omega^{\leftrightarrows}$ annihilate a left/right-moving photon with frequency ω, and obey the bosonic canonical commutation relations, $[a_\omega^{\leftarrow}, (a_{\omega'}^{\leftarrow})^\dagger] = [a_\omega^{\rightarrow}, (a_{\omega'}^{\rightarrow})^\dagger] = \delta(\omega - \omega')$ and $[a_\omega^{\leftarrow}, (a_{\omega'}^{\rightarrow})^\dagger] = [a_\omega^{\rightleftarrows}, a_{\omega'}^{\rightleftarrows}] = 0$. Finally, we note that in the continuum limit, (3) changes into

$$\partial_t p_0 = -\frac{\partial_x \Phi(0^-)}{L_0}. \tag{9}$$

To describe the system dynamics, we first need to specify the incoming, right-moving field

$$\Phi^{\text{in}}(t) = \Phi_{\rightarrow}(0^-, t).$$

Given this initial condition, we can then calculate the SCB dynamics, as well as the outgoing field

$$\Phi^{\text{out}}(t) = \Phi_{\leftarrow}(0^-, t),$$

propagating to the left in the line. The flux at $x = 0$ is simply the sum of the incoming and outgoing flux fields

$$\Phi_0(t) = \Phi(0^-, t) = \Phi^{\text{in}}(t) + \Phi^{\text{out}}(t) + V_{\text{dc}} t, \tag{10}$$

where for simplicity we also explicitly extracted the dc voltage bias V_{dc}, implying that Φ^{in} and Φ^{out} have no dc components. Now, solving for p_0 from (4) gives

$$p_0 = \frac{C_c C_J}{C_\Sigma}\left[V_{\text{dc}} + \partial_t(\Phi^{\text{in}} + \Phi^{\text{out}})\right] - \frac{C_c}{C_\Sigma} p_J \tag{11}$$

and inserting this expression into (6), we arrive at

$$\partial_t \Phi_J = \frac{p_J + C_c\left[V_{\text{dc}} + \partial_t(\Phi^{\text{in}} + \Phi^{\text{out}})\right]}{C_\Sigma}. \tag{12}$$

We then insert Φ_0 from (10) in (13) and arrive at

$$\partial_t p_0 = -\frac{\partial_x \Phi(0^-)}{L_0} = \frac{\partial_t(\Phi^{\text{in}} - \Phi^{\text{out}})}{Z_0}, \tag{13}$$

where we used the relation $\partial_x \Phi_{\rightleftarrows}(0^-) = \mp v^{-1} \partial_t \Phi_{\rightleftarrows}(0^-)$ to change the spatial derivative into a time derivative. Inserting the expression for p_0 from (11) into the left-hand side of this equation and integrating once with respect to time leads to

$$\Phi^{\text{out}} = \Phi^{\text{in}} + Z_0 \frac{C_c}{C_\Sigma} p_J - \tau_{\text{RC}} \partial_t(\Phi^{\text{in}} + \Phi^{\text{out}}), \tag{14}$$

where the time $\tau_{\text{RC}} = C_c C_J Z_0 / C_\Sigma$ is the characteristic RC time for discharging the SCB through the TL. Equations (5), (12) and (14), in principle, give the full time evolution of the SCB operators Φ_J and p_J as well as the out-field, in terms of the in-field. However, to solve these nonlinear equations straightforwardly, we need to make some approximations.

2.3. Voltage-biased single Cooper-pair box approximation

In the following, we will neglect the last term in (14). Since the time derivative enters the product with τ_{RC}, this will be a good approximation as long as the relevant frequencies of the incoming field Φ^{in} and of the SCB dynamics (p_{J}) are much lower than the inverse RC time. Under this approximation, the final equations of motion are

$$\partial_t \Phi_{\mathrm{J}} = \frac{p_{\mathrm{J}} + C_{\mathrm{c}} \left(V_{\mathrm{dc}} + 2\partial_t \Phi^{\mathrm{in}} + \frac{\tau_{\mathrm{RC}}}{C_{\mathrm{J}}} \partial_t p_{\mathrm{J}} \right)}{C_\Sigma}, \tag{15}$$

$$\partial_t p_{\mathrm{J}} = -E_{\mathrm{J}} \frac{2e}{\hbar} \sin\left(\frac{2e}{\hbar} \Phi_{\mathrm{J}} \right), \tag{16}$$

$$\Phi^{\mathrm{out}} = \Phi^{\mathrm{in}} + \frac{\tau_{\mathrm{RC}}}{C_{\mathrm{J}}} p_{\mathrm{J}}. \tag{17}$$

Here we also note that this approximation is valid in recent experiments [22, 23], where $Z_0 = 50\,\Omega$, $C_{\mathrm{c}} \sim 10\,\mathrm{fF}$ and $C_{\mathrm{J}} \sim 25\,\mathrm{fF}$, giving an inverse RC timescale of $1/(2\pi\tau_{\mathrm{RC}}) \sim 400\,\mathrm{GHz}$, which is around 50 times higher than the relevant frequency of Φ^{in} and p_{J}, set by the qubit frequency $\sim$7.5 GHz.

The above set of equations (15)–(17) corresponds to the Hamiltonian

$$H = H_{\mathrm{sys}} + H_{\mathrm{int}} + H_{\mathrm{bath}}, \tag{18}$$

$$H_{\mathrm{sys}} = \frac{[p_{\mathrm{J}} + C_{\mathrm{c}} V_{\mathrm{dc}}]^2}{2C_\Sigma} - E_{\mathrm{J}} \cos\left(\frac{2e}{\hbar} \Phi_{\mathrm{J}} \right), \tag{19}$$

$$H_{\mathrm{int}} = \frac{C_{\mathrm{c}}}{C_\Sigma} (p_{\mathrm{J}} + C_{\mathrm{c}} V_{\mathrm{dc}}) \partial_t \Phi(0^-, t), \tag{20}$$

$$H_{\mathrm{bath}} = \frac{\left[C_{\mathrm{c}} \partial_t \Phi(0^-, t) \right]^2}{2C_\Sigma} + \int_{-\infty}^{0} \frac{p(x,t)^2}{2C_0} + \frac{[\partial_x \Phi(x,t)]^2}{2L_0} \, \mathrm{d}x. \tag{21}$$

Thus, we have arrived at the Hamiltonian of a voltage-biased SCB, weakly coupled to the TL voltage at $x = 0$, i.e. $V_0(t) = \partial_t \Phi_0(t)$. (Here, we note that for the uncoupled TL, without SCB, $\Phi_0(t) = 2\Phi^{\mathrm{in}}(t)$ due to the perfect reflection.) Truncating the Hilbert space of H_{sys} to two levels, (18) is just the spin-boson Hamiltonian. From this point, we can proceed with a Bloch–Redfield derivation of a master equation for the SCB only [38]. By comparing to section 3.2 in [34], we also note that the equations of motion (15)–(16) can be interpreted as quantum Langevin equations (QLE) of the form

$$\dot{Y} = \frac{\mathrm{i}}{\hbar} [H_{\mathrm{sys}}, Y] + \frac{\mathrm{i}}{2\hbar} [\gamma \dot{X} - 2\sqrt{\gamma v} \dot{A}^{\mathrm{in}}, [X, Y]]_+, \tag{22}$$

whereas (17) stands for the input–output relation

$$A^{\mathrm{out}}(t) = A^{\mathrm{in}}(t) - \sqrt{\frac{\gamma}{v}} X(t) \tag{23}$$

using the identifications $Y = \Phi_{\mathrm{J}}$, $X = -(p_{\mathrm{J}} + C_{\mathrm{c}} V_{\mathrm{dc}})$, $A^{\mathrm{in}} = \sqrt{C_0} \Phi^{\mathrm{in}}$ and where

$$\gamma = Z_0 \left(\frac{C_{\mathrm{c}}}{C_\Sigma} \right)^2 \tag{24}$$

is the damping constant that accounts for spontaneous emission.

2.4. Master equation

From the QLE (22), we can derive a master equation for the reduced density matrix of the SCB in the transmon regime. As the input field, we first consider a thermal background at temperature T, giving rise to a photon occupation number of

$$n_\omega = \frac{1}{\exp(\hbar\omega/k_B T) - 1}. \tag{25}$$

We assume that the density matrix initially can be written as a direct product, as well as Markovian properties and short correlation times for the TL variables. In the case when the damping (24) is much smaller than the system eigenenergies, we arrive, after also employing the rotating wave approximation, at the following quantum optical master equation,

$$\dot{\rho}(t) = -\frac{\mathrm{i}}{\hbar}[H_{\mathrm{sys}}, \rho] + \frac{2\gamma}{\hbar}\sum_m \omega_m[(n_{\omega_m}+1)\mathcal{D}(X_m^-)\rho + n_{\omega_m}\mathcal{D}(X_m^+)\rho] \tag{26}$$

with the Lindblad operator defined by $\mathcal{D}(c)\rho = c\rho c^\dagger - \frac{1}{2}\left(c^\dagger c\rho + \rho c^\dagger c\right)$. Also, X has been decomposed into eigenoperators of H_{sys},

$$\left[H_{\mathrm{sys}}, X_m^\pm\right] = \pm\hbar\omega_m X_m^\pm, \quad \omega_m > 0, \tag{27}$$

which is always possible as long as the eigenstates of H_{sys} form a complete set.

Projecting the master equation onto the SCB eigenstates $|i\rangle$, $H_{\mathrm{sys}}|i\rangle = \omega_i|i\rangle$ ($i \in \{0, 1, 2, \ldots\}$), we arrive at the following equation for the diagonal elements,

$$\dot{\rho}_{ii} = \sum_{j\neq i}\Gamma_{ji}\rho_{jj} - \Gamma_{ij}\rho_{ii}, \tag{28}$$

where the relaxation ($\omega_{ij} = \omega_i - \omega_j > 0$) rates are

$$\Gamma_{ij} = \frac{2\gamma}{\hbar}\omega_{ij}\left(1 + n_{\omega_{ij}}\right)|\langle i|X|j\rangle|^2 \tag{29}$$

and the excitation ($\omega_{ij} < 0$) rates are

$$\Gamma_{ij} = \frac{2\gamma}{\hbar}|\omega_{ij}|n_{\omega_{ij}}|\langle i|X|j\rangle|^2. \tag{30}$$

Noting that $X = -(p_J + C_c V_{dc})$ is the charge operator, the matrix elements can be calculated numerically from the SCB Hamiltonian in (19). Denoting the SCB charging energy by $E_C = e^2/2C_\Sigma$, the transmon regime is found for $E_J \gg E_C$ [33]. Here, the SCB spectrum approaches a linear oscillator with the junction plasma frequency $\omega_p = \sqrt{8E_J E_C}/\hbar$, and the charge operator asymptotically couples only neighboring eigenstates [33]. We find the non-zero relaxation rates

$$\Gamma_{(j+1)j} = \pi(j+1)\kappa^2\frac{E_J}{\hbar}\frac{Z_0}{R_K}(1 + n_{\omega_p}) \tag{31}$$

and excitation rates

$$\Gamma_{j(j+1)} = \pi(j+1)\kappa^2\frac{E_J}{\hbar}\frac{Z_0}{R_K}n_{\omega_p}, \tag{32}$$

where $R_K = h/e^2 \approx 25\,\mathrm{k}\,\Omega$ denotes the quantum of resistance. The off-diagonal ($i \neq j$) elements are subject to a pure exponential decay,

$$\dot{\rho}_{ij} = -\gamma_{ij}\rho_{ij} \tag{33}$$

with dephasing rates

$$\gamma_{ij} = \Gamma_\phi^i + \Gamma_\phi^j + \frac{1}{2}\left(\sum_{k\neq i}\Gamma_{ik} + \sum_{k\neq j}\Gamma_{jk}\right), \tag{34}$$

equal to half the sum of all rates for transitions from states $|i\rangle$ and $|j\rangle$, as well as the pure dephasing rates

$$\Gamma_\phi^k = \frac{2\gamma}{\hbar}\frac{k_\mathrm{B}T}{\hbar}|\langle k|X|k\rangle|^2. \tag{35}$$

The pure dephasing rates depend on the dc voltage, through the SCB spectrum, according to

$$|\langle k|X|k\rangle| = \frac{e}{4E_\mathrm{C}}\left|\frac{\partial\omega_k(n_\mathrm{g})}{\partial n_\mathrm{g}}\right|, \tag{36}$$

where $n_\mathrm{g} = C_\mathrm{c}V_\mathrm{dc}/2e$ is the dimensionless gate charge of the SCB. In the transmon regime the spectrum is well approximated by

$$\omega_k(n_\mathrm{g}) = \omega_k(n_\mathrm{g} = 1/4) - \frac{\epsilon_k}{2}\cos(2\pi n_\mathrm{g}), \tag{37}$$

where

$$\epsilon_k \simeq (-1)^k E_\mathrm{C}\frac{2^{4k+5}}{k!}\sqrt{\frac{2}{\pi}}\left(\frac{E_\mathrm{J}}{2E_\mathrm{C}}\right)^{\frac{k}{2}+\frac{3}{4}} \mathrm{e}^{-\sqrt{8E_\mathrm{J}/E_\mathrm{C}}}, \tag{38}$$

giving a maximum thermal pure dephasing rate (for $n_\mathrm{g} = \pm 1/4$) of

$$\max\Gamma_\phi^k = \kappa^2\frac{Z_0}{R_K}\frac{k_\mathrm{B}T}{\hbar}\frac{\pi^3}{8}\left|\frac{\epsilon_k}{E_\mathrm{C}}\right|^2. \tag{39}$$

Here, we also note that in addition to small-amplitude thermal charge noise there can also be a slow but large-amplitude charge drift. In some cases, the effect of this drift can be taken into account by averaging over the range of transition frequencies involved. In the transmon regime, for the transition from $|k\rangle$ to $|k+1\rangle$ this is given by $\epsilon_{k+1} - \epsilon_k \approx \epsilon_{k+1}$.

2.5. Coherent drive

In the next section, we will examine the scattering of coherent signals on the transmon in the two-level and three-level approximations. To include a coherent drive in the description, we take the input field $\Phi^\mathrm{in}(t)$ to consist of a classical part $\Phi^\mathrm{in}_\mathrm{cl}(t)$ on top of the thermal background. Deriving the master equation for this case, it turns out that (26) is modified by adding the following time-dependent term to the system Hamiltonian,

$$H_\mathrm{d}(t) = -2\sqrt{\frac{\gamma}{Z_0}}\dot{\Phi}^\mathrm{in}_\mathrm{cl}(t)X. \tag{40}$$

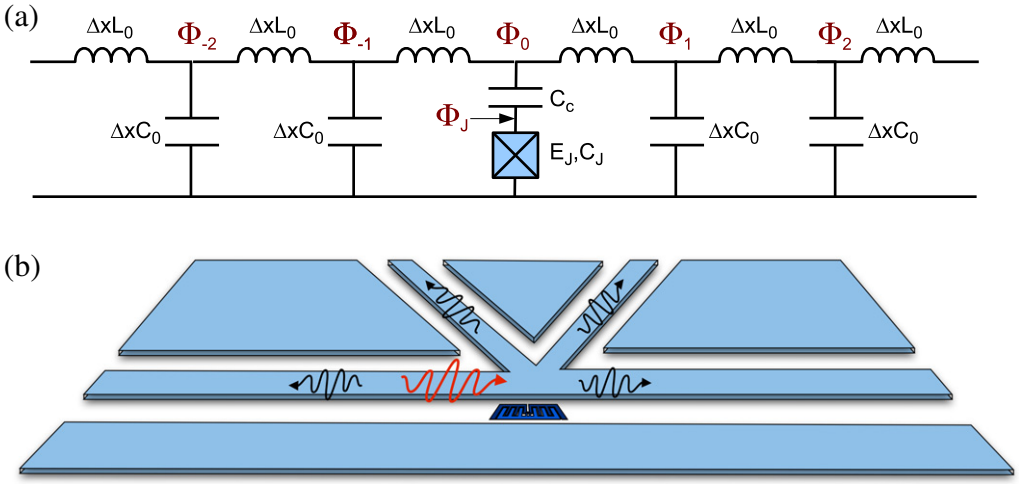

Figure 2. (a) Discretized circuit describing the interaction of an SCB with microwave photons propagating in an infinite TL. (b) Generalization of the input–output formalism to an arbitrary number of ports connected by an artificial atom.

2.6. Adding more transmission lines

In this section, we generalize the above master equation by adding more semi-infinite TLs to the SCB. First, by adding one more semi-infinite line, we arrive at the important case of an SCB capacitively coupled to an infinite TL. The discretized circuit is shown in figure 2(a), and the corresponding Hamiltonian is obtained from (1) by adding the TL terms for $x > 0$

$$H'_{\rm d} = H_{\rm d} + \frac{1}{\Delta x}\sum_{i>0}\left(\frac{p_i^2}{2C_0} + \frac{(\Phi_{i-1}-\Phi_i)^2}{2L_0}\right). \tag{41}$$

From a similar analysis as that above, we arrive at exactly the same master equation for the transmon's reduced density matrix, with the replacements

$$\Phi^{\rm in} = \frac{1}{2}\left(\Phi_{\rm L}^{\rm in} + \Phi_{\rm R}^{\rm in}\right), \quad \tau_{\rm RC} = \frac{Z_0}{2}\frac{C_{\rm c}C_{\rm J}}{C_\Sigma}, \ \gamma = \frac{Z_0}{2}\left(\frac{C_{\rm c}}{C_\Sigma}\right)^2 \tag{42}$$

and the output fields are obtained from

$$\Phi_{\rm L/R}^{\rm out} = \Phi_{\rm R/L}^{\rm in} + (\tau_{\rm RC}/C_{\rm J})\,p_{\rm J}. \tag{43}$$

We note that the damping constant γ as well as the RC time $\tau_{\rm RC}$ are both halved compared to the semi-infinite case, since the impedance to ground is halved to $Z_0/2$. The in-field is the sum of the fields incoming from the left and right, but compared to the semi-infinite case the coupling coefficient is halved, since there is (almost) no reflection at $x = 0$. Indeed, for a more general scenario with N symmetrically coupled incident fields, as illustrated in figure 2(b), the mapping would be

$$\Phi^{\rm in} = \frac{1}{N}\sum_{n=1}^{N}\Phi_n^{\rm in}, \quad \tau_{\rm RC} = \frac{Z_0}{N}\frac{C_{\rm c}C_{\rm J}}{C_\Sigma}, \quad \gamma = \frac{Z_0}{N}\left(\frac{C_{\rm c}}{C_\Sigma}\right)^2 \tag{44}$$

and using the relation $\Phi_0 = \Phi_n^{\text{in}} + \Phi_n^{\text{out}}$ $(\forall n)$, the output fields are given as

$$\Phi_n^{\text{out}} = \Phi_0 - \Phi_n^{\text{in}} = \left(\frac{2}{N} - 1\right)\Phi_n^{\text{in}} + \frac{\tau_{\text{RC}}}{C_{\text{J}}} p_{\text{J}} + \frac{2}{N}\sum_{m\neq n}^{N} \Phi_m^{\text{in}}. \tag{45}$$

3. Applications: scattering by the transmon

3.1. Two-level dynamics

In this section, we examine the scattering of coherent signals on the transmon in an open TL. The input field is a constant coherent signal with a single frequency ω_{p}, close to resonance with the first transition frequency ω_{10} of the transmon. Thus, we can safely describe the transmon as a two-level system. The master equation is given by (26) with a coherent drive and generalized to the case of an infinite TL (see sections 2.5 and 2.6), in the special case of only one system eigenfrequency ω_{10}. Moreover, we include an additional term due to pure dephasing, so that the total dephasing rates are given by (34). We represent our operators by the following Pauli matrices (using the notation $X_{ij} \equiv \langle i|X|j\rangle$):

$$H_{\text{sys}} = -\hbar\frac{\omega_{10}}{2}\sigma_z, \quad X^{\pm} = \pm \text{i}|X_{10}|\sigma^{\pm}. \tag{46}$$

Below, we will determine reflection and transmission coefficients for coherent signals scattered on the transmon. In the previous section, the incoming and outgoing fields were described in terms of the flux, since that gives a simpler description of the transmon. However, the voltage is a more intuitive quantity than the flux and is also usually what is measured in experiments. Therefore, in this section, we will describe the inputs and outputs in terms of the voltage.

We consider an incoming coherent voltage field,

$$V_{\text{L}}^{\text{in}}(t) = \Omega_p \sin\omega_{\text{p}} t, \tag{47}$$

impinging on the transmon from the left. For simplicity, we set the temperature to zero ($n_{\omega_{10}} = 0$). The reflected voltage field is the output to the left of the transmon. Using (42) and (43), we have

$$V_{\text{L}}^{\text{out}}(t) = -\sqrt{\frac{\gamma Z_0}{2}}\langle \dot{X}(t)\rangle, \tag{48}$$

where the expectation value can be written as

$$\langle \dot{X}(t)\rangle = \text{i}\omega_{10}\left(\langle X^{+}(t)\rangle - \langle X^{-}(t)\rangle\right) = -\omega_{10}|X_{10}|\langle\sigma^x\rangle. \tag{49}$$

Inserting (49) into (48) yields

$$V_{\text{L}}^{\text{out}}(t) = \frac{1}{2}\sqrt{\hbar\omega_{10}\Gamma_{10}Z_0}\langle\sigma^x\rangle = \sqrt{\hbar\omega_{10}\Gamma_{10}Z_0}Re\left[\rho_{01}\right], \tag{50}$$

where ρ_{01} is a density matrix element in the transmon eigenbasis.

To solve the master equation, we perform a unitary transformation to a frame rotating with the driving frequency ω_{p}. In this frame, the equation becomes time independent after employing the rotating-wave approximation. Solving the equation in the steady state ($\dot{\rho} = 0$) and transforming back to the non-rotaing frame yields the following expression for the desired density matrix element,

$$\rho_{01} = \frac{1}{2}\frac{\sqrt{\hbar\omega_{10}\Gamma_{10}Z_0}\left(\Delta + \text{i}\gamma_{10}\right)\Omega_p}{\hbar\omega_{10}Z_0\gamma_{10}^2 + \hbar\omega_{10}Z_0\Delta^2 + \gamma_{10}\Omega_{\text{p}}^2}\text{e}^{\text{i}\omega_{\text{p}}t}, \tag{51}$$

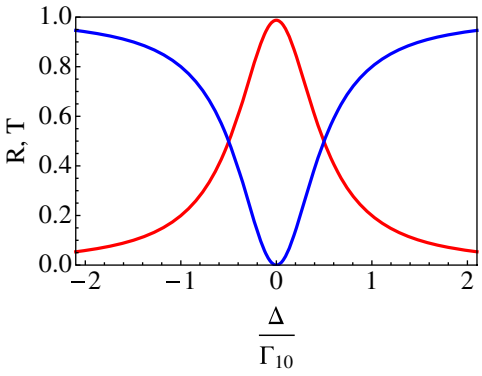

Figure 3. Reflectance R (red) and transmittance T (blue) for a two-level transmon as a function of detuning, with the average number of incoming photons per interaction time being $N_{\text{in}}/(\Gamma_{10}/2\pi) = 0.01$.

where $\Delta \equiv \omega_{\text{p}} - \omega_{10}$ is the detuning. Now, plugging this expression into (50) results in

$$V_{\text{L}}^{\text{out}}(t) = -\frac{\Omega_p}{2}\frac{\sin\omega_{\text{p}}t - \frac{\Delta}{\gamma_{10}}\cos\omega_{\text{p}}t}{\frac{\gamma_{10}}{\Gamma_{10}} + \frac{\Delta^2}{\Gamma_{10}\gamma_{10}} + 2\frac{N_{\text{in}},}{\Gamma_{10}}}, \tag{52}$$

where $N_{\text{in}} = \Omega_{\text{p}}^2/(2Z_0\hbar\omega_{10})$ is the average number of incoming photons per second. Thus, the reflection coefficient for the negative frequency part of the field is given by

$$r = -r_0\frac{1 - \text{i}\frac{\Delta}{\gamma_{10}}}{1 + \left(\frac{\Delta}{\gamma_{10}}\right)^2 + 2\frac{N_{\text{in}}}{\gamma_{10}}}, \tag{53}$$

with $r_0 \equiv \Gamma_{10}/2\gamma_{10}$. For the transmitted field, (43) yields

$$V_{\text{R}}^{\text{out}}(t) = V_{\text{L}}^{\text{in}}(t) - \sqrt{\frac{\gamma Z_0}{2}}\langle\dot{X}(t)\rangle \tag{54}$$

which directly gives us the following expression for the transmission coefficient:

$$t = 1 + r = \frac{1 - r_0 + \left(\frac{\Delta}{\gamma_{10}}\right)^2 + 2\frac{N_{\text{in}}}{\gamma_{10}} + \text{i}r_0\frac{\Delta}{\gamma_{10}}}{1 + \left(\frac{\Delta}{\gamma_{10}}\right)^2 + 2\frac{N_{\text{in}}}{\gamma_{10}}}. \tag{55}$$

In figure 3, we plot the reflectance $R = |r|^2$ and transmittance $T = |t|^2$ as a function of the detuning, in the case of a weak input signal and no pure dephasing. For a resonant drive ($\Delta = 0$), we see that perfect reflection is approached, in agreement with [12, 13, 39].

3.2. Three-level dynamics

In section 3.1, we showed that a low-amplitude input signal is totally reflected when it resonantly scatters off a transmon in the two-level approximation. In this section, we instead study the scattering off of a transmon in the three-level approximation. By strongly driving the second transition, the transmon becomes transparent to frequencies in resonance with the first

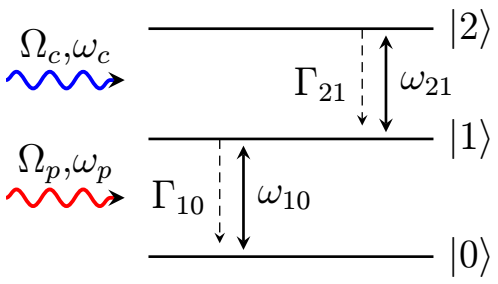

Figure 4. Internal levels of the transmon in the three-level approximation. A strong control field drives the $|1\rangle \rightarrow |2\rangle$ transition, rendering a transparency for the $|0\rangle \rightarrow |1\rangle$ transition.

transition. This effect is due to the Autler–Townes splitting and has been observed in recent experiments [22].

We consider an incoming voltage field from the left, consisting of a probe field $\Omega_\mathrm{p} \sin \omega_\mathrm{p} t$ close to resonance with the first transition (with detuning $\Delta_\mathrm{p} = \omega_\mathrm{p} - \omega_{10}$) and a control field $\Omega_\mathrm{c} \sin \omega_\mathrm{c} t$ close to resonance with the second transition (with detuning $\Delta_\mathrm{c} = \omega_\mathrm{c} - \omega_{21}$). Figure 4 shows the energy levels of the transmon in this approximation. In the transmon eigenbasis, the relevant operators are (with the ground state energy $\omega_0 = 0$)

$$H_\mathrm{sys} = \hbar \sum_{i=1}^{2} \omega_i \, |i\rangle \, \langle i| \,, \tag{56}$$

$$X = \mathrm{i} \sum_{i=1}^{2} |X_{i(i-1)}| (\sigma_i^+ - \sigma_i^-) \tag{57}$$

with $\sigma_i^+ = |i\rangle\langle i-1|$ and $\sigma_i^- = (\sigma_i^+)^\dagger$. In the same way as in the two-level case ((49)–(50)), we obtain the following expression for the reflected signal:

$$V_\mathrm{L}^\mathrm{out}(t) = -\sqrt{\frac{\gamma Z_0}{2}} \langle \dot{X}(t) \rangle = \frac{1}{2} \sum_{i=1}^{2} \sqrt{\hbar \omega_{i(i-1)} Z_0 \Gamma_{i(i-1)}} \langle \sigma_i^x \rangle, \tag{58}$$

with $\sigma_i^x = \sigma_i^+ + \sigma_i^-$. Thus, the reflected field consists of one part with frequencies around the probe frequency ω_p and one part with frequencies around the control frequency ω_c. Since we are interested in the reflectance and transmittance properties of the probe, we concentrate on the corresponding part of the reflected field

$$V_\mathrm{p}^\mathrm{ref}(t) = \frac{1}{2} \sqrt{\hbar \omega_{10} Z_0 \Gamma_{10}} \langle \sigma_1^x \rangle = \sqrt{\hbar \omega_{10} Z_0 \Gamma_{10}} Re(\rho_{10}). \tag{59}$$

The master equation is given by (26) for the case of two system eigenfrequencies, again with a coherent drive and generalized to the case of an infinite TL (see sections 2.5 and 2.6). Also, terms accounting for pure dephasing are added. To transform the master equation into a time-independent picture, we use the following unitary transformation matrix,

$$U(t) = \begin{pmatrix} 1 & 0 & 0 \\ 0 & \mathrm{e}^{-\mathrm{i}\omega_\mathrm{p} t} & 0 \\ 0 & 0 & \mathrm{e}^{-\mathrm{i}(\omega_\mathrm{p} + \omega_\mathrm{c}) t} \end{pmatrix} \tag{60}$$

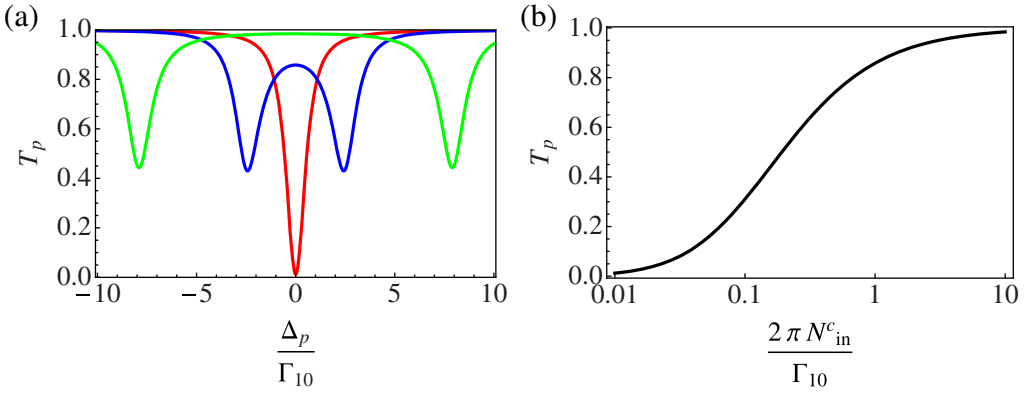

Figure 5. (a) Transmittance $T_{\rm p}$ of the probe as a function of detuning for three different control field strengths: $N^{\rm c}_{\rm in}/(\Gamma_{10}/(2\pi)) = 0.01$ (red), $N^{\rm c}_{\rm in}/(\Gamma_{10}/(2\pi)) = 1$ (blue) and $N^{\rm c}_{\rm in}/(\Gamma_{10}/(2\pi)) = 8$ (green). (b) Transmittance as a function of the control field strength for a resonant probe field ($\Delta_{\rm p} = 0$).

and employ the rotating-wave approximation. As before, we solve the master equation in the steady state to determine ρ_{10}, but we now consider two different cases.

Firstly, by setting $\Omega_{\rm c} = 0$, we recover exactly the same expression for the reflected field as in the two-level case. Thus, with the control field turned off, we see almost full reflection for weak probe fields in resonance with the first transition frequency of the transmon.

Secondly, we consider the case of a strong control field ($\Omega_{\rm c} \gg \Omega_{\rm p}$). Solving the master equation and expanding ρ_{10} to first order in $(\Omega_{\rm p}/\Omega_{\rm c})$, we obtain the following expression:

$$\rho^{(1)}_{10} = -\frac{2{\rm i}\hbar\omega_{21} Z_0 \sqrt{\frac{\Gamma_{10}}{\hbar\omega_{10} Z_0}} \left(\gamma_{20} - {\rm i}\left(\Delta_{\rm c} + \Delta_{\rm p}\right)\right) \Omega_{\rm p}}{4\hbar\omega_{21} Z_0 \left(\gamma_{10} - {\rm i}\Delta_p\right) \left(\gamma_{20} - {\rm i}\left(\Delta_{\rm c} + \Delta_{\rm p}\right)\right) + \Gamma_{21}\Omega_{\rm c}^2} {\rm e}^{-{\rm i}\omega_{\rm p} t}. \tag{61}$$

Inserting (61) into (59), we can determine the reflection coefficient. For a resonant control field ($\Delta_{\rm c} = 0$), the result is

$$r = -\frac{2\Gamma_{10}\left(\gamma_{20}^2 + \Delta_{\rm p}^2\right)\left(\gamma_{10} - {\rm i}\Delta_{\rm p}\right) + \Gamma_{10}\Gamma_{21}\left(\gamma_{20} + {\rm i}\Delta_{\rm p}\right) N^{\rm c}_{\rm in}}{4\left(\gamma_{10}^2 + \Delta_{\rm p}^2\right)\left(\gamma_{20}^2 + \Delta_{\rm p}^2\right) + 4\Gamma_{21}\left(\gamma_{10}\gamma_{20} - \Delta_{\rm p}^2\right) N^{\rm c}_{\rm in} + \Gamma_{21}^2 N^{\rm c2}_{\rm in}}, \tag{62}$$

where $N^{\rm c}_{\rm in} = \Omega_{\rm c}^2/(2Z_0\hbar\omega_{21})$ is the average number of incoming photons per second in the control field. The transmission coefficient is again given by $t = 1 + r$. Figure 5 shows the transmittance $T = |t|^2$ for different probe detunings and control field strengths. In these plots, we have neglected pure dephasing and used (29) to express Γ_{21} in terms of Γ_{10}.

We can clearly see that, for strong control fields, the transmittance of a resonant probe approaches unity. Thus, by turning on and off a strong resonant control field, we can switch between the cases of full transmission and full reflection for the resonant probe.

3.3. Second-order correlations

In a recent experiment [23], the second-order statistics of the field scattered off a transmon was measured. In this section, inspired by the experiment, we analyze the second-order correlation

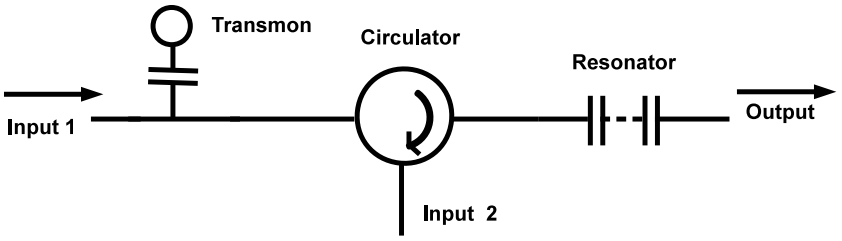

Figure 6. Schematic model of a transmon cascaded with a resonator. The circulator prevents the field reflected from the resonator to reach the transmon. Using input port 1 (2), the output is the filtered transmitted (reflected) signal.

functions in our system. The normalized second-order correlation function is in the steady state given as [40]

$$g^{(2)}(\tau) = \frac{\langle V^+(t)V^+(t+\tau)V^-(t+\tau)V^-(t)\rangle}{\langle V^+(t)V^-(t)\rangle^2} \tag{63}$$

and is proportional to the conditional probability of detecting a photon at time $t+\tau$, given that one was detected at time t. Here, $V^{\pm}(t)$ are the positive and negative frequency parts of the voltage field.

We calculate $g^{(2)}(\tau)$ for the transmitted and reflected fields from a transmon driven by a resonant coherent signal. We treat the transmon as a two-level system and use the same notation as in section 3.1. To be able to compare with the experiments in [23], we perform the calculations for finite temperatures and a finite detection bandwidth on the output signal. For zero temperature and infinite bandwidth, we recover the results of [41]: perfect antibunching in the reflected field and bunching in the transmitted field.

Including the effect of a finite detection bandwidth is straighforward by including a filter in the calculations. The approach we have taken is to model the filter by a single-mode TL resonator in resonance with the transmon, with the Hamiltonian

$$H_{\rm res} = \hbar\omega_{10} a^\dagger a \tag{64}$$

and cascade it with the transmon. We start from the QLE (22) for the transmon, generalized to the case of an infinite TL (see section 2.6), and a similar equation for the resonator. Our coherent input signal is the voltage field $V_{\rm L}^{\rm in}(t) = \Omega_{\rm d}\sin\omega_{\rm d}t$, just like in section 3.1. We can then use the formalism of cascaded quantum systems in [34] to arrive at a master equation for the joint density matrix of the transmon and the resonator. In this formalism, the output from the transmon (reflected or transmitted) is taken as input to the resonator, without any signals going the opposite way (see figure 6). For the field reflected from the transmon, the resulting master equation is

$$\begin{aligned}\dot\rho = {}& \frac{\rm i}{\hbar}[\rho, H_{\rm sys}+H_{\rm res}] + \Gamma_{10}\mathcal{D}(\sigma^-)\rho + \Gamma_{01}\mathcal{D}(\sigma^+)\rho + \gamma_{\rm BW}\left[\left(\frac{n_{\omega_{10}}}{2}+1\right)\mathcal{D}(a)\rho + \frac{n_{\omega_{10}}}{2}\mathcal{D}(a^\dagger)\rho\right] \\ & + \frac{1}{2}{\rm i}\sqrt{\Gamma_{10}(n_{\omega_{10}}+1)\gamma_{\rm BW}}\left([a,\rho\sigma^+]+[a^\dagger,\sigma^-\rho]\right) \\ & + \frac{1}{2}{\rm i}\sqrt{\Gamma_{01}n_{\omega_{10}}\gamma_{\rm BW}}\left([\sigma^+\rho,a]+[\rho\sigma^-,a^\dagger]\right) + {\rm i}\sqrt{\frac{\Gamma_{10}N_{\rm in}}{2(n_{\omega_{10}}+1)}}[\rho,\sigma^x],\end{aligned} \tag{65}$$

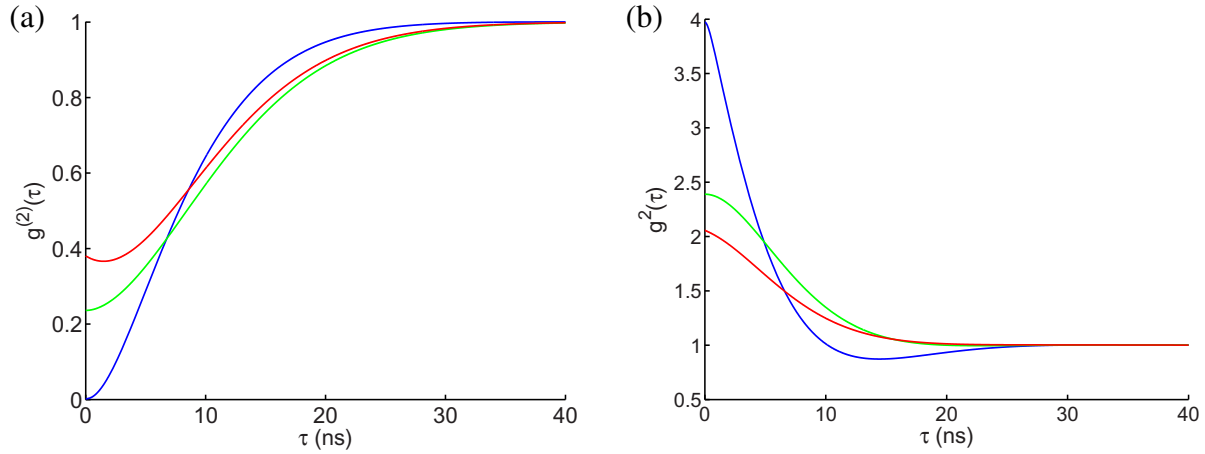

Figure 7. $g^{(2)}(\tau)$ for the fields reflected from and transmitted through a transmon for different temperatures and detection bandwidths. Typical parameter values from recent experiments are used ($\Gamma_{10}/2\pi = 41$ MHz, $\omega_{10}/2\pi = 5.12$ GHz). (a) Reflected field: blue ($T = 0$, BW $= 1$ GHz), green ($T = 0$, BW $= 55$ MHz), red ($T = 50$ mK, BW $= 55$ MHz), with $P = -131$ dBm. (b) Transmitted field: blue ($T = 0$, BW $= 1$ GHz), green ($T = 0$, BW $= 55$ MHz), red ($T = 80$ mK, BW $= 55$ MHz), with $P = -127$ dBm.

where we have denoted the filter bandwidth by γ_{BW}. For the field transmitted through the transmon, (65) is modified by simply adding the following term to the right-hand side:

$$\sqrt{\frac{\gamma_{\mathrm{BW}} N_{\mathrm{in}}}{2}}[\rho, a^\dagger - a]. \tag{66}$$

The output we are interested in is the voltage field leaking out at the right side of the resonator, whose positive and negative frequency parts are proportional to $a(t)$ and $a^\dagger(t)$, respectively. Thus, $g^{(2)}(\tau)$ can be calculated as

$$g^{(2)}(\tau) = \frac{\langle a^\dagger(t)a^\dagger(t+\tau)a(t+\tau)a(t)\rangle}{\langle a^\dagger(t)a(t)\rangle^2} = \frac{\mathrm{Tr}\left[a^\dagger a P(\tau)(a\rho_{\mathrm{s}}a^\dagger)\right]}{\mathrm{Tr}\left[a^\dagger a\rho_{\mathrm{s}}\right]^2}, \tag{67}$$

where ρ_{s} is the steady-state density matrix and $P(\tau)$ the propagator super-operator, defined by $\rho(t+\tau) = P(\tau)\rho(t)$. Both ρ_{s} and $P(\tau)$ are obtained by solving the master equations (65) and (66). For the case without filter, $g^{(2)}(\tau)$ for the reflected field is given by (67) with a replaced by σ^-. Since $(\sigma^-)^2 = 0$, it directly follows that $g^{(2)}(0) = 0$, i.e. perfect antibunching.

In figure 7(a), we plot $g^{(2)}(\tau)$ for the reflected field for different temperatures and detection bandwidths. Typical parameter values from recent experiments [23] are used. For zero temperature and large bandwidth we see perfect antibunching, as expected. For a decreased bandwidth the full time dynamics of the antibunching cannot be resolved, which results in a less pronounced antibunching dip. For finite temperatures, we see even less antibunching, due to a nonzero probability of detecting bunched thermal photons. In figure 7(b), we plot $g^{(2)}(\tau)$ for the transmitted field for different temperatures and detection bandwidths. Here we see a decrease of the superbunching for higher temperatures and smaller bandwidths. These results explain the qualitative features of the experimental data in [23] well.

4. Summary and conclusions

Summing up, we have performed a thorough analysis of the qubit–photon scattering in a one-dimensional continuum from a microscopic point of view. In particular, we have derived a master equation description using a superconducting transmon qubit as our scatterer. When we consider the two lowest levels of the transmon, it behaves like a mirror for the incoming photons. Then, going beyond to the two-level approximation, we can use a control field resonant with a second transition of the transmon to suppress this reflection of photons at the probe frequency. Finally, we discussed how the photon antibunching observed in the reflected field is reduced by finite temperature and finite detection bandwidth.

Acknowledgments

We thank T Willemen and Tauno Palomaki for valuable discussions. We acknowledge financial support from the Swedish Research Council, the Wallenberg Foundation, the STINT and from the EU through the ERC and the projects SOLID and PROMISCE. This work was also supported by the Spanish MICINN project FIS2009-10061 and the CAM research consortium QUITEMAD S2009-ESP-1594. BP acknowledges support from the CSIC grant JAE-PREDOC2009.

References

[1] Clarke J and Wilhelm F K 2008 Superconducting quantum bits *Nature* **453** 1031–42
[2] Schoelkopf R J and Girvin S M 2008 Wiring up quantum systems *Nature* **451** 664–9
[3] Blais A, Huang R-S, Wallraff A, Girvin S M and Schoelkopf R J 2004 Cavity quantum electrodynamics for superconducting electrical circuits: an architecture for quantum computation *Phys. Rev.* A **69** 062320
[4] Wallraff A, Schuster D I, Blais A, Frunzio L, Huang R-S, Majer J, Kumar S, Girvin S M and Schoelkopf R J 2004 Strong coupling of a single photon to a superconducting qubit using circuit quantum electrodynamics *Nature* **431** 162–7
[5] Schuster D I, Wallraff A, Blais A, Frunzio L, Huang R-S, Majer J, Girvin S M and Schoelkopf R J 2005 ac Stark shift and dephasing of a superconducting qubit strongly coupled to a cavity field *Phys. Rev. Lett.* **94** 123602
[6] Schuster D I *et al* 2007 Resolving photon number states in a superconducting circuit *Nature* **445** 515–8
[7] Majer J *et al* 2007 Coupling superconducting qubits via a cavity bus *Nature* **449** 443–7
[8] Houck A A *et al* 2007 Generating single microwave photons in a circuit *Nature* **449** 328–31
[9] Fink J M, Göppl M, Baur M, Bianchetti R, Leek P J, Blais A and Wallraff A 2008 Climbing the Jaynes–Cummings ladder and observing its nonlinearity in a cavity QED system *Nature* **454** 315–8
[10] Karyn Le Hur 2012 Kondo resonance of a microwave photon *Phys. Rev.* B **85** 140506
[11] Knill E, Laflamme R and Milburn G J 2001 A scheme for efficient quantum computation with linear optics *Nature* **409** 46–52
[12] Shen J-T and Fan S 2005 Coherent single photon transport in a one-dimensional waveguide coupled with superconducting quantum bits *Phys. Rev. Lett.* **95** 213001
[13] Shen J T and Fan S 2005 Coherent photon transport from spontaneous emission in one-dimensional waveguides *Opt. Lett.* **30** 2001–3
[14] Micheli A and Zoller P 2006 Single-atom mirror for one-dimensional atomic lattice gases *Phys. Rev.* A **73** 043613
[15] Zheng H, Gauthier D J and Baranger H U 2010 Waveguide QED: many-body bound-state effects in coherent and Fock-state scattering from a two-level system *Phys. Rev.* A **82** 063816

[16] Zheng H, Gauthier D J and Baranger H U 2012 Strongly correlated photons generated by coupling a three- or four-level system to a waveguide *Phys. Rev.* A **85** 043832
[17] Kocabaş S E, Rephaeli E and Fan S 2012 Resonance fluorescence in a waveguide geometry *Phys. Rev.* A **85** 023817
[18] Astafiev O, Zagoskin A M, Abdumalikov A A, Pashkin Yu A, Yamamoto T, Inomata K, Nakamura Y and Tsai J S 2010 Resonance fluorescence of a single artificial atom *Science* **327** 840–3
[19] Astafiev O V, Abdumalikov A A, Zagoskin A M, Pashkin Yu A, Nakamura Y and Tsai J S 2010 Ultimate on-chip quantum amplifier *Phys. Rev. Lett.* **104** 183603
[20] Abdumalikov A A, Astafiev O, Zagoskin A M, Pashkin Yu A, Nakamura Y and Tsai J S 2010 Electromagnetically induced transparency on a single artificial atom *Phys. Rev. Lett.* **104** 193601
[21] Abdumalikov A A, Astafiev O V, Pashkin Yu A, Nakamura Y and Tsai J S 2011 Dynamics of coherent and incoherent emission from an artificial atom in a 1D space *Phys. Rev. Lett.* **107** 043604
[22] Hoi I-C, Wilson C M, Johansson G, Palomaki T, Peropadre B and Delsing P 2011 Demonstration of a single-photon router in the microwave regime *Phys. Rev. Lett.* **107** 073601
[23] Hoi I-C, Palomaki T, Lindkvist J, Johansson G, Delsing P and Wilson C M 2012 Generation of nonclassical microwave states using an artificial atom in 1D open space *Phys. Rev. Lett.* **108** 263601
[24] Hoi I-C, Wilson C M, Johansson G, Palomaki T, Stace T M, Fan B and Delsing P 2012 Giant cross Kerr effect for propagating microwaves induced by an artificial atom arXiv:1207.1203
[25] Hoi I-C, Wilson C M, Johansson G, Lindkvist J, Peropadre B, Palomaki T and Delsing P 2013 Microwave quantum optics with an artificial atom in one-dimensional open space *New J. Phys.* **15** 025011
[26] Bouchiat V, Vion D, Joyez P, Esteve D and Devoret M H 1998 Quantum coherence with a single Cooper pair *Phys. Scr.* **T76** 165–70
[27] Nakamura Y, Pashkin Y A and Tsai J S 1999 Coherent control of macroscopic quantum states in a single Cooper-pair box *Nature* **398** 786–8
[28] Makhlin Y, Schön G and Shnirman A 2001 Quantum-state engineering with Josephson-junction devices *Rev. Mod. Phys.* **73** 357–400
[29] Lehnert K W, Bladh K, Spietz L F, Gunnarsson D, Schuster D I, Delsing P and Schoelkopf R J 2003 Measurement of the excited-state lifetime of a microelectronic circuit *Phys. Rev. Lett.* **90** 027002
[30] Bladh K, Duty T, Gunnarsson D and Delsing P 2005 The single Cooper-pair box as a charge qubit *New J. Phys.* **7** 180
[31] Büttiker M 1987 Zero-current persistent potential drop across small-capacitance Josephson junctions *Phys. Rev.* B **36** 3548–55
[32] Duty T, Gunnarsson D, Bladh K and Delsing P 2004 Coherent dynamics of a Josephson charge qubit *Phys. Rev.* B **69** 140503
[33] Koch J, Yu T M, Gambetta J, Houck A A, Schuster D I, Majer J, Blais A, Devoret M H, Girvin S M and Schoelkopf R J 2007 Charge-insensitive qubit design derived from the Cooper pair box *Phys. Rev.* A **76** 042319
[34] Gardiner C W and Zoller P 1991 *Quantum Noise* (Berlin: Springer)
[35] Yurke B and Denker J S 1984 Quantum network theory *Phys. Rev.* A **29** 1419–37
[36] Devoret M H 1997 Quantum fluctuations in electrical circuits *Quantum Fluctuations* (*Les Houches Session LXIII*) (Amsterdam: Elsevier) pp 351–86
[37] Johansson G, Tornberg L, Shumeiko V S and Wendin G 2006 Readout methods and devices for Josephson-junction-based solid-state qubits *J. Phys.: Condens. Matter* **18** S901
[38] Rau I, Johansson G and Shnirman A 2004 Cavity quantum electrodynamics in superconducting circuits: susceptibility at elevated temperatures *Phys. Rev.* B **70** 054521
[39] Romero G, García-Ripoll J J and Solano E 2009 Microwave photon detector in circuit QED *Phys. Rev. Lett.* **102** 173602
[40] Gerry C C and Knight P L 2005 *Introductory Quantum Optics* (Cambridge: Cambridge University Press)
[41] Chang D E, Sørensen A S, Demler E A and Lukin M D 2007 A single-photon transistor using nanoscale surface plasmons *Nature Phys.* **3** 807–12

3.3.3 Demonstration of a single photon router

The astonishing one-dimensional photon-transport properties presented in publication P5 can be used to control propagating photons with high precision. This can be of central importance in the development of photonic quantum networks [OFV09, Kim08], where quantum nodes have to process and distribute quantum information (codified in propagating photons) among different quantum channels. The task of controlling photons turns out to be nontrivial, since photons do not interact with themselves and hardly do it with real atoms.

In publication P6 we take advantage of the high-efficient scattering in one dimension to control photons, demonstrating a rudimentary quantum node: the single photon router. The active element of the router is a transmon qubit strongly coupled to an open transmission line. By exploiting the phenomenon of electromagnetically induced transparency (EIT), we manage to route single photons to different output ports with a 99% efficiency. Below we summarize the most important results. In particular, we results shown below stand for the best of the transmon samples[15].

- We have experimentally observed the transport properties shown in P5 in the scattered wave, namely: perfect reflection at low-power incoming drives (mean number of photons per unit time $N \ll 1$), perfect transmission at high-power drives ($N \gg 1$)[16], and EIT with the third level of the transmon qubit. This will be further discussed in P7.

- We take advantage of the EIT in the transmon to build up a single-photon router, which is depicted in Fig. 3.6a, and whose working principle is the following:

    1. We send a constant weak probe at the single photon level $N_p \ll 1$ at the ω_{01} frequency. A second strong control pulse ($N_c \gg 1$) at the ω_{12} frequency is alternatively switched on and off. This is clearly shown in the inset of Fig.3.6a.
    2. When the control is turned off, the photons at the probe frequency are reflected by atom, and are routed to the output port 1 through

[15]The limiting factor in the switching efficiency of the router is the pure dephasing rate. This can be attenuated using transmon qubits with large E_J/E_C factors. The best of our samples have $E_J/E_C \sim 60$, which hardly suffers from pure dephasing.

[16]We should not confuse this perfect transmission with EIT. In this case, the perfect transmission is due to the saturation of the qubit, which can not reflect more than one photon at a time.

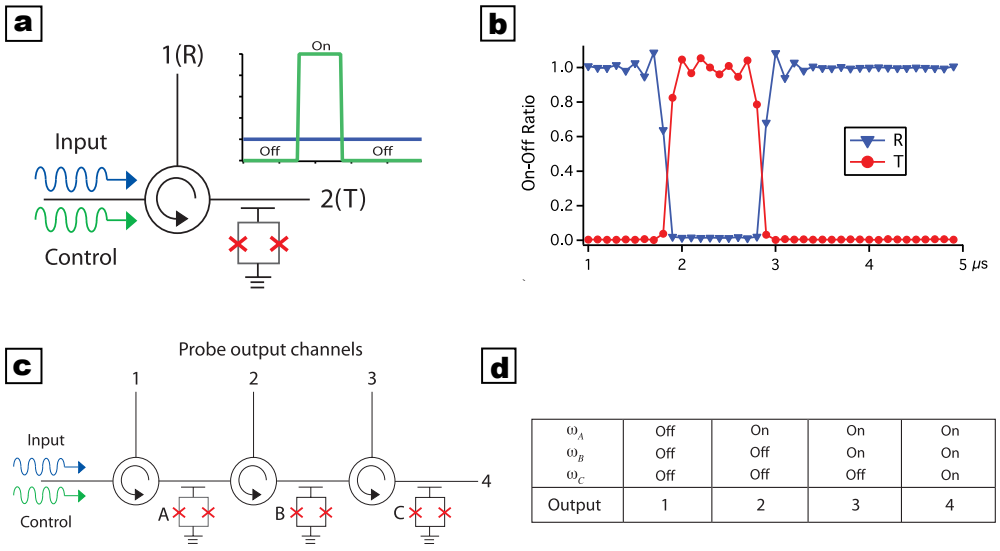

ω_A	Off	On	On	On
ω_B	Off	Off	On	On
ω_C	Off	Off	Off	On
Output	1	2	3	4

Figure 3.6: a) Schematics of a one-port single photon router. b) Transmittance (red) and Reflectance (blue) of the input signal measured simultaneously. The probe photons are routed with an on-off ratio $\sim$ 99%. c) Cartoon of a four port-router with three transmon qubits. All qubits posses the same ω_{01} energy, and three different $1-2$ transitions, $\omega_A \neq \omega_B \neq \omega_C$ d). Sequence of the control-tone frequencies for routing a probe photon for any of the four output ports of the network.

the circulator[17].

3. By contrast, when the control is turned on, EIT occurs in the transmon and the photons at the probe frequency are perfectly transmitted to the output port 2.
4. By turning on or off the control tone, we can decide which port the input photons go to at any time.

- We measure the router efficiency, reaching a 99% on-off ratio both in the reflected and transmitted signal, as it is shown in Fig.3.6b. To make sure that the photon transport carried out by the router is a fully coherent process, we *simultaneously* measure the reflected and transmitter signals, obtaining that $r + t = 1$.
- We study the router response to ultrashort gaussian pulses, observing a high on-off ration up to 10 nanoseconds. The time operation can

[17] A circulator is a passive three-port device, designed in such a way that light entering any port exits from the next, in a direction fixed by an external magnetic field.

be further improved to the subnanosecond scale, by reducing the pure dephasing rate, the limiting factor of the routing efficiency. This can be done by either enhancing the E_J/E_C ratio of the transmon, or increasing its coupling to the transmission line.

- The router can be multiplexed to distribute photons to many channels. This is achieved by putting the transmon in series along the transmission line, separated by circulators, as sketched in Fig.3.6c. We can route photons to any of the four ports by properly applying the control tones at the various frequencies ω_{12}.

In conclusion, in publication P6 we demonstrate the operation principle of a rudimentary quantum node in the microwave regime, which allows us to route single photons by different ports of a network, with high speed and efficiency. Combined with the undeniably better telecom technology for distributing photons over large distances, our setup can pave the way for future quantum networks.

Fundamental Quantum Optics in 1D Open Space

In publication P7 we extend our analysis on the scattering with the transmon qubit, and report on recent experiments that reveal the quantum nature of the artificial atom, as well as diverse quantum optical phenomena in open space. In particular, we have developed the theoretical tools that supports the experimental results shown in P7, which we present below:

- As pointed out in P6, we observe the strong non-linearity of the transmon qubit by probing it with an incident coherent drive, on resonance with the $0-1$ transition. For a drive amplitude in the low-photon regime $N \ll 1$, we observe a 99.6% extinction of the transmitted signal (see Fig.3.7a). Analogously, we also measure the reflected channel, obtaining the complementary result, i.e. perfect reflection of the incoming signal.

- As we increase the power of the drive, we observe an enhancement in the transmission signal, that eventually reaches $t = 1$ in the limit $N \gg 1$ (Fig.3.7a). This is a clear signature of the non-linear nature of the artificial atom[18].

[18]Since the transmon can only absorb and reemit one photon at a time, the atom becomes saturated by the incident photons of the drive.

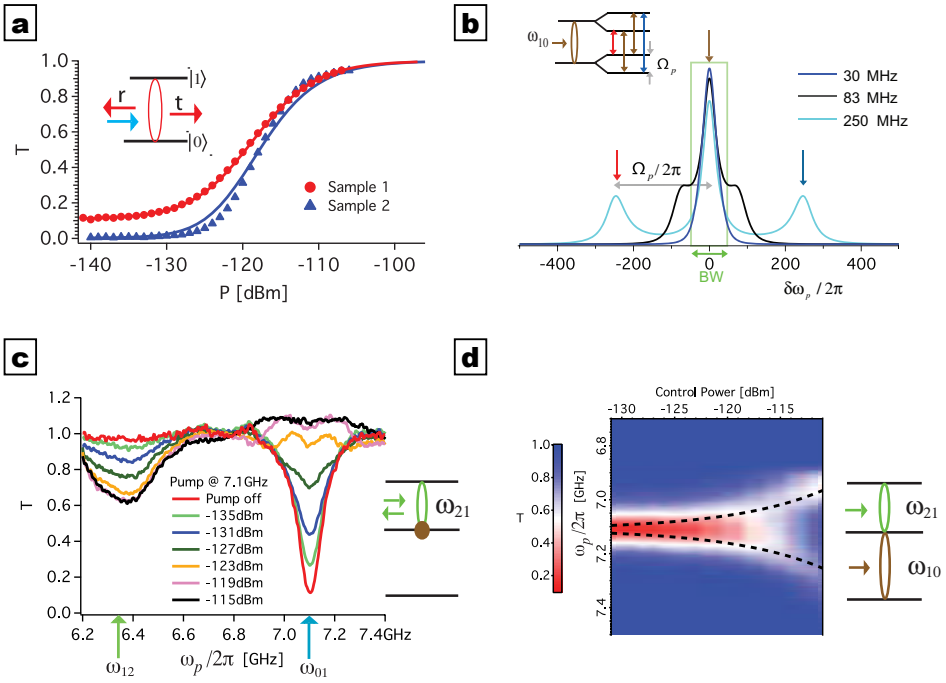

Figure 3.7: a) Transmittance as a function of the probe power. b)Transmission power at different bandwidth detection ranges, revealing the Mollow triplet due to the incoherent scattering. c) Two tone spectroscopy of the transmon qubit for different probe powers, showing the three-level structure of the transmon. d) Transmittance in the probe frequency ω_p as a function of the control power. As the power increases, we observe EIT due to the Autler Townes splitting.

- We observe the Mollow-Triplet [Mol69], due to the inelastic scattering by the transmon (see theoretical curve in Fig.3.7b). Due to the dressing of the atom with the field, the two energy levels split into two, and there appears four transition lines. In the limit of large number of photons in the pump, one of this becomes degenerate leading to the Mollow triplet. It is worth mentioning that it has been measured in the transmittance of the field and not in the emission spectrum.

- We explore higher levels of the transmon. In particular, we send a second coherent drive (the control pulse) on resonance with the 1-2 transition of the transmon, and scan the transmission at the ω_{01} frequency (see Fig.(3.7c). For large probe fields, we expect all the population in the first excited state, so we detect the second state as a dip in the trans-

mission spectrum of the control field.

- Finally, we observe the Autler-Townes splitting[19]. (Fig.3.7d). In particular, for sufficiently strong amplitudes of the control pulse, we can generate EIT in the $0-1$ transition, assisted by the Autler Townes splitting.

- Aside from the single photon router application, this device can be used as a photon-number filter, and a single-photon source –due to the scattered wave in the reflected channel.

In conclusion, based on superconducting qubits and the 1D scattering, in publication P7 we study several fundamental quantum optical effects with a transmon qubit, such as photon scattering, Mollow triplet and Autler-Townes splitting. This results has led to the development of a single photon router, presented in P6.

[19]The atom gets dressed with the strong control field, yielding a splitting at the $1-2$ transition, with energy splitting proportional to the Rabi frequency of the drive Ω_c.

3.3.4 Publication 6: Demonstration of a Single-Photon Router in the Microwave Regime. I.-C. Hoi, C.M. Wilson, G. Johansson, T. Palomaki, B. Peropadre, P. Delsing. Phys. Rev. Lett. 107, 073601 (2011)

Demonstration of a Single-Photon Router in the Microwave Regime

Io-Chun Hoi,[1] C. M. Wilson,[1] Göran Johansson,[1] Tauno Palomaki,[1] Borja Peropadre,[2] and Per Delsing[1]
[1]*MC2, Chalmers University of Technology, Göteborg, Sweden*
[2]*Instituto de Física Fundamental Serrano, CSIC, Madrid, Spain*
(Received 21 February 2011; revised manuscript received 4 June 2011; published 9 August 2011)

We have embedded an artificial atom, a superconducting transmon qubit, in an open transmission line and investigated the strong scattering of incident microwave photons (~ 6 GHz). When an input coherent state, with an average photon number $N \ll 1$ is on resonance with the artificial atom, we observe extinction of up to 99.6% in the forward propagating field. We use two-tone spectroscopy to study scattering from excited states and we observe electromagnetically induced transparency (EIT). We then use EIT to make a single-photon router, where we can control to what output port an incoming signal is delivered. The maximum on-off ratio is around 99% with a rise and fall time on the order of nanoseconds, consistent with theoretical expectations. The router can easily be extended to have multiple output ports and it can be viewed as a rudimentary quantum node, an important step towards building quantum information networks.

DOI: 10.1103/PhysRevLett.107.073601 PACS numbers: 42.50.Gy, 03.67.Hk, 85.25.Cp

In recent years, quantum information science has advanced rapidly, both at the level of fundamental research and technological development. For instance, quantum cryptography systems have become commercially available [1]. These systems are examples of quantum channels, serving mainly to distribute quantum information. There is a significant effort to combine these quantum channels with quantum nodes that would offer basic processing and routing capability. The combination of these channels and nodes would create a quantum network enabling applications simply impossible today [2]. Quantum networks connecting simple quantum processing nodes are also a promising architecture for a scalable quantum computer.

In this Letter, we demonstrate an example of a rudimentary quantum node, a single-photon router. The active element of the router is a single ''artificial atom'', a superconducting qubit, strongly coupled to a superconducting transmission line. Exploiting the phenomenon of electromagnetically induced transparency (EIT), we show that we can route a single-photon signal from an input port to either of two output ports with an on-off ratio of 99%. The switching time of the device is shown to be a few nanoseconds, consistent with theoretical expectations and the device parameters. The device is a nanofabricated circuit offering a clear path to scalability. For instance, it is straight forward to extend this router to select between multiple output channels.

An obvious requirement of a quantum channel is the ability to coherently distribute quantum information over relatively large distances. This typically implies the use of photons as information carriers, as opposed to other quantum systems such as atoms. This presents a problem when trying to implement a quantum node, as the interaction of photons with themselves is vanishingly small. Without interactions, photons cannot be controlled or directed. We can however look to control the photons by using matter as an intermediary [3–5], exploiting the strong interactions of electrons for instance. Still, the coupling of single-photon signals to bulk nonlinear materials is too weak for efficient control. A number of authors [6–9] have suggested that this problem could be overcome by resonantly coupling the signals to single atoms, which are highly nonlinear systems. While impressive technical achievements have been demonstrated in experiment, the coupling of single atoms to light remains relatively inefficient. For instance, in the prototypical experiment of scattering light from a single atom, the reduction in the intensity (extinction) of the incident light does not exceed 12% [10–13]. However, it was recently demonstrated that microwave photons can be coupled extremely efficiently to a single artificial atom, showing extinction efficiencies in an open transmission line greater than 90% [14,15]. Here we demonstrate an extinction of 99.6%, an order of magnitude increase, and use this approach as the basis of our single-photon router.

Our artificial atom is a superconducting transmon [16] qubit, consisting of two Josephson junctions in a SQUID configuration with a total capacitance C_Σ. It is capacitively coupled to a 1D transmission line [see Fig. 1(a)] in a coplanar waveguide configuration. The two lowest energy states $|0\rangle$, $|1\rangle$ have a transition energy $\hbar\omega_{01}(\Phi) \approx \sqrt{8E_J E_c} - E_c \sim 7.1$ GHz where E_J is the Josephson energy of the SQUID, E_C is the charging energy and Φ is the external magnetic flux. This type of qubit has been extensively studied [17–20] and successfully used to, for example, perform quantum algorithms [21] as well as produce single photons [22].

The electromagnetic field in the transmission line can be described by incoming $(+)$ and outgoing $(-)$ voltage waves on the left (L) and the right (R), $V^{\pm}_{L,R}$. In Fig. 1(a), the transmission coefficient $t = V^-_R/V^+_L$ and the reflection coefficient $r = V^-_L/V^+_L$ are related by the definition,

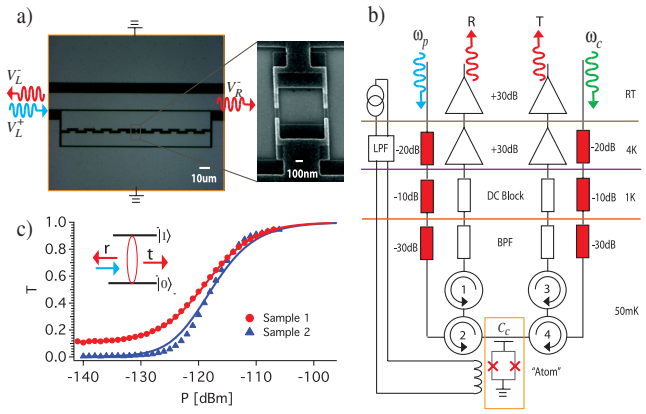

FIG. 1 (color online). Scattering from a single artificial atom. (a) A micrograph of our artificial atom, a superconducting transmon qubit embedded in a 1D open transmission line. The light regions are Al while the dark regions are the oxidized silicon substrate. We see the center conductor of the CPW in between the two ground planes and the two plates of the interdigitated capacitance of the transmon. The enlargement is a scanning-electron micrograph of the SQUID loop of the transmon, which allows us to tune its transition frequency with an external magnetic flux Φ. The junctions are formed using the standard double-angle evaporation technique. (b) Schematic of the measurement setup. A strong control pulse at $\omega_c = \omega_{12}$ is used to route a weak microwave signal at the probe frequency ω_{01}. We measure the transmitted and reflected probe simultaneously in the time domain. The circulators, numbered 1–4, allow us to separate signals propagating in different directions in the lines. (c) Transmittance, $T = |t|^2$, on resonance as a function of incident power. For $N \ll 1$ we see extinction of the coherent probe of 90% and 99.6% for sample 1 and 2, respectively. $N = 1$ for a power of -125 dBm (-123 dBm) for sample 1 (2). The symbols are data while the lines are fits based on Eq. (1). (Inset) A weak, resonant coherent state is scattered by the atom.

$t = r + 1$. When the applied probe frequency ω_p is equal to ω_{01}, the reflection coefficient is given by [14]

$$r = -r_0 \frac{1}{1 + \Omega_p^2/\Gamma_{10}\gamma_{10}}, \tag{1}$$

where the maximum reflection amplitude is $r_0 = 1/(1 + 2\Gamma_\phi/\Gamma_{10})$. Γ_{10} is the relaxation rate of the atom from $|1\rangle$ to $|0\rangle$, $\gamma_{10} = \Gamma_{10}/2 + \Gamma_\phi$ is the 0–1 decoherence rate, and Γ_ϕ is the 0–1 pure dephasing rate. A coherent input signal (probe) will drive coherent oscillations of the atom at a Rabi frequency which is linear in the probe amplitude and can be written as [16]

$$\Omega_p = \frac{2e}{\hbar}\frac{C_c}{C_\Sigma}\left(\frac{E_J}{8E_c}\right)^{1/4}\sqrt{PZ_0}, \tag{2}$$

where $P = |V_L^+|^2/2Z_0$ is the probe power, $Z_0 \sim 50\ \Omega$ is the impedance of the transmission line and C_c is the coupling capacitance between the qubit and the transmission line [Fig. 1(b)]. For a weak resonant probe ($\Omega_p \ll \Gamma_{10}, \gamma_{10}$) and in the absence of both pure dephasing ($\Gamma_\phi = 0$) and unknown loss channels, such as relaxation of the qubit not associated with the coupling to the transmission line, we expect to see full reflection of the incoming probe [7,8,23]. This perfect reflection can be understood as the coherent interference between the incoming wave and the wave scattered from the atom.

TABLE I. Parameters for samples 1 and 2. All values in GHz (except for the extinction), with an uncertainty of 5%.

Sample	E_J/h	E_c/h	$\Gamma_{10}/2\pi$	$\Gamma_\phi/2\pi$	Ext.
1	12.7	0.59	0.073	0.018	90%
2	21.5	0.35	0.096	0.002	99.6%

We have measured the reflection and transmission coefficients in two different samples as a function of incident probe power using homodyne detection (See Supplemental Material [24]). By fitting the frequency and power dependence of this data, we extract the parameters shown in Table I.

In Fig. 1(c), we plot the transmittance $T = |t|^2$ on resonance as a function of P. We can define an average number of photons per interaction time $2\pi/\Gamma_{10}$ as $N \equiv 2\pi P/(\hbar\omega_p\Gamma_{10})$. For $N \ll 1$, we see an extinction of propagating photons of up to 90% for sample 1 and 99.6% for sample 2. The strong saturation of the extinction already at single-photon powers is an indication that the scattering is caused by a single atom, since the atom can only absorb and emit one photon at a time. The reflected power (not shown) also varies with power as expected.

So far, we have considered only the lowest two energy levels of our artificial atom. In reality, the transmon has several higher states, in particular, it has a second excited state with the 1–2 transition frequency ω_{12}. This second transition can be directly measured using two-tone spectroscopy, as is illustrated in Fig. 2(a) for sample 1. We extract $\omega_{12}/2\pi = 6.38$ GHz, giving an anharmonicity of $\alpha = 720$ MHz between the two transitions. The linewidth of the 1–2 transition is dominated by the charge dispersion of $|2\rangle$. Further increasing the pump power, we observe the well-known Mollow triplet [14,25,26] (not shown). The Rabi splitting of the triplet was used to calibrate the applied microwave power at the atom.

By pumping the system at $\omega_c = \omega_{12}$, we can observe the phenomenon of electromagnetically induced transparency (EIT)[15,27–29] based on the Autler-Townes splitting [30,31]. With the pump off, we have seen that an incident, low-power probe at ω_{01} is reflected. For large control powers, however, the original line splits into a doublet with a separation of Ω_c [see Fig. 2(b)], and the atom becomes transparent to the probe beam at ω_{01}.

We exploit EIT to create a single-photon router. The operation principle is explained as follows [see Fig. 2(c)].

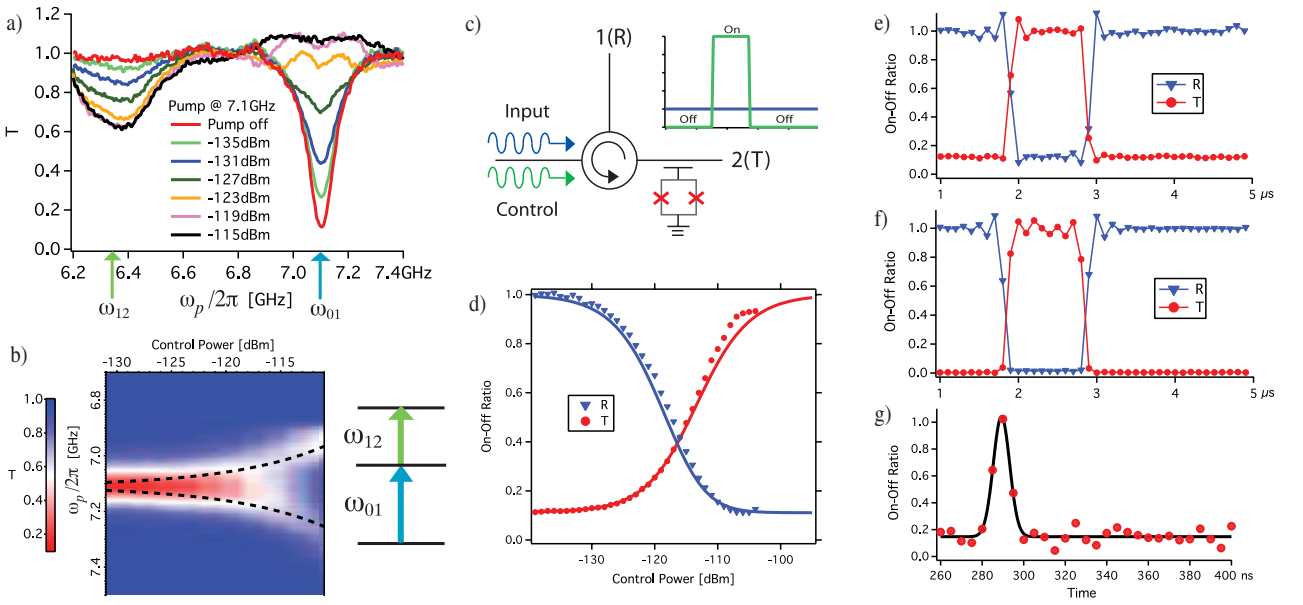

FIG. 2 (color online). (a) Two-tone spectroscopy of sample 1. A microwave pump is continuously applied at ω_{01} with increasing power while a weak probe tone is swept in frequency. As the population in the first state is increased, due to the drive at ω_{01}, scattering at ω_{12} becomes possible, appearing as another dip in the transmittance. From this, we extract $\omega_{12}/2\pi = 6.38$ GHz. (b) The microwave pump is now applied at ω_{12}. As the power of the ω_{12} pump increases, we see electromagnetically induced transparency (EIT) at ω_{01} as the Autler-Townes doublet splits with a separation equal to the Rabi frequency $\Omega_c/2\pi$ (black dashed lines). (inset) Energy level diagram. (c) Cartoon of the router. With the control off, the input probe is reflected from the transmon, and is routed to port 1 through the circulator. When the control is on, the input is transmitted to port 2. Inset: the control pulse sequence. (d) Normalized on-off ratio (see text) of the transmittance (T) and reflectance (R) as a function of control pulse power, measured simultaneously on sample 1. The symbols are the data and the solid lines are fits. (e) Time dependence of T and R at ω_{01}, measured simultaneously for sample 1, while a control pulse is applied. (f) Same for sample 2, although T and R are measured separately. We see that the input signal is routed with an on-off ratio of $\sim$90% ($\sim$ 99%) for sample 1 (2). (g) The response of sample 1 to a 10 ns Gaussian control pulse (circles), along with a Gaussian fit (solid line). We see that the transmittance smoothly follows the control on the few ns time scale while maintaining the high on-off ratio.

We input a weak, continuous probe in the single-photon regime at ω_{01}. We then apply a strong control pulse, around 30 dB stronger than the probe, at $\omega_c = \omega_{12}$. When the control is off, the photons are reflected by the atom and travel through the circulator to output 1. When the control is on, the photons are transmitted due to EIT, and travel to output 2. The measurement setup is shown in Fig. 1(b), which enables us to measure the reflected and transmitted probe power simultaneously in the time domain. This is crucial to demonstrate that the extinction of the transmitted beam is due to reflection instead of loss. One could also envision making a photon router by simply detuning the 0–1 transition of the atom via magnetic flux through the SQUID loop. However, the power needed to generate a flux sufficient to detune our atom is several orders of magnitude higher [19].

The operation of the router is demonstrated in Figs. 2(e)–2(g). As expected, when the control is on, most of the signal is transmitted while little is reflected. For sample 2 (1), we achieve an on-off ratio of nearly 99% (90%) in both the reflectance and transmittance. We also characterized the time response of the router. For both devices, we saw no reduction in the on-off ratio down to the shortest pulses, which had a Gaussian full width at half maximum of 10 ns. An example is shown for sample 1 in Fig. 2(g). We see that the transmission follows the control on the few ns time scale, limited by the 5 ns time resolution of our instruments. We would expect the limit of the device to be $\sim 1/\Gamma_{01} = 2$ ns.

In Fig. 2(d), we characterize the on-off ratio as a function of control power for sample 1. We use the experimentally accessible on-off ratio here, because it is not possible to do a full calibration of r (see below). For a probe power in the single-photon regime ($\Omega_p \ll \Gamma_{01}$) with the control and probe on resonance, the transmission of the probe, for a control amplitude corresponding to Ω_c, is [15]

$$t(\Omega_c) = 1 - \frac{\Gamma_{10}}{2\gamma_{10} + \frac{\Omega_c^2}{2\gamma_{20}}}, \tag{3}$$

where γ_{20} is the decoherence rate of the 0–2 transition. Because of the larger dipole moment of the 1–2 transition [16], we have $\Omega_c(P) = \sqrt{2}\ \Omega_p(P)$. We define the *coherent* transmittance and reflectance as $T(\Omega_c) = |t(\Omega_c)|^2$ and

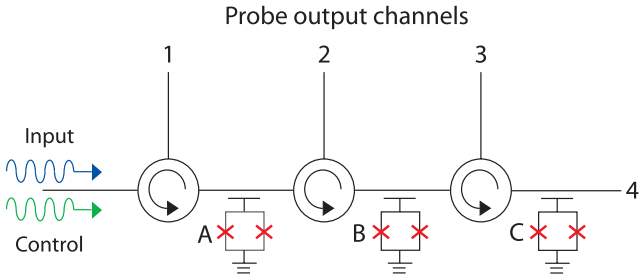

ω_A	Off	On	On	On
ω_B	Off	Off	On	On
ω_C	Off	Off	Off	On
Output	1	2	3	4

FIG. 3 (color online). Cartoon of a multiport router. The router demonstrated here can easily be cascaded to distribute photons to many channels. Here we show a four-port router using 3 atoms (A,B,C) in series, each separated by a circulator. The 0–1 transition frequencies of the atoms are the same, while the 1–2 transition frequencies, $\omega_A \neq \omega_B \neq \omega_C$, are different. This arrangement can be designed in a straightforward manner by controlling the ratio of E_J/E_c. By turning on and off control tones at the various 1–2 transition frequencies, we can determine the output channel of the probe field, according to the table. For instance, if we wish to send the probe field to channel 3, we apply two control tones at ω_A and ω_B. We note that all the control tones can be input through the same port regardless of the number of output channels, reducing the complexity of the design.

$R(\Omega_c) = |1 - t(\Omega_c)|^2$, respectively. An important point is that not all of the input power is necessarily transmitted and reflected coherently. For intermediate values of Ω_c, a significant fraction of the power, quantified by $1 - R(\Omega_c) - T(\Omega_c)$, is lost to spontaneous emission at various frequencies. This power is not detected by our phase-sensitive voltage measurement. To fit the reflection data, we use the theoretical on-off ratio $[R(\Omega_c) + R_b]/[R(0) + R_b]$, where R_b accounts for background reflections in the line and leakage through circulator 2 [Fig. 1(b)]. Using the same values of Γ_{10} and γ_{10} as before, we extract the additional parameters $\gamma_{20}/2\pi = 145$ MHz and $R_b = 0.05$. These values agree with our expectations based on the charge dispersion of $|2\rangle$ and circulator leakage in our system.

It is natural to ask, why sample 2 outperforms sample 1. Within the current model, the switching efficiency η is limited by the maximum reflectance $R_{\max} = (\Gamma_{10}/2\gamma_{10})^2 \approx 1\text{–}4\Gamma_\varphi/\Gamma_{10}$, which is limited by pure dephasing. The major improvement therefore comes from the reduction of the pure dephasing from 18 MHz to 2 MHz. This reduction can largely be attributed to the increase of E_J/E_c from 22 to 60, which dramatically reduces the sensitivity of the transmon to charge noise [16]. A smaller effect is the increased coupling, with $\Gamma_{10}/2\pi$ changing from 73 to 96 MHz.

The operation scheme of the router is scalable in a straightforward manner, as is explained in detail in Fig. 3. For an n-port router, the routing efficiency to the kth port is $\eta_k = T^{k-1}R$ for $k \neq n$ and $\eta_n = T^{n-1}$ for $k = n$. For sample 2, we measure $T \approx 99\%$ and $R \approx 92\%$. Therefore, the efficiency of a four-port router would still exceed 90%. This could be further improved by further reducing the dephasing.

In conclusion, we have demonstrated a basic single-photon router with high speed and efficiency operating in the microwave regime. While microwave circuits are a promising technology for quantum nodes, it is clear that optical photons are advantageous for use in quantum channels. This identifies the development of an optical-microwave quantum interface as a key enabling technology for a hybrid quantum network. Early steps to this type of interface have recently been achieved by a number of groups [32,33].

We acknowledge financial support from the Swedish Research Council, the Wallenberg foundation and from the EU through the European Research Council and the integrated project SOLID. B. P. acknowledges CSIC JAE-PREDOC2009, FIS2009-10061, and QUITEMAD S2009-ESP-1594. We would also like to acknowledge O. Astafiev for fruitful discussions and M. Sandberg and F. Persson for fabrication and experimental help.

[1] V. Scarani *et al.*, Rev. Mod. Phys. **81**, 1301 (2009).
[2] H. J. Kimble, Nature (London) **453**, 1023 (2008).
[3] D. A. Braje *et al.*, Phys. Rev. A **68**, 041801 (2003).
[4] S. E. Harris and L. V. Hau, Phys. Rev. Lett. **82**, 4611 (1999).
[5] S. E. Harris and Y. Yamamoto, Phys. Rev. Lett. **81**, 3611 (1998).
[6] J. T. Shen and S. H. Fan, Opt. Lett. **30**, 2001 (2005).
[7] J. T. Shen and S. H. Fan, Phys. Rev. Lett. **95**, 213001 (2005).
[8] G. Zumofen *et al.*, Phys. Rev. Lett. **101**, 180404 (2008).
[9] D. Witthaut and A. S. Sorensen, New J. Phys. **12**, 043052 (2010).
[10] M. K. Tey *et al.*, Nature Phys. **4**, 924 (2008).
[11] J. Hwang *et al.*, Nature (London) **460**, 76 (2009).
[12] G. Wrigge *et al.*, Nature Phys. **4**, 60 (2007).
[13] I. Gerhardt *et al.*, Phys. Rev. Lett. **98**, 033601 (2007).
[14] O. Astafiev *et al.*, Science **327**, 840 (2010).
[15] A. A. Abdumalikov *et al.*, Phys. Rev. Lett. **104**, 193601 (2010).
[16] J. Koch *et al.*, Phys. Rev. A **76**, 042319 (2007).
[17] D. I. Schuster *et al.*, Nature (London) **445**, 515 (2007).
[18] J. M. Fink *et al.*, Nature (London) **454**, 315 (2008).
[19] M. Sandberg *et al.*, Phys. Scr. **T137**, 014018 (2009).
[20] F. Mallet *et al.*, Nature Phys. **5**, 791 (2009).
[21] L. DiCarlo *et al.*, Nature (London) **460**, 240 (2009).
[22] A. A. Houck *et al.*, Nature (London) **449**, 328 (2007).
[23] D. E. Chang *et al.*, Nature Phys. **3**, 807 (2007).
[24] See Supplemental Material at http://link.aps.org/supplemental/10.1103/PhysRevLett.107.073601 for measurements and fitting of the transmission coefficient.
[25] M. Baur *et al.*, Phys. Rev. Lett. **102**, 243602 (2009).

[26] B. R. Mollow, Phys. Rev. **188**, 1969 (1969).
[27] M. Fleischhauer *et al.*, Rev. Mod. Phys. **77**, 633 (2005).
[28] W. R. Kelly *et al.*, Phys. Rev. Lett. **104**, 163601 (2010).
[29] L. Slodička *et al.*, Phys. Rev. Lett. **105**, 153604 (2010).
[30] S. H. Autler and C. H. Townes, Phys. Rev. **100**, 703 (1955).
[31] P. M. Anisimov *et al.*, arXiv:1102.0546v1.
[32] Y. Kubo *et al.*, Phys. Rev. Lett. **105**, 140502 (2010).
[33] D. Schuster *et al.*, Phys. Rev. Lett. **105**, 140501 (2010).

3.3.5 Publication 7: Microwave Quantum Optics with an Artificial Atom in 1D Open Space. I.-C. Hoi, C.M. Wilson, G. Johansson, J. Lindkvist, B. Peropadre, T. Palomaki, P. Delsing. New J. Phys. 15 025011 (2013)

New Journal of Physics
The open access journal for physics

Microwave quantum optics with an artificial atom in one-dimensional open space

Io-Chun Hoi[1], C M Wilson[1,3], Göran Johansson[1], Joel Lindkvist[1], Borja Peropadre[2], Tauno Palomaki[1] and Per Delsing[1,3]

[1] Department of Microtechnology and Nanoscience (MC2), Chalmers University of Technology, SE-412 96 Göteborg, Sweden
[2] Instituto de Física Fundamental, CSIC, Calle Serrano 113-bis, Madrid E-28006, Spain
E-mail: per.delsing@chalmers.se and chris.wilson@chalmers.se

New Journal of Physics **15** (2013) 025011 (15pp)
Received 10 October 2012
Published 7 February 2013
Online at http://www.njp.org/
doi:10.1088/1367-2630/15/2/025011

Abstract. We address recent advances in microwave quantum optics with artificial atoms in one-dimensional (1D) open space. This field relies on the fact that the coupling between a superconducting artificial atom and propagating microwave photons in a 1D open transmission line can be made strong enough to observe quantum coherent effects, without using any cavity to confine the microwave photons. We investigate the scattering properties in such a system with resonant coherent microwaves. We observe the strong nonlinearity of the artificial atom and under strong driving we observe the Mollow triplet. By applying two resonant tones, we also observe the Autler–Townes splitting. Exploiting these effects, we demonstrate two quantum devices at the single-photon level in the microwave regime: the single-photon router and the photon-number filter. These devices provide important steps toward the realization of an on-chip quantum network.

[3] Authors to whom any correspondence should be addressed.

Contents

1. Introduction

During the last decade, circuit QED based on superconducting circuits has become a promising platform to investigate strong coupling between light and matter as well as enable quantum information processing technology [1–3]. Some of the exciting results include the following: strong coupling between a superconducting qubit and a single photon [4], resolving photon-number states [5], synthesizing arbitrary quantum states [6], three-qubit quantum error correction [7], implementation of a Toffoli gate [8], quantum feedback control [9] and architectures for a superconducting quantum computer [10]. The nonlinear properties of Josephson junctions have also been used to study the dynamical Casimir effect [11] and build quantum limited amplifiers [12, 13].

More recently, theoretical and experimental work has begun to investigate the strong interaction between light and a single atom even without a cavity [14–17]. In this system, the destructive interference between the excited dipole radiation and the incident field gives rise to the extinction of the forward propagating wave for a weak incident field. This effect was first demonstrated for a single atom/molecule in three-dimensional space, where the extinction of the forward incident wave did not exceed 12% [14, 16]. This is due to the spatial mode mismatch between the incident and scattered waves.

However, by taking advantage of the confinement of the propagating fields in a one-dimensional (1D) open transmission line and the huge dipole moment of an artificial atom [18–25], strong coupling between an artificial atom and a propagating field can be achieved. Extinctions in excess of 99% have been observed [19, 20]. This system represents a potential key component in the field of microwave quantum optics, which is the central scope of this paper.

This paper is organized as follows. The elastic and inelastic scattering properties of the single artificial atom are presented in section 2. Well-known quantum optics effects, such as the Mollow triplet and Autler–Townes splitting (ATS), are presented in section 3. In section 4, we demonstrate two quantum devices based on these effects which operate at the single-photon level in the microwave regime, namely the single-photon router and the photon-number filter. In section 5, we discuss the possibilities of a quantum network using these devices.

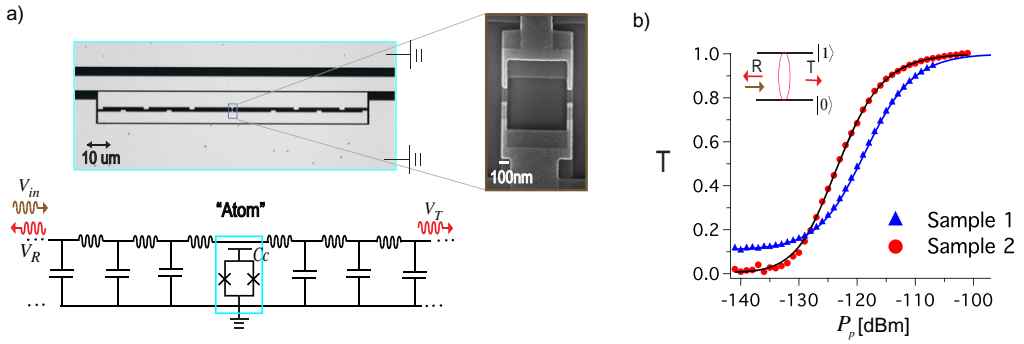

Figure 1. (a) Top: a micrograph of the artificial atom, a superconducting transmon qubit embedded in a 1D open transmission line. (Magnified section) Scanning-electron micrograph of the superconducting quantum interference device (SQUID) loop of the transmon. Bottom: the corresponding circuit model. (b) Measured transmittance, $T = |t|^2$, on resonance as a function of the incoming probe power, P_p, for samples 1 and 2. At low power, very little is transmitted whereas at high power T approaches unity. (Inset) A weak, resonant coherent field is reflected by the atom.

2. Elastic and inelastic scattering

In figure 1(a), a transmon qubit [26] is embedded in a 1D open transmission line with a characteristic impedance $Z_0 \simeq 50\,\Omega$. The 0–1 transition energy of the transmon, $\hbar\omega_{10}(\Phi) \approx \sqrt{8E_\mathrm{J}(\Phi)E_\mathrm{C}} - E_\mathrm{C}$, is determined by two energies, where $E_\mathrm{C} = \mathrm{e}^2/2C_\Sigma$ is the charging energy, C_Σ is the total capacitance of the transmon, $E_\mathrm{J}(\Phi) = E_\mathrm{J}|\cos(\pi\Phi/\Phi_0)|$ is the Josephson energy which can be tuned by the external flux Φ, E_J is the maximum Josephson energy and $\Phi_0 = h/2e$ is the magnetic flux quantum.

With a coherent state input, we investigate the transmission and reflection properties of the field. The input field, transmitted field and reflected field are denoted as V_in, V_T and V_R, respectively, indicated in the bottom panel of figure 1(a). The reflection coefficient, r, can be expressed as [18]

$$r = \frac{V_\mathrm{R}}{V_\mathrm{in}} = -r_0 \frac{1 - \mathrm{i}\delta\omega_\mathrm{p}/\gamma_{10}}{1 + (\delta\omega_\mathrm{p}/\gamma_{10})^2 + \Omega_\mathrm{p}^2/(\Gamma_{10} + \Gamma_l)\gamma_{10}}, \tag{1}$$

where the maximum reflection amplitude is given by $r_0 = \Gamma_{10}/2\gamma_{10}$. Γ_{10} is the relaxation rate of the 0–1 transition of the atom. $\gamma_{10} = \Gamma_{10}/2 + \Gamma_{\phi,l}$ is the 0–1 decoherence rate and $\delta\omega_\mathrm{p} = \omega_\mathrm{p} - \omega_{10}$ is the detuning between the applied probe frequency, ω_p, and the 0–1 transition frequency, ω_{10}. $\Gamma_{\phi,l} = \Gamma_\phi + \Gamma_l/2$, where $\Gamma_{\phi,l}$ is the sum of the non-radiative rates, i.e. the intrinsic losses, Γ_l and the pure dephasing rate, Γ_ϕ. We see that both r_0 and γ_{10} are uniquely dependent on $\Gamma_{\phi,l}$ and Γ_{10}. Ω_p is the Rabi oscillation frequency induced by the probe, which is proportional to V_in [26],

$$\Omega_\mathrm{p} = \frac{2e}{\hbar}\frac{C_\mathrm{c}}{C_\Sigma}\left(\frac{E_\mathrm{J}}{8E_C}\right)^{1/4}\sqrt{P_\mathrm{p}Z_0}, \tag{2}$$

where $P_\mathrm{p} = |V_\mathrm{in}|^2/2Z_0$ is the probe power. By definition, the transmission coefficient $t = V_\mathrm{T}/V_\mathrm{in} = 1 + r$. The level of V_in is assumed to be the same as the off resonance value. The

relaxation process is dominated by coupling to the 1D transmission line through the coupling capacitance C_c (see the bottom panel of figure 1(a)) and assuming that photon emission to the transmission line dominates the relaxation, we find that $\Gamma_{10} \simeq \omega_{10}^2 C_c^2 Z_0/(2C_\Sigma)$. This relaxation originates from coupling to a continuum of modes, as opposed to the cavity case, where the artificial atom is coupled solely to a single mode.

According to equation (1), for a weak ($\Omega_p \ll \gamma_{10}$) resonant probe ($\delta\omega_p = 0$), in the absence of both pure dephasing ($\Gamma_\phi = 0$) and non-radiative decay ($\Gamma_l = 0$), we should see full reflection ($|r| = 1$) of the incoming probe field [24, 25, 27]. In that case, we also have full extinction, $|t| = 0$, of the propagating wave. This full extinction (perfect reflection) can be described as a coherent interference of the incoming wave and the scattered wave from the atom. This is what we observe in figure 1(b), where we measure the transmittance, $T = |t|^2$, on resonance as a function of P_p with two samples. We see an extinction in the resonant microwaves of up to 90% (99%) for sample 1 (2) at low incident probe power, where $\Omega_p \ll \gamma_{10}$. For increasing P_p, we see the strong nonlinearity of the atom which becomes saturated by the incident microwave photons. Since the atom can only scatter one photon at a time, at high incident power, $\Omega_p \gg \gamma_{10}$, most of the photons pass the atom without interaction and are thus transmitted. Therefore $|t|$ tends toward unity for increasing P_p, consistent with equation (1). We define the average probe photon number coming to the transmon per interaction time as $\langle N_p \rangle = P_p/(\hbar\omega_p(\Gamma_{10}/2\pi))$.

We measure t as a function of P_p and ω_p. In figure 2, the experimental magnitude, $|t|$, and phase response, φ_p, for sample 1 are shown in panels (a), (b), respectively. The top and bottom panels display two-dimensional plots and the corresponding line cuts indicated by the arrows, respectively. For $\langle N_p \rangle \ll 1$, the magnitude response shows a strong extinction of resonant microwaves, up to 70% in amplitude or $\sim 90\%$ in power (figure 1(b)). The solid curves of figure 2 show fits to all magnitude and phase curves simultaneously, with three fitting parameters, $\Gamma_{10}/2\pi = 73$ MHz, $\Gamma_{\phi,l}/2\pi = 18$ MHz and $\omega_{10}/2\pi = 7.1$ GHz. This corresponds to $C_c = 25$ fF, $\gamma_{10}/2\pi = 55$ MHz and $r_0 = 0.67$. We find very good agreement between theory and experiment. We also see that r varies as a function of P_p and ω_p, as expected (data not shown).

In order to measure the resonant scattered field, V_R, from the atom, we need to cancel background reflections and circulator leakage in the setup. In figure 3(a), after splitting the input field, the phase and amplitude in one arm are varied such that the field through a directional coupler destructively interferes with the coherent leakage from the circulator and background reflections (see green curves). We send a pulse at ω_{10} and measure the scattered (reflected) fields from the artificial atom. We use a phase-sensitive average $\langle V_R \rangle^2$ to capture the elastic (coherent) component of the scattered field. For the total scattered field, the sum of the elastically and inelastically scattered fields, we use a phase-insensitive average $\langle V_R^2 \rangle$. By pulsing the input, we are able to subtract amplifier noise from our measurement of the total scattered field.

In figure 3(b), we show $\langle V_R^2 \rangle$ and $\langle V_R \rangle^2$ as a function of resonant incident power for two different measurement bandwidths (BW). We see that the amount of the inelastic field that we capture depends on the BW. The solid curves are theory fits using the model in figure 3(c) (integrating the Mollow triplet), with the parameters in table 1, sample 2. As expected, at low incident power, we see the $\langle V_R \rangle^2 \simeq \langle V_R^2 \rangle \simeq \langle V_{in}^2 \rangle$. This suggests that both the dephasing and non-radiative decay are small, and not resolvable from the data. At high incident fields, where $\Omega_p > \Gamma_{10}$, the main contribution to the total field is from inelastic scattering. The power associated with intrinsic losses is $P_l = P_p - P_R - P_T$, where P_R, P_T are the total power reflected and transmitted, respectively. For a resonant probe, we can estimate the loss rate Γ_l using the

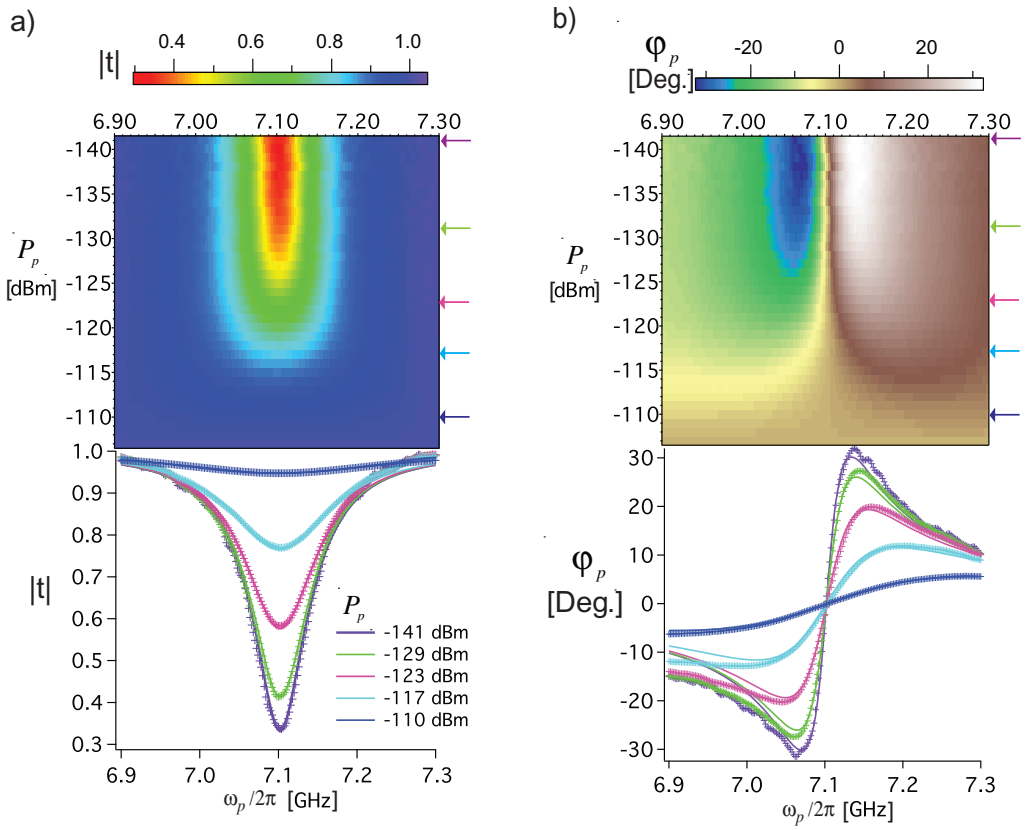

Figure 2. t as a function of P_p and ω_p (sample 1). (a) The magnitude response; (b) the phase response. Top panel: experimental data. Bottom panel: we show the line cuts for five different powers, as indicated by the arrows on the top panel. The experimental data (markers) are fit simultaneously using equation (1) (curves). The magnitude response demonstrates a strong coupling between the atom and resonant propagating microwaves, whereas the phase response shows anomalous dispersion [18].

following expression:

$$P_l = \hbar\omega_{10}\rho_{11}\Gamma_l = \frac{2r_0\Gamma_l/(\Gamma_{10}+\Gamma_l)}{1+\Omega_\mathrm{p}^2/(\Gamma_{10}+\Gamma_l)\gamma_{10}}P_\mathrm{p},$$

where ρ_{11} is the probability for the atom to be in the first excited state. We do not have sufficiently accurate data to extract the loss rate for these measurements. We can, however, set an upper limit on the loss rate. For sample 2, $\Gamma_{\phi,l}/2\pi \simeq 1.1$ MHz, which means that $\Gamma_l/2\pi$ is less than 2.2 MHz.

To further characterize sample 1, the frequency of the resonance dip in transmission in figure 2(a) is mapped as a function of Φ with a weak probe, $\Omega_\mathrm{p} \ll \gamma_{10}$ (see figure 4(a)), in the transmon regime, where $E_\mathrm{J}/E_\mathrm{C} \geqslant 20$, $\delta\omega_\mathrm{p} \approx \omega_\mathrm{p} - [\sqrt{8E_\mathrm{J}|\cos(\pi\Phi/\Phi_0)|E_\mathrm{C}} - E_\mathrm{C}]/\hbar$. If we increase P_p to a level such that the 0–1 transition is saturated, two-photon (0–2) transitions occur, as indicated by the gray curve of figure 4(b). The transition frequency corresponds to $(\omega_{10}+\omega_{21})/2$, where ω_{21} is the 1–2 transition energy. We use a Cooper pair box [26] Hamiltonian with 50 charge states to fit the spectrum of the atom and extract $E_\mathrm{J} = 12.7$ GHz,

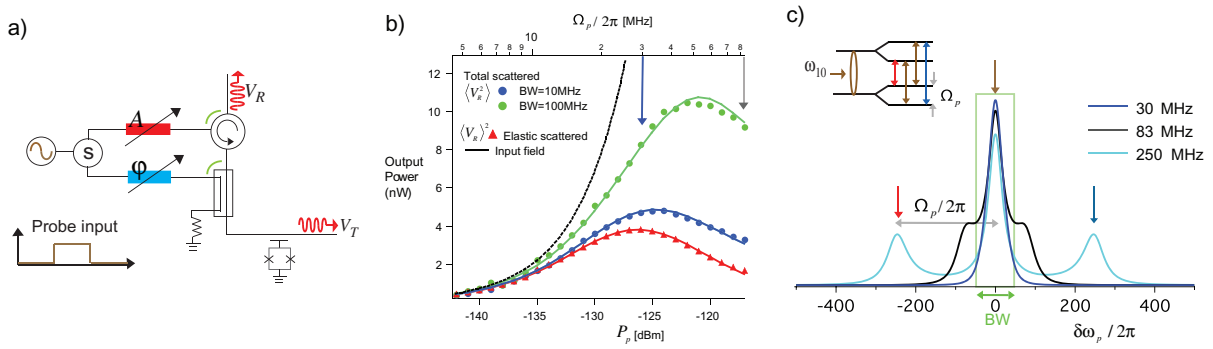

Figure 3. Elastic versus inelastic scattering from the artificial atom (sample 2). (a) Measurement setup, with calibration of background reflection, i.e. leakage from the circulator. The green curves represent the leakage fields from the circulator and the fields through the directional coupler. By tuning the phase (blue box) and attenuation (red box), these two fields can cancel each other. (b) The coherently/elastically reflected power (phase-sensitive average, red curve) or total reflected power (phase-insensitive average, green and blue curves) as a function of resonant $P_{\rm p}$ for different BW. The total power reflected is the sum of both the elastic and inelastic fields. Solid curves are the theory fits to experimental data, with extracted parameters of table 1. The black curve shows the input power for comparison. At low powers, $\langle N_{\rm p}\rangle \ll 1$, we observed that $\langle V_{\rm R}\rangle^2 \simeq \langle V_{\rm R}^2\rangle \simeq \langle V_{\rm in}^2\rangle$. At high powers, $\langle N_{\rm p}\rangle > 1$, more and more photons are inelastically scattered as the Mollow triplet begins to emerge. The wider the BW, the more of the Mollow triplet we capture. Note that the output power includes the 79 dB gain of the amplifiers. (c) Theory plot for the situation when a microwave pump is applied at ω_{10}. As the power of the ω_{10} pump increases, the Mollow triplet appears in the spectrum with peak separation equal to the Rabi frequency $\Omega_{\rm p}$. (Inset) Dressed state picture of the energy levels.

Table 1. Parameters for samples 1–3. All values are in GHz (except for the extinction and $E_{\rm J}/E_{\rm C}$).

Sample	$E_{\rm J}/h$	$E_{\rm C}/h$	$E_{\rm J}/E_{\rm C}$	$\omega_{10}/2\pi$	$\omega_{21}/2\pi$	$\Gamma_{10}/2\pi$	$\Gamma_{\phi,l}/2\pi$	Extinction (%)
1	12.7	0.59	21.6	7.1	6.38	0.073	0.018	90
2	10.7	0.35	31	5.13	4.74	0.041	0.0011	99
3	–	–	–	4.88	4.12	0.017	0.0085	75

$E_{\rm C} = 590$ MHz for sample 1. The extracted parameters are summarized in table 1. Note that one of the Josephson junctions is broken in sample 3; therefore, the transition frequency could not be tuned with Φ.

The extinction efficiency of sample 2 is much better than that of sample 1. This is because sample 1 has a low $E_{\rm J}/E_{\rm C} \sim 21.6$, which is barely in the transmon limit. For this value of $E_{\rm J}/E_{\rm C}$, charge noise still plays an important role as the energy band of the 0–1 transition is still dependent on charge [26]. For sample 1, we find that the charge dispersion is 7 MHz and the dephasing is dominated by charge noise. By increasing $E_{\rm J}/E_{\rm C}$ to 31, we see much less dephasing in sample 2, which gives nearly perfect extinction of propagating resonant

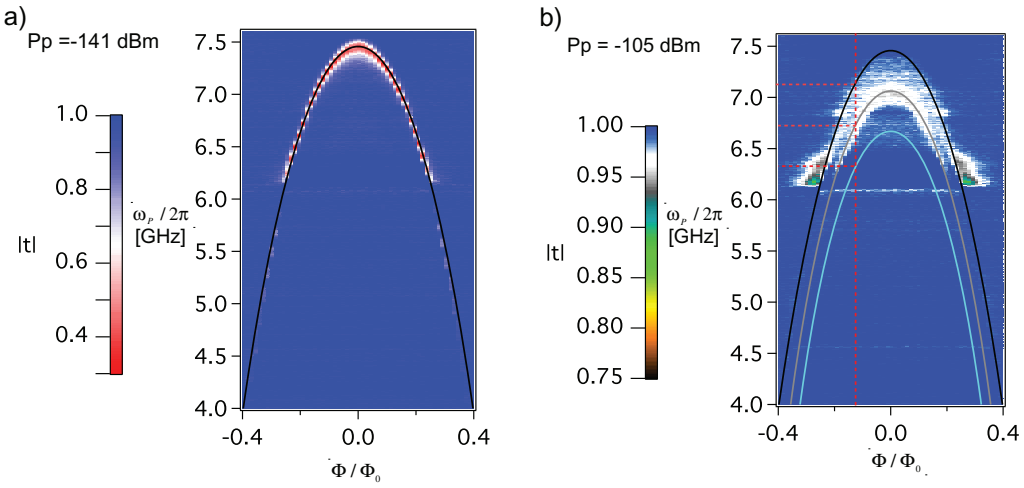

Figure 4. $|t|$ as a function of Φ for sample 1. (a) At weak probe power, where $\Omega_p \ll \gamma_{10}$. The black curve is the theory fit to the 0–1 transition. (b) At high probe power, where $\Omega_p \gg \gamma_{10}$. The black and blue curves correspond to the 0–1 and 1–2 transitions, respectively. The gray curve is the two-photon (0–2) transition. The red dashed line indicates the flux bias point and the corresponding ω_{10}, $\omega_{20}/2$, ω_{21} for figure 2 and figures 5(a), (c) and (d). There is a stray resonance around 6.1 GHz.

microwaves. Note that the anharmonicity between ω_{10} and ω_{21} of sample 2 is close to E_C. This is not quite the case for sample 1 due to its low E_J/E_C [26].

3. Mollow triplet and Autler–Townes splitting

As shown in the previous section, the transmon also has higher level transitions; in particular, we are interested in the 1–2 transition with frequency ω_{21}. By using two-tone spectroscopy, the ω_{21} transition can be directly measured. We can saturate the ω_{10} transition by applying a pump field at $\omega_{10} = 7.1$ GHz, and measure the transmission properties using a weak probe ω_p. As the pump power is increased, the population of the first excited state increases; therefore, we start observing photon scattering from the 1–2 transition, which appears as a dip in transmission at $\omega_p = \omega_{21}$, see figure 5(a). The dip in transmission grows until the 0–1 transition becomes fully saturated. From this, we extract $\omega_{21}/2\pi = 6.38$ GHz for sample 1. Therefore, the two-photon (0–2) transition should be equal to 6.74 GHz, consistent with the observation in figure 4(b). The linewidth of ω_{21} is around 120 MHz; this dephasing mainly comes from the charge dispersion. Further increasing the pump power at ω_{10}, we observe the well-known Mollow triplet [18, 28] (figure 5(b), sample 3). The Rabi splitting of the triplet can be used to calibrate the power at the atom. The Mollow triplet can be explained in the dressed state picture, where the two lowest levels are split by the Rabi frequency. These four states give three different transitions, indicated by red, brown and blue arrows in the inset of figure 5(b), consistent with figure 3(c). Note that the way we observed the triplet here is different from that in [18]. We probe the transmission of these triplet transitions instead of looking at the emission spectrum. We see that the center transition is much less visible, because we pump at the frequency which saturates the transition.

With a weak resonant probe field, $\Omega_p \ll \gamma_{10}$, $\omega_p = \omega_{10}$, and a strong resonant, $\omega_c = \omega_{21}$, control field, the 0–1 resonance dip splits with the magnitude of Ω_c [22]; this is known as the

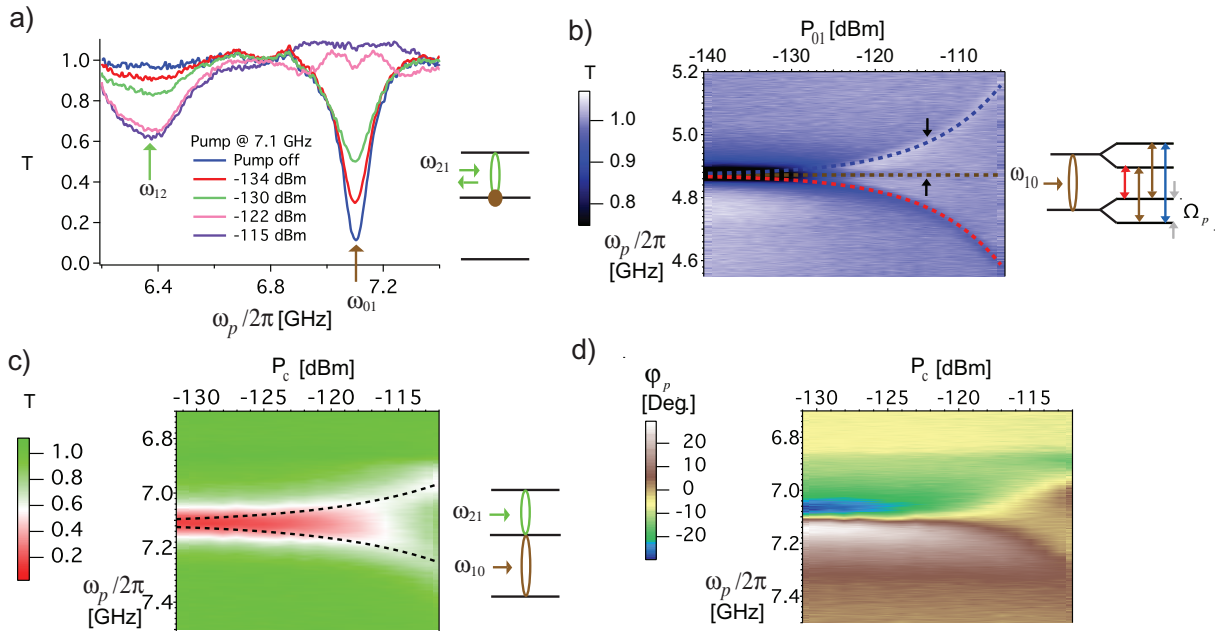

Figure 5. Two-tone spectroscopy. (a) As the frequency of a weak probe field is swept, a second microwave drive is continuously applied at ω_{10} with increasing powers. We see that another dip gradually appears in the probe transmission response. (b) T as a function of the probe frequency and pump power. As the power of ω_{10} further increases, we see the Mollow triplet. The dashed lines indicate the calculated position of the triplet. (Inset) Schematic picture of triplet transitions in the dressed state picture. Note that we use sample 3, where $\omega_{10}/2\pi = 4.88$ GHz. (c) A second microwave drive is applied at ω_{21} with variable power, P_c. Magnitude response in (c). As P_c increases, we see induced transmission at $\omega_p = \omega_{10}$. With a strong drive applied, the ATS appears with the magnitude of $\Omega_c/2\pi$ (black dashed lines). (d) Phase response of the probe.

ATS [29]. The magnitude and phase response are shown in figures 5(c) and (d), respectively. In the magnitude response, we see that the transmon becomes transparent for the probe at $\omega_p = \omega_{10}$ at sufficiently high control power. In the phase response, we see that the probe phase, φ_p, depends on the control power, P_c.

In the following section, we demonstrate two devices based on these effects which could be utilized in a microwave quantum network. By making use of the ATS, we demonstrate a router for single photons. By using the high nonlinearity of the atom, we demonstrate a photon-number filter, where we convert classical coherent microwaves into a non-classical microwave field.

4. Applications

4.1. The single-photon router

The operation principle of the single-photon router is explained as follows. In the time domain (see figure 6(a)), we input a constant weak probe in the single-photon regime, $\langle N_p \rangle \ll 1$, at $\omega_p = \omega_{10}$. We then apply a strong control pulse, around 30 dB more than the probe power, at

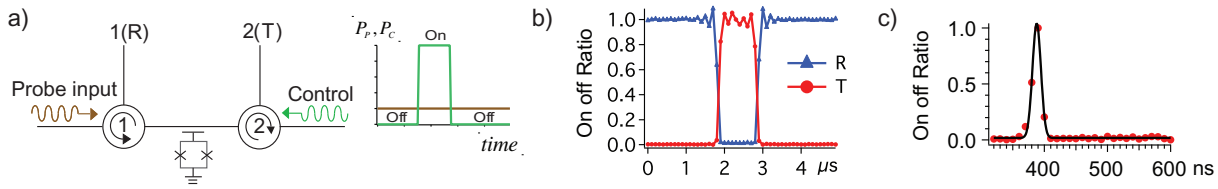

Figure 6. The single-photon router, data for sample 2. (a) Measurement setup and the control pulse sequence. A strong control pulse at $\omega_c = \omega_{21}$ is used to route a weak continuous microwave $\omega_p = \omega_{10}$. Depending on whether the control pulse is on or off, the probe field is delivered to output port 2 or 1, respectively. (b), (c) Normalized on–off ratio (see text) of the transmittance (T) and reflectance (R) of ω_p measured simultaneously. (b) The control pulse is shaped as a square pulse with 1 μs duration. (c) A Gaussian pulse with a duration of 10 ns; we see up to 99% on–off ratio. The black curve in panel (c) is a Gaussian fit to the data.

the ω_{21} frequency. When the control is off, the probe photons are reflected by the atom, and delivered to output port 1. When the control is on, the probe photons are transmitted based on ATS and delivered to output port 2. We measure the reflected and the transmitted probe power simultaneously in the time domain. It is crucial to investigate if the microwave photon transport is a fully coherent process, i.e. the transmission dip seen in figure 2(a) is because the photons are being reflected (not due to dissipation). Note that the measurement quantity is phase sensitive, since we measure $\langle V\rangle^2$ rather than $\langle V^2\rangle$; this means that $\langle V\rangle^2$ is only sensitive to the coherent part of the signal. The experimental setup is shown in figure 6(a).

The results are shown in figures 6(b) and (c) with two different control pulses for sample 2. In figures 6(b) and (c), we use a square (Gaussian) control pulse with a duration of 1 μs (10 ns). As expected, when the control signal is on, the probe power of the transmitted signal is increased and we see a corresponding decrease in the reflected probe signal. A 99% probe on–off ratio is achieved in both reflection and transmission for sample 2. We also see that the on–off ratio does not depend on the control time. In figure 6(c), the time resolution of our digitizer detector/arbitrary waveform generator is 5 ns, which prevents us from accurately measuring pulses less than about 10 ns. The ringing signals appearing in figure 6(b) are artifacts of the digitizer. In the setup of figure 6(a), we send ω_{10} and ω_{21} in opposite directions with respect to each other. We can also send pulses in the same direction by using a microwave combiner at one of the input ports and get the same results, as expected. Note that we use the on–off ratio $[R(\Omega_c) + R_b]/[R(0) + R_b]$ [19], where $R(\Omega_c)$ and $R(0)$ represent reflectance when the control is on and off, respectively, and R_b accounts for background reflections in the line and leakage through circulator 1 (figure 6(a)). We note that these data were taken without canceling the leakage as shown in figure 3. For the on–off ratio of the transmittance $T(0)/T(\Omega_c)$, we can calibrate the transmittance, $T(0) = [T(0)/T(\Omega_c)]T_{VNA}(\Omega_c)$, where $T_{VNA}(\Omega_c) \simeq 98.4\%$ is the transmittance on resonance with the corresponding P_c in figure 5(c). $T(\Omega_c)$ and $T(0)$ represent the transmittance when the control is on and off, respectively. Theoretically, for sample 2, when the control signal is off, we have $R(0) = |\Gamma_{10}/2\gamma_{10}|^2 \simeq 91\%$, $T(0) = |1 - \Gamma_{10}/2\gamma_{10}|^2 \simeq 0.2\%$ and $D_{\phi,l}(0) \simeq 8.8\%$. When the control signal is on, we have $R(\Omega_c) \simeq 0$, $T(\Omega_c) \simeq 1$ and $D_{\phi,l}(\Omega_c) \simeq 0$, where $D_{\phi,l}$ refers to the total dissipation associated with intrinsic losses and pure dephasing.

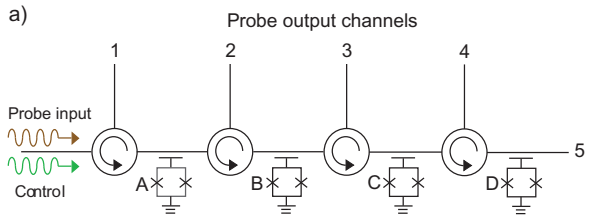

b)

ω_A ω_B ω_C ω_D	Off Off Off Off	On Off Off Off	On On Off Off	On On On Off	On On On On
Output	1	2	3	4	5

Figure 7. A multiport router. (a) Cartoon of a multiport router: single-photon routers cascaded to many output channels. Here we show a five-port router using four atoms (A–D) in series, each separated by a circulator. The ω_{10} of the atoms are the same, whereas the 1–2 transition frequencies, $\omega_{21,A} \neq \omega_{21,B} \neq \omega_{21,C} \neq \omega_{21,D}$, are different. By turning on and off control tones at the various 1–2 transition frequencies, we can determine the output channel of the probe field, according to the table in (b).

The speed of our router sample 1 (2) is predicted to be $1/\Gamma_{10} \sim 2$ ns (4 ns). We show that the router works well down to the time limit of our instruments. By engineering the relaxation rate, it should be possible to achieve even faster switching times in the sub-nanosecond regime. In addition, the routing efficiency, $R = |r_0|^2$, can be improved by further reducing Γ_ϕ. An improvement in sample 2 compared with sample 1 was achieved by increasing the E_J/E_C ratio. This reduced the sensitivity to the charge noise and therefore the dephasing.

Our router can also be easily cascaded to distribute photons to many output channels. Figure 7(a) shows four atoms (A–D) in series, each separated by a circulator. The ω_{10} of the atoms are the same, whereas the ω_{21} are different. This arrangement can be designed in a straightforward manner by controlling the ratio of E_J/E_C. By turning on and off control tones at the various 1–2 transition frequencies of different atoms, we can determine the output channel of the probe field, according to the table of figure 7(b). For instance, if we want to send the probe field to channel 4, we apply three control tones at $\omega_{21,A}$, $\omega_{21,B}, \omega_{21,C}$. Note that regardless of the number of output channels, all the control tones and the probe tone can be sent through the same input port. Theoretically, the maximum number of output channels depends on the ratio of the anharmonicity and the width of the 1–2 transition, γ_{21}. Thus, there is a tradeoff between efficiency and the number of outputs.

4.2. The photon-number filter

In figure 1(b), we demonstrated the nonlinear nature of the artificial atom. This naturally comes from the fact that atoms can only reflect one photon at a time. To reveal the non-classical character of the reflected field, we investigate its statistics. In particular, in this section, we show that the reflected field is antibunched [25]. In addition, we also show that the transmitted field is superbunched [25].

The incident coherent state can be written in terms of a superposition of photon number states, with a Poissonian distribution. For a weak probe field with $\langle N_p \rangle < 0.5$, this coherent field can be approximated using the basis of the first three-photon number states. For a one-photon incident state, the atom reflects it, leading to antibunching in the reflected field. Together with the zero-photon state, the reflected field still maintains first-order coherence, as there is a well-defined phase between the zero- and one-photon states. Because the atom is not able to scatter

more than one photon at a time, a two-photon incident state has a much higher probability of transmission, leading to superbunching in the transmitted field [25, 30]. In this sense, our single artificial atom acts as a photon-number filter, which filters and reflects the one-photon number state from a coherent state. This process leads to a photon-number redistribution between the reflected and transmitted fields [30].

A schematic illustration of the measurement setup is shown in figure 8(a). This allows us to measure the Hanbury Brown–Twiss [31] type power–power correlations. We apply a resonant coherent microwave field at $\omega_p = \omega_{10}$. Depending on whether we send the input through circulator 1 or 2, we measure the statistics of the reflected or transmitted field, respectively. The signal then propagates to a beam splitter, which in the microwave domain is realized by a hybrid coupler, where the outputs of the beam splitter are connected to two nominally identical high electron mobility transistor (HEMT) amplifiers with system noise temperatures of approximately 7 K. We assume that the amplifier noise generated in the two independent detection chains is uncorrelated. After further amplification, the two voltage amplitudes of the outputs are captured by a pair of vector digitizers.

The second-order correlation function [32] provides a statistical tool to characterize the field; it can be expressed as

$$g^{(2)}(\tau) = 1 + \frac{\langle \Delta P_1(t) \Delta P_2(t+\tau) \rangle}{[\langle P_1(t) \rangle - \langle P_{1,N}(t) \rangle][\langle P_2(t) \rangle - \langle P_{2,N}(t) \rangle]},$$

where τ is the delay time between the two digitizers, and P_1 and P_2 are the output powers in ports 1 and 2, respectively, see figure 8(a). $P_{1,N}$, and $P_{2,N}$ are the amplifier noise in ports 1 and 2, respectively, when the incident source is off. Therefore, $[\langle P_i(t) \rangle - \langle P_{i,N}(t) \rangle]$ represents the net power of the field from output port i, where $i = 1, 2$. $\langle \Delta P_1 \Delta P_2 \rangle$ is the covariance of the output powers in ports 1 and 2, defined as $\langle (P_1 - \langle P_1 \rangle)(P_2 - \langle P_2 \rangle) \rangle$.

We had a trigger jitter of ± 1 sample between the two digitizers. To minimize the effect of this trigger jitter, we oversample and then digitally filter (average) the data in all the $g^{(2)}$ measurements. Here, the sampling frequency is set to 10^8 samples s^{-1} with a digital filter with a bandwidth BW = 55 MHz applied to each digitizer for all measurements. For a coherent state, we find that $g^{(2)}(\tau) = 1$ with the qubit detuned from ω_{10}.

In figure 8(b), we plot the measured $g^{(2)}(\tau)$ of the reflected field from our atom. At low powers, where $\langle N_p \rangle \ll 1$, we clearly observe antibunching of the field [25]. The trace here was averaged over 2.4×10^{11} measured quadrature field samples (2 Tbyte of data), computed and averaged over 17 h. We correct the slow drifts, e.g. amplifier gain, every 5 min by switching on and off the incident source. In the future, the measurement efficiency can be significantly improved by incorporating a quantum-limited parametric amplifier [12, 13]. The antibunching behavior at $P_p = -131$ dBm ($\langle N_p \rangle \sim 0.4$), $g^{(2)}(0) = 0.55 \pm 0.04$, reveals the non-classical character of the field. Ideally, we would find that $g^{(2)}(0) = 0$ as the atom can only reflect one photon at a time. The non-zero $g^{(2)}(0)$ we measured originates from four effects: (i) a thermal field at 50 mK temperature, (ii) a finite filter BW, (iii) a trigger jitter between the two digitizers and (iv) stray fields including background reflections in the line and leakage through circulator 1 (figure 8(a)). The complete theory curves include all four non-idealities; the partial theory curves include (i) and (ii), but not (iii) and (iv). The effects of these factors on our measured antibunching are shown in the theory plot figure 8(c). For small BW, within the long sampling time, the atom is able to scatter multiple photons. If BW $\ll \Gamma_{10}, \Omega_p$, the antibunching dip we measure vanishes entirely. This interplay between BW and Ω_p yields a power-dependent $g^{(2)}(0)$,

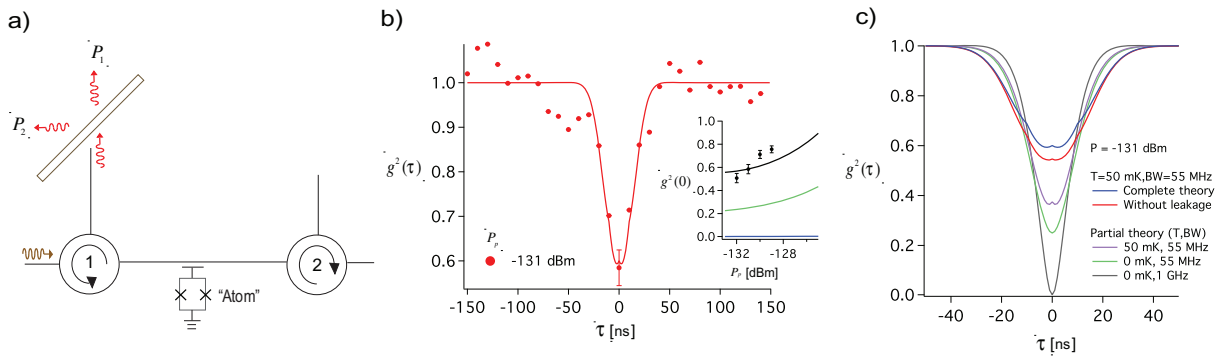

Figure 8. Second-order correlation function of reflected fields generated by the artificial atom (sample 2). (a) A schematic illustration of the physical setup, including circulators (labeled 1, 2) and the hybrid coupler which acts as a beam splitter for the Hanbury Brown–Twiss measurements [31]. Depending on the choice of the input port, we can measure $g^{(2)}$ of the reflected or the transmitted field. (b) $g^{(2)}$ of a resonant reflected field as a function of delay time. We see the antibunched behavior of the reflected field. Inset: $g^{(2)}(0)$ as a function of incident power. The black curve includes all four non-idealities (complete theory) with BW = 55 MHz and $T = 50$ mK. The green curve only includes a finite temperature and bandwidth (partial theory) with $T = 50$ mK and BW = 55 MHz. The blue curve is the expected result using the partial theory with BW = 1 GHz at 0 mK. As the BW decreases or the incident power increases, the degree of antibunching decreases. The error bar indicated for each data (markers) set is the same for all the points. (c) Influence of BW, temperature, leakage and jitter on antibunching. The solid curves in (b) and (c) are the theory curves. For the curves with leakage, we assume that the phase between the leakage field and the field reflected by the atom is 0.37π.

as shown in the inset of figure 8(b). In the ideal case, i.e. for a sufficiently wide BW (1 GHz) at 0 mK, the theory gives $g^{(2)}(0) = 0$, as expected.

In figure 9(a), we see superbunching of the photons [25] with $g^{(2)}(\tau = 0) = 2.31 \pm 0.09 > 2$ at $P_{\rm p} = -129$ dBm ($\langle N_{\rm p}\rangle \simeq 0.8$) for the transmitted field. Superbunching occurs because the one-photon state of the incident field has been selectively reflected and thus filtered out from the transmitted signal, whereas the two-photon state is more likely transmitted. The three-photon state and higher number states are negligible. The transmitted state generated from our qubit is thus bunched even more than a thermal state, which has $g^{(2)}_{\rm therm}(\tau = 0) = 2$. Figure 9(b) shows the theoretical curves of $g^{(2)}(\tau)$ for the transmitted field under the influence of various effects. For the case of BW = 1 GHz at 0 mK, indicated by the black curve, $g^{(2)}$ exhibits very strong bunching at $\tau = 0$. At a later delay $\tau \sim 15$ ns, $g^{(2)}$ for the transmitted field even appears antibunched [25]; this is, however, not resolved in the experimental data. For the other curves, we see the degrading of superbunching due to the influence of BW, temperature and jitter. In figure 9(c), we plot $g^{(2)}(0)$ as a function of incident power, and clearly see that the (super)bunching behavior decreases as the incident power increases. For high powers, where $\langle N_{\rm p}\rangle \gg 1$, we find that $g^{(2)}(\tau) = 1$. This is because most of the coherent signal then passes through the transmission line without interacting with the qubit owing to saturation of the atomic response. We also plot the theoretical curves (blue) at 0 mK for two different BW.

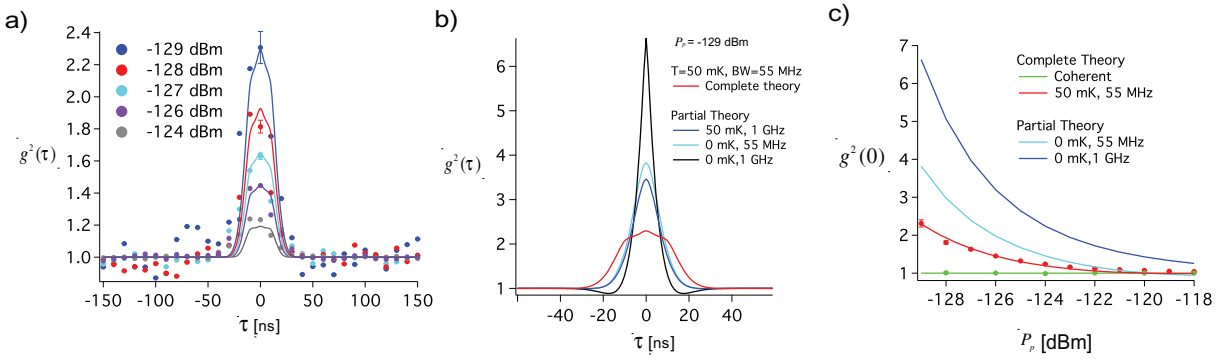

Figure 9. Second-order correlation function of the transmitted fields generated by the artificial atom (sample 2). (a) $g^{(2)}$ of the resonant transmitted microwaves as a function of delay time for five different incident powers. The peculiar feature of $g^{(2)}$ around zero in the theory curves is due to the trigger jitter model. (b) Influence of BW, temperature and jitter on superbunching. (c) $g^{(2)}(0)$ of the resonant transmitted field as a function of incident power. The result for a coherent state is also plotted. We see that the transmitted field statistics (red curve) approach those of a coherent field at high incident power, as expected. For BW = 1 GHz at 0 mK, we see very strong bunching at low incident power in the theory plot. The error bar indicated for each data (markers) set is the same for all the points. The solid curves in (a)–(c) are the theory curves. For all measurements shown here, we find that $g^{(2)}(\infty) = 1$, as expected.

A single-mode resonator is used to model the digital filter. The theoretical curves in figures 8 and 9 are based on a master equation describing both the transmon and the resonator using the formalism of cascaded quantum systems [33]. The trigger jitter is modeled by the following: the value of $g^{(2)}(\tau)$ at each point is replaced by the average value of $g^{(2)}(\tau\text{-}10\,\text{ns})$, $g^{(2)}(\tau)$ and $g^{(2)}(\tau{+}10\,\text{ns})$. We extract 50 mK from all these fits, with no additional free fitting parameters.

As we have shown, the single artificial atom acts as a photon-number filter, which selectively filters out the one-photon number state from a coherent state. This provides a novel way of generating single microwave photons [34–36].

5. Discussion

Microwave quantum optics with a single artificial atom opens up a novel way of building up a quantum network based on superconducting circuits. In such a system, superconducting processors can act as quantum nodes, which can be linked by quantum channels, to transfer flying photons (quantum information) from site to site on-chip with high fidelity. In this way, the single-photon router can switch quantum information on nanosecond timescales and with 99% efficiency, with the possibility of multiple outputs. The photon-number filter can act as the source of generation of flying microwave photons. These components have the advantage of a wide frequency range compared to cavity-based systems [35, 37, 38]. In addition, the recent development of a cross-Kerr phase shifter at the single-photon level based on superconducting circuits is also beneficial for a microwave quantum network [21].

While microwave quantum optics with artificial atoms is a promising technology for quantum information processing, optical photons have clear advantages for long-distance quantum communication via a quantum channel. The development of hybrid quantum networks would combine both advantages of these two systems. The early stages of optical–microwave interface have been demonstrated [39–41], with other potential coupling mechanisms under investigation [42–45].

6. Summary

Based on superconducting circuits, we study various fundamental quantum optical effects with a single artificial atom, for example photon scattering, Mollow triplet and Autler–Townes splitting. We further demonstrate two potential elements for an on-chip quantum network: the single-photon router and the photon-number filter.

Acknowledgments

We acknowledge financial support from the EU through the ERC and the project PROMISCE, from the Swedish Research Council and from the Wallenberg Foundation. B P acknowledges support from the CSIC grant JAE-PREDOC2009. We also acknowledge Thomas M Stace, Bixuan Fan, G J Milburn, Tim Duty and O Astafiev for fruitful discussions.

References

[1] Schoelkopf R J and Girvin S M 2008 *Nature* **451** 664
[2] Clarke J and Wilhelm F K 2008 *Nature* **453** 1031
[3] Wendin G and Shumeiko V S 2007 *Low Temp. Phys.* **33** 724
[4] Wallraff A, Schuster D I, Blais A, Frunzio L, Huang R S, Majer J, Kumar S, Girvin S M and Schoelkopf R J 2004 *Nature* **431** 162–7
[5] Schuster D I *et al* 2007 *Nature* **445** 515–8
[6] Hofheinz M *et al* 2009 *Nature* **459** 546–9
[7] Reed M D, DiCarlo L, Nigg S E, Sun L, Frunzio L, Girvin S M and Schoelkopf R J 2012 *Nature* **482** 382
[8] Fedorov A, Steffen L, Baur M, da Silva M P and Wallraff A 2012 *Nature* **481** 170–2
[9] Vijay R, Macklin C, Slichter D H, Weber S J, Murch K W, Naik R, Korotkov A N and Siddiqi I 2012 *Nature* **490** 77
[10] Mariantoni M *et al* 2011 *Science* **334** 61
[11] Wilson C M, Johansson G, Pourkabirian A, Simoen M, Johansson J R, Duty T, Nori F and Delsing P 2011 *Nature* **479** 376–9
[12] Castellanos-Beltran M A, Irwin K D, Hilton G C, Vale L R and Lehnert K W 2008 *Nature Phys.* **4** 929
[13] Bergeal N, Schackert F, Metcalfe M, Vijayand R, Manucharyan V E, Frunzio L, Prober D E, Schoelkopf R J, Girvin S M and Devoret M H 2010 *Nature* **465** 64
[14] Tey M K, Chen Z L, Aljunid S A, Chng B, Huber F, Maslennikov G and Kurtsiefer C 2008 *Nature Phys.* **4** 924–7
[15] Hwang J, Pototschnig M, Lettow R, Zumofen G, Renn A, Gotzinger S and Sandoghdar V 2009 *Nature* **460** 76–80
[16] Wrigge G, Gerhardt I, Hwang J, Zumofen G and Sandoghdar V 2008 *Nature Phys.* **4** 60–6
[17] Gerhardt I, Wrigge G, Bushev P, Zumofen G, Agio M, Pfab R and Sandoghdar V 2007 *Phys. Rev. Lett.* **98** 033601

[18] Astafiev O, Zagoskin A M, Abdumalikov A A, Pashkin Y A, Yamamoto T, Inomata K, Nakamura Y and Tsai J S 2010 *Science* **327** 840
[19] Hoi I C, Wilson C, Johansson G, Palomaki T, Peropadre B and Delsing P 2011 *Phys. Rev. Lett.* **107** 073601
[20] Hoi I C, Palomaki T, Johansson G, Lindkvist J, Delsing P and Wilson C M 2012 *Phys. Rev. Lett.* **108** 263601
[21] Hoi I C, Wilson C M, Johansson G, Palomaki T, Stace T M, Fan B and Delsing P 2012 arXiv:1207.1203v1
[22] Abdumalikov A A, Astafiev O, Zagoskin A M, Pashkin Y A, Nakamura Y and Tsai J S 2010 *Phys. Rev. Lett.* **104** 193601
[23] Astafiev O V, Abdumalikov A A, Zagoskin A M, Pashkin Y A, Nakamura Y and Tsai J S 2010 *Phys. Rev. Lett.* **104** 183603
[24] Shen J T and Fan S H 2005 *Phys. Rev. Lett.* **95** 213001
[25] Chang D E, Sorensen A S, Demler E A and Lukin M D 2007 *Nature Phys.* **3** 807–12
[26] Koch J, Yu T M, Gambetta J, Houck A A, Schuster D I, Majer J, Blais A, Devoret M H, Girvin S M and Schoelkopf R J 2007 *Phys. Rev.* A **76** 042319
[27] Zumofen G, Mojarad N M, Sandoghdar V and Agio M 2008 *Phys. Rev. Lett.* **101** 180404
[28] Mollow B R 1969 *Phys. Rev.* **188** 1969
[29] Autler S H and Townes C H 1955 *Phys. Rev.* **100** 703–22
[30] Zheng H, Gauthier D J and Baranger H U 2010 *Phys. Rev.* A **82** 063816
[31] Brown R H and Twiss R Q 1956 *Nature* **177** 27–32
[32] Loudon R 2000 *The Quantum Theory of Light* (Oxford: Oxford University Press)
[33] Peropadre B, Lindkvist J, Hoi I C, Wilson C M, Garcia-Ripoll J, Delsing P and Johansson G 2012 arXiv:1210.2264v1
[34] Mallet F, Castellanos-Beltran M A, Ku H S, Glancy S, Knill E, Irwin K D, Hilton G C, Vale L R and Lehnert K W 2011 *Phys. Rev. Lett.* **106** 220502
[35] Bozyigit D *et al* 2011 *Nature Phys.* **7** 154
[36] Wilson C M, Duty T, Sandberg M, Persson F, Shumeiko V and Delsing P 2010 *Phys. Rev. Lett.* **105** 233907
[37] Rebic S, Twamley J and Milburn G J 2009 *Phys. Rev. Lett.* **103** 150503
[38] Sandberg M, Persson F, Hoi I C, Wilson C M and Delsing P 2009 *Phys. Scr.* **T137** 014018
[39] Kubo Y *et al* 2011 *Phys. Rev. Lett.* **107** 220501
[40] Kubo Y *et al* 2010 *Phys. Rev. Lett.* **105** 140502
[41] Staudt M U *et al* 2012 *J. Phys. B: At. Mol. Opt. Phys.* **45** 124019
[42] Kielpinski D, Kafri D, Woolley M J, Milburn G J and Taylor J M 2012 *Phys. Rev. Lett.* **108** 130504
[43] Wang Y D and Clerk A A 2012 *Phys. Rev. Lett.* **108** 153603
[44] Kim Z *et al* 2011 *AIP Adv.* **1** 042107
[45] Tian L 2012 *Phys. Rev. Lett.* **108** 153604

3.3.6 Application to single-photon detection

We finish this part of the Thesis by addressing a challenging and hitherto open problem in circuit QED: the detection of *propagating single photons*. In order to efficiently carry out quantum communications, quantum cryptography or more precisely all-optical quantum information processing, we must be able to analyze the radiation field with high efficiency. While straightforward in the optical domain, the low cross-section between light and matter in the microwave regime makes of photodetection a challenging task[20]. For this reason, we point at the microwave single-photon detector as the ultimate goal in circuit QED. There are promising proposals for microwave photodetection that rely on the scattering of microwaves on absorbing elements, such as phase qubits [RGRS09a]. However, for a photodetector like this to be efficient, it becomes necessary to have many of these absorbers placed in the transmission line, which makes its physical implementation challenging. The highly desirable setup with just one absorber finds an upper threshold of 50% in the detection efficiency[21] [RGRS09b].

In publication P8 we outperform this upper limit, with a proposal of a single-shot single-photon detector that successfully achieves 100% efficiency, *using only one absorber*. Our setup consist of a single absorber placed at a distance L from the end of a semi-infinite transmission line, which acts as a highly reflecting mirror (see Fig.3.8). The absorber is a phase qubit, with two internal states $|0\rangle$ and $|1\rangle$, and a large decay rate Γ from the excited state $|1\rangle$ to a metastable state $|g\rangle$. The photodetection process would be the following: an incoming photon propagating along the transmission line can be trapped in the pseudo-cavity defined by the absorber and the mirror. The photon bounces back and forth between the qubit and the mirror, while the qubit gradually absorbs the photon, and leaves it in the metastable state $|g\rangle$, which can be eventually measured. A thorough description of this photodetector is the main topic of publication P8, whose main results can be summarized as follows:

- Working in real space, we solve the scattering problem shown in Fig.3.8: a photon coming from the left interacting with one absorber place in the line at a distance L from the mirror. To this end, we solve the system of delay differential equations, solution of the Schrödinger equation of

[20] Even though there exist photodetectors based on linear and parametric amplifiers, they still introduce too much noise to talk about single-shot single-photon detection.

[21] For a perfect detection with only one qubit, we must reconstruct the time reversed process of spontaneous emission. Given that the photon approached the qubit either from the left or the right direction, it only represents half of the process and thus half of the efficiency.

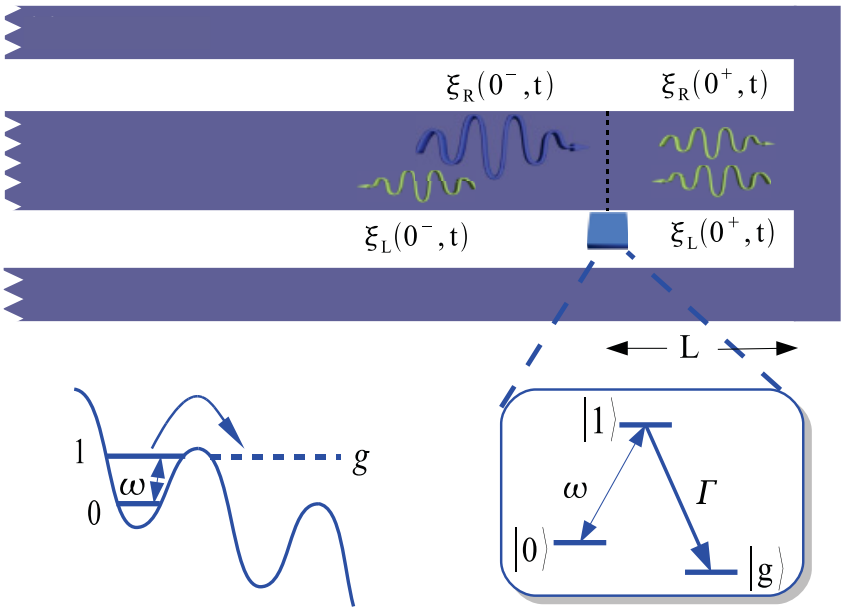

Figure 3.8: a) Schematics of the perfect microwave photodetector. The phase qubit (blue box) and the mirror defines a pseudo-cavity that traps the incoming photon. Part of the photon is reemitted by the qubit to the cavity, and part is detected through the decay channel $|1\rangle \rightarrow |g\rangle$. For sufficiently long times, all the photon is eventually detected.

the system. In particular, we focus on the limit where $L \ll \lambda$, where λ is the wavelength associated with the phase qubit energy gap.

- By controlling the various parameters of our system, such as the distance L, the coupling V to the line, and the decay rate Γ to the metastable state $|g\rangle$, we can control the reflection and transmission coefficients. In particular, we can confine the propagating photon in the pseudo-cavity defined by the qubit and the mirror (which corresponds to $r = 0$).

- We study the photon population inside the pseudo-cavity as the time passes by. In particular, we observe a complete extinction of the photon wavefunction, that results from the full absorption of the photon by the phase qubit

- We define the detection efficiency as the fraction of the wavepacket that has been absorbed. In turn, the absorption efficiency is defined as the amount of radiation that is neither reflected by the qubit, nor stored in

the pseudocavity as a quasibound state [DGI+09]. By virtue of the previous results, we conclude that a propagating photon has been perfectly detected with an efficiency of 100%, using solely a single absorber in the transmission line.

- We validate these results for different incoming wavepackets, ranging from Fock states to more realistic situations where the incoming photons possess Gaussian envelopes. For all the considered cases, we reach outstanding detection efficiencies, even for slightly detuned photons.
- For the sake of completeness, we consider the case of more than one phase qubit in the transmission line, separated by a distance d. We study its detection efficiency as a function of different fluctuating parameters, such as the distance between absorbers and the detuning between the incoming photon and the absorbers. We observe that as we put more absorbers in the line, the detection efficiency becomes robust to highly-detuned incoming photon and to imperfections in the fabrication process.
- We finally consider the case where the photon enters the cavity through the mirror. This new setup is in close resemblance to a recent photodetector proposal [CHS+11], that injects the photon through the mirror, and trap it in the qubit-mirror pseudocavity. Our theory predicts a 90% detection efficiency, with an asymptotic limit of 100% efficiency in the limit $\Gamma \to 0$. This result can be easily interpreted as follows: for a perfect detection, we need the absorber to behave as a perfect mirror, yielding the condition $\Gamma \to 0$. But at the same time, the detection time diverges as $1/\Gamma$, so this scheme would only yield to a perfect detection at infinite time.

In conclusion, in publication P8 we have exploited the 1D photon-transport properties to propose a perfect single-photon detector. The active element of the detector is a three-level system with an irreversible state that we use to perform the detection. The photodetector itself consists of a single absorber confronting the end of a semi-infinite transmission line. With this minimal model, we manage to reach a perfect 100% efficiency of a propagating photon in a single-shot, improving the fundamental limit of 50% efficiency with only one absorber: due to the presence of the mirror in our setup, we are able to reconstruct the time reversed process of spontaneous emission. Our proposal is as well robust against imperfections in the fabrication process, and non-radiative decay channels. For all these reasons, we do believe that this photodetector proposal will be part of the future circuit QED architectures for the satisfactory performance of all-optical quantum information processing.

3.3.7 Publication 8: Approaching perfect microwave photodetection in circuit QED. B. Peropadre, G. Romero, G. Johansson, C. M. Wilson, E. Solano, J. J. García-Ripoll. Phys. Rev. A 84, 063834 (2011)

PHYSICAL REVIEW A **84**, 063834 (2011)

Approaching perfect microwave photodetection in circuit QED

B. Peropadre,[1] G. Romero,[2] G. Johansson,[3] C. M. Wilson,[3] E. Solano,[2,4] and J. J. García-Ripoll[1]

[1]*Instituto de Física Fundamental, CSIC, Calle Serrano 113-bis, E-28006 Madrid, Spain*

[2]*Departamento de Química Física, Universidad del País Vasco–Euskal Herriko Unibertsitatea, Apartado 644, E-48080 Bilbao, Spain*

[3]*Department of Microtechnology and Nanoscience, Chalmers University of Technology, Göteborg, Sweden*

[4]*IKERBASQUE, Basque Foundation for Science, Alameda Urquijo 36, E-48011 Bilbao, Spain*

(Received 12 January 2011; published 14 December 2011)

In order to apply all ideas from quantum optics to the field of quantum circuits, one of the missing ingredients is a high-efficiency single-photon detector. In this work we propose a design for such a device which successfully reaches 100% efficiency with only one absorber. Our photon detector consists of a three-level system (a phase qubit) coupled to a semi-infinite one-dimensional waveguide (a microwave transmission line) which performs highly efficient photodetection in a simplified manner as compared to previous proposals. Using the tools of quantum optics we extensively study the scattering properties of realistic wave packets against this device, thereby computing the efficiency of the detector. We find that the detector has many operating modes, can detect detuned photons, is robust against design imperfections, and can be made broadband by using more than one absorbing element in the design. Many of these ideas could be translated to other single-mode photonic or plasmonic waveguides interacting with three-level atoms or quantum dots.

DOI: 10.1103/PhysRevA.84.063834 PACS number(s): 42.50.Pq, 85.25.Pb, 85.60.Gz

I. INTRODUCTION

The field of quantum circuits is an interdisciplinary one which combines ideas and tools from quantum optics with the novel possibilities brought by superconducting circuits. This field is undergoing a silent revolution, which started with the first superconducting qubits [1–4], greatly advanced in the matter-wave interaction field [5–7], and is now preparing the foundations of an entirely new technology: propagating quantum microwaves. The first ingredients in this new field are the generation of nonclassical propagating waves—either through qubits and cavities [8,9], or through nonlinearities [10]—and the analysis of those fields, currently done using quantum homodyne detection techniques [8,9,11–13]. In order to consolidate and complete the field, we still lack two other ingredients: photon-photon interactions and single-shot photon detection and counting. In particular, photodetection is the ultimate and most desired goal. It is common to quantum optics and quantum-information protocols, from trivial homodyne detection methods up to sophisticated all-optical quantum-computing protocols [14]. Developing such a tool in circuit QED would open the door to quantum communication, quantum cryptography, and general-purpose quantum-information processing with propagating photons. In short, circuit QED allows quantum opticians to explore novel physics and technologies that are not yet available for real atoms interacting with electromagnetic fields.

In previous work [15,16], we identified photodetectors as the ultimate missing tool in circuit QED, and helped in specifying the desired properties of such a device: it should be single shot, work outside the cavity [17], achieve great efficiency, be broadband, and be passive. In that same work, we proposed a rather minimal design that performed the task [15,16]: coupling phase qubits to open transmission lines. In our design the phase qubit acts as a metastable three-level system which can absorb individual photons from the one-dimensional photonic waveguide and transition into a third, easily detectable state, in a process that implements single-photon detection [Fig. 1(b)] with strict upper limit of 50%. We showed that by adding more qubits this value could be easily increased up to 100%. This also had the side effect of improving both the bandwidth and robustness of the detector.

In this work, we show that a slight modification of our design boosts its efficiency up to 100% for a single-qubit detector, without affecting the bandwidth or robustness of the original design. The small change consists of embedding the three-level system in a semi-infinite line, at some distance from the end, which behaves as a perfect mirror. Qualitatively, in this new setup the end mirror allows incoming photons to bounce back from the end of the line and have several chances to be detected just by a single qubit. Alternatively, the setup can be seen as a one-dimensional implementation of the idea in Ref. [18], by which a two-level system is made to absorb a photon whose wave function is the complex conjugate of that from a spontaneously emitted photon.

Our present work is also related to two recent developments. The first one is the implementation of a microwave photodetector using phase-biased Josephson junctions in Ref. [19]. This setup contains some ingredients that are needed for the proposals in this and previous papers [15,16], and in particular its layout closely resembles the ones put forward in this paper. The second work is devoted to the study of the quasibound states that appear when a qubit is confronted with a mirror [20]. Those resonances are to a large extent responsible for the high efficiency and long interaction times between incoming photons and our detector. This is further evidenced in our study of photodetection when the photons are directly injected between the qubit and the mirror (Sec. IV).

Finally, we want to remark that the developments in this and previous works [15,16] are very general. The formalism is based on one-dimensional waveguides and three-level systems, and it could be trivially exported to novel and fascinating experimental setups, such as single-mode fibers or photonic waveguides interacting with atoms [21], or plasmonic waves coupled to quantum dots or nitrogen-vacancy (NV) centers

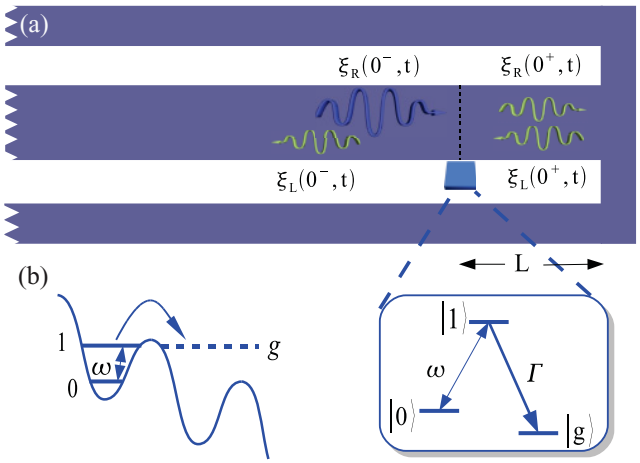

FIG. 1. (Color online) Scheme of our microwave photon detector proposal. (a) The setup consists of a metastable quantum circuit positioned at a distance L from the right mirror of a one-sided cavity, forming a pseudocavity. (b) The quantum circuit can be made from a current-biased Josephson junction, in which a washboard potential confines two metastable states that can decay into a continuum of current states.

[22,23], where the degree of controllability and interaction strength are expected to approach those of circuit QED in the near future.

This work is organized as follows. In Sec. II we study in detail a design that consists of a three-level system sitting on a semi-infinite transmission line and how it interacts with a finite-width propagating photon. We work in the strong-interaction, rotating-wave-approximation regime, in which the number of excitations is preserved, and develop an analytic approximation to the dynamics (Sec. II A), including a simple analyitical expression for long wave packets (Sec. II B). With these tools we can demonstrate that for a wide variety of parameters a single photon may be perfectly absorbed by the three-level detector, even when it is detuned (Sec. II C). In Sec. III we develop a simplified theory based on scattering of plane waves which reproduces the previous results and allows us to study setups with more than one three-level system. The main result is that an increased number of absorbers enhances the robustness, the bandwidth, and the overall performance of the detector. In Sec. IV we slightly modify our theory to study what happens when photons are not coming from the semi-infinite transmission line, but rather injected through the end of the line. We will show that efficient photodetection is still possible and is mediated by quasilocalized states between the qubit and the mirror, at the expense of longer detection times. Finally in Sec. V we summarize our results.

II. A QUBIT AND A MIRROR

In this section, we discuss the simple setup of a semi-infinite transmission line coupled to a metastable quantum circuit located at a distance L from the end of the waveguide, which acts as a mirror (see Fig. 1). Studying the problem in real space, we derive the relevant equations describing the dynamics of the system. These models are used to study the scattering of a photon wave packet, showing that, under realistic conditions, it is completely absorbed by the metastable quantum circuit which represents the detector itself. More precisely, we demonstrate that when the photon is not reflected, the fraction that bounces back and forth between the absorber and the end mirror is also absorbed and thus detected. This will be the starting point for a more general and simpler theory in the following section.

A. One absorber interacting with a single photon

As sketched before, the basis of our work, as in our previous proposal [15,16], is the real-space representation of a one-dimensional waveguide interacting with a single qubit [24]. The model consists of a non-Hermitian Hamiltonian that contains terms for the metastable quantum circuits or "absorbers," modeled as three-level systems, and the radiation fields ψ_R and ψ_L propagating to the right and to the left with group velocity v_g,

$$H = \sum_i \hbar\left(\omega_i - i\frac{\Gamma_i}{2}\right)|1\rangle_i\langle 1| + i\hbar v_g\int[\psi_L^\dagger\partial_x\psi_L - \psi_R^\dagger\partial_x\psi_R]dx + \sum_i \hbar V\int\delta(x-x_i)[(\psi_R+\psi_L)|1\rangle_i\langle 0| + \text{H.c.}]dx. \quad (1)$$

Note how the interaction between photons and circuits is modeled using a δ potential of strength V located at the positions of the latter, x_i. In this notation, $|0\rangle$ and $|1\rangle$ represent the two states of the absorber connected by the photon [see Fig. 1(b)], Γ_i stands for the decay rate from the metastable state $|1\rangle$, and ω_i is the frequency separation between $|0\rangle$ and $|1\rangle$.

The simplest scenario that we consider is a single photon interacting with one absorber placed at $x = 0$, as shown in Fig. 1(a). The photon coming from the left with energy $E = \hbar|k|v_g$ will exchange its excitation. The most general wave function that describes this process is [24]

$$|\Psi\rangle = \int[\xi_R(x)\psi_R^\dagger(x) + \xi_L(x)\psi_L^\dagger(x)]|0,\text{vac}\rangle + e(t)|1,\text{vac}\rangle. \quad (2)$$

The first part of the state constitutes the most general form in which the field contains just a single photon, moving right, $\xi_R(x)$, or left, $\xi_L(x)$, with the detector or absorber in the metastable state $|0\rangle$. As soon as this photon interacts with the three-level system, there is some probability that the field excitation gets absorbed and the three-level system jumps into the unstable level $|1\rangle$. When this happens, the excited-state population of the absorber, $e(t)$, increases. We will derive the evolution equations for general wave packets, $\xi_{R,L}(x)$, but in order to compute the absorption efficiency we need to impose constraints on the bandwidth and the shape of these photons.

We want to emphasize the possibility of having input states other than (2). Consider for instance an attenuated coherent state. This basically consists on Eq. (2) plus a dominant term $|0,\text{vac}\rangle$ and higher-order terms with two and more photons. The

higher-order terms can be neglected and thus the absorption efficiency basically coincides with the one derived using (2). Another possibility would be an incoherent mixture of different single-photon wave packets $\rho = \int p[\xi]|\psi_\xi\rangle\langle\psi_\xi|\mathcal{D}\xi$, with some distribution over wave-packet shapes and properties, $p[\xi]$. One example of this is a statistical mixture of single photons whose emission time and phase cannot be precisely determined, as would be the case of photons emitted by a driven qubit [8] or scattered by a two-level system [25]. In this simple case the total efficiency will be the average over the possible input states. However, given that the same source will produce identical photons through time, and that our single-photon detector will be insensitive to the arrival time and to the phase (Sec. II B), we will find that it is enough to work with the ansatz (2).

Solving the Schrödinger equation with the non-Hermitian Hamiltonian (1) leads to a set of equations containing the field and absorber amplitudes:

$$\begin{aligned} i\partial_t \xi_R(x,t) &= -iv\partial_x \xi_R(x,t) + V\delta(x)e, \\ i\partial_t \xi_L(x,t) &= +iv\partial_x \xi_L(x,t) + V\delta(x)e, \\ \left(i\partial_t - \omega + i\frac{\Gamma}{2}\right)e &= \frac{V}{2}[\xi_R^+ + \xi_R^- + \xi_L^+ + \xi_L^-], \end{aligned} \tag{3}$$

where we abbreviate $\xi_{R,L}^{\pm}(t) := \xi_{R,L}(0^{\pm},t)$. As explained elsewhere [16], our quantum jump description allows us to compute the population of the level $|g\rangle$ as $P_g = 1 - ||\Psi||^2$. Indeed, the value of P_g at long times is what we call the detector efficiency and can be fully determined from the previous equations, after a few manipulations.

Note that two equations in (3) can be turned into boundary conditions around the absorber

$$\xi_R^+ = \xi_R^- - i\frac{V}{v_g}e, \quad \xi_L^- = \xi_L^+ - i\frac{V}{v_g}e. \tag{4}$$

This allows us to express the amplitude of the unstable state $|1\rangle$ in terms of the left and right incoming fields, that is,

$$\left[i\partial_t - \omega + i\frac{\Gamma}{2} + i\frac{V^2}{v_g}\right]e = V[\xi_R^- + \xi_L^+]. \tag{5}$$

The above procedure is standard in any single-photon scattering problem, but in this case the mirror to the right end imposes another key boundary condition, which is a coupling between right- and left-propagating fields. More precisely, the only independent variable will be the field coming from the left, $\xi_R(0^-,t) = \phi(t)$, since the incoming field from the right, $\xi_L(0^+,t)$, is generated by the former, after being reflected by the mirror and affected by a phase factor κ. In other words,

$$\xi_L^+(t) = \kappa\xi_R^+(t-a) = \kappa\phi(t-a) - \kappa i\frac{V}{v_g}e(t-a), \tag{6}$$

with $a = 2L/v_g$ depending on the distance between the absorber and the mirror and the group velocity of the photons. This boundary condition provides us with a closed delay differential equation (DDE) for the amplitude of state $|1\rangle$,

$$\begin{aligned} i\partial_t e(t) = &\left[\omega - i\frac{\Gamma}{2} - i\frac{V^2}{v_g}\right]e(t) - \kappa i\frac{V^2}{v_g}e(t-a) \\ &+ V\phi(t) + \kappa V\phi(t-a), \end{aligned} \tag{7}$$

thereby specifying the complete dynamics of the system for any incoming signal.

B. Adiabatic limit

DDEs are very complicated mathematical objects which rarely have analytic solutions and which typically lead to nonlinear phenomena. In order to simplify the treatment, avoid critical behavior, and get some understanding of the detection of realistic wave packets, we will make some additional simplifications. More precisely, we will assume an incoming wave packet with frequency ω_0 and phase η and adiabatically modulate

$$\phi(t) = \chi(t)\exp(-i\omega_0 t + i\eta), \quad |\partial_t\chi| \ll \omega_0. \tag{8}$$

This ansatz has various consquences for the dynamics. First of all, the absorber itself will evolve according to the main frequency, $e(t) = v_g x(t)\exp(-i\omega_0 t + i\eta)/V$. Second, introducing the constants $\theta = \omega_0 a$ and $a = v_g\Delta/V^2$ and making the change of variables $t = v\tau/V^2$, we will obtain a simplified equation

$$\begin{aligned} i\partial_\tau x(\tau) = &-i(1+\gamma)x(\tau) - izx(\tau-\Delta) \\ &+ \chi(\tau) + z\chi(\tau-\Delta), \end{aligned} \tag{9}$$

with only two free parameters

$$\gamma = \frac{v_g}{V^2}\left[\frac{\Gamma}{2} + i(\omega-\omega_0)\right], \quad z = \kappa e^{i\theta}. \tag{10}$$

Finally, using the *adiabatic approximation*, that is, the smoothness of the envelope, $|\partial_\tau\chi| \ll \omega_0$, we may replace $\chi(\tau-\Delta)$ by $\chi(\tau)$, and integrate the resulting equation

$$x(\tau) = -i(1+z)\int_{-\infty}^{\tau} e^{-(1+\gamma+z)(\tau-s)}\chi(s)ds. \tag{11}$$

The whole problem has simplified considerably, and in particular the dependency on the global phase η has disappeared completely.

C. Test wave packets

Starting from expression (11) we would like to compute the efficiency of the detector. The integral in that equation is roughly a Fourier transform of the adiabatic modulation, and we expect that the the left-hand-side term, in the limit $t \to \infty$, does not depend much on the fine details of the driving field. One may now study, for instance, a normalized Gaussian wave packet

$$\chi(\tau) = \frac{1}{\sqrt{\sigma\sqrt{\pi}}}\exp[-\tau^2/(2\sigma^2)], \tag{12}$$

and how it is scattered by the three-level system. The Gaussian form is chosen for convenience, but it is in no way essential for the results. This Gaussian has the advantage that in the limit $\sigma \to \infty$ it contains the case of infinite plane waves, a limit which we used in previous works and which we would like to recover. However, as long as the wave packet remains adiabatic, that is, $\sigma \gg \omega_0^{-1}$, none of the results will depend dramatically on its precise shape, as we confirmed numerically.

We are now in a position to compute the transmitted and reflected wave packets $\xi_R^+(t), \xi_L^-(t)$, the dynamics of the

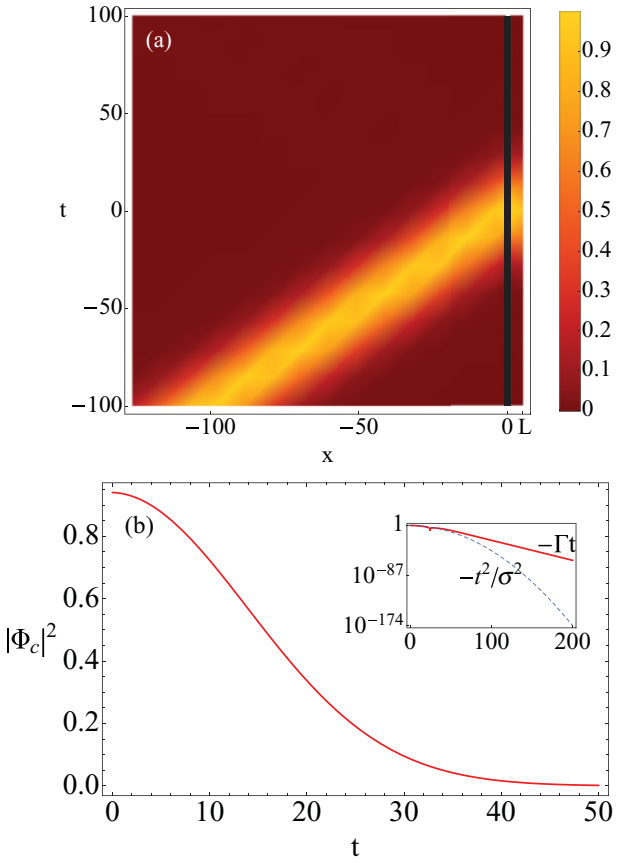

FIG. 2. (Color online) (a) Time evolution of an incident wave packet that undergoes no reflection, leading to a confined field to the right of the absorber. (b) Decay of the field inside the absorber-mirror cavity. The inset shows a logarithmic plot of the field amplitude, exhibiting a time scale with decay.

detector $x(t)$, and even the detection probability mentioned before, all as a function of the parameters σ, γ, and z. The first result that we show in Fig. 2(a) is that there indeed exist configurations for which no incoming photon is reflected. In such setups the photon tunnels through the qubit and bounces back and forth between the qubit and the mirror. If this process continued indefinitely, our system could not perform as a photodetector, as it would never capture the photon and switch. In order for the photodetection to succeed, the three-level system must be able to absorb the confined field completely and undergo an irreversible transition to the "click" state $|g\rangle$. Fortunately, as Fig. 2(b) shows, the population of the field inside the qubit-mirror pseudocavity dissipates very quickly, and in a time scale determined by the decay channel of the absorber, Γ^{-1}, the absorber fully detects the confined photon.

The above results give us a hint that a single absorber with a mirror could reach 100% detection efficiency, but this result must be confirmed for a larger variety of experimental parameters. In order to make the study more systematic, we introduce the detector efficiency as the fraction of the wave packet that was absorbed, given by

$$\alpha = 1 - \frac{\int_{-\infty}^{\infty} |\xi_L(0^-,t)|^2}{\int_{-\infty}^{\infty} |\xi_R(0^-,t)|^2}. \tag{13}$$

This value is computed numerically for different photon profiles σ and varying setup parameters ω, ω_0, θ, and Γ. With respect to the pulse width, we have found that any value of $\sigma > 10$ gives approximately the same result. For the other parameters we have to distinguish the resonant and nonresonant cases, and in the latter study the dependence of the efficiency on the detuning, $\delta = \omega - \omega_0$. As shown in Fig. 3(a), for a resonant incident photon the efficiency reaches a maximum of 100% around $\theta = \pi$ and $\Gamma = 2$ [Fig. 3(a)], where Γ is in units of V^2/v_g. When the photon is off resonant, $\delta \neq 0$, we obtain two remarkable results. First of all, theoretical perfect detection is still possible, and second, this happens for two different sets of parameters, as shown in Fig. 3(b). The relative position of the two maxima depends on the coupling strength V. These solutions approach each other [Fig. 3(c)] until the detuning reaches a threshold $\delta \leqslant V^2/v_g$, where the two solutions merge and disappear. Using parameters in the range used in Ref. [15], this sets the limit of the bandwidth around $\delta \sim 10$–100 MHz for just a single detector, but it increases for larger couplings.

III. SCATTERING THEORY

In the previous section we demonstrated two important results. The first one is that the scattering of a realistic wave packet through a single three-level system indicates the existence of a regime of theoretically perfect photodetection. The second one is that we can analytically compute all scattering properties for a sufficiently large wave packet and that these values are almost insensitive to the wave-packet size. This result motivates us to replace the previous formalism with a simpler one, based on the scattering of plane waves through one or multiple three-level systems. This method, developed in Ref. [24] and applied in our photodetector works [15,16], has the advantage that it scales well to setups with multiple detectors, an ingredient which is crucial for enhancing the robustness and the bandwidth of the detector.

Consider an incident monochromatic beam interacting with more qubits, using the scattering theory developed in Refs. [15, 16,24]. The idea is that the fields on the left and on the right of the absorbers are related by a scattering matrix

$$\begin{pmatrix} \xi_R' \\ \xi_L' \end{pmatrix} = T \begin{pmatrix} \xi_R \\ \xi_L \end{pmatrix}, \tag{14}$$

where T stands for the transfer matrix and takes the form

$$T = \prod_j^N e^{i\frac{2\pi L_j}{\lambda}\sigma_z} T_j, \quad T_j = \begin{pmatrix} 1-1/\gamma & -1/\gamma \\ 1/\gamma & 1+1/\gamma \end{pmatrix}. \tag{15}$$

Compared to Ref. [15], the main difference now is that after leaving the scatterers and confronting the mirror, the field has to satisfy a boundary condition

$$\begin{pmatrix} 1 \\ \kappa \end{pmatrix} = \exp(i\theta\sigma^z) T \begin{pmatrix} \xi_R \\ \xi_L \end{pmatrix}. \tag{16}$$

The parameter θ is the phase acquired by the photon between the last scatterer and the mirror, while κ is the boundary condition for the mirror to have zero field, typically -1. The previous equations hide a relation between the incoming

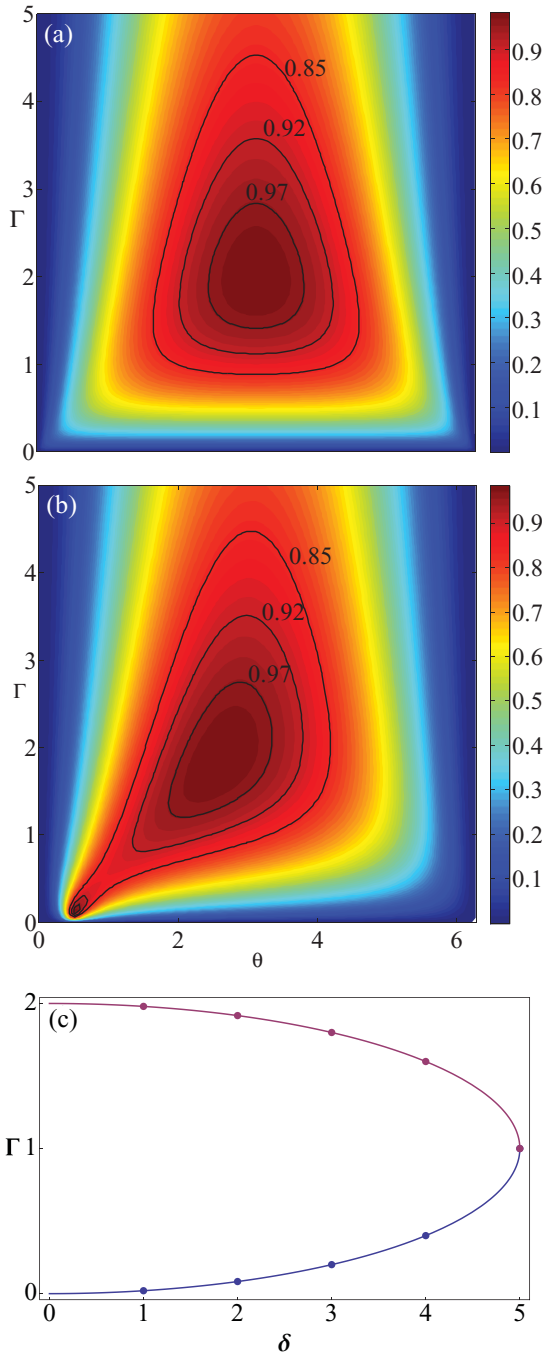

FIG. 3. (Color online) (a) Detection efficiency as a function of the decay γ and the phase θ when the three-level system is on resonance with the incident photon. (b) Real part of the detection efficiency for the off-resonance case. (c) Position of the efficiency maxima as a function of the detuning (off-resonance case).

field ξ_R^- and the reflected one ξ_L^-, which can be revealed by projecting onto an orthogonal subspace

$$\left(\kappa\ -1\right)\exp(i\theta\sigma^z)T\begin{pmatrix}\xi_R\\ \xi_L\end{pmatrix}=0. \tag{17}$$

In the case of a single absorber ($N=1$), we directly obtain an analytic expression for the outgoing field,

$$\xi_L=\left[\frac{\gamma(z+1)}{1+\gamma+z}-1\right]\xi_R, \tag{18}$$

which becomes exactly zero for

$$\gamma=1+z^{-1}, \tag{19}$$

reflecting the limit in which no photon is reflected and all photons are absorbed, in perfect agreement with the exact results for Gaussian wave packets developed in the previous section.

Using this formalism, we can go beyond one absorber, studying the optical properties of a setup with multiple three-level systems in front of a mirror. Inspired by our previous works we expect that a setup with multiple scatterers will help, first, by increasing the robustness of the detector and, second, by enlarging the band of frequencies for which almost perfect detection takes place. Furthermore, as shown in those works, the way in which we place the absorbers is very relevant, as placing them too close together does not have any influence in the detector efficiency or bandwidth. For simplicity, we will adopt the optimal configuration from the open line, with equally spaced absorbers. From the elements of the transfer matrix given by Eq. (15), we can compute the absorption efficiency (13) using the formula

$$\alpha=1-\left|\frac{T_{11}+e^{i\theta}T_{12}}{T_{21}+e^{i\theta}T_{22}}\right|^2, \tag{20}$$

where now T_{ij} depends on the number of absorbers, N, and the previous two parameters Γ and θ.

As an illustration, in Fig. 4 we show three plots that demonstrate the enhanced bandwidth and decreased sensitivity to the qubit and setup properties Γ and θ. To start with, let us look at Fig. 4(a), which plots the detector efficiency for $N=4$ absorbers. Compared with Fig. 3(a), the maximum efficiency is extended to a larger region of mirror separations, now centered around $\pi/2,3\pi/2$, and tolerates also a larger set of decay rates Γ. This is further confirmed when we study the evolution of the efficiency for increasing number of absorbers. For instance, Fig. 4(b) represents the efficiency as a function of the phase $\theta=4\pi L/\lambda$, where L stands for the distance between absorbers. Notice that, for $N=8$ absorbers, the efficiency reaches more than 90% almost independently of θ, the relative position between absorbers becoming less important. A similar effect happens with the detuning, and as Fig. 4(c) shows, the set of multiple detectors very quickly acquires a large bandwidth, even faster than in our previous works [15,16].

IV. DETECTING THROUGH THE MIRROR

On looking at our setup a natural question arises: what happens if the photon is not coming from the semi-infinite transmission line, but instead it "tunnels" through the mirror, which is not perfect? This is an interesting question for a number of reasons. The first one is that if the photon is directly injected between the mirror and the cavity it has a great chance to probe quasibound states existing between both, providing further evidence that the qubit and the mirror form

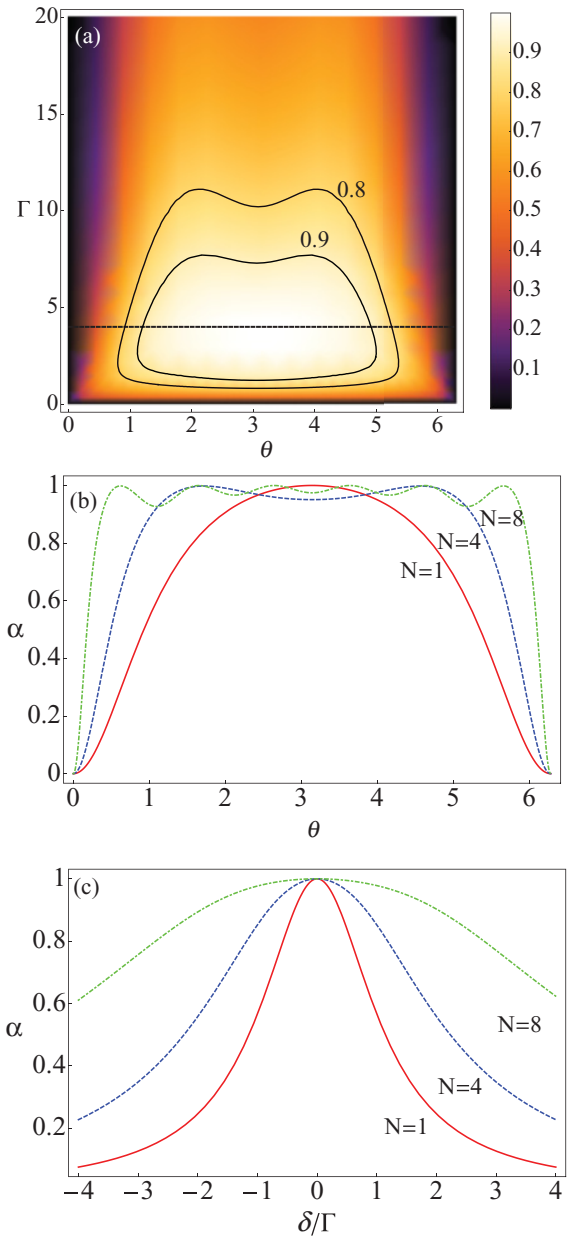

FIG. 4. (Color online) (a) Absorption efficiency for four qubits as a function of the decay and phase θ. (b) Performing a cut along the optimal value of Γ (dashed line), we compute the efficiency as a function of θ for $N = 1, 4$, and 8 absorbers. (c) Efficiency dependence on the detuning rate

a pseudocavity [20]. The second reason is that this setup is close to the recent experiment [19] which demonstrates the photodetection capabilities of a phase-biased junction.

Describing a semi-infinite line with an imperfect mirror would severely depart from the methods introduced in this paper, requiring the introduction of environments, decoherence, and master equations. Fortunately, there is a simple "toy" model that contains the essential ingredients of the problem and which can still be treated with the scattering formalism. In our model the photon is directly tunneling between the qubit and the mirror, as shown in Fig. 5(a), and the only way it

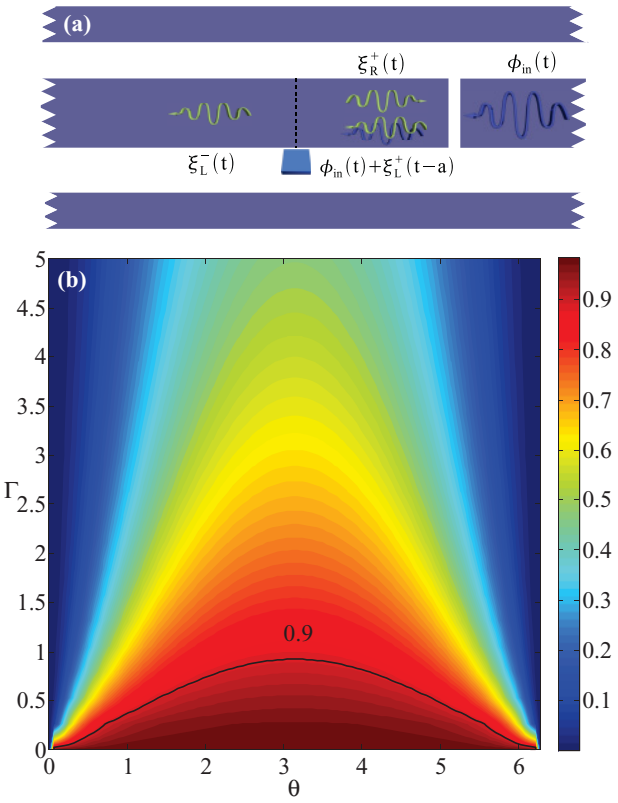

FIG. 5. (Color online) (a) Photodetector scheme for an incident photon coming from the right. (b) Detection efficiency associated with this detector.

may leak is by passing through the qubit again. The incoming photon profile will be denoted by $\phi_{in}(t)$, and we expect that the wave packet is partially trapped into the pseudocavity formed by the mirror and the absorber and is partially transmitted. Working with our previous single-photon formalism we obtain the following set of equations for the field amplitudes:

$$\xi_R^-(t) = 0, \quad \xi_R^+(t) = \xi_R^-(t) - i\frac{V}{v_g}e(t),$$
$$\xi_L^-(t) = \xi_L^+(t) - i\frac{V}{v_g}e(t), \quad \xi_L^+(t) = \phi_{in}(t) + \kappa\xi_R^+(t-a), \tag{21}$$

where the presence of the time-delayed amplitude field ξ_R^+ is due to the iterative feedback with the mirror. Using the same tools, we can now compute the detection efficiency associated with the switching process of the three level system. As shown in Fig. 5(b), the contour plots of the efficiency suffer a radical change. While the maxima are still at a resonant distance between mirror and qubit, the 100% detection efficiency is strictly achieved for $\Gamma \to 0$.

The previous analytical results have a very clear interpretation. In order to have a large detection efficiency, the photon has to spend a long time bouncing between the mirror and the qubit. However, as shown previously [24], the qubit acts as a perfect mirror only strictly for $\Gamma = 0$. The consequence is that in this setup the decay time of the three-level system, Γ, must

approach zero to increase the efficiency, and at the same time the detection time diverges as $1/\Gamma$. In other words, while this setup seems quantitatively similar to the previous ones, it does not work in practice, because, first, the tunneling probability of the photon through the mirror will be small and, second, the detection times are so long that the process will be damaged by decoherence and losses.

V. SUMMARY AND CONCLUSIONS

The main result of this work is that a three-level system, implemented as a phase qubit, a biased Josephson junction, or whatever seems adequate, is an almost perfect photodetector. The efficiency of this device is limited only by how it couples to the waves that contain the photons it has to detect. In particular, it seems that the setup we originally proposed [15,16] can be improved by replacing a completely open transmission line with a semi-infinite line that brings the photons to the detector, allowing repeated interactions. We have studied this absorber-mirror system in detail. Instead of a simple scattering model [15,16], we now have a delay differential equation that allows for nonlinear behavior and in particular for a constructive interference effect. We have demonstrated that, thanks to this effect, when an incoming photon passes through the only qubit without reflection it is actually absorbed. This first result is quite important, because it rules out that the photon gets trapped in a metastable confined state between the absorber and the mirror [19], and because it allows us to develop a much simplified theory based on the scattering of plane waves. With this theory we confirmed the 100% efficiency of a single absorber, and extended our design to include multiple qubits in front of a mirror, a setup that shows enhanced bandwidth and very much decreased sensitivity to the detector properties.

The insensitivity of the detector to the phase and its large bandwidth can be used to prove numerically, as in Ref. [16], its robustness against imperfections in the qubit specifications and dephasing, which are the most important sources of decoherence. Furthermore, since we use the same ingredients as in our previous proposal, all other considerations about robustness still apply. For instance, spontaneous decay from the 1 to the 0 level is also not a problem, because this mainly happens through radiative decay in which the qubit switches its state and deposits a photon on the line. But, as we have seen above, this decay process is contemplated in the theory through the coupling "V": in other words, spontaneous emission is part of what makes the detector work. We can also neglect photon losses, nonradiative qubit decay, and leaky mirrors, because they operate on time scales which are much longer than the photon wave packet. Finally, the greatest technical difficulty of the setup is the control of the three-level system, to avoid dark counts, that is, spontaneous transitions of the phase qubit from the 0 state to the "g" states. This can be dealt with by controlling the ratio between decay rates of the 0 and the 1 levels to the continuum. As is currently done with phase qubits, by tuning the bias it is possible make the jump probability of $0 \rightarrow g$ a thousand times smaller than Γ, which is typically longer than the photon wave packets considered here. Another possibility is to periodically refresh the detector, resetting it to the 0 state, similar to the periodic refreshing that happens with some photodetectors in the optical regime.

Overall, a small change in the photodetector design has been shown to provide an enormous increase in detection efficiency, revealed a different dynamics with a great potential for further development, while making the setup simpler and much more attractive for actual implementation. We strongly believe that this setup is now suitable for integration in ongoing circuit QED experiments with two-level systems and single photons [8,9,25–27]. In this case one might need to use circulators to prevent reflection from the detector and mutual interactions spoiling the emitter signal. A realistic example is found in Ref. [25], where the photons scattered by a two-level system are shown to have widths of about 1 ns (a few centimeters) and can be efficiently routed by circulators on the same chip.

Finally, we expect that many of the ideas in this work can be translated to other physical systems that combine fiber, photonic, or plasmonic waveguides with atoms, quantum dots or NV centers [21–23], once the current degree of controllability and interaction strength of circuit QED is achieved.

ACKNOWLEDGMENTS

We thank Anders Sørensen for pointing out the relation between our work and Refs. [18,28], and the discussions that sparked this research. B.P. thanks Jordi Mur-Petit for useful discussions. This work was supported by Spanish MICINN Project No. FIS2009-10061, and CAM research consortium QUITEMAD Project No. S2009-ESP-1594. B.P. acknowledges funding by a CSIC JAE-PREDOC2009 Grant. G.R. acknowledges funding from the Juan de la Cierva program. G.J. and C.M.W. thank the Swedish Research Council (VR) and European Research Council for funding. E.S. acknowledges funding from Basque Government Grant No. IT472-10, Spanish MICINN Project No. FIS2009-12773-C02-01, the SOLID European project, and the EU CCQED project.

[1] Y. Nakamura, C. D. Chen, and J. S. Tsai, Phys. Rev. Lett. **79**, 2328 (1997).

[2] V. Bouchiat, D. Vion, P. Joyez, D. Esteve, and M. H. Devoret, Phys. Scr., T **76**, 165 (1998).

[3] J. E. Mooij, T. P. Orlando, L. Levitov, L. Tian, C. H. van der Wal, and S. Lloyd, Science **285**, 1036 (1999).

[4] J. M. Martinis, S. Nam, J. Aumentado, and C. Urbina, Phys. Rev. Lett. **89**, 117901 (2002).

[5] A. Blais, R.-S. Huang, A. Wallraff, S. M. Girvin, and R. J. Schoelkopf, Phys. Rev. A **69**, 062320 (2004).

[6] A. Wallraff, D. Schuster, A. Blais, L. Frunzio, R.-S. Huang, J. Majer, S. Kumar, S. M. Girvin, and R. J. Schoelkopf, Nature (London) **431**, 162 (2004).

[7] I. Chiorescu, P. Bertet, K. Semba, Y. Nakamura, C. J. P. M. Harmans, and J. E. Mooij, Nature (London) **431**, 159 (2004).
[8] D. Bozyigit *et al.*, Nat. Phys. **7**, 154 (2011).
[9] C. Eichler, D. Bozyigit, C. Lang, L. Steffen, J. Fink, and A. Wallraff, Phys. Rev. Lett. **106**, 220503 (2011).
[10] F. Mallet, M. A. Castellanos-Beltran, H. S. Ku, S. Glancy, E. Knill, K. D. Irwin, G. C. Hilton, L. R. Vale, and K. W. Lehnert, Phys. Rev. Lett. **106**, 220502 (2011).
[11] M. Mariantoni, M. J. Storcz, F. K. Wilhelm, W. D. Oliver, A. Emmert, A. Marx, R. Gross, H. Christ, and E. Solano, e-print arXiv:cond-mat/0509737.
[12] M. Mariantoni, E. P. Menzel, F. Deppe, M. A. Araque Caballero, A. Baust, T. Niemczyk, E. Hoffmann, E. Solano, A. Marx, and R. Gross, Phys. Rev. Lett. **105**, 133601 (2010).
[13] E. P. Menzel, F. Deppe, M. Mariantoni, M. A. Araque Caballero, A. Baust, T. Niemczyk, E. Hoffmann, A. Marx, E. Solano, and R. Gross, Phys. Rev. Lett. **105**, 100401 (2010).
[14] E. Knill, R. Laflamme, and G. J. Milburn, Nature (London) **409**, 46 (2001).
[15] G. Romero, J. J. García-Ripoll, and E. Solano, Phys. Rev. Lett. **102**, 173602 (2009).
[16] G. Romero, J. J. García-Ripoll, and E. Solano, Phys. Scr. **2009**, 014004 (2009).
[17] F. Helmer, M. Mariantoni, E. Solano, and F. Marquardt, Phys. Rev. A **79**, 052115 (2009).
[18] D. Pinotsi and A. Imamoglu, Phys. Rev. Lett. **100**, 093603 (2008).
[19] Y. Chen, D. Hover, S. Sendelbach, L. Maurer, S. T. Merkel, E. J. Pritchett, F. K. Wilhelm, and R. McDermott, Phys. Rev. Lett. **107**, 217401 (2011).
[20] H. Dong, Z. R. Gong, H. Ian, L. Zhou, and C. P. Sun, Phys. Rev. A **79**, 063847 (2009).
[21] E. Vetsch, D. Reitz, G. Sagué, R. Schmidt, S. T. Dawkins, and A. Rauschenbeutel, Phys. Rev. Lett. **104**, 203603 (2010).
[22] D. E. Chang, A. S. Sørensen, P. R. Hemmer, and M. D. Lukin, Phys. Rev. Lett. **97**, 053002 (2006).
[23] A. V. Akimov, A. Mukherjee, C. L. Yu, D. E. Chang, A. S. Zibrov, P. R. Hemmer, H. Park, and M. D. Lukin, Nature (London) **450**, 402 (2007).
[24] J.-T. Shen and S. Fan, Phys. Rev. Lett. **95**, 213001 (2005).
[25] I.-C. Hoi, C. M. Wilson, G. Johansson, T. Palomaki, B. Peropadre, and P. Delsing, Phys. Rev. Lett. **107**, 073601 (2011).
[26] O. Astafiev, A. M. Zagoskin, A. A. Abdumalikov, Y. A. Pashkin, T. Yamamoto, K. Inomata, Y. Nakamura, and J. S. Tsai, Science **327**, 840 (2010).
[27] A. A. Abdumalikov, O. V. Astafiev, Y. A. Pashkin, Y. Nakamura, and J. S. Tsai, Phys. Rev. Lett. **107**, 043604 (2011).
[28] D. Witthaut and A. S. Sørensen, New J. Phys. **12**, 043052 (2010).

4
Conclusions

Throughout this thesis we have thoroughly studied the control of superconducting quantum circuits, within the framework of circuit QED. Superconducting circuits are mesoscopic solid-state devices that are cooled down to cryogenic temperatures, and which behave quantum mechanically. More precisely, this quantum behavior is manifested in the form of microwave photons and localized quantum systems of a few energy levels such as qubits and qutrits. We have studied the interaction between these quantum systems, and how the control of their interactions yields different applications of great interest in the fields of quantum optics, quantum simulation and quantum computing, and even in relativistic quantum information.

In the first part of the Thesis we have focused on the control of ultrastrong interactions between superconducting circuits, by means of coupling devices such as rf- and dc-SQUID's. Firstly, we have proposed several designs that allows for a tunable interaction between light-matter in the ultrastrong regime, either in a resonator or in an open transmission line. With our proposals, it becomes possible not only to connect/disconnect the coupling in extremely fast times, but also to arbitrary rotate the interaction basis. This ranges from transversal and longitudinal linear interactions, to arbitrary non-linear couplings between light an matter. For the proposed devices, we have listed a number of amazing applications. To name a few, we stress the development of ultrafast two-qubit gates for quantum computing, the qubit isolation from the environment, which both protects the qubit from decoherence and improves its measurement, and the simulation of nonlinear media via Kerr interactions. Of particular importance has been its application to the field of relativistic quantum information: based on a switchable light-matter interaction, we put forward a protocol for extracting past-future quantum correlations from the vacuum field to a pair of superconducting qubits. Moreover, we show how to

perform quantum teleportation in time with our proposal, and how this can be seen as an exotic quantum memory that stores a quantum bit of information in the vacuum.

Aside from the tunability of the light-matter interaction, we focus our attention in the ultrastrong interaction in arrays of superconducting resonators. Using SQUID's as superconducting couplers, we demonstrate a full control of the resonator-resonator coupling. In particular, we show how to fully switch off the geometric coupling ubiquitous in any circuit QED layout, just applying a constant magnetic field through the SQUID. We also demonstrate the possibility of engineering multiphoton interactions via sidebands generation, by judiciously varying the aforementioned magnetic field. Our designs would find application along the following fields: i)quantum optics with the development of tunable beam splitters and squeezed states, ii) condensed matter for testing quantum phase transitions and critical phases, and entanglement dynamics in many-body systems, iii) quantum simulations, with the development of Bose-Hubbard and spin models, and the simulation of gauge potentials. Our theoretical results have inspired several experiments implementing resonator-resonator interactions. In particular, in this Thesis we present the development of an ultrafast beam splitter that can swap photons between the resonators in a few nanoseconds.

The second part of this Thesis is devoted to the study and control of propagating microwave photons through their scattering on superconducting qubits. We theoretically analyze the coherent interaction between a propagating field and a transmon qubit from a microscopic viewpoint, observing that the scattering problem is fully determined by the reflection and transmission coefficients of the outgoing field. For the transmon in the two-level approximation we observe perfect reflection of the incoming field, whereas in the three-level approach we observe perfect transmission assisted by EIT. This versatility of photon transport properties suggests that we can fully control the incoming propagating photons. Along those lines, in this Thesis we propose a practical application for this scattering with the transmon qubit: a single photon router that can distribute photons to two output ports of a transmission line, with high speed and efficiency. We also show that our proposal can be scaled up by adding more transmon qubits, resulting in a multiport router that could distribute photons to arbitrary ports of a quantum network. We have also analyzed both theoretical and experimentally very well-known quantum optics phenomena that can also be observed through the scattering with the transmon: the observation of the transmon anharmonicity, the Autler-Townes splitting, the Mollow-Triplet and the EIT are the most significative results.

We conclude the second part of the Thesis with the proposal of a perfect single-photon detector, which is widely considered as the ultimate missing tool in circuit QED. Our proposal relies on the scattering of propagating photons on a single phase qubit facing a single-end open transmission line. By properly choosing the various system parameters, such as the qubit-mirror distance, and the decay rate to the irreversible state, we can confine the incoming photon in the pseudocavity defined by the qubit and the mirror. The resulting quasibound state bounces back and forth inside the cavity, and meanwhile it is gradually absorbed by the qubit. The photon is eventually detected with a theoretical 100% efficiency in a finite time. The proposed model is robust to detuned incoming photons and small fluctuations in the system parameters.

This Thesis provides a countless number of designs that allows for a full control of interactions in the framework of circuit quantum electrodynamics, particularly in the rather unexplored ultrastrong regime. Our designs would allow for fascinating applications in a wide range of disciplines of physics, which we do believe will pave the way for the forthcoming quantum technologies.

Appendix A: Fluxoid Quantization

In this section we derive the fluxoid quantization condition that we have used throughout this Thesis. Let us consider a superconducting loop, either interrupted or not by Josephson junctions. The macroscopic wavefunction that describes the whole ensemble of Cooper pairs in the superconductor reads

$$\Psi(r) = \sqrt{n(r,t)}e^{-i\theta(r,t)}. \tag{4.1}$$

The probability density $\rho = |\Psi(r,t)|^2 = \Psi^*(r,t)\Psi(r,t)$ satisfies the continuity equation

$$\frac{\partial \rho}{\partial t} = \Psi^* \frac{\partial \Psi}{\partial t} + \Psi \frac{\partial \Psi^*}{\partial t}. \tag{4.2}$$

Using the Schrödinger equation $i\hbar\partial_t\Psi = H\Psi$ we can rewrite the above equation as:

$$\frac{\partial \rho}{\partial t} = \frac{i}{\hbar}(\Psi^* H\Psi - \Psi^* H\Psi). \tag{4.3}$$

In particular, for a superconductor in the presence of an electromagnetic field, the above Hamiltonian takes the form:

$$H = \frac{1}{2m}(-i\hbar\nabla - 2eA(r,t))^2 + 2e\phi(r,t). \tag{4.4}$$

Substituting (4.4) into (4.3), and using the expression for the wavefunction $\Psi(r,t)$, we finally obtain the continuity equation expressed in terms of the supercurrent:

$$\frac{\partial \rho}{\partial t} = \nabla \cdot J, \tag{4.5}$$

where the supercurrent J is defined as:

$$J = 2en(r,t) \cdot \mathrm{Im}\left(i\frac{\hbar}{2m}\nabla\theta(r,t) - i\frac{e}{m}A(r,t)\right). \tag{4.6}$$

Let $n(r,t) = n$ be a constant. This is well justified since the density of Cooper pairs is homogeneous in the superconducting phase. Under this condition, the equation for the supercurrent can be written as:

$$\Lambda J = \frac{\hbar}{2e}\nabla\theta(r,t) - A(r,t), \tag{4.7}$$

where $\Lambda = m/(2e^2 n)$ is the London parameter.

In order to obtain the flux quantization condition, we take the line integral of the supercurrent around a closed contour well inside the superconductor. In doing so, eq. () becomes:

$$\oint_C \Lambda J \cdot \mathrm{d}r + \frac{\hbar}{2e}\oint_C A \cdot \mathrm{d}r = \oint_C \nabla\theta \cdot \mathrm{d}r, \tag{4.8}$$

where the left-hand side of (4.8) is called the fluxoid of the superconductor.

Let us firstly describe a superconducting loop with zero junctions. We compute each term of (4.8) separately, obtaining:

1. The first term
$$\oint \Lambda J \cdot \mathrm{d}r = 0 \tag{4.9}$$
since there circulating current inside the superconductor is $J = 0$[1].

2. The second term
$$\oint A \cdot \mathrm{d}r = \iint (\nabla \times A) \cdot \mathrm{d}S = \iint B \cdot \mathrm{d}S = \Phi_{\mathrm{ext}} + \Phi_{\mathrm{L}}, \tag{4.10}$$
where, Φ_{ext} is the external magnetic flux threading the loop, and Φ_{L} is the one induced by the self inductance of the loop L.

3. Finally the third term yields
$$\oint \nabla\theta \cdot \mathrm{d}r = \lim_{r_b \to r_a} (\theta(r_b) - \theta(r_a)) = 2\pi n. \tag{4.11}$$

The above equation stands for the single valuedness of the macroscopic wave-function, which imposes that the superconducting phase can vary at most an integer multiple of 2π.

[1] This can be easily seen according to the Meissner effect, and the Maxwell equations. The superconductor expels the external magnetic field B, which is zero inside the superconductor. Applying the Ampere's law, we find that inside the superconductor the circulating current is $I = \int_C B \cdot \mathrm{d}r$. Provided that $B = 0$, it trivially follows that $I = 0$ inside the superconductor.

Gathering all equations we finally obtain the flux quantization condition

$$\Phi_{\text{ext}} = n\Phi_0, \tag{4.12}$$

where $\Phi_0 = h/2e$ stands for the flux quantum.

If we now consider a superconducting ring interrupted by one or more Josephson junctions, the first term of the left hand side in (4.8) is no longer zero, but equals the phase drop across each of the junctions. In particular, for a superconducting loop interrupted by k Josephson junctions, each contribution is given by:

$$\int_{a_k}^{b_k} \Lambda J \cdot \mathrm{d}r = \frac{\Phi_0}{2\pi}\varphi_k, \tag{4.13}$$

where a_k, b_k defines defines the position of each junction in the superconducting loop. Inserting this equation into (4.8), we finally get the desired fluxoid quantization condition:

$$\frac{\Phi_0}{2\pi}\sum_{k=1}^{n}\varphi_k + \Phi_{\text{ext}} + \Phi_{\text{L}} = n\Phi_0. \tag{4.14}$$

In particular, for small loops $\Phi_{\text{L}} \to 0$, and we obtain the fluxoid quantization condition ubiquitous in this Thesis

$$\frac{\Phi_0}{2\pi}\sum_{k=1}^{n}\varphi_k + \Phi_{\text{ext}} = n\Phi_0. \tag{4.15}$$

Resumen

Introducción y objetivos

El rápido avance tecnológico que experimenta nuestra sociedad se debe en gran medida al excelente progreso en los procesos de miniaturización de los dispositivos electrónicos. Ello ha permitido llevar al transistor, piedra angular de la electrónica y ubicuo en cualquier circuito integrado, a la escala nanométrica, mejorando con ello el procesado de la información. Sin embargo este proceso de miniaturización no se puede realizar de forma indefinida, y dicho avance tecnológico tal y como los conocemos actualmente, verá su fin cuando los microchips alcancen un tamaño en el que la mecánica cuántica rija dinámica de sus constituyentes. A esas escalas microscópicas los electrones que circulasen por un circuito integrado, lejos de estar confinados en la guía de ondas por la que se propagan, podrían atravesar la misma (suceso conocido como efecto túnel) destruyendo así toda transmisión de información que estuviesen llevando a cabo. Se hace así imprescindible un avance cualitativo que permita reconciliar dicho progreso tecnológico con las leyes de la mecánica cuántica.

Dicho avance nace durante la última década de la mano de las ciencias de la *información y computaciones cuánticas* [NC00]. Se trata de un campo emergente y multidisciplinar cuyo objetivo es aprovechar fenómenos genuinos de la mecánica cuántica, como la superposición y el entrelazamiento cuántico, para mejorar la codificación, transporte y procesado de la información. Aparece así un nuevo marco paradigmático en la que la información se almacena y transporta por medio de bits cuánticos (qubits), y se procesa en un nuevo prototipo de procesador, el *computador cuántico* [Deu85]. Esta revolucionaria idea no sólo resolvería el problema de la miniaturización, sino que además permitiría resolver problemas completamente inaccesibles con un ordenador clásico, como el problema de la factorización [Sho97] o la propia dinámica de sistemas cuánticos de muchos cuerpos [AL97].

Para que estos computadores cuánticos puedan superar las capacidades computacionales de sus compañeros clásicos se hace imprescindible que centenares de qubits operen entre sí sin perder sus propiedades cuánticas. Sin embargo hasta la fecha sólo se ha conseguido que sistemas de unos pocos qubits preserven sus propiedades cuánticas, lo cual no es suficiente para poder hablar de una revolución en el campo de la computación. No obstante no todo son malas noticias, y hasta que se desarrolle un computador cuántico universal de un tamaño suficiente que permita resolver problemas como los comentados anteriormente, existe una alternativa que permite simular de forma efectiva un conjunto más reducido de problemas, como la dinámica de algunos sistemas cuánticos de interés. Se trata de la *simulación cuántica* [Fey82, Llo96]: un simulador cuántico[2] [BN09] es un dispositivo experimental sobre el que tenemos un alto grado de control, de forma que podemos manipular el estado cuántico del sistema, así como las interacciones entre las partículas, y hacer que este sistema reproduzca la dinámica de un modelo determinado.

Existen diversos prototipos para implementar tanto computadores como simuladores cuánticos, todos ellos están basados en diferentes sistemas físicos; iones atrapados en trampas electromagnéticas [CZ95, FSG+08], átomos ultrafríos en redes ópticas [JZ05], sistemas de resonancia magnética nuclear [VC05], puntos cuánticos [BKKY08] o circuitos superconductores [HTK12] son algunos ejemplos de simuladores cuánticos. Cada una de estas plataformas presenta distintas ventajas e inconvenientes respecto a las demás, como pueden ser la facilidad de aislar partículas, manipular sus interacciones, controlar su decoherencia, o el propio coste económico que conlleva su realización. Sin embargo, todas ellas comparten un ingrediente común: el excelente control que se tiene sobre partículas cuánticas individuales, tales como átomos, electrones y fotones. Trabajos pioneros tanto en el marco teórico como experimental durante la última década han conseguido que esto sea una realidad, y así ha sido reconocido por la comunidad científica con el Premio Nobel de Física en 2012 a D. Wineland y S. Haroche por sus *"innovadores técnicas experimentales que permiten la medición y manipulación de sistemas cuánticos individuales"*. No es de extrañar que la escalabilidad y control de dichos sistemas cuánticos centre los esfuerzos de la comunidad científica, hacia una nueva revolución que permita resolver problemas cuya solución es imposible hoy en día.

En esta Tesis perseguimos también este objetivo, y estudiamos el control

[2] A diferencia de un computador cuántico universal, un simulador cuántico no requiere de corrección cuántica de errores para reproducir correctamente la dinámica de un modelo sistema cuántico concreto.

de sistemas cuánticos en una plataforma concreta: los *circuitos superconductores*.

Los circuitos supercondutores [CW08], también llamados circuitos cuánticos, son circuitos integrados cuyos grados de libertad están cuantizados. A diferencia de un circuito clásico donde los grados de libertad[3] pueden tomar un conjunto continuo de valores, los grados de libertad de un circuito cuántico[4] sólo pueden tomar valores discretos. El requisito fundamental para que un circuito se comporte cuánticamente es la ausencia de disipación en el mismo. Por ello estos circuitos están construidos con materiales superconductores, ya que estos no presentan resistencia al paso de la corriente eléctrica [5]. Si finalmente el circuito superconductor se enfría hasta temperaturas criogénicas (del orden de decenas del milikelvin) donde las fluctuaciones térmicas sean despreciables, podremos observar su naturaleza cuántica.

En particular, circuitos construidos a partir de elementos lineales tales como bobinas y capacitores, manifiestan su naturaleza cuántica en forma de excitaciones de los campos electromagnéticos que oscilan en él, esto es, *fotones de microondas*. Si por el contrario añadimos elementos no lineales al circuito, tales como uniones de Josephson[6], podemos construir sistemas cuánticos localizados de dos o más niveles, creando de esta forma lo que se conoce como *átomos artificiales* o qubits superconductores. Estos átomos artificiales interaccionan con los fotones de microondas de la misma manera que átomos reales interaccionan con fotones del rango óptico, es decir, regidos por las leyes de la *electrodinámica cuántica* (QED por sus siglas en inglés), dando lugar al campo conocido como electrodinámica cuántica de circuitos [BHW+04] (también llamada en la literatura *circuit QED* , y como nos referiremos a ella de ahora en adelante).

Considerada en sus orígenes como la implementación en un chip de su análoga en cavidades ópticas cavity QED, circuit QED estudia la interac-

[3]Los grados de libertad de un circuito clásico son el voltaje V y al intensidad I a lo largo del circuito.

[4]En lugar de voltaje e intensidad, utilizaremos como grados de libertad de un circuito cuántico las variables de flujo ϕ y carga q, por su relación físca con la fase condensada del circuito superconductor, y los quantos de carga presentes en éste. No obstante estas variables se derivan trivialmente de V e I sin más que integrar dichas variables en el tiempo.

[5]Los materiales más comunes para el diseÃśo de circuitos cuánticos son el Aluminio y el Niobio, superconductores de tipo I a temperaturas de 4 Kelvin.

[6]Una unión de Josephson se forma por la unión de dos superconductores separados por una fina lámina de aislante, típicamente del tamaÃśo de nanómetros. Esta débil unıón permite el tunneling coherente de pares de Cooper de un superconductor a otro. Este tuneleo produce una corriente oscilante en el circuito que finalmente se modeliza como una inductancia no lineal.

ción entre materia y radiación a su nivel más fundamental *en una dimensión*. Como veremos a lo largo de esta Tesis, esta naturaleza unidimensional dota a la circuit QED de una gran ventaja frente al resto de plataformas, pues la interacción entre materia y radiación sucede de una forma más efectiva. La otra gran ventaja que presenta la circuit QED frente a la electrodinámica de cavidades ópticas, es que tanto átomos artificiales como fotones de microondas emergen del mismo material. Esto no sólo hace que tengan la misma escala de energías, sino que la interacción entre ambos sistemas, caracterizada por el parámetro de acoplo "g", también esté dentro de esa escala energética; es lo que se conoce como *régimen de acoplo ultrafuerte* [BGA+09, NDH+10, FLM+10]. Este régimen, imposible de alcanzar en un sistema óptico, ha hecho del campo de los circuitos superconductores una plataforma privilegiada para estudiar nuevos regímenes en la interacción entre materia y radiación [CRL+10, NC10b], permitiendo alcanzar y explorar fuertes interacciones fotón-fotón [HBP06, PZW+12] asÃ■ como el estudio de la fśica del modelo de Kondo en modelos de espín-bosón [LH12]. Desde la perspectiva de las tecnologías cuánticas, el régimen de acoplo ultrafuerte encuentra aplicación en el desarrollo de puertas cuánticas ultrarrápidas [RBW+12] y memorias cuánticas [SPdRMM12] para computación cuántica con circuitos superconductotes [NC11]. Por todas estas razones, la circuit QED se erige como una plataforma única para el estudio de nuevos fenómenos en óptica cuántica, así como un fuerte candidato en ser el primer sistema en que se desarrolle un computador cuántico[7].

En esta Tesis estudiamos cómo manipular la interacción fuerte y ultrafuerte entre materia y radiación en circuit QED de una manera controlada, tanto estática como dinámicamente, así como sus posibles aplicaciones a las tecnologías cuánticas. Los trabajos derivados de esta Tesis se pueden clasificar en dos frentes distintos, a saber:

- Control de la interacción entre fotones y qubits superconductores, confinados en resonadores de microondas o en una línea de transmisión infinita, por medio de un parámetro de acoplo ajustable g.
- Control de la interacción de fotones propagantes de microondas en una línea de transmisión abierta, por medio de sus propiedades de dispersión por un átomo artificial.

[7] Entre los principales problemas en la realizaciÓn de un computador cuántico están su escalabilidad y tiempo de decoherencia. Los circuitos superconductores son fácilmente escalables al estar fabricados de elementos pasivos, y estar impresos en un chip. Por otro lado, el tiempo de operación de una puerta cuántica es inversamente proporcional al parámetro de acoplo g, luego en el régimen de acoplo ultrafuerte se pueden implementar puertas ultrarrápidas que realicen multitud de operaciones antes de sufrir decoherencia.

En el primer punto, veremos cómo por medio de dispositivos de interferencia cuántica (SQUID's de su acrónimo inglés *superconducting quantum interference device*), podemos controlar de forma dinámica el parámetro de acoplo entre un qubit y un fotón de microondas, conectando y desconectando la interacción en tiempos que están en la escala del nanosegundo. Los diseños propuestos en este trabajo funcionan como un interruptor cuántico que permitiría la implementación de puertas cuánticas ultrarrápidas, la generación de fotones individuales, así como la simulación de problemas en información cuántica relativista, como la extracción de entrelazamiento del vacío. Estos diseños no sólo permiten encender y apagar la interacción, sino que además permiten rotarla de forma coherente, pasando de interacciones transversales a longitudinales. A parte de encontrar aplicación en computación cuántica mediante su uso para puertas lógicas, nuestros diseños permiten la simulación de medios no lineales tipo Kerr con los que generar pares de fotones entrelazados. Asimismo, por medio de estos dispositivos de interferencia cuántica, es posible sintonizar dinámicamente y de forma controlada la interacción entre resonadores superconductores, permitiendo así el estudio y simulación de transiciones de fase cuánticas en modelos de materia condensada, como modelos de Bose-Hubbard.

En el segundo punto adoptamos un enfoque distinto. Motivados por los recientes experimentos [WGH+07, AZA+10] en los que se observa que materia y radiación pueden interaccionar fuertemente incluso en ausencia de cavidades confinantes, estudiamos el control de fotones propagantes en una línea de transmisión infinita por medio de su dispersión por átomos artificiales. Observamos que la dispersión de fotones propagantes por un átomo de dos niveles resulta en una reflexión perfecta del fotón sobre la línea. Por el contrario, la dispersión por un átomo de tres niveles conduce a la transmisión completa del fotón propagante. De esta forma, controlando la estructura interna de nuestro átomo artificial, podemos hacer que los fotones propagantes sean dirigidos por distintos canales de una red cuántica. Finalmente, abordamos la dispersión de fotones por átomos artificiales como posible método de detección en el régimen de microondas. Dada la baja energía y sección eficaz que poseen los fotones de microondas, no ha sido posible diseñar detectores eficientes que trabaje en el régimen de un sólo fotón sin introducir ruido en el proceso de detección. Basados en la teoría de scattering, proponemos un sencillo diseño de un qubit en una línea de transmisión semi-infinita que permite detectar de forma perfecta de un fotón de microondas. A continuación presentamos los resultados más significativos derivados de esta Tesis.

Resultados y aportaciones fundamentales

Sintonización de acoplo ultrafuerte en circuit QED

La fuerte interacción que se puede inducir entre átomos y radiación en un circuito cuántico ha permitido alcanzar los regímenes de acoplo fuerte [BHW+04, WSB+04] y ultrafuerte [BGA+09]. En particular, en este último régimen, la constante de acoplo es comparable a las energías del átomo y del fotón ($g \simeq \omega_0, \Omega$), y la aproximación de onda rotante (RWA), y el célebre modelo de Jaynes-Cummings no describen correctamente la física de nuestro sistema. Este régimen, lejos de ser una prueba de principio [BGA+09], ha sido alcanzado en diversos experimentos [FLM+10, NDH+10], abriendo la puerta al poco explorado campo de la óptica cuántica más allá de la aproximación de onda rotante. Este acoplo es, sin embargo, difícilmente ajustable. Sólo en el caso de qubits confinados en una cavidad es posible controlar el acoplo, pero el precio a pagar es tener que desintonizar el qubit. El caso del qubit en un continuo es aún peor, ya que incluso en desintonía el qubit está acoplado a todos los modos. Estos problemas se pueden resolver introduciendo elementos externos tales como SQUID's, lo cual ha sido uno de los resultados de esta Tesis, y que se puede resumir en los siguiente puntos:

- Hemos propuesto un diseño de acoplo ajustable, válido tanto en resonadores como en líneas de transmisión infinitas, por medio de un SQUID conectado galvánicamente al circuito para preservar el régimen ultrafuerte. Por medio del campo magnético que atraviesa este SQUID, podemos rotar la interacción entre materia y radiación, pasando de interacciones transversales tipo $H_{\text{int}} = g\sigma_x(a + a^\dagger)$ a interacciones longitudinales de la forma $H_{\text{int}} = g\sigma_z(a + a^\dagger)$, en tiempos inferiores al nanosegundo, preservando el naturaleza ultrafuerte de la interacción.

- Por medio de un lazo superconductor adicional, proponemos un diseño más versátil que permiten desconectar distintos órdenes de la interacción de forma completa. De este modo, es posible encender y apagar interacciones no lineales, donde la contribución dominante en el Hamiltoniano es del tipo $H_{\text{int}} = g\sigma_x(a + a^\dagger)^2$.

- Finalmente presentamos un dispositivo que permite la desconexión de todos los acoplos presentes en el sistema, tanto lineales como no lineales, así como posibles acoplos residuales a canales capacitivos.

Estos dispositivos superconductores tienen diversas aplicaciones. La primera de ellas sería la creación de puertas cuánticas ultrarrápidas [RBW+12] entre parejas arbitrarias de átomos artificiales en una red de qubits. Esto es posible desacoplando todas las interacciones de los qubits con la línea, excepto de aquellos que han de implementar la puerta cuántica a dos qubits. La segunda aplicación sería proteger al qubit de decoherencia desconectándolo del continuo [GHB11], así como congelar su dinámica para hacer medidas en el mismo. Otra aplicación es la generación determinista de fotones individuales (pares de fotones entrelazados) propagantes. Esto se realiza mediante el siguiente protocolo: preparamos el qubit en el estado fundamental. Mediante un forzado excitamos el qubit, y acto seguido conectamos una interacción transversal lineal (no lineal) con la línea. El qubit, ultrafuertemente acoplado al campo, decaerá por emisión espontánea emitiendo un fotón (pares de fotones) propagante. Finalmente, un acoplo ajustable con fotones propagante es de utilidad en el campo de la información cuántica relativista. Gracias a estos diseños, es posible medir el cono del luz de los fotones, así como la propagación de correlaciones cuánticas entre qubits en una línea de transmisión.

En conclusión, hemos propuesto distintos dispositivos que permiten un control preciso de la interacción ultrafuerte tanto en resonadores como en líneas abiertas, así como una plétora de aplicaciones a diversos campos, como son la óptica cuántica de microondas, la computación cuántica con circuitos superconductores, o la información cuántica relativista. Un aplicación particular de estos dispositivos en información cuántica relativista se estudia en profundidad en la siguiente publicación.

Extracción de correlaciones de vacío entre pasado y futuro utilizando circuit QED

El vacío de un campo cuántico es un estado entrelazado. Este hecho, considerado en un principio como un mero resultado teórico, ha adquirido un gran interés como posible fuente de entrelazamiento para diferentes tareas en información cuántica. Como demostraron B. Reznik y colaboradores [RRS05, RCR05], se puede extraer entrelazamiento del vacío a un par de átomos separados espacialmente que interaccionan con un campo a un tiempo t, generando así estados de Bell. Este resultado ha sido brillantemente generalizado por T. Ralph y J. Olson [OR11] a un escenario en el que los átomos extraen las correlaciones del vacío cuando interaccionan con ese vacío *a tiempos distintos*. Es lo que se conoce como entrelazamiento *pasado-futuro*.

La enorme dificultad inherente a estas propuestas es su implementación física [OR12]. Para poder extraer entrelazamiento del vacío, necesitamos un continuo de modos que describa adecuadamente un campo cuántico. Por otro lado, las interacciones con el campo deben alcanzar regímenes ultrafuertes para amplificar las débiles correlaciones cuánticas del vacío, y al mismo tiempo poder ser desconectadas de forma ultrarrápida. La circuit QED nos proporciona todos estos ingredientes, ya que como hemos visto es posible alanzar el régimen de acoplo ultrafuerte con un continuo de modos, y desconectar el mismo de forma súbita.

En esta parte de la Tesis proponemos un experimento que permita extraer correlaciones cuánticas del vacío del tipo "pasado-futuro" a un par de qubits de flujo superconductores. El protocolo que proponemos para realizar dicha extracción de entrelazamiento es el siguiente: consideramos dos qubits superconductores P (de pasado) y F (de futuro) separados una distancia fija d en una línea de transmisión abierta, que contiene un campo en el estado de vacío. Conectamos la interacción entre el qubit P y el campo por un tiempo T_{on}, mientras el qubit F permanece desconectado. Pasado ese tiempo, desconectamos el qubit P del campo durante un tiempo T_{off}, evolucionando el sistema libremente. Finalmente, conectamos la interacción de F con el campo, mientras P permanece desconectado. Después de este protocolo, evaluamos la concurrencia entre los qubits P y F como medida de su entrelazamiento en función de los diferentes parámetros de nuestro sistema, como son la distancia d, y los tiempos T_{on} y T_{off} Los resultados principales se resumen a continuación.

- Cuando la separación entre qubits d es mucho menor que la longitud de onda asociada a su gap λ, observamos que los qubits están entrelazados fuera del cono de luz. Esto es, incluso cuando el intercambio de fotones reales no está permitido, los qubits P y F presentan fuertes correlaciones cuánticas. Esto es posible a que los qubits han extraído esas correlaciones del vacío.

- Para distancias $d > \lambda$, no hay entrelazamiento en regiones desconectadas causalmente, y todo su entrelazamiento es debido al intercambio de fotones reales. Sin embargo, se trata de un entrelazamiento no trivial, ya que el alto grado de entrelazamiento observado incluso en ausencia de medidas proyectivas sobre el campo es debido a la peculiar naturaleza de la circuit QED.

- Discutimos la posibilidad de realizar teleportación en el tiempo basados en el entrelazamiento "pasado-futuro". Ya que podemos generar pares

de Bell P, F entrelazados en el tiempo, podemos teleportar el estado de un qubit Q de la siguiente forma. Hacemos interaccionar el sistema conjunto P, Q por un tiempo T_{on} con el vacío del campo. Después de este tiempo, desconectamos la interacción y hacemos una medida de Bell en P, Q. Finalmente conectamos la interacción del qubit F con el campo, y dado que éste está entrelazado con P, podemos recuperar el estado de Q por medio de operaciones locales y comunicación clásica *con independencia del estado de* P. Nótese que, a diferencia con un protocolo de teleportación usual, el canal cuántico se ha creado *después* de la medida de Bell en P, Q.

En resumen, en esta parte de la Tesis hemos estudiado una aplicación de los dispositivos de desacoplo cuánticos al campo de la información cuántica relativista. Hemos propuesto un protocolo de extracción de entrelazamiento del vacío, en los que generar pares de Bell entrelazados *en distintos instantes de tiempo*. Discutimos a su vez un protocolo de teleportación temporal, utilizando dichos estados de Bell. Esta teleportación temporal, entendida como la codificación en el vacío del estado de un átomo Q, para recuperalo pasado un tiempo,se puede interpretar como un prototipo exótico de memoria cuántica.

Ingeniería de acoplos ajustables entre resonadores superconductores

En los primeros trabajos de esta Tesis hemos visto cómo la circuit QED es un excelente banco de pruebas para explorar la interacción entre materia y radiación en el régimen de acoplo ultrafuerte, así como una herramienta muy versátil para controlar sus interacciones. Además de un laboratorio de óptica cuántica unidimensional, *circuit QED* es una plataforma fácilmente escalable, y muy útil para estudiar la dinámica de muchos cuerpos. Por poner un ejemplo, acoplando sistemas qubit-resonador, es posible crear redes de estos en los que estudiar la dinámica de polaritones[8], como puede ser el modelo de Bose-Hubbard [LH10]. La única desventaja que presenta respecto a otras plataformas es que la interacción entre resonadores queda fijada por el geometría concreta de la red.

En esta parte de la Tesis centramos nuestra atención en cómo resolver este problema. Diseñando un acoplo ajustable entre resonadores a primeros vecinos por medio de SQUID's somos capaces de desacoplar localmente las

[8] el polaritón es una cuasipartícula que resulta de la interacción fuerte entre un fotón y un átomo de dos niveles. En nuestro ejemplo, este polaritón es la excitación del sistema qubit-resonador, y éste puede saltar entre distintos resonadores por medio un acoplo ajustable.

interacciones entre resonadores. Dicho acoplo representa a su vez un avance en este tipo de sistemas, si bien la ajuste dinámico del acoplo permite una gran variedad de interacciones fotón-fotón, como *sidebands* roja y azul, o simulación de campos de gauge. Los resultados más importantes derivados de esta Tesis en sistemas de resonadores acoplados son los siguiente:

- Hemos estudiado un modelo microscópico de resonadores acoplados geométricamente, derivando sus acoplos estáticos, de naturaleza púramente geométrica, en función de los distintos parámetros libres de los resonadores. Este modelo es interesante en sí mismo, ya que produce un Hamiltoniano de la forma $H = a_1^\dagger a_2 + a_1 a_2^\dagger$, simulando la dinámica de separadores de haz –véase la siguiente subsección.

- Proponemos varios diseños que permiten desacoplar los resonadores, basados en acoplos ajustables. En particular, estos diseños permiten cancelar el acoplo estático anterior. Por otro lado, gracias al acoplo galvánico con el SQUID, el parámetro de acoplo g es comparable a las frecuencias de los resonadores, de forma que interacciones contrarrotantes de la forma $H_{\text{int}} = g(a_1^\dagger a_2^\dagger + h.c)$ contribuyen a la dinámica y pueden volverse importantes.

- Estudiamos correcciones no lineales en los resonadores producidas por qubits superconductores o uniones de Josepshon, dando lugar a interacciones *on site* en cada resonador. Con ello tenemos los ingredientes necesarios para el estudio de modelos de materia condensada como modelos de Bose-Hubbard o modelos de espín, así como sus transiciones de fase [LDM+12]. En este sentido, la velocidad a la que sintonizamos juega un papel crucial: Así pues, si éste se cambia de forma adiabática, podemos estudiar la dinámica de las transiciones de fase cuánticas[9] y sus distintas fases críticas. Por otro lado, si el acoplo se cambia de una manera diabática podemos realizar un *quench*[10] sobre el sistema y estudiar la propagación de excitaciones en la red.

Más allá de acoplos ajustables que no varían en el tiempo, o lo hacen de forma monótona, consideramos propuestas más complejas como es la alimentación del SQUID con campos oscilantes no monocromáticos. Esto hace posible variedad de aplicaciones, siendo las siguientes las de mayor interés:

[9] Un ejemplo paradigmático de transición de fase cuántica es la transición aislante de Mott-superfluido, que ocurre en sistemas cuánticos a temperatura $T = 0K$

[10] Un quench consiste en sacar súbitamente al sistema de su estado fundamental, llevándolo a un estado excitado de no equilibrio.

- Alimentando el SQUID con un forzado de dos colores, es posible implementar interacciones efectivas entre cavidades[11] sólo con términos rotantes o términos contrarrotantes. (sidebands roja y azul respectivamente). En el primer caso, estamos simulando la dinámica de un separador de haz, pilar de la computación cuántica con fotones. Con el segundo, proponemos la generación paramétrica de fotones, y la posibilidad de crear *estados comprimidos* entre distintos modos fotónicos.

- Dado que también podemos controlar la fase de cada uno de los tonos del forzado, es posible generar términos en el Hamiltoniano de la forma $H = g_1 e^{i\phi_1} a^\dagger b + g_2 e^{i\phi_2} ab + \text{H.c.}$ en redes bidimensionales de resonadores, donde los fotones que saltan en plaquetas cerradas adquieren fases no triviales, simulando la dinámica de campos gauge en la red [KHHG10, NKG11].

Desde el punto de vista técnico, cabe mencionar que este tipo de forzados es viable experimentalmente gracias a la avanzada tecnología de los equipos electrónicos, tales como los generadores de señales, por lo que su implementación no supone un problema.

En resumen, por medio de la introducción de lazos superconductores como SQUID's en la geometría de redes de resonadores superconductores, es posible diseñar una gran variedad de modelos Hamiltonianos. Con su simulación, proponemos a su vez una plétora de aplicaciones en diversos campos de interés como son la óptica cuántica, la materia condensada y la física de no equilibrio.

Algunas de estas propuestas teóricas están se están llevando a cabo experimentalmente. Como ejemplo presentamos brevemente aquellas que conciernen a resultados obtenidos en esta Tesis.

Separadores de haz ultrarrápidos a partir de resonadores superconductores:

Dispositivos ubicuos en computación cuántica con fotones son los separadores de haz. Mediante ellos es posible implementar puertas cuánticas a un qubit, y puertas *KLM* a dos qubits[12] [KLM01]. Para poder realizar una computación se necesita ejecutar un conjunto de estas puertas cuánticas antes de que la información se pierda por decoherencia. Por ello es necesario que los separadores de haz hagan las operaciones de forma rápida.

[11] En este caso exigimos que las frecuencias de los resonadores sean distintas, de forma que obtenemos una sideband roja no trivial de frecuencia $\omega_1 - \omega_2$.

[12] Puertas KLM o de Knill-Laflamme-Milburn son puertas a dos qubits de tipo C-NOT desarrolladas sólo mediante óptica lineal.

Como ya hemos visto, acoplando resonadores en circuit QED es posible alcanzar los los regímenes de acoplo fuerte y ultrafuertes, generando interacciones tipo beam-splitter con un tiempo de puerta rápido. El modelo más sencillo experimentalmente que produce este tipo de Hamiltonianos es el acoplo de los resonadores geométricamente. El problema es que, en estos regímenes de interacción, los términos contrarrotantes pueden ser importantes, y contribuir con no-linealidades indeseadas en el sistema. En este primer experimento proponemos un modelo de acoplo geométrico asimétrico, que permite atenuar los efectos debidos a esta no linealidad. La idea se basa en lo siguiente: como el acoplo de los términos rotantes $g_{BS} = g_c + g_i$, y el de los contrarrotantes $g_{TMS} = g_c - g_i$[13], podemos acoplar los resonadores con una geometría tal que $g_c - g_i$ sea mínimo. De esta forma, podemos suprimir o atenuar los efectos no lineales del acoplo, manteniendo el término de beam-splitter. Los aportaciones y resultados obtenidos en este trabajo de la Tesis son los siguientes:

- En este trabajo investigamos siete muestras diferentes de resonadores acoplados con distintas geometrías. Medidas espectroscópicas en transmisión en todas las muestras arrojan un desdoblamiento asimétrico en los modos normales $\omega_\pm$ respecto a la frecuencia libre de los resonadores ω_0. Esto es una signatura clara de la presencia de términos contrarrotantes en el Hamiltoniano.

- Mediante teoría microscópica de circuitos, extraemos los valores de g_c y g_i, y estudiamos su dependencia con la geometría de las distintas muestras. Obtenemos que $g_{BS}/\omega_0 \simeq 20\%$ independiente de la geometría, mientras que g_{TMS} depende linealmente de ella, de acuerdo al modelo teórico propuesto. De las muestras analizadas, obtenemos un valor mínimo de $g_{TMS}/g_{BS} = 16\%$, y un valor máximo de $g_{TMS}/g_{BS} = 43\%$.

- Mediante extrapolación de nuestros resultados, mostramos que es posible tanto alcanzar una interacción de beam-splitter pura ($g_{TMS} = 0$), así como una interacción ultrafuerte entre resonadores ($g_{TMS}/\omega_0 \simeq 13\%$ en ausencia de acoplo galvánico.

Los resultados mostrados en este trabajo son una prueba de principio de la viabilidad de separadores de haz ultrarrápidos para su uso en computación y simulación cuántica con fotones, estén estos confinados en resonadores, o propagándose en una línea de transmisión.

[13] g_{BS} representa el parámetro de acoplo de los términos rotantes (Beam-Splitter), mientras que g_{TMS} representa el de los términos contrarrotantes (Two-Mode Squeezer). En ambos casos, g_c y g_i representan el acoplo capacitivo e inductivo entre resonadores respectivamente

Dispersión de estados coherentes por un átomo artificial en circuit QED

Dejamos a un lado el control de sistemas cuánticos mediante acoplos ajustables, para centrarnos en el segundo objetivo de esta Tesis: el control de fotones propagantes por medio de sus propiedades de dispersión por un átomo artificial [SF05b, SF05a], en lo que se conoce como *óptica cuántica de sistemas abiertos*. Nuestro interés surge a raíz de los primeros experimentos que estudian la fuerte interacción entre radiación y átomos individuales en ausencia de cavidades[14]. El fenómeno más llamativo es que, en aproximación de campo débil, la interferencia entre la radiación emitida por el dipolo con la del campo incidente, resultan en una extinción perfecta de la onda propagante en la dispersión hacia adelante. Este fenómenos fue observado con átomos individuales en tres dimensiones, pero con una extinción del 12% [WGH+07],. Esto es debido a la incompatibilidad en la superposición de frecuencias entre ondas incidentes y dispersadas[15], así como el difícil control sobre átomos individuales mediante láseres. Esta incompatibilidad no ocurre, sin embargo, en circuit QED: el sistema está confinado *en una dimensión*, de forma que la fotón emitido por el dipolo es también una onda plana. En este sentido, los primeros experimentos en circuit QED arrojaron resultados notables, con extinciones del 94% en la dispersión hacia adelante [AZA+10]. Como resultado de este proceso de dispersión observamos que el fotón ha sido prácticamente reflejado por el átomo. De esta manera, nuestras aspiraciones serán explotar esta fuerte interacción radiación materia para su posible uso en computación cuántica con fotones.

En este primer trabajo nos centraremos en un profundo estudio teórico de las propiedades de dispersión de fotones por un átomo artificial en una línea de transmisión abierta, partiendo de un modelo microscópico. A continuación presentamos los resultados más significativos:

- Partiendo de un modelo de elementos puntuales para una línea de transmisión semi-infinita, derivamos las ecuaciones de movimiento de un átomo artificial acoplado a la línea. Discutimos los límites de validez de la aproximación de onda rotante en nuestro sistema. En ese régimen, obtenemos el Hamiltoniano de un qubit superconductor acoplado a un

[14] El hecho de que la interacción radiación-materia en una cavidad sea fuerte se debe a que ésta confina al fotón en una región muy reducida del espacio, aumentando notablemente su probabilidad de interacción con el átomo. Es lo que se conoce como *efecto Purcell* [PTP46].

[15] Nótese que la onda dispersada es una onda esférica, mientras que la onda incidente es una onda plana.

baño de osciladores armónicos[16], y una relación de *input-output* para los campos propagantes. A partir de éste, derivamos una ecuación maestra en la forma de Lindblad [17]. Generalizamos estos resultados para un átomo acoplado a N líneas de transmisión infinitas.

- Utilizando las herramientas derivadas en el apartado anterior, estudiamos la dispersión de un forzado clásico por un *transmon*[18] en función de diferentes parámetros, a saber: la intensidad del forzado y su frecuencia. Caracterizamos la dinámica de los campos por medio de los coeficientes de reflexión y transmisión obtenidos a partir de parámetros del sistema. Observamos que para forzados débiles en resonancia con el átomo artificial, recuperamos el fenómeno observado experimentalmente de reflexión perfecta.

- Estudiamos la dispersión de un forzado en el régimen de un sólo fotón sobre el transmon cuando añadimos un segundo forzado al sistema. Observamos que los coeficientes de reflexión y transmisión del primer forzado dependen de la frecuencia e intensidad del segundo. Por ello, podemos utilizar el segundo forzado para controlar la transmisión del primero.

- Finalmente, estudiamos correlaciones de segundo orden en el campo, y cómo estas correlaciones se ven afectadas por efectos de temperatura y ancho de banda finitos [HPL+12].

En conclusión, hemos realizado un exhaustivo análisis de la dispersión en sistemas abiertos unidimensionales desde el punto de vista microscópico de la teoría de circuitos cuánticos. Hemos derivado una ecuación maestra para un qubit superconductor tipo transmon. Obtenemos que, en la aproximación de dos niveles, el transmon se comporta como un espejo reflejando los fotones incidentes. Por último vemos que, si añadimos un segundo forzado en resonancia con la segunda transición de nuestro átomo artificial, podemos suprimir la reflexión de fotones de la primera transición, fenómeno conocido como *transparencia inducida electromagnéticamente* [BIH91, AAZ+10].

Estos resultados teóricos están en excelente acuerdo con los experimentos

[16] Estos osciladores armónicos representan los distintos modos electromagnéticos de la línea de transmisión

[17] Este resultado es compatible con una derivación más formal de la ecuación maestra a partir de las ecuaciones del movimiento, que representan una ecuación cuántica de Langevin

[18] Un transmon es un átomo artificial cuya estructura interna es la de un átomo de tres niveles, pero con una anarmonicidad suficiente para que pueda comportarse como un átomo de dos niveles, en ausencia de forzados que induzcan la transición $1 - 2$.

que presentamos a continuación, también incluídos en los resultados de esta Tesis.

Demostración de un router de un sólo fotón

Dentro de las ciencias de la información cuántica, las *comunicaciones cuánticas*[19] han alcanzado un gran desarrollo tecnológico. Como ejemplo, sistemas de criptografía cuántica ya se distribuyen comercialmente [SBPC+09]. Esto son algunos ejemplos de canales cuánticos que distribuyen información cuántica, codificada en fotones [20]. Combinando estos canales cuánticos con *nodos cuánticos*, dispositivos capaces de procesar y dirigir la información por los canales, sería posible desarrollar *redes cuánticas*, que además de implementar un computador cuántico escalable, permitirían la distribución de software cuántico [OFV09, Kim08],.

El desafío está en dirigir o enrutar los fotones por distintos canales, pues los fotones no interaccionan entre ellos, y lo hacen débilmente con la materia. En este trabajo queremos aprovechar una vez más el régimen de acoplo fuerte en circuit QED, presentando un prototipo rudimentario de nodo cuántico: el *router de un sólo fotón*. El elemento activo del router es un qubit transmon acoplado capacitivamente a una línea de transmisión. Hacemos incidir un forzado sobre él, y estudiamos el resultado de la dispersión del forzado por este átomo, obteniendo los siguientes resultados:

- Para un forzado en el régimen de fotones $N \ll 1$[21] en resonancia con la transición $0-1$ del transmon, observamos una extinción del 99.6% en el canal de transmisión. A medida que aumentamos la potencia del forzado observamos que la transmisión aumenta, saturando para $N's$ grandes, lo cual es una signatura del carácter cuántico del átomo, ya que éste sólo puede absorber un fotón por unidad de tiempo. A su vez, las medidas en el canal de reflexión muestran el resultado complementario esperado[22].

[19] La comunicación cuántica es un método de comunicar información de forma incondicionalmente segura en una red.

[20] Los fotones son un sistema ideal para transmitir información cuántica, ya que pueden recorrer grandes distancias, del orden de centenas de kilómetro, [ref schmitt manderbach], sin interaccionar entre ellos.

[21] Definimos N como el número medio de fotones por tiempo de interacción.

[22] Un dato importante a tener en cuenta, es que las medidas en reflexión y en transmisión se realizan de forma simultanea, para asegurar que el fotón no es emitido por canales no radiativos.

- Añadimos un forzado de control en resonancia con la transición $1-2$ del transmon. Para forzados fuertes, observamos el fenómeno de transparencia inducida electromagnéticamente (EIT) en la transición $0-1$, como consecuencia de la *separación de Autler-Townes* [AT55] inducida por el forzado de control. Por completitud se mide también el triplete de Mollow.

- Explotamos el fenómeno de la EIT para construir un router de un fotón, cuyo funcionamiento es el siguiente: Un primer pulso débil incide continuamente por un canal de entrada a la frecuencia $0-1$. Un segundo pulso fuerte de control se enciende y apaga alternativamente a la frecuencia $1-2$. Cuando el control está apagado, el primer pulso es reflejado por el átomo, mientras que si el control está encendido, generamos EIT y el primer pulso es transmitido. Mediante un circulador[23] colocado antes del transmon, podemos enrutar el fotón en la frecuencia $0-1$ por distintos canales de salida. De esta forma, queda demostrado el funcionamiento del ruter cuántico.

- Hemos mediado la eficiencia del router, alcanzando un 99% tanto en transmisión como en reflexión. Se caracterizó el tiempo de respuesta del router con pulsos gaussianos ultracortos, preservando la eficiencia anterior para pulsos de un anchura de 10 nanosegundos. Este tiempo de operación se espera mejorarlo aún más, hasta el límite de 2 nanosegundos, compatible con el estado del arte de la electrónica actual.

Cabe destacar que el router propuesto puede ser multiplexado para distribuir fotones por diversos canales. Esto se consigue concatenando la estructura circulador-transmon a lo largo de la línea, y diseñando los transmon con distintas frecuencias de transición $1-2$, manteniendo la misma frecuencia de transición $0-1$.

En resumen, en este trabajo hemos demostrado el funcionamiento de un nodo cuántico rudimentario en el régimen de microondas, que permite dirigir fotones individuales por distintos puertos de una posible red. Es claro que fotones ópticos son más adecuados para comunicaciones cuánticas a distancia, mientras que los circuitos cuánticos son más adecuados para implementar los nodos de la red. Será de sumo interés explorar interfaz que permita convertir fotones ópticos en fotones de microondas, para así construir redes cuánticas híbridas que aprovechen las ventajas de ambos campos.

[23] Un circulador es un dispositivo con tres puertos, uno de entrada para la señal incidente, y dos de salida. El circulador funciona de la siguiente manera: Dado un puerto cualquiera de entrada, un fotón incidente por ese puerto saldrá por el inmediatamente siguiente, fijada una dirección.

Detección perfecta de un fotón en circuit QED

Terminamos esta Tesis mirando a otro problema importante, aún abierto en circuit QED; el problema de la fotodetección de un sólo fotón propagante. A diferencia del rango óptico, donde los fotones se pueden detectar fácilmente[24], los fotones de microondas no tienen suficiente energía ni sección eficaz como para arrancar electrones de un material y ser detectados. Los detectores basados en amplificadores introducen ruido en el sistema, y aunque este puede atenuarse mediante amplificación paramétrica, no es suficiente como para hacer tomografía cuántica de fotones. Resulta crucial resolver este problema para que la computación cuántica con fotones de microondas sea posible. Existen propuestas teóricas basadas en la teoría de dispersión por elementos dispersores en una línea de transmisión abierta [RGRS09a]. Sin embargo, han demostrado un límite fundamental del 50% en la eficiencia de detección cuando sólo tenemos un elemento dispersor[25] [RGRS09b].

En este trabajo proponemos un modelo basado en la teoría de dispersión en la que es posible alcanzar una eficiencia de detección del 100%, utilizando *un único* elemento dispersor, en este caso un qubit de fase[26]. Los aportaciones fundamentales de nuestra investigación se pueden resumir en los siguientes puntos:

- Estudiamos el scattering de un fotón por un qubit de fase situado a una distancia L del final de una línea semi-infinita, actuando como espejo[27]. Para ello, resolvemos el sistema de ecuaciones diferenciales retardadas en el régimen $L \ll \lambda$, siendo λ la longitud de onda asociada al gap de energía del qubit.

- Manipulando los parámetros del qubit, tales como la distancia L y el ratio de decaimiento Γ al estado metaestable de detección, podemos controlar los coeficientes de reflexión y transmisión, confinado el fotón

[24] Por ejemplo por medio de diferencias de potencial generadas por este fotón en fotomultiplicadores. Este potencial finalmente en una corriente que se puede medir.

[25] Para detectar un fotón con una eficiencia del 100%, necesitaríamos reconstruir la *inversión temporal* del proceso de *emisión espontánea*. Esto es, el fotón debe incidir por la izquierda y por la derecha del átomo al mismo tiempo. Esto no es posible ya que el fotón sólo puede provenir de una de las dos direcciones; de ahí el umbral del 50% en la eficiencia de detección.

[26] Un qubit de fase es un átomo de dos niveles, donde el estado excitado tiene un decaimiento muy grande a un estado mesoscópico podemos medir. El proceso de detección está precisamente basado en esto.

[27] Esto se consigue conectado la línea de transmisión a tierra. La línea está así en cortocircuito, y la condición de contorno para el potencial eléctrico es $V = 0$, resultando en una reflexión perfecta sobre la línea.

propagante en la pseudo-cavidad que definen el espejo y el qubit – correspondiente al caso de reflexión cero. Para este último caso, estudiamos la población del fotón confinado en la pseudo-cavidad en función del tiempo.

- Observamos la completa extinción del fotón en la pseudo-cavidad, como resultado de la absorción del fotón por el qubit de fase. Definiendo la eficiencia de absorción como la parte de la radiación que no es reflejada por el qubit, ni queda de forma estacionaria en la pseduo-cavidad, concluimos que se puede detectar un fotón propagante de microondas por un sólo qubit con una eficiencia teórica del 100%.

- Hemos validado estos resultados para distintos tipos de paquetes de onda, desde estados de Fock de momento definido $|k\rangle$, a situaciones más realistas con perfiles gaussianos. En todos ellos, incluso en situaciones de moderada desintonía del fotón con el qubit, se alcanzan excelentes eficiencias de absorción.

- Consideramos también el caso de más de un qubit de fase como elementos dispersores. Observamos que, a medida que ponemos más qubits de fase en la línea separados una distancia proporcional a la longitud de onda λ, la eficiencia en la detección se vuelve robusta a imperfecciones en el diseño de los qubits[28], y a mayores desintonías entre el fotón y los qubits.

- Por último, desarrollamos una teoría que prediga los resultados obtenidos en los primeros experimentos de detección de fotones propagantes [CHS+11]. El experimento mostrado en Ref. [CHS+11] es esencialmente nuestro modelo inicial, pero con el fotón propagante incidiendo a través del espejo, confinándose en la pseudo-cavidad. Nuestra teoría predice los resultados experimentales, en los que se obtiene una eficiencia del 90%, con un límite asintótico del 100% sujeto a la condición $\Gamma \to 0$. Esto es debido a que el qubit sólo actúa como un espejo perfecto en ese límite.

En conclusión, en esta Tesis proponemos un diseño de detector y contador de fotones propagantes basado en la teoría de la dispersión en circuit QED. Nuestra propuesta, basada en un qubit de fase de tres niveles enfrentado a un espejo, rompe el límite del 50% en la eficiencia de detección, intrínseco de la teoría. El diseño propuesto es robusto a posibles imperfecciones en el proceso de fabricación, así como a canales de decaimiento no radiativos,

[28] El gap de energía de un qubit depende del tamaño de las uniones de Josephson que lo componen. Su diseño mediante litografía óptica en una máscara de silicio y evaporación de doble ángulo, típicamente produce errores del 5% en el tamaño de las uniones.

lo que hace de él un buen candidato para formar parte de arquitecturas de circuitos superconductores para procesado de la información cuántica con fotones[29].

Conclusiones

A lo largo de esta Tesis hemos estudiado cómo controlar sistemas cuánticos con circuitos superconductores en el marco de la electrodinámica cuántica de circuitos. Los circuitos superconductores son dispositivos mesoscópicos de estado sólido, que enfriados a temperaturas criogénicas muestran su naturaleza cuántica, que se manifiesta en forma de fotones de microondas, y sistemas de pocos niveles, como qubits y qutrits. Estudiamos la interacción entre ellos, y cómo el control de las mismas da lugar a distintas aplicaciones de gran interés en óptica cuántica, simulación y computaciones cuánticas.

En la primera parte de la Tesis nos centramos en el control de la interacción mediante modelos de acoplo ajustable. Los primeros modelos estudiados se refieren a la interacción qubit-fotón n el régimen de acoplo ultrafuerte, ya sea en un resonador o en un espacio abierto. Demostramos que el acoplo no es sólamente ajustable en intensidad, sino también en tipo, permitiendo rotaciones coherentes de este. Utilizando estos dispositivos, sugerimos cómo realizar puertas cuánticas a dos qubits de forma ultrarrápida, proteger qubits frente a decoherencia, mejorar su medida, así como simular medios no lineales. Una aplicación muy interesante del acoplo ajustable es su uso para extraer correlaciones del vacío como fuente de entrelazamiento, así como una posible memoria cuántica por medio del protocolo de teleportación temporal. Las siguientes propuestas que hemos estudiado en esta Tesis se centran en el acoplo ajustable entre redes escalables de resonadores superconductores. Estudiamos su utilidad para realizar simuladores cuánticos de gran variedad de modelos en materia condensada. El acoplo ajustable permite el estudio dinámico de transiciones de fase cuánticas, así como de quenches en sistemas anarmónicos, y el estudio de cotas de Lieb-Robinson en esos modelos. Demostramos que es posible construir separadores de haz ultrarrápidos con resonadores acoplados geométricamente, y discutimos su utilidad para hacer computación cuántica con fotones.

En la segunda parte de la Tesis tratamos el control de fotones propagantes por medio de su dispersión con átomos artificiales. A partir de un modelo

[29]Como la propuesta de computación cuántica con fotones propuesta por Knill-Lafflamme-Milburn, más conocida como *dual rail encoding*.

microscópico de teoría de circuitos vemos cómo depende el estado de los fotones propagantes en función de la estructura interna de los átomos artificiales. Así, átomos de dos niveles en resonancia con el fotón actúan como espejos perfectos. Por el contrario, un átomo de tres niveles puede dar lugar a transparencia inducida electromagnéticamente (EIT), de forma que el fotón antes reflejado, ahora es completamente transmitido. Utilizamos estos resultados para proponer un prototipo de nodo cuántico, que llamamos router de un fotón. Controlando un pulso de control sobre un qubit transmon, podemos hacer un desdoblamiento de Autler-Townes en los niveles excitados del transmon, y generar así generar la EIT, que regula en última instancia el puerto por el que el router dirige al fotón. Este modelo se puede concatenar en un router multipuerto que dirigiría fotones por distintos puertos de una red cuántica, en tiempos de operación de pocos nanosegundos. Finalmente abordamos en esta Tesis un problema abierto en circuit QED, como es la detección de fotones propagantes. Proponemos un fotodetector que permite alcanzar una eficiencia teórica de detección del 100%, rompiendo un límite fundamental en teoría de detección con un solo qubit. El modelo es escalable a más qubits, lo que hace de él una propuesta realista en posibles experimentos.

Creemos que los resultados presentados en esta Tesis sientan las bases del control de interacciones en régimen de acoplo fuerte y ultrafuerte dentro del campo de circuit QED. A su vez, estos trabajos arrojan luz sobre las posibles aplicaciones que este régimen tiene en las ciencias de la información y computaciones cuánticas.

Abstract

Quantum information science (QIS) [NC00] is an emerging and multidisciplinary field whose ultimate goal is to take advantage of quantum phenomena, such as superposition and entanglement, in order to improve the information storage, commmunication and computation. Among all the disciplines spanned by QIS, quantum computing [Deu85] and quantum simulations [Fey82, Llo96, BN09] have attracted a great deal of attention, as they aim to solve problems which are nowadays impossible to access with classical computers [Sho97, AL97]. There exist several proposals for implementing both quantum computers and quantum simulators, all of them based on different physical systems. Trapped ions [CZ95, FSG+08], ultracold atoms [JZ05], NMR systems [VC05], quantum dots [BKKY08] or superconducting circuits [HTK12] are some examples of quantum simulators. Indeed, superconducting circuits [CW08] are particularly suitable for implementing those devices, since they posess strong interactions, it is straightforward to scale them up, and are easily controllable.

In particular, superconducting circuits made out of linear elements behave as microwave photons, whereas if one adds non-linear elements to the circuit, such as Josephson junctions, superconducting circuits behave as two-level systems, or artificial atoms. These artificial atoms interact with the photons in the same way that real atoms and photons do, i.e., ruled by the laws of quantum electrodynamics, giving rise to the field known as circuit quantum electrodynamics or *circuit QED*. Circuit QED [BHW+04] studies the light-matter interaction in a one-dimensional chip. As we will see in this Thesis, this one-dimensional nature makes of circuit QED an advantageous platform for developing quantum computers and quantum simulators, since the interaction between light and matter happens in a much more efficient way. In particular, it is possible to reach an interaction regime where the coupling strength "g" is comparable to the bare energies of superconducting qubits ω_q, and microwave photons ω_k. Under this condition, light and matter interact in the so-

called *ultrastrong coupling regime* [BGA+09, NDH+10, FLM+10], unachievable in an optical system. In this rather unexplored regime, one can tailor strong photon-photon interactions [HBP06, PZW+12], generate strong correlations between light and matter [CRL+10, NC10b], or study the Kondo physics in the spin-boson model [LH12]. Along the lines of quantum technologies, the ultrastrong coupling regime has found application in the development of ultrafast quantum gates [RBW+12] and quantum memories [SPdRMM12] for quantum computing in circuit QED [NC11]. For all these reasons, circuit QED has become a unique platform for studying new regimes of interaction, as well as a strong candidate to be the first system that implements a quantum computer.

This Thesis is devoted to the study of light-matter interaction in a quantum circuit, and how we can control their interaction in the ultrastrong regime. In addittion to this, we propose different designs that allows for a switchable coupling, both statically and dynamically, and we show their potential application for quantum information science. The Thesis is written in the "article format", where the original publications that this Thesis has produced are presented after a brief summary and discussion of their main results. Our results can be dividied into two different approaches, namely

- Control of the interaction between photons and qubits, either confined in a resonator or an open line, via an engineered switchable coupling "g".
- Control of propagating microwave photons moving in an open transmission line, by means of the scattering properties with an artificial atom.

In the first part of this Thesis, we will show how we can dynamically control the coupling "g" between qubits and microwave photons through superconducting quantum interference devices (SQUID's), connecting and disconnecting the interaction in times that are on the nanosecond scale. The designs proposed in this Thesis can be used as quantum switches that allow for the implementation of ultrafast quantum gates, the generation of single photons on demand, as well as the simulation of relativistic quantum information problems, such as the extraction of quantum entanglement from the vacuum. These designs not only allow for a complete switch of the light-matter interaction, but also for coherent rotations of it, going from transverse to longitudinal interactions. Besides these applications, mostly focused in the development of quantum gates for quantum computing, our designs allow for the simulation of Kerr-type nonlinear media, and the generation of entan-

gled pair of photons. Moreover, we propose different setups of coupled superconducting resonators whose interaction can be dynamically controlled by means of SQUID's. Using this devices, we it becomes possible to study and quantum simulate diverse interesting models in condensed matter physics, such as families of Bose-Hubbard models.

In the second part of the Thesis, we adopt a different approach for controlling the coupling. Motivated by the recent experiments which shows that light and matter can interact strongly even in the absence of confining cavities, we study the control of propagating photons in an open tranmission line through their scattering upon artificial atoms. We observe that the scattering of propagating photons by a two-level system results in a perfect reflection of the photon. By contrast, the photon scattering by a three-level artificial atom can result in perfect transmission of the photon. Hence, by controlling the internal structure of the artificial atom, we can control whether the photons are reflected or transmitted at will. We propose a practical application to address photons to different channels of a quantum network. Finally, we study the photodetection problem of propagating microwaves in circuit QED. Given the low cross section of microwave photons, it has not been possible to design efficient single-photon detectors without introducing noise the detection process. Based on the scattering theory, we propose a simple design with a single phase qubit placed in a semi-infinite transmission line that works as a perfect absorber of the microwave photon. Below we present the most outstanding results derived from this Thesis.

Summary and discussion of results

Switchable ultrastrong coupling in circuit QED

The large dipole moments of artificial atoms combined with the strong vacuum fields attainable in superconducting resonators have made possible the achievement of the strong and ultrastrong coupling regimes in circuit QED [BHW+04, WSB+04, BGA+09, FLM+10, NDH+10]. In this latter regime, the coupling "g" is comparable to the qubit and photon frequencies ($g \simeq \omega_0, \Omega$), and the celebrated Jaynes-Cummings model does not properly describe the dynamics of the system, opening the door to a wide variety of studies around the rather unexplored physics beyond the rotating wave approximation. However, the ultrastrong coupling is not tunable. Only in the case of a qubit confined in a resonator, the coupling might be adjusted by detuning the qubit from the cavity, but at the price of moving the qubit away from its symmetry point, with the subsequent reduction of qubit lifetime. For a qubit placed in an open transmission line this argument is not even valid, since the qubit is coupled to a continuum of field modes, regardless it is detuned or not.

Both problems can be solved at once by adding superconducting couplers such as SQUID's, galvanically coupled to the standard circuit QED architecture. A profound description of an ultrastrong tunable interaction has been one of the central results of this Thesis, whose main results can be summarized in the following points:

- We propose a tunable coupling design, consisting of two superconducting loops galvanically coupled to a transmission line. By controlling the external magnetic flux threading both loops, we can rotate the light-matter interaction basis, going from transversal interactions of the form $H_{\rm int} = g_x\sigma_x(a + a^\dagger)$ to longitudinal Hamiltonians $H_{\rm int} = g_z\sigma_z(a + a^\dagger)$. This rotation can be performed in times that are within the subnanosecond scale, while preserving the ultrastrong nature of the interaction.

- By means of an additional loo, we propose a more versatile design that allows us to switch on and off *different orders* of the interaction Hamiltonian. Thus, it becomes possible to enhance the relevance of non-linear contributions of the form $H_{\rm int} = g_x^{(2)}\sigma_x(a + a^\dagger)^2$, by switching off only the light-matter interaction at first order.

- Finally, we present a device that could disconnect *all the couplings* at a

time, both linear, non-linear and possible spurious couplings that might arise from capacitive channels.

We envision numerous applications for all these proposals. The immediate one would concern the field of Quantum Information Processing, with the creation of ultrafast quantum gates [RBW+12] between two arbitrary pair of qubits in a row coupled to a transmission line. The second application would be the qubit protection from decoherence. By switching off all the couplings we can isolate the qubit from the environment [GHB11]. Moreover, this can be used for measuring the qubit once its ultrafast dynamics is frozen. Another application is the generation of propagating single-photons (two-photons) on demand. This is accomplished by the following protocol: we prepare the qubit in its ground state. We drive the qubit the qubit to the excited state, and immediately connect an ultrastrong linear (nonlinear) interaction to the line, as described above. The qubit finally decays by emitting a propagating single-photon (two-photons). Lastly, a tunable coupling with propagating photons can be of paramount importance in the field of relativistic quantum information. With these designs, it becomes possible to measure the light-cone of photons, as well as the propagation of quantum correlations between qubits in a common transmission line.

Application to Relativistic Quantum Information

In the second work of this Thesis, we exploit the fascinating properties of ultrastrong coupling in circuit QED and the aforementioned switchability, to propose a realistic experiment that would permit for the extraction of past-future quantum correlations from the quantum vacuum to a pair of superconducting qubits. The extraction protocol is the following: two superconducting flux qubits P (for the past) and F (for the future), are interact with the vacuum field of an open transmission line *at different times*. By means of the switchable device presented before, we connect an ultrastrong interaction between the qubit P and the field for a time T_{on}, while keeping the qubit F disconnected. After this time, we switch off the coupling for a time T_{off}. Finally, we switch on the interaction of the qubit F with the field for a time T_{on}, while keeping P disconnected. After this protocol, the system ends up in a highly correlated state. We study this correlations as a function of different parameters, such as the distance between qubits d, and the interaction times T_{on} and T_{off}. The main results of this work are:

- When the distance between qubits d is much smaller than the typical

wavelength of the qubit energy gap λ, we observe that the qubits are entangled outside their mutual light cone; even when the exchange of real photons is not allowed, qubits P and F exhibit strong quantum correlations. This is due to the extraction of entanglement from the vacuum state $|0\rangle$.

- As the distance d increases, past-future quantum correlations vanish. However, we observe a high degree of entanglement concentrated in the vicinity of the light-cone, even in the absence of projective measurements. This non-trivial correlations can only be explained by the one dimensional nature of circuit QED, which allows for a much more efficient interaction.

- We discuss the possibility of using our setup for developing *quantum teleportation in time*. Moreover, we show that this teleportation protocol can be seen as a rudimentary quantum memory, where the state of a qubit P' is codified in the vacuum for a time T_{off}, and recovered in the future.

In summary, taking advantage of switchable ultrastrong interactions, we propose a doable circuit QED experiment to test the extraction of quantum correlations between different times contained in the vacuum of a quantum field. We have shown in particular that sizable past-future vacuum correlations can be transferred to a pair of qubits P and F, which only interact with the field in the past or the future respectively, and *do not coexist at the same time*.

Tunable coupling in arrays of superconducting resonators

Besides studying light-matter intereaction with superconducting circuits, in this Thesis we focus on circuit QED as a playground for testing the many-body dynamics of low-dimensional quantum systems. In particular, we extend these models to scenarios with tunable coupling, by coupling superconducting resonators. This allows us for the generation of multi-photon interactions, that find application in many different fields, such as Quantum Optics or Condensed matter physics. The main results derived from our research are:

- We derive a microscopic model of geometrically coupled superconducting resonators. We show that the resonators are always coupled, re-

gardless their geomertric layout. In particular, the Hamiltonian of the resonators is that of a beam-splitter interaction

- Based once again on simple devices such as SQUID's, we propose a tunable coupling design between superconducting resonators. The coupling relies on the flux quantization over the SQUID loop, that merges the photon operators of different resonators $\Delta\psi_1$, $\Delta\psi_2$ in a linear or non-linear way, depending on the value of the external flux threading the SQUID $\Phi_{\circlearrowleft}$. Applying a proper external constant magnetic flux, we can cancel the geometric coupling between the resonators.

- Alternatively to the full decoupling, one can strongly couple the resonators. In particular, due to the galvanic nature of the interaction, this coupling can be brought to the ultrastong regime.

- We study non-linear corrections to the resonator-resonator coupling produced by qubits or Josephson junctions, giving rise to an on-site interaction on each resonator. With this, we have all the ingredients to study condensed matter models, such as the Bose-Hubbard model [LH10, LDM+12], or spin-like systems. Along these lines, the speed on tuning of the coupling constant plays a fundamental role: in particular, if it changes in an adiabatic way, we can study dynamical quantum phase transitions of these models, and their critical phases. On the other hand, if we change it an a fast way, we can perform quantum quenches and track how correlations propagate in the lattice, and more generally how the system relaxes.

Apart from constant magnetic fluxes $\Phi_{\circlearrowleft}$ or monotonic variations of the flux, we consider time-dependent oscillating magnetic fields through the SQUID's. This yields an incredibly large number of applications, being the most relevant the following ones:

- Feeding the SQUID with a two-tone driving, we can create the blue and the red sideband between the resonators. This makes possible the simulation of tunable beam splitters (with the red sideband), or the frequency conversion of photons and generation of squeezed states (with the blue sideband)

- By controlling the phase of each tone of the driving, we can generate terms of the form $H = g_1 e^{i\theta_1} a_1^\dagger a_2 + g_2 e^{i\theta_2} a_1^\dagger a_2^\dagger$H.c. in 2D lattices, where the photons hop around closed plaquettes acquiring a non-trivial phase, which simulates the dynamics of gauge fields.

Summing up, we have presented the tunability of coupled superconducting resonators via galvanic coupling with SQUID's. We show that it is possible to go from ultrastrong coupling, to perfect decoupling. Moreover, we propose arbitrary linear and nonlinear couplings in arrays of resonators, as well as countless applications to the fields of microwave quantum optics and condensed matter physics. We envision that all these proposals can be realized in the near future. In particular, in the next work we present a first experiment on coupled resonators, which is a proof-of-principle towards multiresonator experiments.

Ultrafast beam splitters from superconducting resonators:

Beam splitters are ubiquitous devices for quantum computing with photons. Thanks to these devices, it is possible to engineer one-qubit and two-qubit KLM gates[30] [KLM01] for quantum information processing. In order to perform quantum operations before the information is lost by decoherence, it is convenient that beam splitters operate sufficiently fast. In this work we experimentally show that this can be done in the framework of circuit QED by coupling superconducting resonators.

As shown before, the simplest model that yields a beam splitter dynamics is that of geometrically coupled resonators. Moreover, since the coupling can reach the ultrastrong regime, they are well suited to perform fast quantum operations. On the other hand, within this interaction regime, counterrotating terms become important and can jeopardize the well-functioning of a beam splitter, via the two-mode squeezer term g_{TMS}. Fortunately, since the beam splitter term is given by $g_{\mathrm{BS}} = g_{\mathrm{i}} + g_{\mathrm{c}}$, and the two mode squeezer term is $g_{\mathrm{TMS}} = g_{\mathrm{i}} - g_{\mathrm{c}}$[31], we can couple the resonators in such a way that $g_{\mathrm{TMS}} = 0$ while maximizing the beam splitter term. Below we show the main results of this work:

- We look for asymmetric designs that can suppress the effect of the counterrotating terms, by studying the dependence of g_{i} and g_{c} with the physical coupling positions of the layout.
- We have experimentally validated our model, by analyzing seven samples with different geometries. We perform spectroscopic measure-

[30] Knill-Laflamme-Milburn or KLM gates [KLM01], are heralded C-NOT gates for scalable quantum computation with photons using solely linear devices such as beam splitters, ancillary photons and measurements.

[31] The terms g_{i}, g_{c} respectively stand for the inductive and capacitive coupling between the resonators.

ments in transmission for the coupled resonators, observing asymmetrical splitting of the normal modes $w_{\pm}$ with respect to the bare resonator frequencies w_0. This is a clear signature of the presence of counterrotating terms.

- Using a distributed coupling model we obtain the couplings g_{i} and g_{c} as a function of the geometry of the resonators. Using realistic parameters, we obtain that $g_{\mathrm{BS}}/\omega_0 \simeq 20\%$ regardless the geometry design, whereas g_{TMS} depends lineraly on it, according to the proposed model. In particular, for the analyzed samples we demonstrated a tunability of the coupling ratio $g_{\mathrm{TMS}}/g_{\mathrm{BS}}$ between 16% and 43%.

- By extrapolation of our results, we show that it would be possible to reach a pure ultrastrong beam-splitter interaction (this is, $g_{\mathrm{BS}}/\omega_0 \simeq 20\%$ and $g_{\mathrm{TMS}} = 0$), as well as standard ultrastrong interaction between resonators in absence of galvanic coupling (with $g_{\mathrm{BS}}/\omega_0 \simeq 20\%$, $g_{\mathrm{TMS}}/\omega_0 \simeq 13\%$,).

To sum up, we have proposed a fast beam splitter with geometrically coupled resonators. Our results are a proof-of-principle of the viability of ultrafast beam splitters for quantum computing and quantum simulations with photons.

Scattering by an artificial atom

In the second part of the Thesis, we leave aside the control of quantum systems using switchable couplers, to rather focus on the control of propagating photons through their scattering on an artificial atom [SF05b, SF05a]. Our interest stems from the first experiments showing the strong interaction between light and individual atoms in the absence of confining cavities. The coherent coupling between the photon and the atoms manifests as a quantum interference in the scattering process, that can result in a perfect extinction of the forward propagating wave. This fascinating effect has been observed in light scattered by individual atoms [WGH+07], but with just a 12% of extinction in the forward direction. This is because of the frequency mismatch between incident and scattered waves[32], and the extremely challenging task of addressing individual atoms with lasers.

[32]Notice that the spontaneously emitted wave by the atom is an spherical wave, while the incident one is a plane wave.

By contrast, this frequency mismatch does not occur in circuit QED, where light-matter interaction takes place in one dimension, which is by far much more efficient than in 3D. In one dimension, the spontaneous emission by the artificial atom produces a photon propagating either backwards of forward in the open line, that is, the emitted photon is a plane wave as the incident photon. Recent experiments in circuit QED have confirmed the theoretical predictions with impressive results, showing extinctions of 94% in the transmitted wave [AZA+10]. This brings with it important consequences in the photon dynamics: as the photon can only propagate forward or backwards, the overall effect is that the photon has been reflected by the atom.

In this Thesis we will exploit this coherent coupling to control the transport properties of propagating photons in an open transmission line. In particular, we focus on an in-depth theoretical study of propagating microwaves in an open transmission line scattering off on a transmon qubit[33]. For the transmon qubit working in the two-level approximation, the qubit acts as a saturable mirror for the incident photons. On the other hand, by driving a strong coherent field to the second transition of the transmon, the atom becomes transparent, yielding to perfect transmission of the incident photons. The main results of this work are:

- We derive the equations of motion of a transmon qubit coupled to a semi-infinite transmission line from a fully microscopi viewpoint. These equations are quantum Langevin equations for the transmon, and an input-output relation for quantum fields.
- Since Langevin equations are generally not solvable, we derive a master equation for the transmon in its Lindblad form. Using the master equation and the input-output relation, we study the scattering of a coherent signal by a transmon qubit in the two-level approximation. The scattering process is fully determined by the reflection and transmission coefficients. In particular, for a low-amplitude drive on resonance with the qubit, we obtain the experimentally observed perfect reflection of the photon by the atom.
- We consider the scattering problem in the three-level approximation of the transmon: a coherent probe at the single photon level scatters off the transmon at the first transition, while a strong control pulse drives the second transition. For sufficiently strong control pulses, we observe Electromagnetically Induced Transparency (EIT) [BIH91, AAZ+10], which

[33] A transmon is a superconducting circuit with three-energy levels in ladder configuration. Nevertheless, the system is sufficiently anharmonic to behave as a two level system.

in this case is assisted by the splitting of the second transition –usuall called Autler-Townes splitting [AT55].

- Finally, we study second order correlations functions $g_2(\tau)$ for the reflected and the transmitted field through the transmon . For low amplitude drives, we observe strong antibunching in the reflected field, and strong bunching in the transmitted one. The transmon acts as a photon-number filter, reflecting back to the line the one-photon Fock state $|1\rangle$ and transmitting higher multiphoton states [HPL+12]. We include finite temperature and finite detection bandwidth in the system. This can be done by adding a single-mode transmission line resonator in resonance with the transmon, acting as a frequency filter.

Summing up, we have reported on an in-depth study of the scattering of coherent states on a single transmon, from a microscopic viewpoint. Our results show that the transmon in the two-level approximation behaves as a saturable mirror for the incoming photons. On the other hand, a strong control pulse addressing the second transition of the transmon induces an Autler-Townes splitting on the excited energy levels, yielding to perfect transmission at the probe frequency. Our theoretical results are in excellent agreement with circuit QED experiments. In particular with those we present in the following work.

Demonstration of a single photon router

The timely one-dimensional photon-transport properties before can be used to control propagating photons with high precision. This can be of great interest in the development of photonic quantum networks [OFV09, Kim08], where quantum nodes have to process and distribute quantum information (codified in propagating photons) among different quantum channels. The task of controlling photons turns out to be nontrivial, since photons do not interact with themselves and hardly do it with real atoms.

In this work, we exploit of the high-efficient scattering in one dimension to control photons, demonstrating a rudimentary quantum node: the single photon router. The active element of the router is a transmon qubit strongly coupled to an open transmission line. By exploiting the phenomenon of electromagnetically induced transparency (EIT), we manage to route single photons to different output ports with a 99% efficiency. Below we summarize the most important results:

- We have experimentally observed perfect reflection on the scattering of a coherent field at the single photon level ($N \ll 1$) with the transmon qubit in the two-level approximation. On the other hand, at high drive powers ($N \gg 1$) we observe perfect tranmission of photons, as a clear signature of the non-linear nature of the transmon, which can only reflect one photon at a time.

- By sending a second coherent drive on resonance with the 1-2 transition of the transmon, we observe the third level of the transmon qubit, which can be used to induce EIT in the system. Moreover, we take advantage of this phenomenon to build up a single-photon router, whose working principle is the following: A weak incoming probe at the single photon level $N_p \ll 1$ scatters the qubit at the ω_{01} frequency. A second strong control pulse ($N_c \gg 1$) at the ω_{12} frequency is alternatively switched on and off. When the control is turned off, the photons at the probe frequency are reflected by atom, and are routed to one output port (let's call it port 1) through a circulator[34]. On the other hand, when the control is on, EIT occurs in the transmon and the photons at the probe frequency are perfectly transmitted to a different output port 2.

- We measure the router efficiency, reaching a 99% on-off ratio both in the reflected and transmitted signal. We check this router efficiency for incoming ultrashort gaussian pulses, observing a high on-off ration up to 10 nanoseconds. The time operation can be further improved to the subnanosecond scale, by reducing the pure dephasing rate of the transmon.

It is worth pointing out that the router can be multiplexed to distribute photons to many channels. This is achieved by putting the transmon in series along the transmission line, separated by circulators.

In summary, we demonstrate the operation principle of a rudimentary quantum node in the microwave regime, which allows us to route single photons by different ports of a network, with high speed and efficiency. Combined with the undeniably better telecom technology for distributing photons over large distances, our setup can pave the way for future quantum networks. In particular, we envision the realization of a quantum interface between micro- and telecom wavelengths as the ultimate goal for developing hybrid quantum networks.

[34] A circulator is a passive three-port device, designed in such a way that light entering any port exits from the next, in a direction fixed by an external magnetic field.

Application to single-photon detection

We finish this Thesis by addressing an open problem in circuit QED: the detection of *propagating microwave photons*. In contrast to thes optical domain, where photons are straightforwardly detected, the low cross-section between light and matter in the microwave regime makes of photodetection a challenging task. For this reason, we point at the microwave single-photon detector as the ultimate goal in circuit QED for developing all-optical quantum information processing. There are promising proposals for microwave photodetection that rely on the scattering of microwaves on absorbing elements, such as phase qubits[35] [RGRS09a]. However, these proposals face a fundamental limit in the detection efficiency when trying to detect with a single absorber[36] [RGRS09b].

In this work we outperform this fundamental thresholdt, by proposing a single-shot single-photon detector that successfully achieves 100% efficiency, *using only one absorber* –which will be a phase qubit as well. The main results of this work can be summarized in the following points:

- Our photodetector proposal consists of a phase qubit placed at a distance L from the end of a semi-infinite transmission line, which acts as a highly reflecting mirror. We solve the scattering problem for this model: a photon coming from the left interacts with the qubit. We solve the Schrödinger equation in the limit where $L \ll \lambda$, where λ is the wavelength associated with the phase qubit energy gap.

- By controlling the various parameters of our system, such as the distance L, the coupling V to the line, and the decay rate Γ to the metastable state $|g\rangle$, we can control the reflection and transmission coefficients. In particular, we can confine the propagating photon in the pseudo-cavity defined by the qubit and the mirror (which corresponds to $r = 0$).

- We observe the full extintion of the photon in the pseudo-cavity as the time passes by, due to the full absorption of the photon by the phase qubit. Defining the detection efficiency as the fraction of the wavepacket that has been neither reflected by the qubit, nor stored in the pseudocavity, we conclude that a propagating photon has been perfectly detected

[35] A phase qubit is a superconducting qubit that possesses two internal states $|0\rangle$ and $|1\rangle$, and a large decay rate Γ from the excited state $|1\rangle$ to a metastable state $|g\rangle$.

[36] For a perfect detection with only one qubit, we must reconstruct the time reversed process of spontaneous emission. Given that the photon approached the qubit either from the left or the right direction, it only represents half of the process and thus half of the efficiency.

with an efficiency of 100%, using solely a single absorber in the transmission line.

- We validate these results for different incoming wavepackets, ranging from Fock states to more realistic situations where the incoming photons possess Gaussian envelopes. For all the considered cases, we reach outstanding detection efficiencies, even for slightly detuned photons.

- We consider the case of more than one phase qubit in the transmission line, separated by a distance d. We study its detection efficiency as a function of different fluctuating parameters, such as the distance between absorbers and the detuning between the incoming photon and the absorbers. We observe that as we put more absorbers in the line, the detection efficiency becomes robust to highly-detuned incoming photon and to imperfections in the fabrication process.

- Finally, we propose a theoretical model that predicts the experimental results of [CHS+11]. This photodetector proposal is in close resemblance with our model, but the photon is injected through the mirror, and trap it in the qubit-mirror pseudocavity. Our theory predicts a 90% detection efficiency, with an asymptotic limit of 100% efficiency in the limit $\Gamma \to 0$. This result can be easily interpreted as follows: for a perfect detection, we need the absorber to behave as a perfect mirror, yielding the condition $\Gamma \to 0$. But at the same time, the detection time diverges as $1/\Gamma$, so this scheme would only yield to a perfect detection at infinite time.

With this minimal model, we manage to reach a perfect 100% efficiency of a propagating photon in a single-shot, improving the fundamental limit of 50% efficiency with only one absorber: due to the presence of the mirror in our setup, we are able to reconstruct the time reversed process of spontaneous emission.

General conclusions

Throughout this Thesis we have thoroughly studied the control of superconducting quantum circuits, within the framework of circuit QED. Superconducting circuits are mesoscopic solid-state devices that are cooled down to cryogenic temperatures, and which behave quantum mechanically. More precisely, this quantum behavior is manifested in the form of microwave photons and localized quantum systems of a few energy levels such as qubits and qutrits. We have studied the interaction between these quantum systems, and how the control of their interactions yields different applications of great interest in the fields of quantum optics, quantum simulation and quantum computing, and even in relativistic quantum information.

In the first part of the Thesis, we have focused on the control of ultrastrong interactions between superconducting circuits, by means of coupling devices such as SQUID's. Firstly, we have proposed several designs that allows for a tunable interaction between light-matter in the ultrastrong regime, either in a resonator or in an open transmission line. We demonstrate that the coupling can not only be tuned in strength but also in kind. We suggest several applications, as the development of ultrafast two-qubit gates for quantum computing, qubit protection from the environment, or simulation of nonlinear media. Particularly interesting has been its application to the field of relativistic quantum information, where we propose a protocol for extracting past-future quantum correlations from the vacuum field to a pair of superconducting qubits. Moreover, we propose an exotic quantum memory that codifies quantum information in the vacuum, based on quantum teleportation in time. Aside from tunable interactions in light-matter setups, we demonstrate this tunability in scalable networks of superconducting resonators. Our proposals find applications in the following fields: i)quantum optics with the development of tunable beam splitters and squeezed states, ii) condensed matter for testing quantum phase transitions and critical phases, and entanglement dynamics in many-body systems, iii) quantum simulations, with the development of Bose-Hubbard and spin models, and the simulation of gauge potentials. Our theoretical results have inspired several experiments implementing resonator-resonator interactions. In particular, in this Thesis we present the development of an ultrafast beam splitter that can swap photons between the resonators in a few nanoseconds.

In the second part of this Thesis, we explore how to control propagating microwave photons through their scattering on superconducting qubits. We theoretically analyze the coherent interaction between a propagating field and a transmon qubit from a microscopic viewpoint. For the transmon in the

two-level approximation we observe perfect reflection of the incoming field, whereas in the three-level approach we observe perfect transmission assisted by EIT. We combine both features to demonstate a redimentary quantum node: a single photon router that can distribute photons to different output ports of a transmission line or quantum network, with high speed and efficiency. The detection of these propagating photons still remains as an open problem in circuit QED. In this Thesis we contribute to this problem with the proposal of a perfect single-photon detector. Our proposal relies on the scattering of propagating photons on a single phase qubit facing a single-end open transmission line. The proposed model shows a theoretical 100% detection efficiency in a finite time, and robustness to detuned incoming photons and small fluctuations in the system parameters.

This Thesis provides a countless number of designs that allows for a full control of interactions in the framework of circuit QED, particularly in the rather unexplored ultrastrong regime. Our designs would allow for fascinating applications in a wide range of disciplines of physics, which we do believe will pave the way for the forthcoming quantum technologies.

Bibliography

[AAAN+08] Jr. A. Abdumalikov, O. Astafiev, Y. Nakamura, Y. A. Pashkin, and J. Tsai, *Vacuum Rabi splitting due to strong coupling of a flux qubit and a coplanar-waveguide resonator*, Phys. Rev. B **78** (2008), no. 18, 180502.

[AAZ+10] A. A. Abdumalikov, O. Astafiev, A. M. Zagoskin, Yu. A. Pashkin, Y. Nakamura, and J. S. Tsai, *Electromagnetically induced transparency on a single artificial atom*, Phys. Rev. Lett. **104** (2010), 193601.

[AL97] Daniel S. Abrams and Seth Lloyd, *Simulation of many-body fermi systems on a universal quantum computer*, Phys. Rev. Lett. **79** (1997), 2586–2589.

[AT55] S. H. Autler and C. H. Townes, *Stark effect in rapidly varying fields*, Phys. Rev. **100** (1955), 703–722.

[AZA+10] O. Astafiev, A. M. Zagoskin, A. A. Abdumalikov, Yu. A. Pashkin, T. Yamamoto, K. Inomata, Y. Nakamura, and J. S. Tsai, *Resonance Fluorescence of a Single Artificial Atom*, Science **327** (2010), no. 5967, 840–843.

[BGA+09] J. Bourassa, J. M. Gambetta, A. A. Abdumalikov, O. Astafiev, Y. Nakamura, and A. Blais, *Ultrastrong coupling regime of cavity qed with phase-biased flux qubits*, Phys. Rev. A **80** (2009), no. 3, 032109.

[BHW+04] Alexandre Blais, Ren-Shou Huang, Andreas Wallraff, S. M. Girvin, and R. J. Schoelkopf, *Cavity quantum electrodynamics for superconducting electrical circuits: An architecture for quantum computation*, Phys. Rev. A **69** (2004), no. 6, 062320.

[BIH91] K.-J. Boller, A. Imamolu, and S. E. Harris, *Observation of electromagnetically induced transparency*, Phys. Rev. Lett. **66** (1991), 2593–2596.

[BKKY08] Tim Byrnes, Na Young Kim, Kenichiro Kusudo, and Yoshihisa Yamamoto, *Quantum simulation of fermi-hubbard models in semiconductor quantum-dot arrays*, Phys. Rev. B **78** (2008), 075320.

[BN09] I. Baluta and F. Nori, *Nmr techniques for quantum control and computation*, Science **326** (2009), 108–111.

[BP07] H.P. Breuer and F. Petruccione, *The theory of open quantum systems*, OUP Oxford, 2007.

[BVJ+98] V. Bouchiat, D. Vion, P. Joyez, D. Esteve, and M. H. Devoret, *Quantum Coherence with a Single Cooper Pair*, Physica Scripta Volume T **76** (1998), 165–170.

[Car91] H. J. Carmichael, *An open systems approach to quantum optics*, Université Libre de Bruxelles, 1991.

[CBC05] Cristiano Ciuti, Gérald Bastard, and Iacopo Carusotto, *Quantum vacuum properties of the intersubband cavity polariton field*, Phys. Rev. B **72** (2005), no. 11, 115303.

[CHS+11] Y.-F. Chen, D. Hover, S. Sendelbach, L. Maurer, S. T. Merkel, E. J. Pritchett, F. K. Wilhelm, and R. McDermott, *Microwave photon counter based on josephson junctions*, Phys. Rev. Lett. **107** (2011), 217401.

[Cla89] J. Clarke, *Principles and applications of SQUIDs*, Proceedings of the IEEE **77** (1989), no. 8, 1208–1223.

[CRL+10] Jorge Casanova, Guillermo Romero, Ion Lizuain, Juan José García-Ripoll, and Enrique Solano, *Deep strong coupling regime of the jaynes-cummings model*, Physical review letters **105** (2010), no. 26, 263603.

[CW08] J. Clarke and F. K. Wilhelm, *Superconducting quantum bits*, Nat. Phys.**453** (2008), 1031–1042.

[CZ95] J. I. Cirac and P. Zoller, *Quantum computations with cold trapped ions*, Phys. Rev. Lett. **74** (1995), 4091–4094.

[Deu85] D. Deutch, *Quantum theory, the church-turing principle and the univer- sal quantum computer*, Royal Society of London Proceedings Series A. **400** (1985), 97–117.

[Dev95] M. H. Devoret, *Quantum fluctuations in electrical circuits*, Les Houches Session LXIII, Quantum Fluctuations (1995), 351–386.

[DGI+09] H. Dong, Z. R. Gong, H. Ian, Lan Zhou, and C. P. Sun, *Intrinsic cavity qed and emergent quasinormal modes for a single photon*, Phys. Rev. A **79** (2009), no. 6, 063847.

[DGS07] M.H. Devoret, Steven Girvin, and Robert Schoelkopf, *Circuit-qed: How strong can the coupling between a josephson junction atom and a transmission line resonator be?*, Annalen der Physik **16** (2007), no. 10-11, 767–779.

[Dir27] P. A. M. Dirac, *The quantum theory of the emission and absorption of radiation*, Proceedings of the Royal Society of London. Series A **114** (1927), no. 767, 243–265.

[DWM] M. H. Devoret, A. Wallraff, and J. M. Martinis, *Superconducting qubits: A short review*, arXive:cond-mat/0411174v1.

[Fey82] RichardP. Feynman, *Simulating physics with computers*, International Journal of Theoretical Physics **21** (1982), no. 6-7, 467–488 (English).

[FLM+10] P. Forn-Díaz, J. Lisenfeld, D. Marcos, J. J. García-Ripoll, E. Solano, C. J. P. M. Harmans, and J. E. Mooij, *Observation of the Bloch-Siegert Shift in a Qubit-Oscillator System in the Ultrastrong Coupling Regime*, Physical Review Letters **105** (2010), no. 23, 237001.

[FSG+08] A. Friedenauer, H. Schmitz, J. T. Glueckert, D. Porras, and T. Schaetz, *Simulating a quantum magnet with trapped ions*, Nature Physics **4** (208), 757–761.

[GAH+09] G. Günter, A. A. Anappara, J. Hees, A. Sell, G. Biasiol, L. Sorba, S. de Liberato, C. Ciuti, A. Tredicucci, A. Leitenstorfer, and R. Huber, *Sub-cycle switch-on of ultrastrong light-matter interaction*, Nat. Phys.**458** (2009), 178–181.

[GHB11] J. M. Gambetta, A. A. Houck, and Alexandre Blais, *Superconducting qubit with purcell protection and tunable coupling*, Phys. Rev. Lett. **106** (2011), 030502.

[GZ91] C. W. Gardiner and P. Zoller, *Quantum noise*, Springer, 1991.

[HBP06] M. J. Hartmann, F. G. S. L. Brandão, and M. B. Plenio, *Strongly interacting polaritons in coupled arrays of cavities*, Nature Physics **2** (2006), 849–855.

[HK89] Serge Haroche and Daniel Kleppner, *Cavity quantum electrodynamics*, Physics Today **42** (1989), no. 1, 24–30.

[HPL+12] Io-Chun Hoi, Tauno Palomaki, Joel Lindkvist, Göran Johansson, Per Delsing, and C. M. Wilson, *Generation of nonclassical microwave states using an artificial atom in 1d open space*, Phys. Rev. Lett. **108** (2012), 263601.

[HR06] S. Haroche and J.-M. Raymond, *Exploring the quantum*, Oxford Univ. Press Inc., New York, 2006.

[HTK12] A. A. Houck, H. E. Türeci, and J. Koch, *On-chip quantum simulation with superconducting circuits*, Nature Physics **8** (2012), 292–299.

[HWJ+11] Io-Chun Hoi, C. M. Wilson, Göran Johansson, Tauno Palomaki, Borja Peropadre, and Per Delsing, *Demonstration of a single-photon router in the microwave regime*, Phys. Rev. Lett. **107** (2011), 073601.

[JC63] E.T. Jaynes and F. W. Cummings, *Comparison of quantum and semiclassical radiation theories with application to the beam maser*, Proceedings of the IEEE **51** (1963), no. 1, 89–109.

[Jos62] B. D. Josephson, *Possible new effects in superconductive tunnelling*, Phys. Lett **1** (1962), 251.

[JZ05] D. Jaksch and P. Zoller, *The cold atom hubbard toolbox*, Annals of Physics **315** (2005), no. 1, 52 – 79, Special Issue.

[KHHG10] Jens Koch, Andrew A. Houck, Karyn Le Hur, and S. M. Girvin, *Time-reversal-symmetry breaking in circuit-qed-based photon lattices*, Phys. Rev. A **82** (2010), 043811.

[Kim08] H. J. Kimble, *The Quantum Internet*, Nat. Phys.**453** (2008), 1023.

[KLM01] E. Knill, R. Laflamme, and G. J. Milburn, *A scheme for efficient quantum computation with linear optics*, Nat. Phys.**409** (2001), 46–52.

[KYG+07] Jens Koch, Terri M. Yu, Jay Gambetta, A. A. Houck, D. I. Schuster, J. Majer, Alexandre Blais, M. H. Devoret, S. M. Girvin, and

R. J. Schoelkopf, *Charge-insensitive qubit design derived from the cooper pair box*, Phys. Rev. A **76** (2007), no. 4, 042319.

[LDM+12] Martin Leib, Frank Deppe, Achim Marx, Rudolf Gross, and Michael Hartmann, *Networks of nonlinear superconducting transmission line resonators*, New Journal of Physics (2012), no. 14, 075024.

[Leg80] A. J. Leggett, *Macroscopic quantum systems and the quantum theory of measurement*, Progress of Theoretical Physics Supplement **69** (1980), 80–100.

[LH10] Martin Leib and Michael J Hartmann, *BoseâĂŞhubbard dynamics of polaritons in a chain of circuit quantum electrodynamics cavities*, New Journal of Physics **12** (2010), no. 9, 093031.

[LH12] Karyn Le Hur, *Kondo resonance of a microwave photon*, Phys. Rev. B **85** (2012), 140506.

[Llo96] Seth Lloyd, *Universal quantum simulators*, Science **273** (1996), no. 5278, 1073–1078.

[LWH+07] T Lindström, C H Webster, J E Healey, M S Colclough, C M Muirhead, and A Ya Tzalenchuk, *Circuit qed with a flux qubit strongly coupled to a coplanar transmission line resonator*, Superconductor Science and Technology **20** (2007), no. 8, 814.

[MDC85] John M. Martinis, Michel H. Devoret, and John Clarke, *Energy-level quantization in the zero-voltage state of a current-biased josephson junction*, Phys. Rev. Lett. **55** (1985), no. 15, 1543–1546.

[MKGD09] Vladimir E. Manucharyan, Jens Koch, Leonid I. Glazman, and Michel H. Devoret, *Fluxonium: Single cooper-pair circuit free of charge offsets*, Science **326** (2009), no. 5949, 113–116.

[Mol69] B. R. Mollow, *Power spectrum of light scattered by two-level systems*, Phys. Rev. **188** (1969), 1969–1975.

[MOL+99] J. E. Mooij, T. P. Orlando, L. Levitov, Lin Tian, Caspar H. van der Wal, and Seth Lloyd, *Josephson Persistent-Current Qubit*, Science **285** (1999), no. 5430, 1036–1039.

[NC00] M. A. Nielsen and I. L. Chuang, *Quantum computation and quantum information*, Cambridge Univ. Press, Cambridge, 2000.

[NC10a] P. Nataf and C. Ciuti, *Vacuum degeneracy of a circuit qed system in the ultrastrong coupling regime*, Physical review letters **104** (2010), no. 2, 023601.

[NC10b] Pierre Nataf and Cristiano Ciuti, *No-go theorem for superradiant quantum phase transitions in cavity qed and counter-example in circuit qed*, Nature Communications **1** (2010), 72.

[NC11] P. Nataf and C. Ciuti, *Protected quantum computation with multiple resonators in ultrastrong coupling circuit qed*, Physical Review Letters **107** (2011), no. 19, 190402.

[NDH+10] T. Niemczyk, F. Deppe, H. Huebl, E. P. Menzel, F. Hocke, M. J. Schwarz, J. J. Garcia-Ripoll, D. Zueco, T. Hümmer, E. Solano, A. Marx, and R. Gross, *Circuit quantum electrodynamics in the ultrastrong-coupling regime*, Nature Physics **6** (2010), 772–776.

[NKG11] A Nunnenkamp, Jens Koch, and S M Girvin, *Synthetic gauge fields and homodyne transmission in jaynesâĂŞcummings lattices*, New Journal of Physics **13** (2011), no. 9, 095008.

[OD91] T. P. Orlando and K. A. Delin, *Foundations of applied superconductivity*, Addison-Wesley Publishing Company, New York, 1991.

[OFV09] J. L. O'Brien, Akira Furusawa, and Jelena Vuckovi, *Photonic quantum technologies*, Nature Photonics **3** (2009), 687 – 695.

[OMT+99] T. P. Orlando, J. E. Mooij, Lin Tian, Caspar H. van der Wal, L. S. Levitov, Seth Lloyd, and J. J. Mazo, *Superconducting persistent-current qubit*, Phys. Rev. B **60** (1999), 15398–15413.

[OR11] S. Jay Olson and Timothy C. Ralph, *Entanglement between the future and the past in the quantum vacuum*, Phys. Rev. Lett. **106** (2011), 110404.

[OR12] S. J. Olson and T. C. Ralph, *Extraction of timelike entanglement from the quantum vacuum*, Phys. Rev. A **85** (2012), 012306.

[Pau94] C. R. Paul, *Analysis of multiconductor transmission lines*, Wiley-Interscience, New York, 1994.

[PFHM09] F. G. Paauw, A. Fedorov, C. J. P. M Harmans, and J. E. Mooij, *Tuning the gap of a superconducting flux qubit*, Phys. Rev. Lett. **102** (2009), 090501.

[PTP46] E. M. Purcell, H. C. Torrey, and R. V. Pound, *Resonance absorption by nuclear magnetic moments in a solid*, Phys. Rev. **69** (1946), 37–38.

[Pur01] R.R. Puri, *Mathematical methods of quantum optics*, Physics and astronomy online library, Springer, 2001.

[PZW+12] Borja Peropadre, David Zueco, Friedrich Wulschner, Frank Deppe, Achim Marx, Rudolf Gross, and JJ García-Ripoll, *Tunable coupling engineering between superconducting resonators: from sidebands to effective gauge fields*, arXiv preprint arXiv:1212.2240 (2012).

[RBH01] J. M. Raimond, M. Brune, and S. Haroche, *Manipulating quantum entanglement with atoms and photons in a cavity*, Rev. Mod. Phys. **73** (2001), 565–582.

[RBW+12] G. Romero, D. Ballester, Y. M. Wang, V. Scarani, and E. Solano, *Ultrafast quantum gates in circuit qed*, Phys. Rev. Lett. **108** (2012), 120501.

[RCR05] A. Retzker, J. I. Cirac, and B. Reznik, *Detecting vacuum entanglement in a linear ion trap*, Phys. Rev. Lett. **94** (2005), 050504.

[RGRS09a] G. Romero, J. J. García-Ripoll, and E. Solano, *Microwave photon detector in circuit qed*, Phys. Rev. Lett. **102** (2009), no. 17, 173602.

[RGRS09b] Guillermo Romero, Juan José García-Ripoll, and Enrique Solano, *Photodetection of propagating quantum microwaves in circuit qed*, Physica Scripta **2009** (2009), no. T137, 014004.

[RLSH12] Alessandro Ridolfo, Martin Leib, Salvatore Savasta, and Michael J Hartmann, *Photon blockade in the ultrastrong coupling regime*, Physical Review Letters **109** (2012), no. 19, 193602.

[RRS05] Benni Reznik, Alex Retzker, and Jonathan Silman, *Violating bell's inequalities in vacuum*, Phys. Rev. A **71** (2005), 042104.

[RSH13] Alessandro Ridolfo, Salvatore Savasta, and Michael J Hartmann, *Nonclassical radiation from thermal cavities in the ultrastrong coupling regime*, Physical Review Letters **110** (2013), no. 16, 163601.

[RVDS+10] Alessandro Ridolfo, Rocco Vilardi, Omar Di Stefano, Stefano Portolan, and Salvatore Savasta, *All optical switch of vacuum rabi*

oscillations: The ultrafast quantum eraser, Physical Review Letters **106** (2010), no. 1, 013601.

[SBPC+09] Valerio Scarani, Helle Bechmann-Pasquinucci, Nicolas J. Cerf, Miloslav Dušek, Norbert Lütkenhaus, and Momtchil Peev, *The security of practical quantum key distribution*, Rev. Mod. Phys. **81** (2009), 1301–1350.

[SDRGRL11] Carlos Sabín, Marco Del Rey, Juan José García-Ripoll, and Juan León, *Fermi problem with artificial atoms in circuit qed*, Physical Review Letters **107** (2011), no. 15, 150402.

[SF05a] J. T. Shen and Shanhui Fan, *Coherent photon transport from spontaneous emission in one-dimensional waveguides*, Opt. Lett. **30** (2005), no. 15, 2001–2003.

[SF05b] Jung-Tsung Shen and Shanhui Fan, *Coherent single photon transport in a one-dimensional waveguide coupled with superconducting quantum bits*, Physical Review Letters **95** (2005), no. 21, 213001.

[SG08] R. J. Schoelkopf and S. M. Girvin, *Wiring up quantum systems*, Nat. Phys.**451** (2008), 664–669.

[SGRSL10] Carlos Sabín, Juan José García-Ripoll, Enrique Solano, and Juan León, *Dynamics of entanglement via propagating microwave photons*, Physical Review B **81** (2010), no. 18, 184501.

[Sho97] Peter W. Shor, *Polynomial-time algorithms for prime factorization and discrete logarithms on a quantum computer*, SIAM J. Comput. **26** (1997), no. 5, 1484–1509.

[SPdRMM12] Carlos Sabín, Borja Peropadre, Marco del Rey, and Eduardo Martín-Martínez, *Extracting past-future vacuum correlations using circuit qed*, Physical Review Letters **109** (2012), no. 3, 33602.

[SRDS+13] R. Stassi, A. Ridolfo, O. Di Stefano, M. J. Hartmann, and S. Savasta, *Spontaneous conversion from virtual to real photons in the ultrastrong-coupling regime*, Physical Review Letters **110** (2013), no. 24, 243601.

[SZ97] M.O. Scully and S. Zubairy, *Quantum optics*, Cambridge University Press, 1997.

[VAC+02] D. Vion, A. Aassime, A. Cottet, P. Joyez, H. Pothier, C. Urbina, D. Esteve, and M. H. Devoret, *Manipulating the quantum state of an electrical circuit*, Science **296** (2002), 886–889.

[VC05] L. M. K. Vandersypen and I. L. Chuang, *Nmr techniques for quantum control and computation*, Rev. Mod. Phys. **76** (2005), 1037–1069.

[WGH+07] Gert Wrigge, Ilja Gerhardt, Jaesuk Hwang, Gert Zumofen, and Vahid Sandoghdar, *Efficient coupling of photons to a single molecule and the observation of its resonance fluorescence*, Nature Physics **4** (2007), no. 1, 60–66.

[WM08] D. F. Walls and G. J. Milburn, *Quantum optics / d.f. walls, gerard j. milburn*, 2nd ed. ed., Springer Berlin, 2008 (English).

[WSB+04] A. Wallraff, D. I. Schuster, A. Blais, L. Frunzio, R.-S. Huang, J. Majer, S. Kumar, S. M. Girvin, and R. J. Schoelkopf, *Strong coupling of a single photon to a superconducting qubit using circuit quantum electrodynamics*, Nat. Phys.**431** (2004), 162–167.

[WVEB06] H. Walter, B. T. H. Varcoe, B. G. Englert, and T. Becka, *Cavity quantum electrodynamics*, Rep. Prog. Phys. **69** (2006), 1325.

[YD84] Bernard Yurke and John Denker, *Quantum network theory*, Physical Review A **29** (1984), no. 3, 1419–1437.

[Zag11] A.M. Zagoskin, *Quantum engineering: Theory and design of quantum coherent structures*, Quantum Engineering: Theory and Design of Quantum Coherent Structures, Cambridge University Press, 2011.